Lecture Notes in Physics 901

Gottfried H. Bauer

Photovoltaic Solar Energy Conversion

Springer

Lecture Notes in Physics

Volume 901

The Lecture Notes in Physics

The series Lecture Notes in Physics (LNP), founded in 1969, reports new developments in physics research and teaching-quickly and informally, but with a high quality and the explicit aim to summarize and communicate current knowledge in an accessible way. Books published in this series are conceived as bridging material between advanced graduate textbooks and the forefront of research and to serve three purposes:

- to be a compact and modern up-to-date source of reference on a well-defined topic
- to serve as an accessible introduction to the field to postgraduate students and nonspecialist researchers from related areas
- to be a source of advanced teaching material for specialized seminars, courses and schools

Both monographs and multi-author volumes will be considered for publication. Edited volumes should, however, consist of a very limited number of contributions only. Proceedings will not be considered for LNP.

Volumes published in LNP are disseminated both in print and in electronic formats, the electronic archive being available at springerlink.com. The series content is indexed, abstracted and referenced by many abstracting and information services, bibliographic networks, subscription agencies, library networks, and consortia.

Proposals should be sent to a member of the Editorial Board, or directly to the managing editor at Springer:

Christian Caron
Springer Heidelberg
Physics Editorial Department I
Tiergartenstrasse 17
69121 Heidelberg/Germany
christian.caron@springer.com

More information about this series at
http://www.springer.com/series/5304

Gottfried H. Bauer

Photovoltaic Solar Energy Conversion

Springer

Gottfried H. Bauer
Institut für Physik
Carl von Ossietzky Universität
AG Halbleiterphysik
Oldenburg, Germany

ISSN 0075-8450 ISSN 1616-6361 (electronic)
Lecture Notes in Physics
ISBN 978-3-662-46683-4 ISBN 978-3-662-46684-1 (eBook)
DOI 10.1007/978-3-662-46684-1

Library of Congress Control Number: 2015937388

Springer Heidelberg New York Dordrecht London

Printed on acid-free paper

Springer-Verlag GmbH Berlin Heidelberg is part of Springer Science+Business Media (www.springer.com)

Preface

These notes on photovoltaic solar energy conversion result from lectures given to graduate students in the Physics Department of Carl von Ossietzky University Oldenburg over the last two decades, the aim being to increase the number of young people getting expertise in 'photovoltaics,' to motivate young colleagues and graduate and Ph.D. students in physics, chemistry, and eventually electrical engineering, as well as researchers involved in basics and applications of these disciplines, to reflect upon the conversion of solar light with fundamental concepts, to ask themselves questions, and to try to find consistent answers on how photovoltaic solar energy conversion works and contribute successfully to its progress. If senior scientists and colleagues interested in or already working in the field also find here some new aspects of the problem, this would be a further positive point.

The contents of these notes have been developed on the basis of contributions in the form of textbooks by two well-known experts, in particular A. deVos (*Endoreversible Thermodynamics for Solar Energy Conversion*) and P. Würfel (*Physics of Solar Cells*), and have been garnished by some of my own ideas on how to understand and visualize the microscopic physical mechanisms and effects.

These personal ideas have, of course, been influenced by contacts, feedback, and very fruitful discussions and collaborations with friends and colleagues over the last few decades, including in particular Peter Würfel and Tom Markvart, as well as Gion Calzaferri, Reinhard Carius, Jean-François Guillemol, Wolfram Jägermann, Jean-Paul Kleider, Uwe Rau, Harald Ries, Helmut Tributsch, and many others not explicitly listed here. I am grateful for the opportunity to meet and exchange ideas and concepts with numerous attendees of conferences, workshops, and meetings on general physics, on photovoltaics and solar energy conversion, and I must not forget the stimulus of questions and comments from my closer scientific environment during my stay at Carl von Ossietzky University in Oldenburg, including in particular Dr. Rudi Brüggemann and my Ph.D. and diploma students.

The impetus to compile this contribution came from Dr. C. Caron at Springer.

Oldenburg, Germany and Soubès, France G.H. Bauer
January 2015

Contents

Symbols, Acronyms, Abbreviations

A	Area, constant, abbreviation factor
A_{12}	Einstein coefficient
$\mathbf{A}$	Vector potential
B	Constant
B_{12}, B_{21}	Einstein coefficients
C	Constant, solar light concentration factor
CB	Conduction band
D	Density of states
D_n, D_p	Diffusion coefficient of electrons, of holes
$E_\mathrm{x,y,z}$	Component of electric field strength
$\mathbf{E}$	Electric field strength (vector)
E_int	Internal energy of 'Landsberg-receiver'
F	Function
H	Hamiltonian
$\mathbf{H}$	Magnetic field strength (vector)
J	Flow, particle current
L	Length
L_n, L_p	Diffusion length of electrons, of holes
M_CV, M_VC	Dipole matrix element ($CB \rightarrow VB$- and $VB \rightarrow CB$-transition)
N	Number
N_V, N_C	Effective density of states in VB, in CB
P	Power, probability
$\mathbf{P}$	Polarization (vector)
Q	Heat
QD	Abbreviation for quantum dot
R	Radius
R_Earth	Radius of Earth
R_Sun	Radius of Sun
R_rec	Radius of receiver
S	Entropy
SQ	Abbreviation for Shockley–Queisser

T	Temperature
$T_{\mathrm{Earth}}, T_{\mathrm{Sun}}$	Temperature of Earth, of Sun
U	Internal energy
V	Volume, voltage
VB	Valence band
W	Work
a	Absorption, heat conduction term
b	Constant, radiation transfer term
c, c_0	Speed of light, in vacuum
d	Thickness
d_{SE}	Distance Sun to Earth
e	Elementary charge ($+1.6 \times 10^{-19}$ As)
f	Distribution function
g	Generation rate
$\hbar$	Planck's constant ($(h/2\pi) = 1.055 \times 10^{-34}$ Ws^2)
i	Current, successive number
j	Electric current density, successive number
k	Boltzmann constant (1.381×10^{-23} Ws/K)
$k_{\mathrm{x,y,z}}$	Components of wave vector
l	Length
m	Mass
$m_{\mathrm{n}}^*, m_{\mathrm{p}}^*$	Effective mass of electrons, of holes
mpp	Maximum power point
n	Mode number, refractive index, electron concentration in CB
$\mathbf{n}_{\mathrm{normal}}$	Normal vector perpendicular to surface element
oc	Open circuit
p	Power density, pressure, hole concentration in VB
q	Heat
r	Rate, reflection factor, resistor term
s	Entropy density
sc	Short circuit
t	Transmission factor
u_ϵ	Energy density
$\mathbf{u}$	Particle velocity (vector)
v	Velocity
w	Work, geometrical width
x	Component of spatial coordinate
$\mathbf{x}$	Spatial vector
z	Component of spatial coordinate
α	Absorptivity, optical absorption coefficient
β	Abbreviation factor
γ	Factor
δ	Increment, slope of E_{C}

ϵ	Electron energy
ϵ_V, ϵ_C	Energy of top of VB, of bottom of CB
$\epsilon_F, \epsilon_{Fp}, \epsilon_{Fn}$	Fermi energy, quasi-Fermi level of holes, of electrons
ε	Emissivity, dielectric susceptibility, etendue
ε_0	Vacuum dielectric susceptibility
ζ	Independent variable, Riemann's zeta-function
η	Conversion efficiency
η_C	Carnot efficiency
θ	Angle
λ	Wave length
μ	Chemical potential
μ_n	Mobility of electrons
μ, μ_0	Magnetic permeability of matter, in vacuum
ξ	Spatial position, independent variable
π	pi (3.141592)
ρ	Radius, space charge
σ_{SB}	Stefan–Boltzmann constant (5.67×10^{-8} (Ws/m^2 K^4))
$\tau_\epsilon, \tau_{\mathbf{k}}$	Relaxation time for energy, for wave vector
τ_{rec}	Recombination lifetime
φ	Angle, electrical potential
χ	Electron affinity
χ_{el}	Electron polarization function
ψ	Electrostatic energy (e.g. for band bending in space-charge regions)
ω	Frequency
Γ	General flux, Gamma function
$\Gamma_\epsilon, \Gamma_\gamma$	Energy flux, particle flux
Δ	Difference
$\triangle$	Delta operator ($\triangle = \bigtriangledown^2$)
$\Delta p, \Delta n$	Excess concentration of holes (in VB), and electrons (in CB)
$\bigtriangledown$	Nabla operator
Θ	Angle
Φ	Electrostatic energy ($\Phi = e \cdot \varphi$)
Ψ	Electron wave function
Ω	Solid angle

Chapter 1
Introduction

The direct conversion of solar light into electrical energy is one option for the use of renewable energies. Since the life expectancy of our source of radiation, the Sun, amounts to another 4.5 billion years, the reservoir of solar radiation is effectively inexhaustible to individual human beings. In the middle and long term future, it will represent the only driving force for departures from thermal-equilibrium conditions, e.g., for biological life on our globe.

At the present time, recognition of the need to use solar energy is growing rapidly, both nationally and internationally, and the technical exploitation of solar energy is in turn expanding at a significant rate. In the context of these growing activities, more and more well educated experts will be required with fundamental knowledge of the principles and limitations of solar light conversion, and with the ability to implement innovative technical concepts and solutions in the design and realization of devices.

This survey of the principles of photovoltaic solar energy conversion has been based upon fundamental relations and seeks to accord with basics of physics presented in undergraduate and graduate courses, such as thermodynamics and statistical physics, the physics of atoms and molecules, quantum mechanics and solid state and semiconductor physics. Although these subjects do not constitute an inescapable precondition for understanding the book's message, a sound knowledge of them would definitely be helpful.

As a consequence of the spectral distribution of solar photons resulting from an emitter in thermal equilibrium at a certain temperature (T_{Sun}), whose energy is to be converted in an absorber at a (substantially lower) temperature, e.g., T_{Earth}, thermodynamic and statistical physics relations need to be introduced into formulations of the performance and fundamental limits of solar energy conversion. In other words, as long as ensembles of particles or quasi-particles, such as photons, electrons and holes, excitons, or phonons, are involved in processes and effects, their respective distributions in energy and/or wave vectors have to be taken into account, and those distributions (i.e., Boltzmann, Fermi-Dirac, Bose-

G.H. Bauer, *Photovoltaic Solar Energy Conversion*, Lecture Notes in Physics 901,
DOI 10.1007/978-3-662-46684-1_1

Einstein distribution functions) contain the variable 'temperature'.[1] Furthermore, thermodynamic relations enter the formalism through the dependence of energy and entropy fluxes on temperature, as well as through entropy production by interactions of the transport medium photons with matter, i.e., absorption, emission, or scattering.

The notes presented here have been established on the basis of these approaches, as formulated in great detail in the textbooks of A. deVos [1] and P. Würfel [2, 3]. They are supplemented by concepts designed to help the reader to understand and visualize the microscopic physical mechanisms and effects underlying photovoltaic solar energy conversion.

This introduction and a brief chapter on the global energy situation are followed by Chap. 3 which contains a short discussion on the source of solar radiation, the Sun, as a thermal-equilibrium radiator (Planck's law), and some related optical properties of radiation, such as its spectral distribution, energy and entropy fluxes.

Chapter 4 discusses the principles and associated formulations of limits for the use of solar radiation, first in thermal absorbers, this being ascribed to 'endoreversible thermodynamics' [1], and second, in electronic band systems such as semiconductors or accumulations of molecules, in which light is generating a photo-excited state that departs from the one at thermal equilibrium. The motion of these photo-excited states towards the boundaries of the absorbing system is understood as resulting from asymmetric electronic properties and leads to the limit for a single band gap configuration due to Shockley and Queisser [4].

Chapter 5 summarizes the most important real electronic systems with a discussion of the photogeneration of species and their relative spatial separations, and hence their motions in different directions, which is generally referred to as charge separation. This effect is initiated by an asymmetry of source and sink for the photogenerated carriers. Using this approach, we avoid the confusion raised by an often erroneously introduced function of an electric field.[2]

In Chap. 6, we explore approaches that go beyond the Shockley–Queisser limit either by exploiting effects that make better use of photon energies exceeding the single band gap absorption, or by modifying photon energies and manipulating the coupling of solar light in absorbers and/or manipulating the coupling of outgoing luminescence photons.

Finally, the appendixes at the end of the book recall some important relations from semiconductor and solid state physics which are also often applied to describe functions of electronic level systems for solar light conversion.

[1] Here we assume that, despite the departure from thermal equilibrium, due to fast energy and momentum relaxation compared to relaxation to the ground states, a maximum entropy distribution in the respective excited states is established which allows for the introduction of a skalar variable 'temperature'.

[2] The driving force is in fact the gradient of the chemical potential of relevant species. A general argument in favor of this viewpoint is also represented by reference to the Schrödinger equation, in which forces do not occur but instead the dependence on potentials emerges.

References

1. A. deVos, *Endoreversible Thermodynamics for Solar Energy Conversion* (Oxford University Press, Oxford, 1992; Wiley-VCH, Weinheim, 2008)
2. P. Würfel, *Physik der Solarzellen* (Spektrum Akademischer Verlag, Heidelberg, 2000)
3. P. Würfel, *Physics of Solar Cells* (Wiley-VCH, Weinheim, 2009)
4. W. Shockley, H.-J. Queisser, J. Appl. Phys. **32**, 510 (1961)

Chapter 2
Global Energy Situation

2.1 Primary Energy Resources

The main global primary energy resources consist of the traditionally used fossil fuels, such as coal, oil, and natural gas, which in the last century have substantially replaced wood, and which have notably been supplemented by nuclear 'fuels' (^{238}U) within the last couple of decades, due to a considerable increase in global primary energy needs.

Solar energy is the driving force for almost all types of 'renewable energy'. The input to the outer atmosphere of our globe amounts to 175,000 TW (see Fig. 2.1) and exceeds the present global primary energy requirement per unit time of about 15 TW by four orders of magnitude.

With an assumed technically usable fraction of only 1 % and a hypothetical overall conversion efficiency of solar light of $\eta = 10^{-2}$, solar radiation would theoretically be sufficient to provide for the primary energy needs of the world, even with further population growth. However, the use of that amount of solar light would have enormous impacts on the global average temperature and thus on the global climate. Despite the fact that solar radiation is available in such huge amounts, for environmental reasons mankind may well be unable to exploit it in the way that primary energies have been used so far.

Amongst all types of light reaching the Earth's surface, such as from stars, from the Moon, solar radiation is by far predominant and is entering almost exclusively into the entire global energy flow balance. Behind solar radiation with $P_{\text{rad, surf}} = 89{,}000\,\text{TW}$, the theoretical potential of wind energy ($P_{\text{kinet. air}} = 400\,\text{TW}$) and of biomass ($P_{\text{biosphere}} = 100\,\text{TW}$), each of them also driven by solar radiation are the next candidates for renewable energy utilization; in comparison with these, the theoretical potential of hydraulic power is relatively small ($P_{\text{hydro}} = 5\,\text{TW}$) ([1–3]

G.H. Bauer, *Photovoltaic Solar Energy Conversion*, Lecture Notes in Physics 901,
DOI 10.1007/978-3-662-46684-1_2

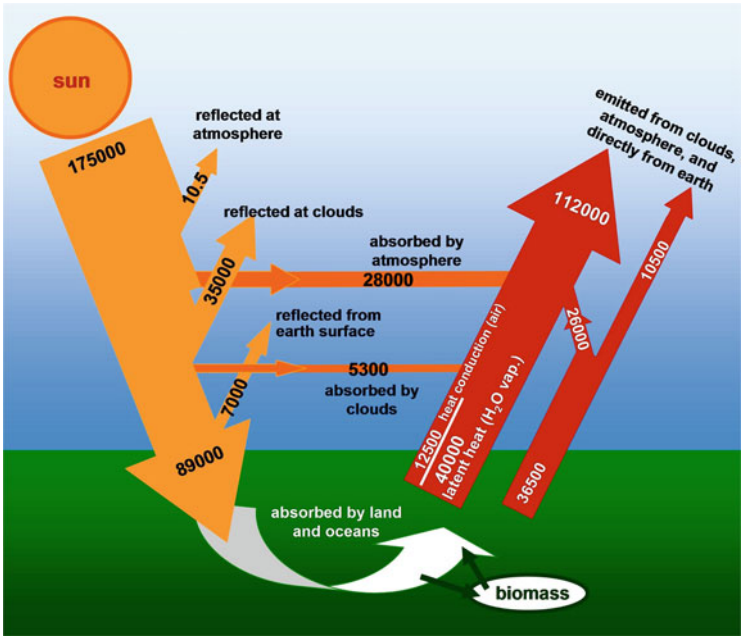

Fig. 2.1 Global energy flow budget. Numbers in TW. Data from [1]

and see Fig. 2.2 for details).[1] Of course, for each of these theoretical potentials, the so-called technically usable part amounts to a substantially smaller fraction only.

2.2 Primary Energy Demand

The present global primary energy demand per time amounts to about 15 TW. Divided amongst 7×10^9 human beings, this implies an average value of 2.2 kW/capita. The distribution of the primary power demand and use diverges widely between 'rich' consumers in industrialized countries (up to 12 kW/capita) and extremely 'poor' consumers elsewhere (< 0.1 kW/capita). The average as well as the individual numbers may be compared with the 'biological' value of (0.06–0.07) W/capita for adult humans not engaging in any specific physical activity, i.e., only sleeping or sitting.

In view of an increase in regional industrial activities and due to the moral requirement to provide a better energy supply to the large number of poor people,

[1] The exploitation of locally available types of renewable energies, such as tidal, geothermal, ocean waves, etc., should certainly be considered. In the global balance, however, their contribution is only marginal.

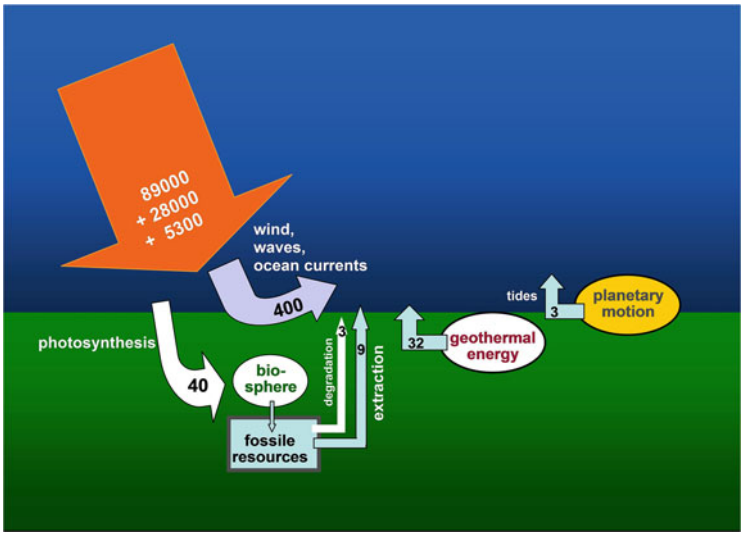

Fig. 2.2 Global budget of renewable energy flows driven by solar insolation of the atmosphere and the Earth's surface. Data from [2]

one must expect an even greater increase in global primary energy demand than would be implied by the corresponding rise in population. In the future, a straight replacement of traditionally used fossil energy carriers by renewable energies, and in particular solar energy, will definitely not suffice for a 'business as usual' strategy. Indeed, we will need to change our appreciation of the value of energy and our relationships with it. In this sense, we should regard the contribution of electrical power delivered from solar cells by conversion of sunlight rather as an option than as a panacea.

2.3 Production of Solar Cells and Modules

Regarding the production of solar cells and modules and their use for solar energy conversion, several aspects must be taken into account, including the total energy needed for preparation versus energy output over lifetime, availability and costs of material and components, cost of investments, and return on investments. For a fast-growing business area like solar cells, the availability of sufficient numbers of personnel with the appropriate training in science, technology, and maintenance may also act as a bottleneck for the necessary speedy development of a photovoltaic industry.

To appreciate what industrial production would involve, we may calculate the energy and material needed to replace the electrical power output of a nuclear power plant with nominal 5 GW production. For this purpose, we assume single-

crystalline silicon (c-Si) solar cells with a module efficiency $\eta_{\text{mod}} = 0.15$, exposed to an average central European insolation of 100 W/m^2. Replacing 5 GW would then require a total module area of $A_{\text{mod}} = 3.3 \times 10^8\,\text{m}^2$ ($18 \times 18\,\text{km}^2$). Furthermore, assuming a mean absorber thickness of the c-Si wafers of $d_{\text{c-Si}} = 250\,\mu\text{m}$, one arrives at a total volume of crystalline silicon[2] of $V_{\text{c-Si}} = 1.65 \times 10^5\,\text{m}^3$. The energy required to produce c-Si wafers presently amounts to about 1,300 kWh/m^2 [4], which corresponds to about 4.3×10^{14} Wh for a 5 GW photovoltaic plant.

At the present time, the lifetime of such c-Si modules is considered to be around 30 years (2.6×10^5 h), which translates to a production rate of $V^*_{\text{c-Si}} = 15\,\text{m}^3$/day. This corresponds to the production of modules with an area $A^*_{\text{mod}} = 3 \times 10^4\,\text{m}^2$/day. The power input for a daily output of 15 m^3 c-Si amounts to about 1.7 MW. Here, we understand that this type of business will no longer be run by a small factory, but will rather resemble an industrial plant for mass production, as for tires, for chemicals, or for cars!

Furthermore, the average production power of a 5 GW photovoltaic plant of 4.3×10^{14} Wh within the 30 years of its lifetime yields about 1.5 GW. Consequently a c-Si photovoltaic power plant (under central European insolation) would pay back its energy needed for production after 9 years. Thin film photovoltaic modules (however, somewhat less efficient) are assumed to need substantially less energy for production (factor 0.1–0.2) and thus their energy pay-back time amounts only to few years or even less.

References

1. http://asd-www.larc.nasa.gov/erbe/components2.gif
2. W.H. Bloss, G.H. Bauer, Survey of renewable energy resources, in *Proceedings of 11th World Energy Conference*, 1980, Munich (D), ed. by O. Kappelmeyer, J. Koch, J. Meyer (Federal Institute for Geosciences and Natural Sciences, Hannover (D), 1980)
3. J. Nitsch, in *Hydrogen as an Energy Carrier*, ed. by C.-J. Winter, J. Nitsch (Springer, Berlin, 1988)
4. G.H. Bauer, in *Hydrogen as an Energy Carrier*, ed. by C.-J. Winter, J. Nitsch (Springer, Berlin, 1988)

[2]Including another 250 μm of powder produced by slicing the ingots, we end up with $d_{\text{tot. mat.}} = 500\,\mu\text{m}$ for the entire necessary material thickness.

Chapter 3
Sun as Energy Source

The Sun is a nuclear fusion reactor with a life expectance of about 4.5×10^9 years. In its core, at a proton density of $10^{25}\,\mathrm{cm}^{-3}$ and a temperature of $1.5 \times 10^7\,\mathrm{K}$, protons ($p^+$) are converted by fusion processes and via several intermediate steps into nuclear products, such as helium ($^4_2$He), amongst others [1]. The average energy gain per nucleon in such fusion reactions amounts to several MeV. The total rate of change of the mass deficit of the Sun amounts to $\dot{m} = 6 \times 10^9\,\mathrm{kg/s}$, corresponding to a total power of $3.6 \times 10^{26}\,\mathrm{W}$ emitted by the outer surface of the Sun, or an energy flux

$$\Gamma_{\epsilon,Sun} = \Gamma_\epsilon(R_{\mathrm{Sun}} = 6.9 \times 10^8\,\mathrm{m}) = 6 \times 10^7\,\mathrm{W/m^2}\ .$$

3.1 Geometrical Configuration

The geometrical configuration of the Sun and planets in our solar system determines the energy flows exchanged between the individual partners and also the balance governing steady-state temperatures [2]. For our treatment here, we regard the Sun as a thermal-equilibrium source of radiation supplied by internal nuclear fusion processes. The planets are 'passive' absorbers of solar radiation, and also emitters of radiation, thus balancing the incoming energy and providing for steady-state conditions, such as an average temperature.

In particular, the planet Earth at mean distance $d_{\mathrm{SE}} = 1.5 \times 10^{11}\,\mathrm{m}$ from the Sun receives the radiation after a strong reduction from $\Gamma_\epsilon(R_{\mathrm{Sun}}) = 6 \times 10^7\,\mathrm{W/m^2}$. At the outer boundary of the Earth's atmosphere, this radiation represents an energy flux $\Gamma_\epsilon(d_{\mathrm{SE}}) = \Gamma_{\epsilon,Sun}(R_{\mathrm{Sun}}/d_{\mathrm{SE}})^2 = 1.27 \times 10^3\,\mathrm{W/m^2}$. Provided it does not suffer from any further directional dispersion (conservation of the etendue), this flux can be reconcentrated by passive elements like lenses or mirrors with maximum theoretical concentration factor $C_{\mathrm{max,\,th}} = (d_{\mathrm{SE}}/R_{\mathrm{Sun}})^2$ to reestablish the original photon and

G.H. Bauer, *Photovoltaic Solar Energy Conversion*, Lecture Notes in Physics 901,
DOI 10.1007/978-3-662-46684-1_3

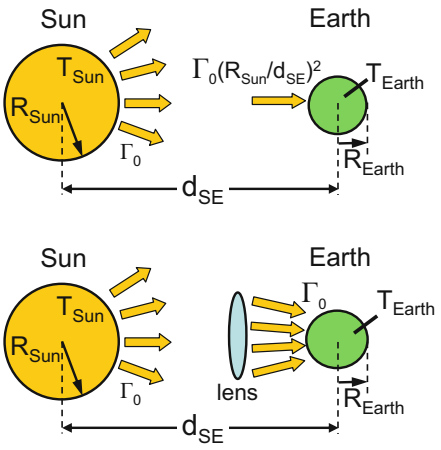

Fig. 3.1 Geometrical configuration of Sun and Earth and solar photon fluxes to Earth without (*top*) and with maximum concentration of sunlight (*bottom*)

energy fluxes at R_{Sun}, which for the photon flux reads $\Gamma_{\gamma,0} = \Gamma_{\gamma}(R_{\mathrm{Sun}})$ (see Fig. 3.1).[1]

3.2 Spectral Distribution of Solar Photons

3.2.1 Thermal Equilibrium Radiation/Planck's Law

To a good approximation, the spectral distribution of solar radiation equals that of a thermal-equilibrium source at $T = T_{\mathrm{Sun}} \approx 6{,}000\,\mathrm{K}$. Here we have neglected the inhomogeneous temperature distribution at the Sun's surface, along with the high-temperature protuberances contributing to the full solar light flow with relatively small surface areas.

To formulate the thermal-equilibrium radiation, we follow a similar approach like that of M. Planck [3], considering as the origin of radiation the photon density in a three-dimensional box with ideally electrically conducting walls and held at temperature T. One novel step taken by Planck was the introduction of discrete modes, and in particular discrete modes of electric field strength. Due to the infinitely conducting walls of the box, the electric field strength vanishes there. Our second input consists of the occupation of these discrete modes in accordance with the Bose–Einstein energy distribution function.[2]

[1] The sunlight arrives at the Earth's position under the solid angle of $\Omega_{\mathrm{Sun}} = \pi(R_{\mathrm{Sun}}/d_{\mathrm{SE}})^2$ and—according to the second law of thermodynamics—might be concentrated only up to the flux per solid angle of the source, known also as conservation of the etendue.

[2] The total energy of thermal radiation using classical electromagnetic theory via the integral $\int_0^{\infty} u_{\omega}(\hbar\omega, T)d(\hbar\omega) \rightarrow \infty$, whereas with the Bose-distribution function equivalently with Planck's approach, the total energy of a thermal radiator gives a finite value (see [4]).

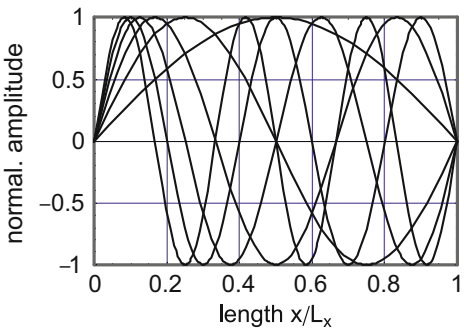

Fig. 3.2 Schematic representation of stationary modes of different wave lengths, e.g., transverse electric field strength, in a box of length L_x with highly conductive walls

Along each of the three Cartesian axes of Planck's box, with lengths L_x, L_y, L_z, the boundary conditions for the transverse electric fields of the electromagnetic wave imply that we get standing waves with wave vectors

$$k_x\,(n_x) = \frac{2\pi}{\lambda_{n_x}} = \frac{2\pi}{2L_x} n_x,$$
$$k_y\,(n_y) = \frac{2\pi}{\lambda_{n_y}} = \frac{2\pi}{2L_y} n_y,$$
$$k_z\,(n_z) = \frac{2\pi}{\lambda_{n_z}} = \frac{2\pi}{2L_z} n_z,$$

where $n_{x,y,z} \in \mathbb{Z}$ (see Fig. 3.2), these being related to the electric field components $E_{n,\text{trans},x} = E_{n,y,z} \sin\left(k_{n_x} x\right)$, $E_{n,\text{trans},y} = E_{n,z,x} \sin\left(k_{n_y} y\right)$, and $E_{n,\text{trans},z} = E_{n,x,y} \sin\left(k_{n_z} z\right)$ in the box.

Superposition of the three independent modes yields the solution for standing waves with independent mode numbers n_x, n_y, and n_z. For standing waves, the change in sign of n_x, n_y, or n_z to $-n_x$, $-n_y$, and $-n_z$ does not alter the solution. In the three-dimensional wave vector space, the resulting wave vector for a particular combination k_x, k_y, k_z gives $k = \sqrt{k_x^2 + k_y^2 + k_z^2}$, and analogously we write $n = \sqrt{n_x^2 + n_y^2 + n_z^2}$ for the resulting mode number. Replacing the k-values for standing waves by $k_i = \pi n_i / L_i$, we finally arrive at

$$k = \sqrt{\left(\frac{\pi}{L_x} n_x\right)^2 + \left(\frac{\pi}{L_y} n_y\right)^2 + \left(\frac{\pi}{L_z} n_z\right)^2}\,.$$

We see from the relation $k_i = \pi n_i / L_i$ that wave vectors k_i and modes n_i are equidistantly distributed along the k_i and n_i axes, respectively.

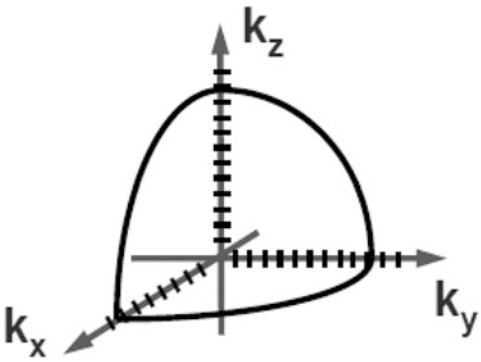

Fig. 3.3 Three-dimensional wave vector space for the visualization of discrete modes of the wave vector $k = \sqrt{k_x^2 + k_y^2 + k_z^2} =$ const. and representation of a section of the $4\pi k^2$ surface

The number of modes in a three-dimensional volume element is $\mathrm{d}N = \mathrm{d}n_x \mathrm{d}n_y \mathrm{d}n_z$ and these have to be summed up (integrated) over the isotropic space (see Fig. 3.3) to yield

$$\mathrm{d}N = \frac{1}{8} \times 4\pi \times 2n^2 \mathrm{d}n \tag{3.1}$$

We only count one octant of the n-space and allow for two directions of polarization, which correspond to each of the two components of the electric field strength oriented transversely with respect to the propagation, e.g., for the x propagation, we consider E_y and E_z.

Since we are interested in the energy distribution of modes rather than the mode distribution, the number of modes dN per mode interval $\mathrm{d}n$ has to be translated via the wave vectors k and $\mathrm{d}k$ into energy $\hbar\omega$ or frequency ω by

$$n = \frac{L}{\pi} k_n = \frac{L}{c\pi} \omega$$

and

$$\mathrm{d}n = \frac{L}{c\pi} \mathrm{d}\omega \ ,$$

respectively, where c and ω are the speed of light, e.g., in vacuum, and the frequency. In this way, for a cubic box with $L_x = L_y = L_z = L$, we arrive at

$$\mathrm{d}N(\omega) = \frac{L^3}{c^3 \pi^2} \omega^2 \mathrm{d}\omega \ . \tag{3.2}$$

A normalization of this number of stationary solutions with respect to volume L^3 and frequency interval $\mathrm{d}\omega$ represents the three-dimensional density of states for these energy quanta, called photons.

The second ingredient of our approach consists of imposing the Bose–Einstein distribution function for the occupation of the density of photon states $\mathrm{d}N(\omega)$. This reads

$$f_{\mathrm{Bose}} = \frac{1}{\exp\left(\dfrac{\hbar\omega - \mu_\gamma}{kT}\right) - 1} , \tag{3.3}$$

where $\hbar\omega$, μ_γ, k, and T are the photon energy of particular modes, chemical potential of the photon field, Boltzmann constant, and temperature. Since the chemical potential of the photon field from a thermal equilibrium radiator at the same temperature T as the environment vanishes ($\mu_\gamma = 0$), the photon density in the box per volume element $\mathrm{d}n_\gamma(\omega) = \mathrm{d}N_\gamma(\omega)/L^3$ is expressed by

$$\mathrm{d}n_\gamma(\omega) = \frac{1}{c^3\pi^2} \frac{\omega^2}{\exp\left(\dfrac{\hbar\omega}{kT}\right) - 1} \mathrm{d}\omega , \tag{3.4}$$

whence the energy density is

$$\begin{aligned} \mathrm{d}u_\epsilon(\omega) = \hbar\omega\, \mathrm{d}n_\gamma &= \frac{\hbar\omega}{c^3\pi^2} \frac{\omega^2}{\exp\left(\dfrac{\hbar\omega}{kT}\right) - 1} \mathrm{d}\omega \\ &= \frac{1}{c^3\pi^2\hbar^3} \frac{(\hbar\omega)^3}{\exp\left(\dfrac{\hbar\omega}{kT}\right) - 1} \mathrm{d}(\hbar\omega) . \end{aligned} \tag{3.5}$$

Figure 3.4 shows the spectral photon densities and spectral energy densities of thermal equilibrium Planck boxes for different temperatures.

The conversion of photon energies into wavelengths is obtained with the help of $\omega = 2\pi c/\lambda$ and $\mathrm{d}\omega = -(2\pi c/\lambda^2)\mathrm{d}\lambda$ for the energy density $\mathrm{d}u_\epsilon(\lambda)$, we obtain the relation

$$\mathrm{d}u_\epsilon(\lambda) = \frac{16\pi^2\hbar c}{\lambda^5} \frac{1}{\exp\left(\dfrac{2\pi\hbar c}{\lambda kT}\right) - 1} (-\mathrm{d}\lambda) . \tag{3.6}$$

Figure 3.5 shows the energy density versus wavelength $\mathrm{d}u_\epsilon(\lambda)$ for different temperatures. The shift of the maximum to lower λ with rising temperature T is known as Wien's law:

$$\lambda(u_\epsilon = \max) = \lambda^* \approx \frac{2\pi\hbar c}{5kT} .$$

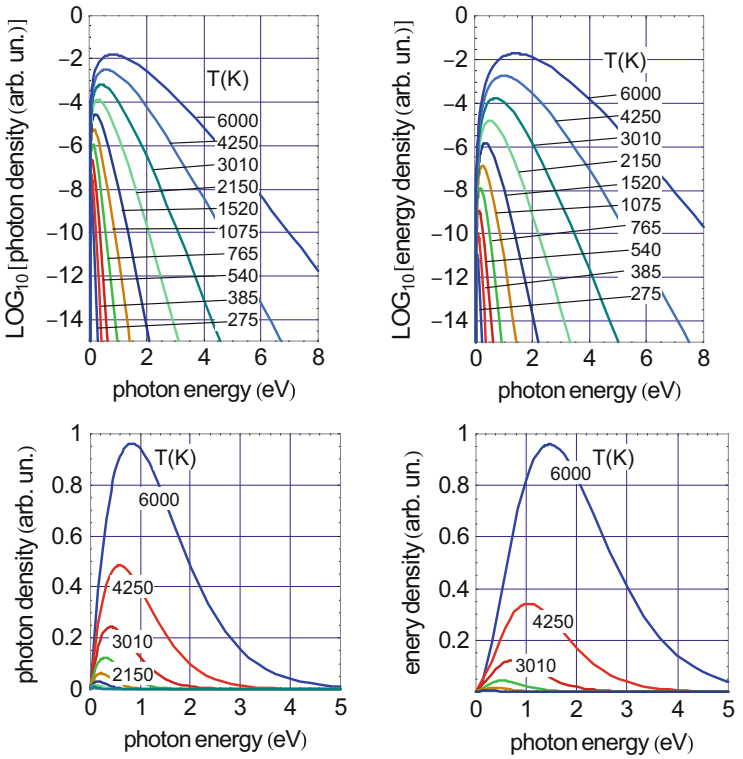

Fig. 3.4 Relative spectral photon densities (*left*) and relative spectral energy densities (*right*) in a thermal equilibrium Planck box for different temperatures (275 K $\leq T \leq$ 6,000 K) in log-linear-plots (*top*) and in linear-linear-plots (*bottom*)

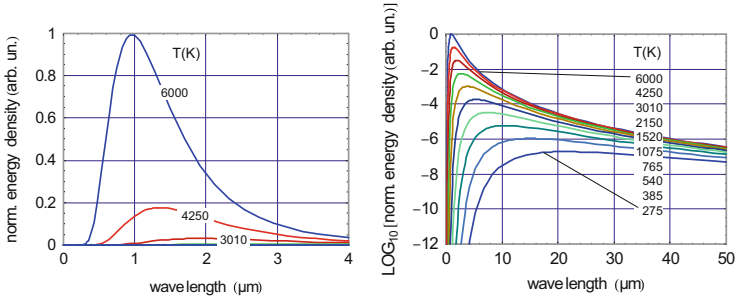

Fig. 3.5 Energy density versus wavelength in a thermal equilibrium Planck box for different temperatures (275 K $\leq T \leq$ 6,000 K)

Another approach based on transition rates of electrons between particular levels within energetic regimes with corresponding densities of state $D_1 = D(\epsilon_1)$ and $D_2 = D(\epsilon_2)$ [5] leads to the same relation for the spectral behavior of photon versus photon energy $\hbar\omega$. The resulting number of energy modes per frequency

interval derived from the photon modes reads equivalently:

$$\mathrm{d}u_\epsilon = \frac{A_{21}}{B}\frac{1}{\exp\left(\dfrac{\hbar\omega}{kT}\right)-1}\mathrm{d}\omega\ , \tag{3.7}$$

which, apart from the prefactor A_{21}/B, whose components originate from the coefficients for transitions between particular upper (2) and lower energy levels (1) [5, 6] for stimulated ($B_{12} = B_{21} = B$) as well as for spontaneous ones (emission) ($2 \rightarrow 1$) with A_{21} [5] equal the frequency dependence in the Planck approach. The prefactor A_{21}/B commonly is derived from the Rayleigh–Jeans law

$$\mathrm{d}u_{\epsilon,\,RJ}(\omega) = \frac{2\omega^2}{\pi c^3}kT\,\mathrm{d}\omega \tag{3.8}$$

by equating $\mathrm{d}u_\epsilon$ for $u_{\epsilon,\mathrm{RJ}}(\omega \rightarrow 0)$:

$$\begin{aligned}\mathrm{d}u_\epsilon(\omega\rightarrow 0) &= \frac{A_{21}}{B}\frac{1}{1+\dfrac{\hbar\omega}{kT}+\dfrac{1}{2!}\left(\dfrac{\hbar\omega}{kT}\right)^2+\cdots-1}\mathrm{d}\omega\\ &\approx \left(\frac{A_{21}}{B}\right)\left(\frac{1}{\hbar\omega/kT}\right)\mathrm{d}\omega,\end{aligned} \tag{3.9}$$

which finally yields

$$\frac{A_{21}}{B} = \frac{2\hbar\omega^3}{\pi c^3} = \frac{2\,(\hbar\omega)^3}{\pi c^3\hbar^2} \tag{3.10}$$

and

$$\mathrm{d}u_\epsilon = \frac{2}{\pi^2c^3\hbar^3}\frac{(\hbar\omega)^3}{\exp\left(\dfrac{\hbar\omega}{kT}\right)-1}\mathrm{d}\,(\hbar\omega)\ . \tag{3.11}$$

3.2.2 *Emission from a Black Body*

The emission of radiation from a source like a black body in thermal equilibrium in which the photons are propagating with homogeneous distribution in the 4π solid angle, can be realized as escape through an aperture with infinitesimally small area $\mathrm{d}A$ (see Fig. 3.6). The entire amount of photons leaving the box per time J_γ (flow of photons to be derived from the spectral particle flux $d\Gamma_\gamma$) is assumed to be so small that it will not affect the photon reservoir. It is also assumed that the photon

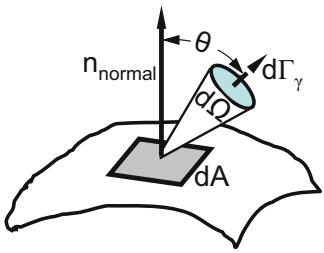

Fig. 3.6 Photon flux $\mathrm{d}\Gamma_\gamma$ through area element $\mathrm{d}A$ into solid angle $\mathrm{d}\Omega$ inclined at angle Θ from normal incidence n_{normal}

flux from the box reflects the spectral composition $\mathrm{d}n_\gamma(\omega)$ of photon modes in the box, which is governed by the temperature (and formally depends on the number of dimensions of the box). Accordingly the emitting aperture is an ideal representation of a black body.

The spectral energy flow $\mathrm{d}J_\epsilon$ through an area element $\mathrm{d}A$ propagating at angle Θ with respect to the normal n_{normal} into the solid angle element $\mathrm{d}\Omega$ with the speed of light in vacuum c_0 is given by

$$\mathrm{d}J_\epsilon = \mathrm{d}u_\epsilon c_0 \frac{\mathrm{d}\Omega}{4\pi} \cos\Theta \, \mathrm{d}A \; . \tag{3.12}$$

The integration of $\mathrm{d}u_\epsilon(\omega)$ over the entire spectral range with upper and lower limits $\omega = 0$ and $\omega \to \infty$, respectively, yields the energy density $u_\epsilon = \int_0^\infty \mathrm{d}u_\epsilon$.

The total energy flow J_ϵ through the aperture $\mathrm{d}A$ thus corresponds to the integral

$$\begin{aligned} J_\epsilon &= u_\epsilon c_0 \frac{\mathrm{d}A}{4\pi} \int_0^{\pi/2} \cos\Theta \sin\Theta \, \mathrm{d}\Theta \\ &= u_\epsilon \frac{c_0}{4\pi} \mathrm{d}A \frac{1}{2} \sin^2(\pi/2) = u_\epsilon \frac{1}{4} c_0 \mathrm{d}A \; , \end{aligned} \tag{3.13}$$

and finally this flow J_ϵ through the aperture $\mathrm{d}A$ is given by

$$J_\epsilon = \mathrm{d}A \frac{1}{4\pi^2 \hbar^3 c_0^2} \int_0^\infty \frac{(\hbar\omega)^3}{\exp(\hbar\omega/kT) - 1} \mathrm{d}(\hbar\omega) \; . \tag{3.14}$$

The upper equation involves a definite integral of type

$$\int \xi^n \frac{1}{\exp(a\xi) - 1} \mathrm{d}\xi \; ,$$

which is analytically solvable (in fact, a Gamma function) and which leads to

$$\frac{J_\epsilon}{\mathrm{d}A} = \Gamma_\epsilon = \frac{\pi^2}{4c_0^2} \frac{k^4}{\hbar^3} \frac{1}{15} T^4 = \sigma_{\mathrm{SB}} T^4 \; , \tag{3.15}$$

where σ_{SB} is the Stefan–Boltzmann constant,[3] with value

$$\sigma_{SB} = 5.667 \times 10^{-8}\,\mathrm{W\,K^{-4}\,m^{-2}}\,.$$

3.3 Radiative Balance Between Sun and Earth

With Planck's law we calculate the total energy flow from the Sun, which illuminates the Earth, and which, assuming steady state, itself emits the very same amount of energy it receives from the source into the surrounding environment. Here, for the radiative balance, we forget about the amount of solar radiation converted into fossil energy, accumulated ago over millions of years and also neglect the contribution of fossil components today released and transformed to oxidized species such as CO_2 or H_2O. We also simplify absorption and subsequent emission of solar radiation by our globe by assuming that Sun and Earth are ideal Planck radiators and absorbers, each exhibiting both absorptivity α and emissivity ε equal to unity irrespective of the energy of the photons, whereupon $\alpha(\omega) = \varepsilon(\omega) = 1$. The energy flow balance is thus

$$\begin{aligned}&\varepsilon_{\mathrm{Sun}}\sigma_{SB}T_{\mathrm{Sun}}^4\Omega_0\alpha_{\mathrm{Earth}}\pi R_{\mathrm{Earth}}^2 + \varepsilon_{\mathrm{Univ}}\sigma_{SB}T_{\mathrm{Univ}}^4\alpha_{\mathrm{Earth}}(4\pi - \Omega_{\mathrm{sun}})R_{\mathrm{Earth}}^2\\ &\quad = \varepsilon_{\mathrm{Earth}}\sigma_{SB}T_{\mathrm{Earth}}^4 4\pi R_{\mathrm{Earth}}^2\,.\end{aligned} \tag{3.16}$$

The contribution of the Universe consists of the 3 K-background radiation and the light of the stars and the Moon, which reaches the Earth in the solid angle $(4\pi - \Omega_{\mathrm{Sun}})$ with $\Omega_0 = (R_{\mathrm{Sun}}/d_{\mathrm{SE}})^2$, where Ω_{Sun} denotes the solid angle under which the Sun appears when observed from the Earth, and Ω_0 may also be regarded as a simple abbreviation for the reduction of the energy flux from $\Gamma_\epsilon(R_{\mathrm{Sun}})$ to $\Gamma_\epsilon(d_{\mathrm{SE}})$

[3] The above deduction of Planck's law for the spectral behavior of thermal equilibrium radiation is based on the density of states of photons, in other words, on the density of three-dimensional modes for stationary solutions of a wave equation resulting in 3D standing waves. Mode numbers and individual wave vectors translate linearly into frequencies and energies of particular photons, and the multiplication of the density of states by the particular photon energy yields the corresponding spectral energy flux. So apart from the Bose term $\left[\exp(\hbar\omega/kT) - 1\right]^{-1}$, the integrand contains the independent variable ω to a power n equal to the number of dimensions, i.e., $(\hbar\omega)^n$. Consequently, the analytically representable solution of the definite integral also contains the number of dimensions, i.e., in the dependence of the total energy flux on temperature $\sim T^{(n+1)}$. Accordingly, σ_{SB} also depends on the number of dimensions [7], and in general reads

$$\sigma_{SB} = 2\pi^{(n-1)/2}\frac{\Gamma_{(n+1)}\zeta_{(n+1)}}{\Gamma_{(n+1)/2}}\frac{k^{n+1}}{(2\pi\hbar)^n c^{n-1}}\,,$$

where Γ and ζ are the Gamma and Riemann zeta functions, respectively.

(see footnote[4]). We solve the above equation with the approximation $\Omega_{\text{Sun}} \ll 4\pi$ and obtain for the steady-state Earth temperature

$$T_{\text{Earth}} \approx \sqrt[4]{\frac{1}{4}\Omega_0 T_{\text{Sun}}^4 + T_{\text{Univ}}^4} \,. \tag{3.17}$$

Due to the low value of the temperature of the background radiation, which enters through a fourth power, and because of the negligible contribution of moonlight and of the input from stars, the above balance implies that the approximate temperature of our globe is

$$T_{\text{Earth}} \approx \sqrt[4]{\frac{1}{4}\Omega_0 T_{\text{Sun}}^4} = 288\,\text{K} \,. \tag{3.18}$$

In this approximation, each of our crude assumptions, such as the constant and ideal absorptivities and emissivities not taking into account the differing values of reflection and absorption of water, land, and ice areas or clouds, lead by lucky coincidence to errors that compensate one another, and we get a reasonable number for the Earth temperature of about 300 K. To conclude, in general terms, we have to describe a system of two temperature reservoirs, namely, a heat source at $T_{\text{Sun}} = 6{,}000\,\text{K}$ and a heat sink at $T_{\text{Earth}} = 300\,\text{K}$ with the transfer of these heats by electromagnetic waves, and unquestionably apply thermodynamic relations to find the behaviour of such configurations.

If we depart from a purely radiative balance in the configuration of one hypothetical hot source (a type of Sun with asterixed properties T_{Sun}^*, etc.) and a single Earth-like absorber/receiver (properties indicated by subscript *rec*) by allowing for a portion of solar radiation to be converted by some procedure of the absorber into chemical energy $\dot{U}$ of components transferred to some kind of storage (see Fig. 3.7 and think of photosynthesis, photobiology, photochemistry, or photovoltaics attached to a battery), the energy flow balance modifies to

$$\begin{aligned} &\varepsilon_{\text{Sun}}\sigma_{\text{SB}}\left(T_{\text{Sun}}^*\right)^4 \Omega_0 \alpha_{\text{rec}} \pi R_{\text{rec}}^2 + \varepsilon_{\text{Univ}}\sigma_{\text{SB}} T_{\text{Univ}}^4 \alpha_{\text{rec}}(4\pi - \Omega_{\text{Sun}}) R_{\text{rec}}^2 \\ &\quad = \varepsilon_{\text{rec}}\sigma_{\text{SB}} T_{\text{rec}}^4 4\pi R_{\text{rec}}^2 + \dot{U} \,. \end{aligned} \tag{3.19}$$

Furthermore we assume once again unit absorptivity and emissivity of source, Universe, and receiver, i.e., $\varepsilon_{\text{Sun}} = \varepsilon_{\text{rec}} = \varepsilon_{\text{Univ}} = \alpha_{\text{rec}} = 1$, $\Omega_{\text{Sun}} \ll 4\pi$, and

[4]The entire flow collected by an ideally absorbing sphere at distance from the Sun d_{SE} is related to the perpendicular projection of the sphere (cross section) and amounts to $\Gamma_\epsilon(d_{\text{SE}})\pi R_{\text{sphere}}^2$ whereas for emission the sphere offers the total surface area of $4\pi R_{\text{sphere}}^2$. Here the maximum solar light concentration would correspond to the illumination of the entire surface of the sphere ($4\pi R_{\text{sphere}}^2$) and vanishing access of the light from the universe.

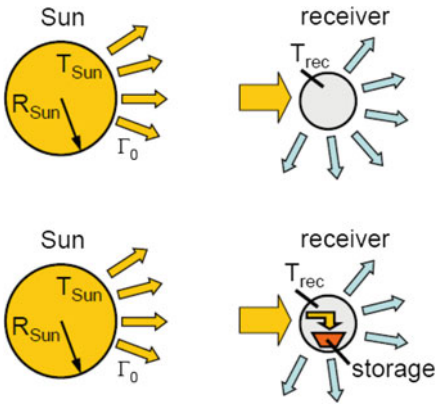

Fig. 3.7 Energy flow balance of Sun and receiver without (*top*) and with conversion of solar energy into chemical energy and subsequent storage (*bottom*)

write the modified steady-state temperature of the receiver, as

$$T_{\mathrm{rec}} \approx \sqrt[4]{\frac{1}{4}\Omega_0 \left(T^*_{\mathrm{Sun}}\right)^4 + T^4_{\mathrm{Univ}} - \frac{\dot{U}}{R^2_{\mathrm{rec}}\sigma_{\mathrm{SB}} 4\pi}} \,. \tag{3.20}$$

We recognize that the receiver temperature T_{rec} decreases when converting a part of the incoming solar energy flow into chemical energy that is put into a reservoir. Equivalently, the receiver temperature rises when energy is released from storage and at least partially converted into heat, an effect which is currently initiated by human beings when using fossil fuels. In essence, the temperature of a receiver depends on what the receiver is doing with the absorbed light.

Assuming further that the performance of the above conversion process depends on the receiver temperature as in a Carnot cycle or similar, the efficiency commonly rises for decreasing T_{rec}, whereupon the part for storage increases as well and T_{rec} decreases even further.

For the use of a Carnot engine to convert a fraction β of the incoming solar energy into chemical energy, the balance of the energy flow of the hypothetic spheric receiver transforms to

$$\begin{aligned} &\varepsilon_{\mathrm{Sun}}\sigma_{\mathrm{SB}} \left(T^*_{\mathrm{Sun}}\right)^4 \Omega_0 \alpha_{\mathrm{rec}} \pi R^2_{\mathrm{rec}} \\ &\quad = \varepsilon_{\mathrm{rec}}\sigma_{\mathrm{SB}} T^4_{\mathrm{rec}} 4\pi R^2_{\mathrm{rec}} + \beta\varepsilon_{\mathrm{Sun}}\sigma_{\mathrm{SB}} \left(T^*_{\mathrm{Sun}}\right)^4 \Omega_0 \alpha_{\mathrm{rec}} R^2_{\mathrm{rec}} \left(1 - \frac{T_{\mathrm{rec}}}{T^*_{\mathrm{Sun}}}\right). \end{aligned} \tag{3.21}$$

After a simple rearrangement and including solar light concentration with factor C, we get the following equation for the receiver temperature T_{rec}:

$$T^4_{\mathrm{rec}} - \beta \frac{C\Omega_0}{4\pi} T_{\mathrm{rec}} \left(T^*_{\mathrm{Sun}}\right)^3 - (1-\beta) \frac{C\Omega_0}{4\pi} \left(T^*_{\mathrm{Sun}}\right)^4 = 0 \,. \tag{3.22}$$

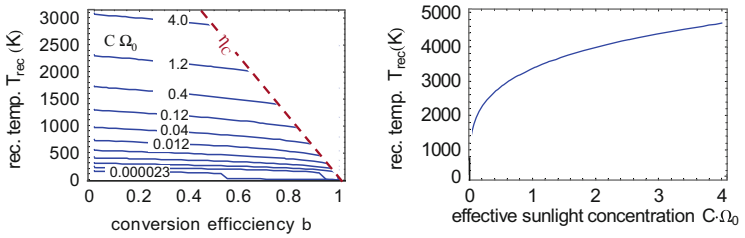

Fig. 3.8 Temperature T_{rec} of a solar-energy receiver (at distance d_{SE} from the Sun) as a function of the fraction β of conversion of the incoming light into chemical energy ($\beta \leq \eta_{\mathrm{C}}$) for different solar light concentration factors C between AM0 and maximum ($1 \leq C \leq C_{max} = 4(\Omega_0)^{-1}$; $\Omega_0 = (R_{\mathrm{Sun}}/d_{\mathrm{SE}})^2$) (*left*), and receiver temperature versus sunlight concentration for conversion with Carnot efficiency ($\eta = \eta_{\mathrm{C}}$) (*right*); for both figures the contribution of the Universe has been neglected

The numerical solution for $T_{\mathrm{rec}} = T_{\mathrm{rec}}(\Omega_0, \beta, C)$ is presented in Fig. 3.8, where the receiver temperature is presented for different light concentration factors C.

Note that any storage of solar radiation or its equivalent release in other bodies (stars, planets, etc.) in our Universe will in principle influence the temperature of any receiver/absorber system in the Galaxy. Although this effect is numerically of little importance, we recognize the coupling of all components of our Universe through exchange of radiation.

3.4 Particular Aspects of Solar Radiation Arriving at the Earth

3.4.1 Solar Energy Flux

At the distance $d_{\mathrm{SE}} = 1.5 \times 10^{11}\,\mathrm{m}$ from the Sun's surface, which corresponds to the average radius of the Earth orbit around the Sun, the energy flux emitted from the surface of the Sun at temperature $T_{\mathrm{Sun}} = 6{,}000\,\mathrm{K}$ is reduced while propagating radially in a homogeneous way in the three-dimensional space and thus is attenuated by the factor $(R_{\mathrm{Sun}}/d_{\mathrm{SE}})^2$ before it enters the Earth's atmosphere.[5] The energy flux at the outer atmosphere $\Gamma_\epsilon(d_{\mathrm{SE}}) = 1.26 \times 10^3\,\mathrm{W\,m^{-2}}$ before it arrives at the Earth's surface is additionally affected by light-matter interaction in the

[5]The flux from the Sun $\Gamma_\epsilon(d_{SE})$ is defined as solar light flux at Air Mass Zero (AM0) since it is not affected by interactions with the Earth atmosphere; corresponding modifications of the spectral distribution of Γ_ϵ, as well as its magnitude by the atmosphere are designed by AM1, AM2 etc. Here Γ_ϵ suffers from absorption, scattering, and reflection by particles of different kinds, like molecules, water clusters, dust, and so on, qualitatively represented by the path length of the light through the atmosphere.

atmosphere (absorption and scattering) and thus it is further reduced; of course the solar flux might be additionally influenced by light concentrating elements (mirrors, lenses) what formally reads in modifying the solid angle $\Omega_0 = (R_{\mathrm{Sun}}/d_{\mathrm{SE}})^2$ by a concentration factor C.

3.4.2 Photon Flux at the Position of the Earth

In order to get the photon flux $\Gamma_\gamma(d_{\mathrm{SE}})$ (number of incident photons per unit area and unit time) at the outer atmosphere of the Earth, we integrate the spectral flux at the Sun's surface and reduce this number by the factor $\Omega_0 = (R_{\mathrm{Sun}}/d_{\mathrm{SE}})^2$, whence

$$\Gamma_\gamma(d_{\mathrm{SE}}) = \frac{1}{4\pi^2}\left(\frac{R_{\mathrm{Sun}}}{d_{\mathrm{SE}}}\right)^2 \int_0^\infty \left(\frac{1}{c_0^2\hbar^3}\right)\left(\frac{1}{\hbar\omega}\right)\frac{(\hbar\omega)^2}{\exp(\hbar\omega/kT_{\mathrm{Sun}})-1}\mathrm{d}(\hbar\omega)\ , \tag{3.23}$$

and finally,

$$\begin{aligned}\Gamma_\gamma(d_{\mathrm{SE}}) &= \frac{1}{4\pi^2}\left(\frac{R_{\mathrm{Sun}}}{d_{\mathrm{SE}}}\right)^2\left(\frac{1}{c_0^2\hbar^3}\right)\left(2k^3T_{\mathrm{Sun}}^3\zeta[3]\right)\\ &= 7.05\times10^{17}\ \mathrm{cm^{-2}\,s^{-1}}\ .\end{aligned} \tag{3.24}$$

3.4.3 Optical Concentration of Solar Light

As it propagates from its spherical origin in three dimensions, the solar energy flux is reduced by a factor equal to the square of its distance from the Sun,[6] so that we have $\Gamma_\epsilon(d) = \Gamma_\epsilon(R_{\mathrm{Sun}})\,(R_{\mathrm{Sun}}/d)^2$. This reduction might be reversed—in a gedanken experiment—by passive optical elements, assumed to exhibit ideal properties, like mirrors (with reflection factor of unity and zero temperature) or lenses with ideal transmission and no reflection). For the concentration of sunlight[7] we distinguish two options.

The first one, usually applied for the determination of the theoretical limit of solar light conversion, where the solar light receiver/absorber is illuminated under a

[6] We have to recognize that the solar light even at the large distance from the sun $d_{\mathrm{SE}} = 1.5\times10^{11}$ m might not be treated as a plane wave and accordingly concentration is limited by conservation of the photon flux per solid angle (etendue).

[7] Instead of balancing the light flows like that of the solar light with its respective concentration reaching the absorber and the light flow emitted by the absorber commonly solid angles, Ω_{in} for the entrance and Ω_{out} for the exit are used, which implicitly contain the factor of sunlight concentration.

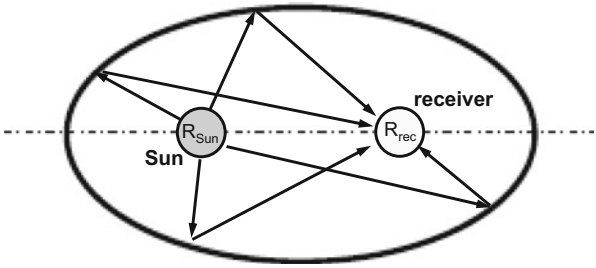

Fig. 3.9 Representation of photon exchange by beam optics of source S and receiver R for maximum light concentration with an ideal ellipsoidal mirror

solid angle Ω_{in} ranging from $\Omega_0 \leq \Omega_{\text{in}} \leq \Omega_{\text{out}} = 4\pi$ which means the receiver for emission sees the entire solid angle in the three-dimensional space.

A schematic representation of this approach with maximum concentration consists of an ideal mirror of shape of a rotational ellipsoid (see Fig. 3.9). The source (the Sun) is located at one of the focal points, while the receiver is located at the second focal point. Thus every photon of the source emitting isotropically into the 4π solid angle is reflected towards the receiver and arrives there.[8] For identical radii of source and receiver ($R_{\text{Sun}} = R_{\text{rec}}$) arguments regarding the reversibility of optical paths show that the originally emitted light flux from the source surface will be exactly equal to that incident on the receiver surface, leading to a concentration factor $C = C_{\max} = (d_{\text{SE}}/R_{\text{Sun}})^2$. This maximum is in agreement with thermodynamic arguments: a higher flux density at the receiver by $R_{\text{rec}} < R_{\text{Sun}}$—in the flow of photons and of the energy balance of the receiver, which in steady state requires input equals output—would be accompanied by a receiver temperature higher than that of the source, in contradiction to the second law of thermodynamics!

In the picture provided by ray optics, a receiver radius $R_{\text{rec}} < R_{\text{Sun}}$ implies a smaller receiver area to get a higher local energy flux $\Gamma_\epsilon(R < R_{\text{rec}}) > \Gamma_\epsilon(R_{\text{Sun}})$. But wave optics does not agree! It should be remembered that ray or beam optics is an approximation that can only be applied if interference effects and superposition of wave amplitudes can be neglected. And since any of the spherical sources of the radiating system (the Sun) emit waves that only interfere constructively at the same radius of the receiver as the source radius, for smaller receiver radii, the image of the Sun is not exactly focused on the receiver. This means that the squared amplitudes of the photon field in the vicinity of the receiver, and in particular at $R_{\text{rec}} < R_{\text{Sun}}$, do not exceed those at R_{Sun}.

A similar conflict seems to emerge when concentrating solar light with an 'ideal' lens system (see Fig. 3.10). Here, even for a lens diameter approaching infinity, one only would collect photons from the solid angle 2π and transfers them to the receiver solid angle, again equal to 2π (optical imaging with curved planes). Of course, the object (the Sun) can be projected onto a smaller image, but this will

[8] This approach is valid provided the spatial extension of source and receiver are small compared to their distance.

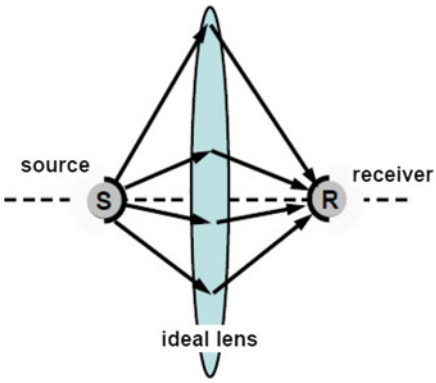

Fig. 3.10 Schematic photon exchange between source (Sun) and receiver for light concentration with an ideal lens

definitely not increase the flux of photons or of energy of the image beyond that of the source.

The second option for the balance of photon flows in and out of an absorber with consideration of sunlight concentration accounts for the particular configuration of flat absorbers, such as solar thermal or photovoltaic panels. For the projection of photons from a spherical source onto a plane[9] the solid angle of the input light ranges from $\Omega_{\text{in}} = \Omega_0$ (no concentration) up to $\Omega_{\text{in,max}} = \pi$ (maximum concentration), whereas the 'effective' solid angle for the absorber's emission into the half hemisphere amounts to $\Omega_{\text{out}} = \pi$. The value $\Omega_{\text{in,max}}$ can be easily derived from the balance of the entire photon flow through the aperture of an optical concentrator, e.g., an ideally assumed lens. For maximum sunlight concentration (see Fig. 3.11) the photons from the Sun, $J_{\gamma,\text{Sun}}$, emitted by the area dA_{S} arrive at the receiver area dA_{r} ($J_{\gamma,\text{Sun}} = J_{\gamma,\text{r}}$) with the identical flux $\Gamma_{\gamma,\text{r}} = J_{\gamma,\text{r}}/dA_{\text{r}}$ like that at the emitting Sun surface $\Gamma_{\gamma,\text{Sun}} = J_{\gamma,\text{Sun}}/dA_{\text{S}}$.[10] The respective flows from the sun and to the receiver read

$$J_{\gamma,\text{Sun}} = \Gamma_{\gamma,\text{Sun}} \int_{\theta_{\text{S}}=0}^{\Theta_{\text{Sun}}} 2\pi \cos\theta_{\text{S}} \sin\theta_{\text{S}} d\theta_{\text{S}} dA_{\text{S}} \tag{3.25}$$

and

$$J_{\gamma,\text{r}} = \Gamma_{\gamma,\text{r}} \int_{\theta_{\text{r}}=0}^{\Theta_{\text{r}}} 2\pi \cos\theta_{\text{S}} \sin\theta_{\text{r}} d\theta_{\text{r}} dA_{\text{r}}. \tag{3.26}$$

[9]This configuration is commonly realized with solar thermal absorbers and with photovoltaic cells and modules, which both are exposed only by one side to the solar insolation on comparatively small areas for which the photons are assumed to propagate parallel and of which the area for light reception equals that for light emission.

[10]The upper limit is again given by thermodynamics, whereas we should not trust ray optics which erroneously would allow for even higher light fluxes of the image than that of the source.

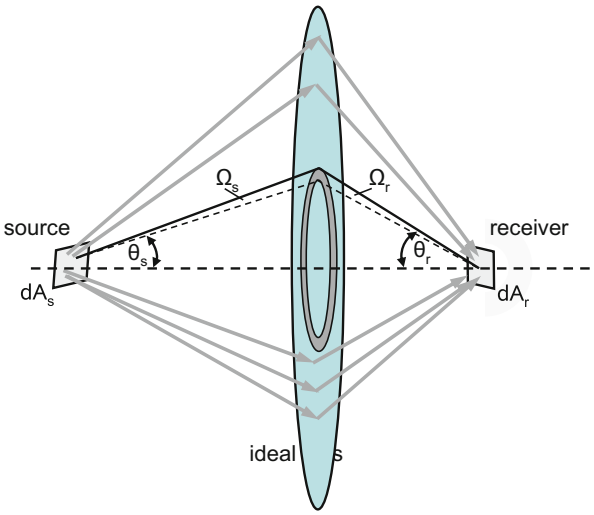

Fig. 3.11 Solar photons fed to a flat receiver with concentration of light from the Sun (source) by an ideal lens

The upper limit of the angle $\theta = \Theta_{\text{Sun}} = \Omega_{\text{Sun}} = \pi\Omega_0$ represents the solid angle under which a terrestrial observer sees the Sun. Of course, due to the optical configuration $dA_{\text{S}} \neq dA_{\text{r}}$. We replace

$$\int_{\text{a}}^{b} \cos\theta \sin\theta d\theta = \int_{\text{a}}^{b} \sin\theta d \sin\theta = \left[(1/2)(\sin\theta)^2\right]_{\text{a}}^{\text{b}}$$

and demand the identity of the fluxes $\Gamma_{\gamma,\text{Sun}} = \Gamma_{\gamma,\text{r}}$ which means the optical image of the Sun at the receiver appears as bright as the Sun's surface (maximum sunlight concentration). Finally we get

$$C_{\max} = \frac{\pi}{\Omega_{\text{Sun}}}(\sin\Theta_{\text{Sun,max}})^2 = \frac{\pi}{\Omega_{\text{Sun}}}(\sin\Theta_{\text{r,max}})^2,$$

with $(\sin\Theta_{\text{r,max}})^2 = 1$, or $\Theta_{\text{r,max}} = (\pi/2)$ equivalently.[11]

3.4.4 Average Energy of Solar Photons

The mean energy of solar photons emitted from the surface of the Sun is related to its surface temperature $T_{\text{Sun}} \approx 6{,}000\,\text{K}$, which corresponds to

$$kT_{\text{Sun}} = 1.38 \times 10^{-23}\,\text{Joule/K} \times 6{,}000\,\text{K} = 8.28 \times 10^{-20}\,\text{Joule} = 0.52\,\text{eV}\ .$$

[11] In real systems the angle $\Theta_{\text{r,max}} = (\pi/2)$ for the collection of photons arriving from the entire hemisphere to which the receiver is exposed to can hardly be realized.

During propagation of these photons in vacuum to the Earth we do not consider any change in spectral distribution, since interaction with matter is excluded and photon–photon interactions in the photon energy range considered do not occur,[12] so the average photon energy ϵ_{phot} is derived as the total solar energy flux divided by the total photon flux:

$$\bar{\epsilon}_{\mathrm{phot}} = \frac{\int_0^\infty \frac{1}{c_0^2 4\pi^2\hbar^3} \frac{(\hbar\omega)^3}{\exp(\hbar\omega/kT_{\mathrm{Sun}})-1} \mathrm{d}\,(\hbar\omega)}{\int_0^\infty \frac{1}{c_0^2 4\pi^2\hbar^3} \frac{(\hbar\omega)^2}{\exp(\hbar\omega/kT_{\mathrm{Sun}})-1} \mathrm{d}\,(\hbar\omega)} \approx 1.405\,\mathrm{eV}. \tag{3.27}$$

3.4.5 *Fraction of Solar Photons Above a Specific Optical Threshold Energy*

For the absorption by matter with a specific optical threshold energy ϵ_{g} above which photon-matter interactions are allowed, we are interested in the fraction of solar photons being absorbed and plot the corresponding ratio of photon fluxes:

$$\xi\left(\epsilon_{\mathrm{g}}\right) = \frac{\int_{\epsilon_{\mathrm{g}}}^\infty \frac{1}{c_0^2 4\pi^2\hbar^3} \frac{(\hbar\omega)^2}{\exp(\hbar\omega/kT_{\mathrm{Sun}})-1} \mathrm{d}\,(\hbar\omega)}{\int_0^\infty \frac{1}{c_0^2 4\pi^2\hbar^3} \frac{(\hbar\omega)^2}{\exp(\hbar\omega/kT_{\mathrm{Sun}})-1} \mathrm{d}(\hbar\omega)} \tag{3.28}$$

Figure 3.12 shows the fraction of solar photons with energies $\hbar\omega$ larger than the optical threshold energy ϵ_{g} for absorption (e.g., the band gap of a semiconductor).

3.4.6 *Momentum Transfer of Solar Photons to Absorbers*

In the course of the interaction of photons with matter by absorption or emission, momentum and spins are also conserved. Accordingly, absorption and reflection of photons induces a transfer of momenta from the photons to the absorbing or reflecting media. (Here, due to the small contribution, we may neglect the conservation of spins.) We accumulate the individual momenta of each of the solar photons, which means integrating the transfer of photon momenta ($\hbar\omega/c_0$) to an ideally absorbing medium (threshold energy ϵ_{g}) per unit area and time interval to

[12] Here we neglect the influence of the spectral shift of solar photons when leaving the gravitational field of the Sun or entering that of the Earth. The curious reader may be inspired to estimate the influence of the gravitational fields of the Sun and the Earth.

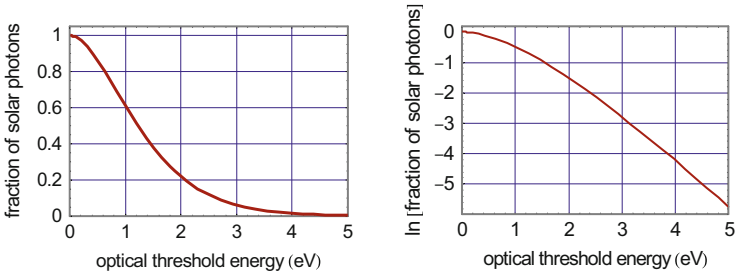

Fig. 3.12 Fraction of solar photons versus optical threshold energy for absorption (optical band gap of a semiconductor) in linear (*left*) and logarithmic representation (*right*)

get the 'pressure' $p_{\mathrm{Sun,\,abs}}(d)$ that solar photons produce at distance d from the Sun:

$$p_{\mathrm{Sun,\,abs}}(d) = \left(\frac{R_{\mathrm{Sun}}}{d}\right)^2 \int_{\epsilon_{\mathrm{g}}}^{\infty} \frac{(h\omega)^2}{c_0^2 4\pi^2\hbar^3} \left(\frac{\hbar\omega}{c_0}\right) \left(\frac{1}{\exp(\hbar\omega/kT_{\mathrm{Sun}}) - 1}\right) \mathrm{d}(\hbar\omega) \,, \tag{3.29}$$

and with exemplarily chosen $\epsilon_{\mathrm{g}} = 0$, with the definite integral of the form

$$\int_0^{\infty} \zeta^n \frac{1}{\exp(\zeta/a) - 1} \mathrm{d}\zeta$$

and the appropriate Gamma function, we obtain

$$p_{\mathrm{Sun,\,abs}}(d) = \left(\frac{R_{\mathrm{Sun}}}{d}\right)^2 \frac{1}{c_0^3} \frac{6}{90} \pi^4 \frac{(kT_{\mathrm{Sun}})^4}{\hbar^3 (2\pi)^2} \,. \tag{3.30}$$

Setting $d = d_{\mathrm{SE}}$ and $T_{\mathrm{Sun}} = 6{,}000\,\mathrm{K}$, gives

$$p_{\mathrm{Sun,\,abs}} = 5.3 \times 10^{-12}\,\mathrm{VAs\,cm^{-3}} = 5.3 \times 10^{-10}\,\mathrm{N\,cm^{-2}} \,. \tag{3.31}$$

For ideally reflecting matter, the momentum transfer doubles and the solar photon pressure becomes

$$p_{\mathrm{Sun,\,refl}} = 2\,p_{\mathrm{Sun,\,abs}} = 1.06 \times 10^{-9}\,\mathrm{N\,cm^{-2}} \,. \tag{3.32}$$

Moreover, the emission of photons from an absorber, e.g., such of thermal radiation, of course, also effects a momentum, that pushes the emitting body in the opposite direction of the photons.

3.4.7 How an Earth-Based Observer Sees the Sun

For an Earth-based observer, the Sun covers a solid angle

$$\Omega_{\mathrm{Sun}} = \pi\,(R_{\mathrm{Sun}})^2\,\frac{1}{(d_{\mathrm{SE}})^2} = 6.7\times 10^{-5}\ .$$

An arbitrarily selected area element $\mathrm{d}A_{\mathrm{S}} = \mathrm{d}\xi\,\mathrm{d}s$ of the Sun's surface (see Fig. 3.13) emits a photon flow $\mathrm{d}J_{\gamma,\Omega} = \Gamma_\gamma \mathrm{d}\xi\mathrm{d}s\mathrm{d}\Omega$ towards a terrestrial observer. Writing $\mathrm{d}s = R_{\mathrm{Sun}}\mathrm{d}\theta$, we obtain the emission $\mathrm{d}J_{\gamma,\Omega}$ in the direction of the Earth, say in the direction of the radius vector from the center, whereupon the flux is modified by a term in the cosine of the angle θ :

$$\mathrm{d}J_{\gamma,\Omega} = \Gamma_\gamma \mathrm{d}\Omega\,\mathrm{d}\xi\cos\theta\,\mathrm{d}s\ . \tag{3.33}$$

Introducing $\rho = R_{\mathrm{Sun}}\sin\theta$ and $\mathrm{d}\rho/\mathrm{d}\theta = R_{\mathrm{Sun}}\cos\theta$, which converts into

$$\mathrm{d}\theta = \frac{1}{R_{\mathrm{Sun}}}\frac{1}{\cos\theta}\mathrm{d}\rho\ ,$$

we arrive at

$$\begin{aligned}\mathrm{d}J_{\gamma,\Omega} &\sim R_{\mathrm{Sun}}\mathrm{d}\Omega\mathrm{d}\xi\cos\theta\,\mathrm{d}\theta \\ &= R_{\mathrm{Sun}}\mathrm{d}\Omega\frac{1}{R_{\mathrm{Sun}}}\cos\theta\frac{1}{\cos\theta}\mathrm{d}\xi\mathrm{d}\rho \sim \mathrm{d}\xi\,\mathrm{d}\rho\ ,\end{aligned} \tag{3.34}$$

which shows that the emission of an area element towards the Earth does not depend on its position ρ and θ.

In a similar approach we may equivalently regard a circular area element $\mathrm{d}A_{\mathrm{S}}$ of the disc-shaped configuration with radius ρ and width $\mathrm{d}s$:

$$\mathrm{d}A_{\mathrm{S}} = 2\pi\rho\mathrm{d}s = 2\pi R_{\mathrm{Sun}}\sin\theta\,\mathrm{d}s\ . \tag{3.35}$$

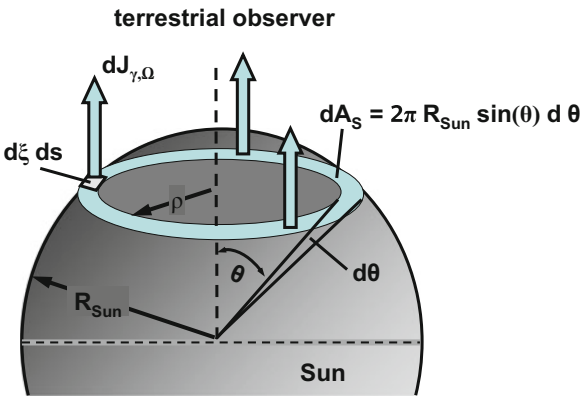

Fig. 3.13 Emission from a spherical source like the Sun towards a terrestrial observer

Introducing $\mathrm{d}s = R_{\mathrm{Sun}}\mathrm{d}\theta$, one arrives at

$$\mathrm{d}A_{\mathrm{S}} = 2\pi\rho\mathrm{d}s = 2\pi R_{\mathrm{Sun}}^2 \sin\theta\,\mathrm{d}\theta\ . \tag{3.36}$$

The emitted entire flow $\mathrm{d}J^*_{\gamma,\mathrm{S}}$ from this circular area element $\mathrm{d}A_{\mathrm{S}}$, into the solid angle $\mathrm{d}\Omega$ yields

$$\mathrm{d}J^*_{\gamma,\mathrm{S}} = \Gamma_\gamma \mathrm{d}A_{\mathrm{S}} \cos\theta\,\mathrm{d}\Omega \tag{3.37}$$

and

$$\mathrm{d}J_{\gamma,\mathrm{S}} = \Gamma_\gamma 2\pi R_{\mathrm{Sun}}^2 \mathrm{d}\Omega \sin\theta\cos\theta\,\mathrm{d}\theta\ . \tag{3.38}$$

Then observing that $\cos\theta\,\mathrm{d}\theta = \mathrm{d}(\sin\theta)$, we get by integration

$$\begin{aligned} J_{\gamma,\Omega} &= \int_0^{\pi/2} \Gamma_\gamma 2\pi R_{\mathrm{Sun}}^2 \mathrm{d}\Omega \sin\theta\,\mathrm{d}(\sin\theta) \\ &= \left[\Gamma_\gamma 2\pi R_{\mathrm{Sun}}^2 \mathrm{d}\Omega \frac{1}{2}(\sin\theta)^2\right]_0^{\pi/2} \\ &= \Gamma_\gamma \pi R_{\mathrm{Sun}}^2 \mathrm{d}\Omega\ , \end{aligned} \tag{3.39}$$

which is identical to the emission of a homogeneously emitting circular disc recorded perpendicularly.

3.4.8 Entropy Flux of Solar Radiation

The energy flux Γ_ϵ of the Sun is related to the fourth power of the surface temperature, viz., $\Gamma_\epsilon = \sigma_{\mathrm{SB}}\varepsilon_{\mathrm{Sun}}T_{\mathrm{Sun}}^4$. By thermodynamic arguments, this energy flux is accompanied by a corresponding entropy flux $\Gamma_{\mathrm{S,Sun}}(T_{\mathrm{Sun}})$, which reduces the free energy of the photons and thus dependent on the temperature of the absorber may also drop the efficiency of their conversion [8]. To determine the corresponding entropy flux the relevant fundamental relation of thermodynamics are applied, i.e., the first law, which relates the change in internal energy $\mathrm{d}U$ with the heat $\delta Q = T\mathrm{d}S$ fed into the system, the work extracted from the system (e.g., mechanical work, formulated in terms of pressure and volume change) $\delta W = p\mathrm{d}V$, and the species $\mathrm{d}N_i$ (here, the photons) with appropriate chemical potential μ_i, also fed into the system:

$$\mathrm{d}U = T\mathrm{d}S - p\mathrm{d}V + \sum \mu_i \mathrm{d}N_i\ . \tag{3.40}$$

Since the internal energy $U = U(S, V, N_i)$ also reads

$$\mathrm{d}U = \left(\frac{\partial U}{\partial S}\right)_{V,N_i} \mathrm{d}S + \left(\frac{\partial U}{\partial V}\right)_{S,N_i} \mathrm{d}V + \sum \left(\frac{\partial U}{\partial N_i}\right)_{S,V} \mathrm{d}N_i \ , \tag{3.41}$$

we deduce the identities

$$\left(\frac{\partial U}{\partial S}\right)_{V,N_i} = T \ , \quad \left(\frac{\partial U}{\partial V}\right)_{S,N_i} = -p \ , \quad \left(\frac{\partial U}{\partial N_i}\right)_{S,V} = \mu_i \ .$$

We imagine a package of photons with energy $\mathrm{d}U$ in a hypothetical volume, travelling with the speed of light in vacuum in a certain direction. Due to the absence of photon–photon interactions, there is no change in spectral distribution, and in fact $\mathrm{d}N_i = 0$. For large distances from the Sun's surface, $d \gg R_{\mathrm{Sun}}$, we also assume the photon flux to be a plane wave, and due to the absence of spatial dispersion (the speed in vacuum is identical for every photon energy/wavelength), no change will thus occur in the hypothetical volume. We assume the component to proceed with the partial derivative

$$\left(\frac{\partial U}{\partial S}\right)_{V,N_i} = T \ ,$$

then substitute in

$$\left(\frac{\partial U}{\partial S}\right)_{V,N_i} = \left(\frac{\partial U}{\partial T}\right)_{V,N_i} \left(\frac{\partial T}{\partial S}\right)_{V,N_i} = T \ ,$$

and introduce $U = \sigma_{\mathrm{SB}} \varepsilon T^4$ to obtain

$$\sigma_{\mathrm{SB}} \varepsilon 4T^3 \left(\frac{\partial T}{\partial S}\right)_{V,N_i} = T \ , \tag{3.42}$$

or

$$\sigma_{\mathrm{SB}} \varepsilon 4T^2 \mathrm{d}T = \mathrm{d}S \ . \tag{3.43}$$

Note that the transition from the internal energy U and the entropy S in a non-moving system to fluxes Γ_ϵ and Γ_S, such as those attributed to photons propagating with the speed of light, neglects—eventually erroneously—the influence of photon wave vectors for the entire balance of energy and momentum [9].

The last equation solves by integration for the entropy S travelling with the speed of light, as well as a byproduct of the energy flux Γ_ϵ emitted from a thermal equilibrium source at temperature T :

$$\Gamma_{\mathrm{S}} = \sigma_{\mathrm{SB}} \varepsilon \frac{4}{3} T^3 + \Gamma_{\mathrm{S},0}, \tag{3.44}$$

with vanishing integration constant since

$$\Gamma_{\mathrm{S},0} = \Gamma_{\mathrm{S}}(T \to 0)) = 0. \tag{3.45}$$

As a further consequence, the measure of the convertible part of the internal energy U is given by the flux of free energy Γ_F, once again traveling with the speed of light, which reads

$$\Gamma_{\mathrm{F}} = \Gamma_{\epsilon} - T\Gamma_{\mathrm{S}} \; .$$

For small distances from a spherical light source $R_{\mathrm{Sun}} \leq d \ll d_{\mathrm{SE}}$, the photon flux into a constant solid angle remarkably decreases, and conversely the hypothetical volume enveloping the photon package rises by a factor of $(d/R_{\mathrm{Sun}})^2$, which in turn for an ideal quantum gas, further increases the entropy flux due to the rise in the number of accessible micro states. This gives another contribution to the reduction of the free energy of solar photons.

3.4.9 Chemical Potential of Light

The chemical potential of light (μ_γ) defines the "quality" of radiation of a light source referenced to a thermal-equilibrium environment with appropriate thermal-equilibrium radiation. Moreover this magnitude μ_γ allows for the formulation of the work that these photons are able to initiate in the ideal case when interacting with matter [10]. By receiving the energy of photons of this type of radiation, electrons and phonons (lattice vibrations) are transferred to a non-thermal equilibrium state, from which they return after a particular time period to their respective ground state either by emitting photons and/or creating phonons which lead to heating of the matter. Here, we are only interested in the light-induced excitation of electrons since the direct excitation of phonons by light (optical modes) is related to photon energies of few tens of meV which are in the neighborhood of kT_{Earth} and thus far below the level worthwhile for photovoltaics, photochemical, or photobiological processes. Under stationary exposure to that light source the excited electrons in the receiver are departed from thermal equilibrium and their excited state may be used for producing work in terms of electrical energy.

Of course, the chemical potential of radiation of a thermal-equilibrium source at T_{rad} is zero for a receiver at the very same temperature $T_{\mathrm{rec}} = T_{\mathrm{rad}}$, exactly like the efficiency of a Carnot engine operated between heat reservoirs with identical temperatures. For this particular case of a thermal-equilibrium photon ensemble in a box, the fundamental relation of thermodynamics, i.e., the first law, reads $\mathrm{d}U = T\mathrm{d}S - p\mathrm{d}V + \sum \mu_i \mathrm{d}N_i = 0$ in the steady state, with T, S, p, V, μ_i, and N_i designating temperature, entropy, pressure, volume, chemical potential of a specific component, and number for that component, respectively. The magnitudes to be 'exchanged' for $\mathrm{d}U = 0$ are entropy (which provides for thermal equilibrium and

governs temperature), volume (which allows for pressure), and particle exchange (which enables chemical equilibrium). Due to photon absorption and emission at the 'black' walls of the radiator, $\mathrm{d}N_i \neq 0$. In order to satisfy $\sum \mu_i \mathrm{d}N_i = 0$, one must therefore have $\mu_i = 0$.

For general determination of the properties of a particular photoexcited state, each of the rates of change of the relevant quantities has to be formulated, which means knowing each of the rates of occupation of specific energy levels as a function of all the relevant levels. This ansatz leads to a system of coupled differential equations that turns out to be extremely complicated and can generally only be solved numerically.

However, a simple approach exists when light source and matter are in the steady state and the matter exhibits electronic levels or bands whose occupation is no longer in thermal equilibrium but substantially perturbed by the influence of the light source with the particular behavior of the species in the excited states to establish comparably fast a maximum entropy distribution (say, a temperature distribution) due to fast intraband relaxation (see Sect. 4.2.2).

The exemplary electronic band system consists of two energetic regimes of a semiconductor with valence (VB) and conduction band (CB) separated by an energy gap $(\epsilon_\mathrm{C} - \epsilon_\mathrm{V}) = \epsilon_\mathrm{g}$ and corresponding densities of state $D_\mathrm{VB}(\epsilon)$, $D_\mathrm{CB}(\epsilon)$. Analogously we could also think of a molecular system with comparatively larger separation of individual energy levels and a separation between highest occupied (HOMO) and lowest unoccupied molecular level (LUMO) called $\epsilon_\mathrm{LUMO} - \epsilon_\mathrm{HOMO}$ that equivalently to the band gap ϵ_g acts as a threshold energy for absorption and emission of photons in the absorber.

Our system, here the semiconductor (see Fig. 3.14), is kept at a particular temperature T by a strong coupling to a heat reservoir. We assume furthermore that it is exposed to photons generating the internal photon density n_γ, which initiates transitions from VB to CB by absorption. The corresponding "back reaction" of the system is assumed to consist ideally only of radiative transitions from CB to VB which are spontaneous and stimulated emission of photons resulting again in a photon flow caused by the photon density n_γ.[13] For steady-state conditions, the occupation of the levels $D_\mathrm{VB}(\epsilon)$ of VB and $D_\mathrm{CB}(\epsilon)$ of CB is stationary and the entire transition rates balance out accordingly:

$$r_\mathrm{abs} = r_\mathrm{em,\,spont} + r_\mathrm{em,\,stim}\ . \tag{3.46}$$

These rates of the transitions depend amongst optical matrix elements (M_CV, M_VC) and photon density on the occupation of initial and final states, which we

[13] Although the photon density absorbed and providing for the excitation of the electron system (flow in) with respect to spectral distribution and entire density might differ from the spectral photon density emitted (flow out) the emission is determined by the excitation state regardless by which spectral distribution this has been achieved as far as the balance of the rates is met. From this point of view we are allowed to also assume the photon density for absorption to equal that of emission.

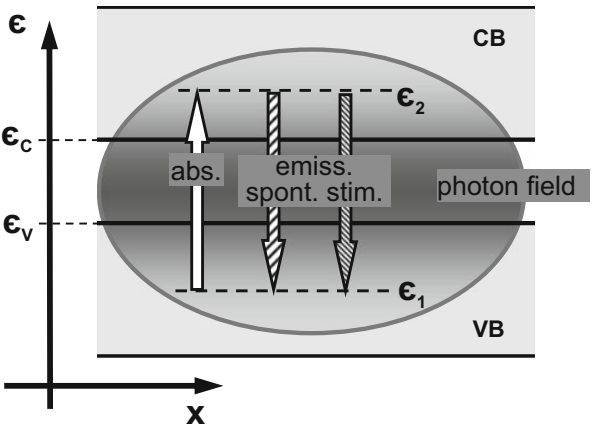

Fig. 3.14 Electronic band system with conduction (*CB*) and valence band (*VB*) and transitions representing absorption, spontaneous and stimulated emission of photons; the respective density of states in CB and VB are $D_{\mathrm{CB}}(\epsilon)$ and $D_{\mathrm{VB}}(\epsilon)$

compose of the respective density of states $D(\epsilon)$ and distribution functions, e.g., for electrons $f(\epsilon)$. Furthermore due to the optical transitions with negligible wave vector changes the initial and final states are energetically separated by the energy $\hbar\omega$ of absorbed or emitted photons,[14] $\epsilon_2 = \epsilon_1 + \hbar\omega$. We introduce the density of states occupied and unoccupied by electrons in the valence band by the distribution function $f(\epsilon)$ and $(1 - f(\epsilon))$ and equivalently in the conduction band as well by $f(\epsilon + \hbar\omega)$ and $(1 - f(\epsilon + \hbar\omega))$ and accordingly we may write the transition rates:

$$r_{\mathrm{abs}} = n_\gamma \int_0^\infty D_{\mathrm{VB}}(\epsilon) f(\epsilon) D_{\mathrm{CB}}(\epsilon)(1 - f(\epsilon + \hbar\omega)) M_{\mathrm{VC}}(\epsilon, \hbar\omega) d\epsilon \tag{3.47}$$

$$r_{\mathrm{em,spont}} = D_\gamma \int_0^\infty D_{\mathrm{CB}}(\epsilon) f(\epsilon + \hbar\omega) D_{\mathrm{VB}}(\epsilon)(1 - f(\epsilon)) M_{\mathrm{CV}}(\epsilon, \hbar\omega) d\epsilon, \tag{3.48}$$

and

$$r_{\mathrm{em,stim}} = n_\gamma \int_0^\infty D_{\mathrm{CB}}(\epsilon) f(\epsilon + \hbar\omega) D_{\mathrm{VB}}(\epsilon)(1 - f(\epsilon)) M_{\mathrm{CV}}(\epsilon, \hbar\omega) d\epsilon, \tag{3.49}$$

where D_γ designates the photon density of states ($D_\gamma = (n^2(\hbar\omega)^2)/(\pi^2\hbar^3c^3)$), with refractive index n, photon energy $\hbar\omega$, and speed of light c.

The assumption that the system is kept at a specific temperature T implies that the electron behavior is to be described by Fermi statistics,[15] which here means

[14] These two states in CB and VB are arbitrarily chosen; in thermal equilibrium—and analogously assumed under excitation—the individual rates for transitions of absorption and spontaneous and stimulated emission, regardless their respective photon energy, also compensate each other.

[15] Due to strong electron-electron interaction and because of efficient electron-phonon coupling within energy bands the electrons after excitation by light undergo a very fast relaxation ($(10^{-13}$–

the density of excited states of electrons in the conduction band and of unoccupied states in the valence band (called holes) can be formulated by quasi-Fermi energies ϵ_{Fn} and ϵ_{Fp} respectively:

$$f(\epsilon + \hbar\omega) = \frac{1}{exp(\frac{\epsilon + \hbar\omega - \epsilon_{\mathrm{Fn}}}{kT}) + 1}, \tag{3.50}$$

$$(1 - f(\epsilon)) = \frac{1}{exp(\frac{-\epsilon + \epsilon_{\mathrm{Fp}}}{kT}) + 1}. \tag{3.51}$$

The functions $(1 - f(\epsilon + \hbar\omega))$ and $f(\epsilon)$ are derived by conservation of states and accordingly we get:

$$\begin{aligned}(1 - f(\epsilon + \hbar\omega)) &= 1 - \frac{1}{exp(\frac{\epsilon + \hbar\omega - \epsilon_{\mathrm{Fn}}}{kT}) + 1} \\ &= \frac{exp(\frac{\epsilon + \hbar\omega - \epsilon_{\mathrm{Fn}}}{kT})}{exp(\frac{\epsilon + \hbar\omega - \epsilon_{\mathrm{Fn}}}{kT}) + 1},\end{aligned} \tag{3.52}$$

and

$$\begin{aligned}f(\epsilon) &= 1 - \frac{1}{exp(\frac{-\epsilon + \epsilon_{\mathrm{Fp}}}{kT}) + 1} \\ &= \frac{exp(\frac{-\epsilon + \epsilon_{\mathrm{Fp}}}{kT})}{exp(\frac{-\epsilon + \epsilon_{\mathrm{Fp}}}{kT}) + 1}.\end{aligned} \tag{3.53}$$

The explicit rate equations above can be converted with respect to the photon density n_γ and read

$$\begin{aligned}n_\gamma &= D_\gamma \frac{\int_0^\infty D_{\mathrm{CB}}(\epsilon) D_{\mathrm{VB}}(\epsilon) M_{\mathrm{CV}}(\epsilon, \hbar\omega) \left[f(\epsilon + \hbar\omega)(1 - f(\epsilon)) \right] d\epsilon}{\Xi} \\ &= \frac{\Theta}{\Xi}\end{aligned} \tag{3.54}$$

10^{-12}) s) and occupy a distribution of maximum entropy which allows for the introduction of the magnitude temperature.

with the abbreviation for the denominator

$$\begin{aligned}\Xi &= \int_0^\infty D_{\mathrm{VB}}(\epsilon) f(\epsilon) D_{\mathrm{CB}}(\epsilon)(1 - f(\epsilon + \hbar\omega)) M_{\mathrm{VC}}(\epsilon, \hbar\omega) d\epsilon \\ &\quad - \int_0^\infty D_{\mathrm{CB}}(\epsilon) f(\epsilon + \hbar\omega) D_{\mathrm{VB}}(\epsilon)(1 - f(\epsilon)) M_{\mathrm{CV}}(\epsilon, \hbar\omega) d\epsilon \\ &= \int_0^\infty D_{\mathrm{VB}}(\epsilon) D_{\mathrm{CB}}(\epsilon) M_{\mathrm{CV}}(\epsilon, \hbar\omega) \\ &\quad \times [f(\epsilon)(1 - f(\epsilon + \hbar\omega)) - f(\epsilon + \hbar\omega)(1 - f(\epsilon))]\, d\epsilon \\ &= \int_0^\infty D_{\mathrm{VB}}(\epsilon) D_{\mathrm{CB}}(\epsilon) M_{\mathrm{CV}}(\epsilon, \hbar\omega)\, (f(\epsilon + \hbar\omega)(1 - f(\epsilon))) \\ &\quad \times \left[\frac{f(\epsilon)(1 - f(\epsilon + \hbar\omega))}{f(\epsilon + \hbar\omega)(1 - f(\epsilon))} - 1 \right] d\epsilon. \end{aligned} \tag{3.55}$$

Except for the term in rectangular brackets in the denominator, numerator Θ and denominator Ξ are identical, and a closer inspection of the bracket term yields

$$\begin{aligned}&\frac{f(\epsilon)(1 - f(\epsilon + \hbar\omega)}{f(\epsilon + \hbar\omega)(1 - f(\epsilon)} - 1 \\ &\quad = \frac{\left(\dfrac{exp(\dfrac{-\epsilon + \epsilon_{\mathrm{Fp}}}{kT})}{exp(\dfrac{-\epsilon + \epsilon_{\mathrm{Fp}}}{kT}) + 1} \right) \left(\dfrac{\dfrac{\epsilon + \hbar\omega - \epsilon_{\mathrm{Fn}}}{exp(\dfrac{\epsilon + \hbar\omega - \epsilon_{\mathrm{Fn}}}{kT})}}{\dfrac{\epsilon + \hbar\omega - \epsilon_{\mathrm{Fn}}}{exp(\dfrac{\epsilon + \hbar\omega - \epsilon_{\mathrm{Fn}}}{kT})+1}} \right)}{\left(\dfrac{\dfrac{1}{\epsilon + \hbar\omega - \epsilon_{\mathrm{Fn}}}}{exp(\dfrac{\epsilon + \hbar\omega - \epsilon_{\mathrm{Fn}}}{kT})+1} \right) \left(\dfrac{\dfrac{1}{-\epsilon + \epsilon_{\mathrm{Fp}}}}{exp(\dfrac{-\epsilon + \epsilon_{\mathrm{Fp}}}{kT})+1} \right)} - 1 \\ &\quad = exp\left(\frac{-\epsilon + \epsilon_{\mathrm{Fp}} + \epsilon + \hbar\omega - \epsilon_{\mathrm{Fn}}}{kT} \right) - 1 \\ &\quad = \left(\frac{\hbar\omega - (\epsilon_{\mathrm{Fn}} - \epsilon_{\mathrm{Fp}})}{kT} \right) - 1), \end{aligned} \tag{3.56}$$

and we recognize this term to be independent of the variable ϵ, so we can substantially simplify the integral expression for n_γ

$$n_\gamma = D_\gamma \frac{\int_0^\infty D_{\mathrm{CB}}(\epsilon) D_{\mathrm{VB}}(\epsilon) M_{\mathrm{CV}}(\epsilon, \hbar\omega)\, [f(\epsilon + \hbar\omega)(1 - f(\epsilon))]\, d\epsilon}{\int_0^\infty D_{\mathrm{CB}}(\epsilon) D_{\mathrm{VB}}(\epsilon) M_{\mathrm{CV}}(\epsilon, \hbar\omega)\, [f(\epsilon + \hbar\omega)(1 - f(\epsilon))] \left(exp\left(\frac{\hbar\omega - (\epsilon_{\mathrm{Fn}} - \epsilon_{\mathrm{Fp}})}{kT} \right) - 1 \right) d\epsilon}, \tag{3.57}$$

and finally arrive at the photon density of the photoexcited semiconductor system in terms of the chemical potential $(\epsilon_{\mathrm{Fn}} - \epsilon_{\mathrm{Fp}})$

$$n_\gamma = D_\gamma \frac{1}{\left(exp\left(\frac{\hbar\omega - (\epsilon_{\mathrm{Fn}} - \epsilon_{\mathrm{Fp}})}{kT} \right) - 1 \right)}. \tag{3.58}$$

For steady state the electron system (fermions) and the photons (bosons) coupled by the rate equations for absorption and emission are in chemical equilibrium and thus their respective chemical potentials are equal

$$(\epsilon_{\mathrm{Fn}} - \epsilon_{\mathrm{Fp}}) = \mu_{\mathrm{np}} = \mu_\gamma. \tag{3.59}$$

By this approach [10] the potential of light (μ_γ)—regardless its spectral distribution—with respect to the light-exposed matter at temperature T can be determined and accordingly μ_γ represents the upper limit of the amount of the energy of photons that can be converted into chemical energy of electrons μ_{np}. This ability to perform work, i.e., via an ideal (fully reversible) process, of course, is governed by the temperature T of the solid state probing the light. In contrast with an incorrect intuition, even thermal-equilibrium radiation such as that from the Sun, emitted at $T_{\mathrm{Sun}} = 6{,}000\,\mathrm{K}$ exhibits a particular non-vanishing chemical potential for an Earth-based receiver at $T_{\mathrm{Earth}} = 300\,\mathrm{K}$.

3.4.10 Kirchhoff's Law for Non-ideal Black Bodies

Kirchhoff's law for non-ideal black bodies (G.R. Kirchhoff, 1859, see [11]) combines the features of absorption and emission of spectrally selective bodies by the interchange of radiative fluxes, as shown schematically in Fig. 3.15. A plate of solid matter with properties indexed by 1 (reflection r_1, absorption a_1, and transmission t_1) is located opposite another plate of solid matter with ideal black-body behavior and properties indexed by 2 (absorption $a_2 = 1$, emissivity $\varepsilon_2 = 1$). The two plates have been inside a box with walls at temperature T_0 for a very long

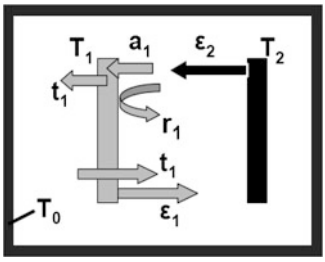

Fig. 3.15 Exchange of radiation between a black-body absorber/receiver (properties indexed by 2) and a 'grey' body (indexed by 1) with absorptivity, emissivity, and transmission $0 < a_1 < 1$, $0 < \varepsilon_1 < 1$, and $0 < t_1 < 1$, respectively

time, in order to ensure steady-state and thermal-equilibrium conditions. The walls of this box also exhibit ideal black-body behavior.

The light flux arriving at plate 1 from plate 2 is partially reflected r_1, partially absorbed a_1, and partially transmitted t_1, so that energy flux conservation reads

$$r_1 + a_1 + t_1 = 1 \, . \tag{3.60}$$

On the other hand, plate 2 also emits, reflects, and absorbs fluxes, and the balance between plate 1 and plate 2 reads

$$\sigma_{\mathrm{SB}} T_2^4 r_1 + \sigma_{\mathrm{SB}} T_1^4 \varepsilon_1 + \sigma_{\mathrm{SB}} T_0^4 \varepsilon_0 t_1 = \sigma_{\mathrm{SB}} T_2^4 \varepsilon_2 \, . \tag{3.61}$$

Thermal equilibrium implies that $T_0 = T_1 = T_2$, and furthermore, as a consequence of the ideal black-body behavior, $\varepsilon_0 = \varepsilon_2 = a_2 = 1$, so

$$r_1 + \varepsilon_1 + t_1 = 1 \, . \tag{3.62}$$

For any photon energy the combination of Eqs. (3.60) and (3.62) yields

$$\varepsilon_1(\omega) = a_1(\omega) \, . \tag{3.63}$$

A violation of this relation would immediately lead to a contradiction with the second law, since a piece of matter exhibiting $\varepsilon_1(\omega) \neq a_1(\omega)$ in a stationary radiative balance with another (reference) body would either heat up more than the reference $\varepsilon_1(\omega) < a_1(\omega)$ or achieve a lower temperature than the reference $\varepsilon_1(\omega) > a_1(\omega)$.

3.4.11 Spectrally Selective Radiators and Absorbers

Real solids always show spectrally selective behavior since they are composed of electrons and ions, both of which provide access for the electric field component of photons to periodically displace these charges from their equilibrium positions. In the simplest ansatz of the one-electron picture, the displacement of a charge is formulated by an oscillator with a resonance frequency ω_0, a force driving the charge back to the equilibrium position dependent on the displacement, and a damping term. This ansatz leads to the well known frequency dependence of the amplitude and the phase of the oscillator (remember the harmonic oscillator), representing here the dependence of the optical properties of the given material on the frequency of the photons (the frequency is easily translated into the wavelength of photons).

With spectrally selective behavior, the input (absorption) of radiation in a specific frequency range can be adjusted very efficiently to where the emission of the Sun is strong (see Fig. 3.16), e.g., for photon energies $\hbar\omega \geq 0.5\,\mathrm{eV}$. The unavoidable emission of the receiver due to its substantially lower temperature

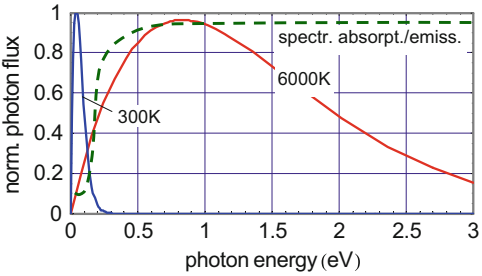

Fig. 3.16 Normalized spectral energy fluxes of a hot (6,000 K) and a cold (300 K) black-body radiator, shown to visualize the option of spectral selectivity

(in the neighborhood of 300 K for an Earth-based receiver) might be minimized by low spectral emissivity/absorption in the low-photon-energy regime ($0 \leq \hbar\omega \leq 0.5\,\mathrm{eV}$).

The approach of tailoring the spectral absorption/emissivity becomes more effective the less spectral overlap exists between the regime of the incoming light to be collected and the emitted output radiation.

References

1. S.M. Chitre, in *Lectures in Solar Physics*, ed. by H.M. Atia, A. Bhatnagar, P. Ulmschneider. Lecture Notes in Physics (Springer, Berlin, 2003)
2. M. Iqbal, *An Introduction to Solar Radiation* (Academic, Toronto, 1983)
3. M. Planck, Ann. Phys. **309**, 564 (1901)
4. D. Kondepudi, I. Prigogine, *Modern Thermodynamics* (Wiley, Chichester, 1998)
5. H. Haken, H.C. Wolf, *Physics of Atoms and Quanta* (Springer, Berlin, 1994)
6. A. Einstein, Verhandl. Deutsch. Phys. Gesellsch. **18**, 318 (1916)
7. A. deVos, *Endoreversible Thermodynamics of Solar Energy Conversion* (Oxford University Press, Oxford, 1992)
8. P.T. Landsberg, J. Appl. Phys. **54**, 2841 (1983)
9. T. Markvart, G.H. Bauer, Appl. Phys. Lett. **101**, 193901 (2012)
10. P. Würfel, J. Phys. C Solid State Phys. **15**, 3967 (1982)
11. E. Hecht, *Optics* (Addison & Wesley, San Francisco, 2002)

Chapter 4
Theoretical Limits for Solar Light Conversion

The conversion of light into different types of energy is based upon the interaction of electromagnetic radiation with matter. The matter might be represented by atoms, molecules, small clusters, liquids, or solids, such as metals, semiconductors, or dielectrics, and the radiation may be formulated in the wave approach with Maxwell's equations. The light-matter interaction also may be expressed in the particle picture with Hamiltonians for each of the relevant species and by the appropriate vector potential for the radiation.

In the particular case of a thermal-equilibrium light source, the Sun, and a receiver on the Earth, thermodynamic principles are applied to express the relevant processes quantitatively, especially for steady-state conditions.

In the first part of this chapter, a general approach is chosen to determine the limits, subdividing the problem as follows:

- Transport of photons from the Sun and their interaction with matter on Earth to achieve a state departing substantially from the Earth's equilibrium temperature which is assumed to be constant and not depending on what is done with the incoming solar radiation in terms of conversion into chemical energy and its storage.
- Transformation of this state by an ideal engine into usable mechanical, electrical, or chemical work. By this approach, we can determine the uppermost limit for terrestrial solar energy harvesting, of which the maximum theoretical efficiency is achieved under highest possible solar light concentration.

In the second part we examine particular details of electronic systems and their excitation by solar light. Here we exploit the insights gained in the first part concerning transport of photons, concentration of sunlight, and spectral splitting,[1] and the possibilities offered by spectrally dependent emissivity and absorption.

[1] Spectral splitting means the subdivision of the solar spectrum into different parts and their subsequent individual conversion.

G.H. Bauer, *Photovoltaic Solar Energy Conversion*, Lecture Notes in Physics 901,
DOI 10.1007/978-3-662-46684-1_4

The analytical description of the performance of solar light collection and its conversion into electrical energy is performed for steady-state conditions with a 'stable' temperature T_{Earth} as that of a heat reservoir at the low-temperature side.

4.1 Endoreversible Thermodynamics

In the approach referred to as endoreversible thermodynamics[2] [1], heat currents from high- and low-temperature reservoirs are supplied in a non-reversible way, i.e., irreversibly, to a reversibly working thermodynamic engine. Figure 4.1 shows a schematic representation of heat reservoirs with high and low temperatures T_{H} and T_{C}, heats $\dot{Q}_{\mathrm{H}}(T_{\mathrm{H}})$ and $\dot{Q}_{\mathrm{C}}(T_{\mathrm{C}})$ supplied in a non-reversible way to the engine, e.g., a Carnot engine (CE), of which the output is work $\dot{W}$. Of course, the efficiency of this setup is the Carnot efficiency η_{C}, expressed in terms of the temperatures T_{l}, T_{m} of the intermediate levels $\eta = \eta_{\mathrm{C}} = 1 - T_{\mathrm{m}}/T_{\mathrm{l}}$. However, for our problem, we wish to know the efficiency as a function of the outer temperatures T_{H} and T_{C}, and the transport terms a_1 and a_2, which govern the heat $\dot{Q}_{\mathrm{i,j}} = a_{\mathrm{i,j}}(T_{\mathrm{i}}^{\mathrm{n}} - T_{\mathrm{j}}^{\mathrm{n}})$ transmitted through the medium. Put simply, for $n = 1$, we describe heat conduction through a medium with thermal conduction a and temperature difference $\delta T = T_{\mathrm{i}} - T_{\mathrm{j}}$, or we formulate a general heat which originates from a source as thermal equilibrium radiation by $\dot{Q}_{\mathrm{rad,ij}} = a_{\mathrm{i,j}}(T_{\mathrm{i}}^4 - T_{\mathrm{j}}^4)$.

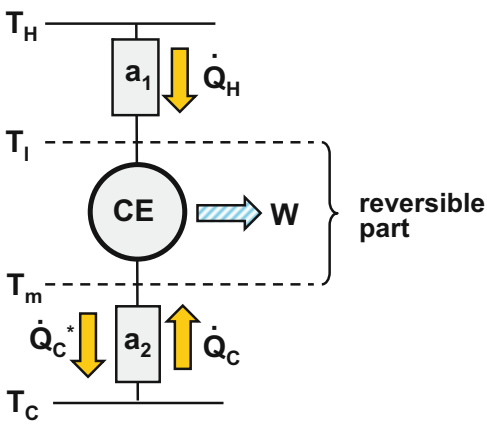

Fig. 4.1 Schematic design of a Curzon–Ahlborn engine with reversible part in the center and irreversible supply of heats for the Carnot engine (CE) through heat conducting media (heat conductor a_1, a_2) from/to the external reservoirs with temperatures T_{H} and T_{C}

[2]The Greek prefix 'endo' means 'internal', so the idea here is that the internal process is reversible.

4.1.1 Curzon–Ahlborn Approach

For didactic reasons, since this approach allows for an analytic solution of the overall efficiency, the heat transport term $\dot{Q}_{\mathrm{i,j}} = a_{\mathrm{i,j}}(T_{\mathrm{i}}^{1} - T_{\mathrm{j}}^{1})$ is chosen and we thus describe thermal conduction of the respective heats[3] supplied to the Carnot engine (see Fig. 4.1) [2, 3]. We have

$$\dot{Q}_{\mathrm{H}} = a_1(T_{\mathrm{H}} - T_{\mathrm{l}}) \,, \tag{4.1}$$

$$-\dot{Q}_{\mathrm{C}} = \dot{Q}_{\mathrm{C}}^{*} = a_2(T_{\mathrm{m}} - T_{\mathrm{C}}) \,, \tag{4.2}$$

and with

$$\eta_{\mathrm{C}} = \eta = 1 - \frac{T_{\mathrm{m}}}{T_{\mathrm{l}}} \,, \tag{4.3}$$

we get

$$T_{\mathrm{m}} = T_{\mathrm{l}}(1 - \eta)$$

or analogously

$$T_{\mathrm{l}} = T_{\mathrm{m}} \frac{1}{1 - \eta} \,.$$

From Clausius's relation for the internal reversible import of heats ($\dot{Q}_{\mathrm{i}}$) to the Carnot engine, viz.,

$$0 = \sum \frac{\dot{Q}_{\mathrm{i}}}{T_{\mathrm{i}}} = \frac{\dot{Q}_{\mathrm{H}}}{T_{\mathrm{l}}} + \frac{\dot{Q}_{\mathrm{C}}}{T_{\mathrm{m}}} = \frac{\dot{Q}_{\mathrm{H}}}{T_{\mathrm{l}}} - \frac{\dot{Q}_{\mathrm{C}}^{*}}{T_{\mathrm{m}}} \,,$$

we rewrite the products of the heats and corresponding temperatures, viz.,

$$\dot{Q}_{\mathrm{H}} T_{\mathrm{m}} = \dot{Q}_{\mathrm{C}}^{*} T_{\mathrm{l}} = -\dot{Q}_{\mathrm{C}} T_{\mathrm{l}} = a_1(T_{\mathrm{H}} - T_{\mathrm{l}}) T_{\mathrm{m}} = a_2(T_{\mathrm{m}} - T_{\mathrm{C}}) T_{\mathrm{l}} \,, \tag{4.4}$$

which can be converted into equations of the form $T_{\mathrm{l}} = T_{\mathrm{l}}(T_{\mathrm{H}}, T_{\mathrm{C}}, a_1, a_2)$ and $T_{\mathrm{m}} = T_{\mathrm{m}}(T_{\mathrm{H}}, T_{\mathrm{C}}, a_1, a_2)$ as functions of the 'outer' temperatures and depending on the transport terms, using

$$a_1(T_{\mathrm{H}} - T_{\mathrm{l}}) T_{\mathrm{l}}(1 - \eta) = a_2\big[T_{\mathrm{l}}(1 - \eta) - T_{\mathrm{C}}\big] T_{\mathrm{l}} \tag{4.5}$$

[3] Heats and work are regarded as flowing magnitudes infinitesimally slowly fed to or extracted from the system, in order to allow for the application of thermal-equilibrium relations.

and

$$a_1\left(T_\mathrm{H}-T_\mathrm{m}\frac{1}{1-\eta}\right)T_\mathrm{m}=a_2(T_\mathrm{m}-T_\mathrm{C})T_\mathrm{m}\frac{1}{1-\eta}\,, \tag{4.6}$$

to obtain

$$T_\mathrm{l}=\frac{a_1}{a_1+a_2}T_\mathrm{H}+\frac{a_2}{a_1+a_2}\frac{1}{1-\eta}T_\mathrm{C} \tag{4.7}$$

and

$$T_\mathrm{m}=\frac{a_1}{a_1+a_2}(1-\eta)T_\mathrm{H}+\frac{a_2}{a_1+a_2}T_\mathrm{C}\,. \tag{4.8}$$

With these expressions, we use $\dot{Q}_\mathrm{H}=a_1(T_\mathrm{H}-T_\mathrm{l})$ and $\dot{W}=\eta\dot{Q}_\mathrm{H}$ to derive the relations

$$\dot{Q}_\mathrm{H}=a_1T_\mathrm{H}-a_1\frac{a_1}{a_1+a_2}T_\mathrm{H}-\frac{a_1a_2}{a_1+a_2}\frac{1}{1-\eta}T_\mathrm{C}=\frac{a_1a_2}{a_1+a_2}\frac{1}{1-\eta}\big[T_\mathrm{H}(1-\eta)-T_\mathrm{C}\big] \tag{4.9}$$

and

$$\dot{Q}_\mathrm{H}=a^*\frac{1}{1-\eta}\big[T_\mathrm{H}(1-\eta)-T_\mathrm{C}\big]\,, \tag{4.10}$$

for the heat, together with

$$\dot{W}=\left(\frac{a_1a_2}{a_1+a_2}\right)\frac{\eta}{1-\eta}\big[T_\mathrm{H}(1-\eta)-T_\mathrm{C}\big]=a^*\frac{\eta}{1-\eta}\big[T_\mathrm{H}(1-\eta)-T_\mathrm{C}\big]\,, \tag{4.11}$$

for the output work.

The efficiency η, which is, of course, still the Carnot efficiency $\eta=1-T_\mathrm{C}/T_\mathrm{H}$, is expressed as a function of the outer temperatures and the transport terms through $a^*=a_1a_2/(a_1+a_2)$, together with the amount of heat $\dot{Q}_\mathrm{H}$ from the high-temperature reservoir:

$$\eta=\frac{a^*T_\mathrm{H}-\dot{Q}_\mathrm{H}-a^*T_\mathrm{C}}{a^*T_\mathrm{H}-\dot{Q}_\mathrm{H}}=1-a^*\frac{T_\mathrm{C}}{a^*T_\mathrm{H}-\dot{Q}_\mathrm{H}}=1-\frac{T_\mathrm{C}}{T_\mathrm{H}-\dot{Q}_\mathrm{H}/a^*}\,. \tag{4.12}$$

This Curzon–Ahlborn efficiency resembles the Carnot efficiency except that the denominator contains $\dot{Q}_\mathrm{H}$ and the transport term a^*. For infinite heat conduction ($a^*\to\infty$) and/or vanishing heat ($\dot{Q}_\mathrm{H}\to 0$), we get the Carnot efficiency

$$\eta_\mathrm{C}=\eta=1-\frac{T_\mathrm{C}}{T_\mathrm{H}}=1-\frac{T_\mathrm{m}}{T_\mathrm{l}}\,.$$

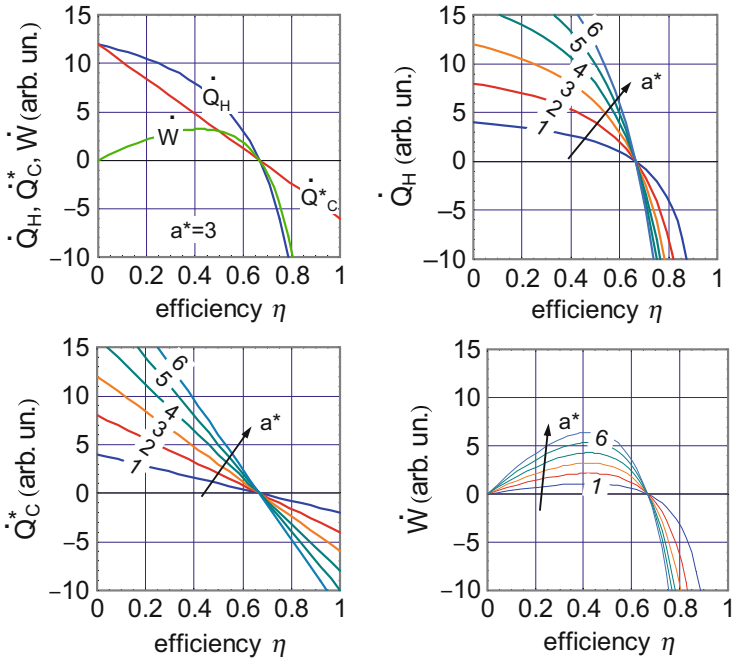

Fig. 4.2 Characteristic magnitudes of the heats $\dot{Q}_H$ and $\dot{Q}^*_C$ and work $\dot{W}$ in arbitrary units for a Curzon–Ahlborn engine as a function of efficiency η and heats and output work (*upper left*) for different transport terms a_1, a_2, $a^* = a_1 a_2/(a_1 + a_2)$; temperatures chosen for these plots $T_H = 3T_C$

The regime $0 \leq \eta \leq \eta_C$ represents the operation as a heat engine, whereas $\eta_C \leq \eta \leq 1$ with $\dot{Q}_H \leq 0$ and $\dot{W} \leq 0$ designate the operation of the device as a heat pump and cooler, respectively (see Fig. 4.2). For approaching internal temperatures $T_l \to T_m$ the Carnot efficiency vanishes and the entire setup acts as simple heat conductor ($\dot{Q}_H = \dot{Q}^*_C = a^*(T_H - T_C)$).

For the extreme situation of $T_C \to 0$, the Carnot efficiency approaches unity $\eta_C \to 1$ and the heat $\dot{Q}_H$ fed to the engine at T_H only depends on the transport term a^*. Since $\dot{Q}_C = a^*(1-\eta)T_H - a^* T_C$ is linear in η and for this particular case $\eta = \eta_C = 1$, the output work $\dot{W}$ and the heat $\dot{Q}_C$ at the low-temperature side superimpose linearly on $\dot{Q}_H$. The situation of $\eta = 1$ can only be prepared with infinite transport term $a^* \to \infty$ or with $\dot{Q}_H \to 0$. For the first option ($a^* \to \infty$), using the Clausius relation for an ideal Carnot cycle $\dot{Q}_H/T_H = \dot{Q}^*_C/T_C$ and $\dot{Q}_C/\dot{Q}_H = T^*_C/T_H$, and for $T_H > 0$ and as $T_C \to 0$, we find $\dot{Q}_H \neq \dot{Q}_H(\eta) =$ constant, and moreover we deduce $\dot{Q}_C \to 0$ neither heat pumping nor cooling can be achieved (see Fig. 4.3)

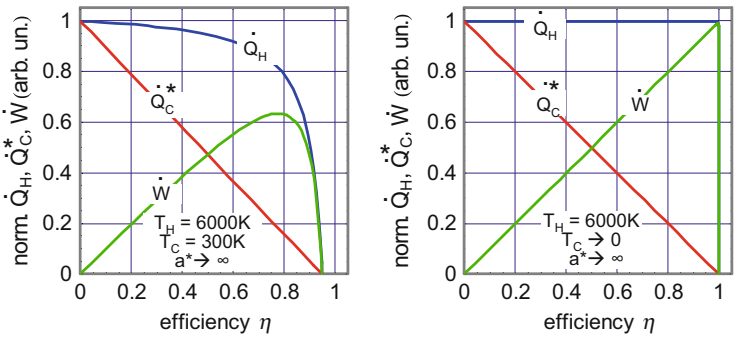

Fig. 4.3 Normalized heats $\dot{Q}_H$, $\dot{Q}_C^*$, and output work $\dot{W}$ of a Curzon–Ahlborn engine for $a^* \to \infty$ and $T_C = 300\,K$ *(left)* resp. $T_C \to 0$ *(right)* versus efficiency η; in both cases $T_H = 6{,}000\,K$

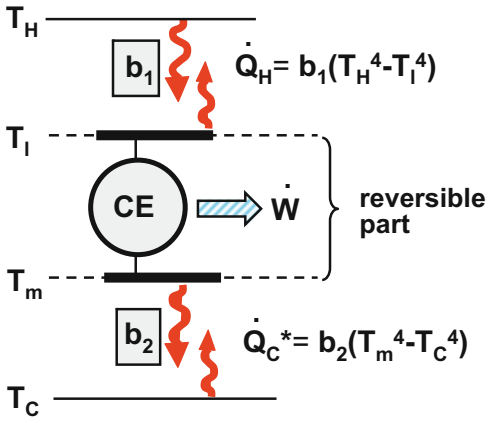

Fig. 4.4 Schematic design of a Boltzmann engine obtained by replacing the exponent unity in the temperature dependence of the transport terms of a Curzon–Ahlborn engine by four, which represents the Stefan–Boltzmann dependence

4.1.2 Stefan–Boltzmann Approach

The Boltzmann engine (as it is called by deVos [3]) looks similar to the Curzon–Ahlborn device, except that the transport terms differ with regard to the exponents of the relevant temperatures. Indeed, instead of the exponent unity in the relation $\dot{Q}_{i,j} = a_{i,j}(T_i^1 - T_j^1)$, which is valid for regular heat conduction, we write the equivalent for Planck's radiation law with $\dot{Q}_{i,j} = b_{i,j}(T_i^4 - T_j^4)$. Figure 4.4 shows the schematic setup for this type of device.

The appropriate set of equations for $\dot{Q}_H$, $\dot{Q}_C$, T_l, and T_m then reads

$$\dot{Q}_H = b_1(T_H^4 - T_l^4)\,, \tag{4.13}$$

$$-\dot{Q}_C = \dot{Q}_C^* = b_2(T_m^4 - T_C^4)\,, \tag{4.14}$$

and we use once again

$$\eta_{\mathrm{C}} = \eta = 1 - \frac{T_{\mathrm{m}}}{T_{\mathrm{l}}}$$

to get the internal temperatures

$$T_{\mathrm{m}} = T_{\mathrm{l}}(1-\eta)\,, \quad T_{\mathrm{l}} = T_{\mathrm{m}}\frac{1}{1-\eta}\,,$$

together with

$$\dot{Q}_{\mathrm{H}} T_{\mathrm{m}} = \dot{Q}_{\mathrm{C}}^{*} T_{\mathrm{l}} = -\dot{Q}_{\mathrm{C}} T_{\mathrm{l}} = b_1(T_{\mathrm{H}}^4 - T_{\mathrm{l}}^4)T_{\mathrm{m}} = b_2(T_{\mathrm{m}}^4 - T_{\mathrm{C}}^4)T_{\mathrm{l}}\,, \tag{4.15}$$

finally yielding

$$T_{\mathrm{l}} = \frac{b_1 T_{\mathrm{H}}^4}{b_1 + b_2(1-\eta)^3} + \frac{b_2 T_{\mathrm{C}}}{b_1(1-\eta) + b_2(1-\eta)^4} \tag{4.16}$$

and

$$T_{\mathrm{m}} = \frac{b_1(1-\eta)^4 T_{\mathrm{H}}^4}{b_1 + b_2(1-\eta)^3} + \frac{b_2(1-\eta)^3 T_{\mathrm{C}}}{b_1 + b_2(1-\eta)^3}\,. \tag{4.17}$$

We thus obtain the heat $\dot{Q}_{\mathrm{H}}$ and work $\dot{W}$ from $\dot{Q}_{\mathrm{H}} = b_1(T_{\mathrm{H}}^4 - T_{\mathrm{l}}^4)$ and $\dot{W} = \eta\dot{Q}_{\mathrm{H}}$ with

$$\dot{Q}_{\mathrm{H}} = b_1 b_2 \frac{T_{\mathrm{H}}(1-\eta)^4 - T_{\mathrm{C}}^4}{b_1(1-\eta) + b_2(1-\eta)^4} \tag{4.18}$$

or

$$\dot{W} = b_1 b_2 \eta \frac{T_{\mathrm{H}}(1-\eta)^4 - T_{\mathrm{C}}^4}{b_1(1-\eta) + b_2(1-\eta)^4}\,. \tag{4.19}$$

Figure 4.5 shows the heat $\dot{Q}_{\mathrm{H}}$ of the hot side and the work $\dot{W}$ as a function of the efficiency η for a set of transport terms b_1, b_2. Here 'heat' transport terms b_i are to be understood as combination of emissivity, Stefan–Boltzmann's constant ($\sigma_{\mathrm{SB}} = 5.68\times10^{-8}\,\mathrm{W\,m^{-2}\,K^{-4}}$), and solid angle into which the radiation is emitted.

The quality of heat and work of the Boltzmann engine are similar to those of the Curzon–Ahlborn engine. However, the shape of the functions $\dot{Q}_{\mathrm{H}} = \dot{Q}_{\mathrm{H}}(\eta)$ and $\dot{W} = \dot{W}(\eta)$ differ due to the fourth power dependence on temperatures, viz., T_{H}^4, T_{C}^4, and $(1-\eta)^4$.

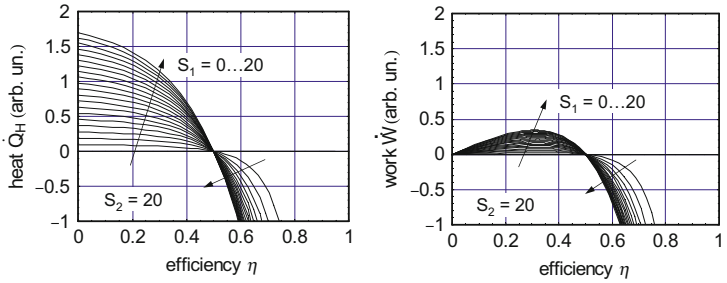

Fig. 4.5 Heat (*left*) and output work (*right*) of a Boltzmann engine versus efficiency for transport terms $0 \leq b_1 \leq 20$, $b_2 = 20$; exemplarily chosen $T_H = 2T_C$

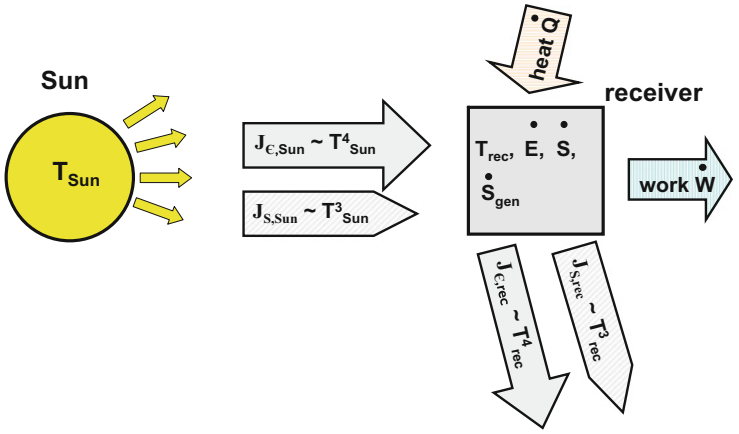

Fig. 4.6 Energy and entropy flows (J_ϵ, $\dot{W}$, J_S, $\dot{S}$) to and from a solar light absorber (receiver) for the derivation the free energy of solar photons

4.1.3 *Maximum Conversion Efficiency of Black Body Radiation with a Thermal Receiver in the Limit of Vanishing Output Power*

By analogy with the free energy concept of an ideal gas $F = U - TS$, which defines that part of the internal energy U of a system that can be converted into mechanical, chemical, or electrical energy, we study the free energy of photons originating from a thermal equilibrium source at T_{Sun} and being absorbed by a receiver in thermal equilibrium and at temperature T_{abs} (see Fig. 4.6).

Here we consider the magnitudes entering a receiver (kept at temperature T_{rec}), such as energy and entropy flows from the sun, defined as $J_{\epsilon,Sun}$, $J_{S,Sun}$, as well as some heat flow $\dot{Q}$ from the environment of the receiver, and accordingly the magnitudes leaving the receiver, like the flows of energy, entropy, $J_{\epsilon,rec}$, $J_{S,rec}$, and of course, the flow of work $\dot{W}_{rec}$.

In order to formulate the balances of energy and entropy of this receiver system we introduce the internal variables as time derivatives of internal energy and entropy, $\dot{E}_{\mathrm{int}}$, $\dot{S}_{\mathrm{int}}$, and in addition of the increase in internal entropy due to irreversible processes in the receiver $\dot{S}_{\mathrm{gen}}$.

The balances of energy and entropy flows are expressed by these rate equations [4]

$$\dot{E}_{\mathrm{int}} = J_{\epsilon,\mathrm{Sun}} - J_{\epsilon,\mathrm{rec}} + \dot{Q} - \dot{W} \tag{4.20}$$

and

$$\dot{S}_{\mathrm{int}} = J_{\mathrm{S,Sun}} - J_{\mathrm{S,rec}} + \frac{\dot{Q}}{T_{\mathrm{rec}}} + \dot{S}_{\mathrm{gen}} \ , \tag{4.21}$$

In the stationary state, each of the internal magnitudes is constant and consequently their time derivatives vanish $\dot{E}_{\mathrm{int}} = 0$, $\dot{S}_{\mathrm{int}} = 0$.

According to the concept of Helmholtz free energy (commonly named F) and with the condition for stationarity of the internal magnitudes[4] we derive

$$\begin{aligned} \dot{F}_{\mathrm{int}} &= \dot{E}_{\mathrm{int}} - \dot{S}_{\mathrm{int}} T_{\mathrm{rec}} = 0 \\ &= J_{\epsilon,\mathrm{Sun}} - J_{\mathrm{S,Sun}} T_{\mathrm{rec}} - (J_{\epsilon,\mathrm{rec}} - J_{\mathrm{S,rec}} T_{\mathrm{rec}}) + \dot{Q} - \frac{\dot{Q}}{T_{\mathrm{rec}}} T_{\mathrm{rec}} - \dot{W} - \dot{S}_{\mathrm{gen}} T_{\mathrm{rec}} \ . \end{aligned} \tag{4.22}$$

After rearrangement, we get

$$\dot{W} = (J_{\epsilon,\mathrm{Sun}} - J_{\mathrm{S,Sun}} T_{\mathrm{rec}}) - (J_{\epsilon,\mathrm{rec}} - J_{\mathrm{S,rec}} T_{\mathrm{rec}}) - \dot{S}_{\mathrm{gen}} T_{\mathrm{rec}} \ , \tag{4.23}$$

where the additional entropy generation in the absorber $\dot{S}_{\mathrm{gen}} \geq 0$ and, of course, $T_{\mathrm{rec}} > 0$. Since $\dot{S}_{\mathrm{gen}}$ depends on the particular process and is not known generally, we drop that term and write instead

$$\dot{W} \leqq (J_{\epsilon,\mathrm{Sun}} - J_{\mathrm{S,Sun}} T_{\mathrm{rec}}) - (J_{\epsilon,\mathrm{rec}} - J_{\mathrm{S,rec}} T_{\mathrm{rec}}) \ . \tag{4.24}$$

This Landsberg efficiency [4] for the conversion of black body radiation $J_{\epsilon,\mathrm{Sun}}(T_{\mathrm{Sun}})$ is defined as $\eta_{\mathrm{PL}} = \dot{W} / J_{\epsilon,\mathrm{Sun}}$, whence

$$\begin{aligned} \eta_{\mathrm{PL}} &\leqq 1 - \frac{J_{\mathrm{S,Sun}} T_{\mathrm{rec}}}{J_{\epsilon,\mathrm{Sun}}} - \left(\frac{J_{\epsilon,\mathrm{rec}}}{J_{\epsilon,\mathrm{Sun}}} - \frac{J_{\mathrm{S,rec}} T_{\mathrm{rec}}}{J_{\epsilon,\mathrm{Sun}}} \right) \\ &= 1 - \frac{J_{\mathrm{S,Sun}} T_{\mathrm{rec}}}{J_{\epsilon,\mathrm{Sun}}} - \frac{J_{\epsilon,\mathrm{rec}}}{J_{\epsilon,\mathrm{Sun}}} \left(1 - \frac{J_{\mathrm{S,rec}} T_{\mathrm{rec}}}{J_{\epsilon,\mathrm{rec}}} \right) \ . \end{aligned} \tag{4.25}$$

[4]Note, that $\dot{E}$, $\dot{S}$, and $\dot{S_{\mathrm{gen}}}$ are time derivatives of the internal magnitudes of the receiver system.

Introducing the dependence of energy and entropy fluxes on the corresponding temperature (Sect. 3.4.8), viz., $J_{\epsilon,\mathrm{i}} = \sigma_{\mathrm{SB}} \epsilon_i T_i^4$ and $J_{\mathrm{S,i}} = \frac{4}{3} \sigma_{\mathrm{SB}} \epsilon_i T_i^3$, into (4.25), it follows that

$$\eta_{\mathrm{PL}} \leqq 1 - \frac{4T_{\mathrm{rec}}}{3T_{\mathrm{Sun}}} - \frac{T_{\mathrm{rec}}^4}{T_{\mathrm{Sun}}^4} \left(1 - \frac{4}{3}\right) \tag{4.26}$$

$$= 1 - \frac{T_{\mathrm{rec}}}{T_{\mathrm{Sun}}} - \frac{1}{3} \left[\frac{T_{\mathrm{rec}}}{T_{\mathrm{Sun}}} - \left(\frac{T_{\mathrm{rec}}}{T_{\mathrm{Sun}}} \right)^4 \right] .$$

We recognize that the efficiency η_{PL} is bounded by the Carnot efficiency $1 - T_{\mathrm{rec}}/T_{\mathrm{Sun}}$ reduced by an additional factor

$$\eta_{\mathrm{PL}} \leqq \eta_{\mathrm{C}} - \frac{1}{3} \left[\frac{T_{\mathrm{rec}}}{T_{\mathrm{Sun}}} - \left(\frac{T_{\mathrm{rec}}}{T_{\mathrm{Sun}}} \right)^4 \right] , \tag{4.27}$$

which accounts for the transport of the generalized heats in form of photons with dependence of the respective energy flows by T^4 at variance with pure heat conduction in a Carnot engine with linear dependence on temperature T.

We have assumed so far that the receiver temperature T_{rec} equals the temperature of the heat sink, which is the temperature T_{env} of the environment, e.g., that of the Earth T_{Earth}. For the heat transport from the low temperature side of the receiver to the environment, a vanishing temperature gradient would be available which would allow only for a vanishing heat flux between receiver and environment, also reducing to zero that fraction of the 'solar heat' to be converted into work. The efficiency η_{PL} accordingly yields the maximum efficiency for conversion of solar radiation for negligible output power (see Fig. 4.7).

With the two temperatures $T_{\mathrm{Sun}} = 6{,}000\,\mathrm{K}$ and $T_{\mathrm{Earth}} = 300\,\mathrm{K}$ for the heat source and heat sink, the regime of the absorber temperature ranges over $300 \leq T_{\mathrm{rec}} \leq 6{,}000\,\mathrm{K}$. For $T_{\mathrm{rec}} = T_{\mathrm{Earth}} = 300\,\mathrm{K}$, the efficiency reaches the maximum

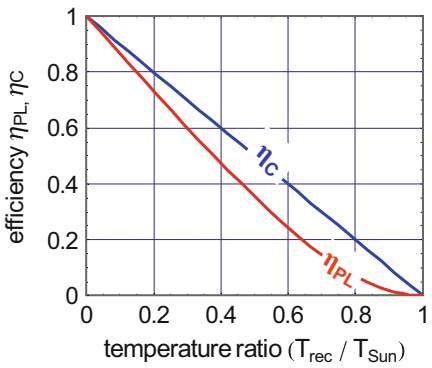

Fig. 4.7 Efficiency η_{PL} of solar energy conversion calculated on the basis of the free energy of solar photons [4] in comparison with the Carnot efficiency η_{C}. For the limit of ($T_{\mathrm{rec}} = T_{\mathrm{Earth}}$), the temperature difference needed for the extraction of heat at the cold side vanishes and in turn the output work also disappears

value $\eta_{\mathrm{PL}} = 0.933$. However, $T_{\mathrm{rec}} = T_{\mathrm{Earth}}$ does not allow for extraction of work from the device ($\dot{W} = 0$).

4.1.4 Mueser Approach

A substantial simplification of the concept of the Stefan–Boltzmann approach consists of directly linking the low temperature side of the reversibly operating heat engine (Carnot engine CE) to the low temperature heat reservoir T_{C} (see Fig. 4.8) [5]. We assume the receiver to get the solar insolation under the solid angle Ω_{in} and to emits its radiation into the solid angle Ω_{out} which in the general case of a spheric receiver amounts to $\Omega_{\mathrm{out}} = 4\pi$. In the language of the Stefan–Boltzmann engine, for the Mueser engine the transport term gets $b_2 \to \infty$ and, setting $T_{\mathrm{H}} = T_{\mathrm{Sun}}$ and $T_{\mathrm{C}} = T_{\mathrm{Earth}}$, the balance for input from Sun and environment and for output energy fluxes from receiver and in particular with the heat flux $\dot{Q}_{\mathrm{H}}$ to the Carnot engine reads

$$\Omega_{\mathrm{in}}\varepsilon_{\mathrm{Sun}}\sigma_{\mathrm{SB}}T_{\mathrm{Sun}}^4\alpha_{\mathrm{rec}} + (4\pi - \Omega_{\mathrm{in}})\,\varepsilon_{\mathrm{env}}\sigma_{\mathrm{SB}}T_{\mathrm{env}}^4\alpha_{\mathrm{rec}} = \Omega_{\mathrm{out}}\varepsilon_{\mathrm{rec}}\sigma_{\mathrm{SB}}T_{\mathrm{rec}}^4 + \dot{Q}_{\mathrm{H}} \tag{4.28}$$

The heat $\dot{Q}_{\mathrm{H}}$ available at the level of T_{rec} is converted to work $\dot{W}$ with the Carnot efficiency η_C. Here, Ω_{in}, Ω_{out}, $\varepsilon_{\mathrm{Sun}}$, $\varepsilon_{\mathrm{env}}$, $\varepsilon_{\mathrm{rec}}$, α_{rec}, designate solid angle for the reception of solar light (including sunlight concentration when $\Omega_{\mathrm{in}} > \Omega_{\mathrm{Sun}}$), solid angle for light emission Ω_{out}, emissivity of the Sun, of the environment, of the receiver, and absorptivity of the receiver.

Setting

$$\dot{Q}_{\mathrm{H}} = \frac{\dot{W}}{\eta_{\mathrm{C}}} = \frac{\dot{W}}{1 - T_{\mathrm{C}}/T_{\mathrm{rec}}}\,,$$

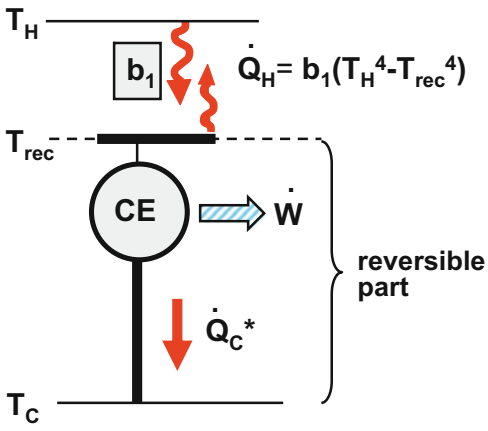

Fig. 4.8 Schematic design of a Mueser engine. The Mueser approach is a simplification of the Boltzmann engine in which the low-temperature side of the Carnot engine is directly connected to the heat reservoir at temperature T_{C}

the above flow balance is rewritten to give the work over the Carnot efficiency, viz.,

$$\Omega_{\mathrm{in}}\varepsilon_{\mathrm{Sun}}\sigma_{\mathrm{SB}}T_{\mathrm{Sun}}^4\alpha_{\mathrm{rec}}+(4\pi-\Omega_{\mathrm{in}})\,\varepsilon_{\mathrm{Univ}}\sigma_{\mathrm{SB}}T_{\mathrm{Univ}}^4\alpha_{\mathrm{rec}}-\Omega_{\mathrm{out}}\varepsilon_{\mathrm{rec}}\sigma_{\mathrm{SB}}T_{\mathrm{rec}}^4=\frac{\dot{W}}{1-T_{\mathrm{Earth}}/T_{\mathrm{rec}}} \tag{4.29}$$

Relating the work $\dot{W}$ to the input from the Sun $\Omega_{\mathrm{in}}\varepsilon_{\mathrm{Sun}}\sigma_{\mathrm{SB}}T_{\mathrm{Sun}}^4$ and assuming ideal black body emitter (Sun, environment), as well as receiver properties with $\varepsilon_{\mathrm{Sun}}=\varepsilon_{\mathrm{env}}=\varepsilon_{\mathrm{rec}}=\alpha_{\mathrm{rec}}=1$, one obtains the efficiency of the Mueser engine

$$\eta_{\mathrm{Mues}}=\left[1-\frac{\Omega_{\mathrm{out}}}{\Omega_{\mathrm{in}}}\left(\frac{T_{\mathrm{rec}}}{T_{\mathrm{Sun}}}\right)^4+\frac{(4\pi-\Omega_{\mathrm{in}})}{\Omega_{\mathrm{in}}}\left(\frac{T_{\mathrm{env}}}{T_{\mathrm{Sun}}}\right)^4\right]\left(1-\frac{T_{\mathrm{Earth}}}{T_{\mathrm{rec}}}\right). \tag{4.30}$$

Basically, the radiation input from the environment might be composed of the contributions from the global neighborhood and from the Universe weighted by their individual solid angles. For the sake of simplicity, one might neglect the term from the environment since its share is weighted by the factor $(T_{\mathrm{env}}/T_{\mathrm{Sun}})^4$ which for $T_{\mathrm{env}}=T_{\mathrm{Earth}}=300\,\mathrm{K}$ and also for $T_{\mathrm{env}}=T_{\mathrm{Univ}}=3\,\mathrm{K}$ is very small. Finally, one obtains with good approximation

$$\eta_{\mathrm{Mues}}=\left[1-\frac{\Omega_{\mathrm{out}}}{\Omega_{\mathrm{in}}}\left(\frac{T_{\mathrm{rec}}}{T_{\mathrm{Sun}}}\right)^4\right]\left(1-\frac{T_{\mathrm{Earth}}}{T_{\mathrm{rec}}}\right). \tag{4.31}$$

This efficiency comprises a term describing the influence of the energy transport by photons (rectangular brackets) together with a second term, the Carnot efficiency. The solid angle in which the Sun appears for an Earth-based observer without light concentration amounts to $\Omega_{\mathrm{in}}=\Omega_{\mathrm{Sun}}=5.3\times10^{-6}$, that may be increased by concentration to $\Omega_{\mathrm{in}}>\Omega_{\mathrm{Sun}}$; accordingly the solid angle for the contribution of the environment under concentrated sunlight $(4\pi-\Omega_{\mathrm{in}})$ decreases. For maximum solar light concentration $(\Omega_{\mathrm{in}}=4\pi)$ the receiver does not see but the Sun and the solid angles for reception and emission are identical $\Omega_{\mathrm{in}}=\Omega_{\mathrm{out}}=4\pi$. In this case, from the fifth order relation of $T_{\mathrm{rec}}=T_{\mathrm{rec}}(T_{\mathrm{Sun}},T_{\mathrm{Earth}},\eta_{\mathrm{Mues}})$ it is easy to see,[5] that the highest receiver temperature achievable is $(T_{\mathrm{rec}}/T_{\mathrm{Sun}})=1$, provided the Mueser efficiency vanishes $(\eta_{\mathrm{Mues}}\to0)$; accordingly no heat must be transferred to the Carnot engine $(\dot{Q}_{\mathrm{H}}=0)$, which likewise means that the output power of the converter vanishes $\dot{W}=0$. In this mode of operation, the entire radiative energy from the Sun to the receiver is given back to the Sun radiatively.

[5] After rearrangement the relation for the Mueser efficiency reads

$$\left(\frac{T_{\mathrm{rec}}}{T_{\mathrm{Sun}}}\right)^5-\left(\frac{T_{\mathrm{Earth}}}{T_{\mathrm{Sun}}}\right)\left(\frac{T_{\mathrm{rec}}}{T_{\mathrm{Sun}}}\right)^4+(\eta_{\mathrm{Mues}}-1)\left(\frac{T_{\mathrm{rec}}}{T_{\mathrm{Sun}}}\right)+\left(\frac{T_{\mathrm{Earth}}}{T_{\mathrm{Sun}}}\right)=0 \tag{4.32}$$

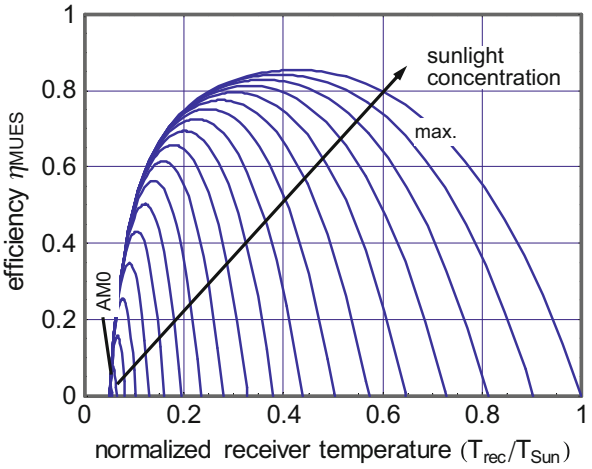

Fig. 4.9 Efficiency η_{Mues} of a Mueser engine versus normalized receiver temperature $T_{\text{rec}}/T_{\text{Sun}}$ for different levels of solar light concentration. Each of these efficiency values has been calculated for a spherical receiver at lower temperature $T_{\text{Earth}} = 300\,\text{K}$. Here the input photons are collected with the area πR_{rec}^2, whereas the output light is emitted from area $4\pi R_{\text{rec}}^2$. For a solar thermal receiver device, one would certainly choose identical input and output areas, e.g., a one sided open flat absorber and thus gain the factor 4 in the balance of flows per area and the factor of $\sqrt[4]{4}$ in the maximum achievable receiver temperature

The lower the temperature of the receiver is adjusted (for any concentration ($\Omega_{\text{in}} > \Omega_{\text{Sun}}$)) the more heat is fed into the engine. However, the more heat, the lower the receiver temperature and the lower the Carnot factor to make work out of it. For the lowest possible receiver temperature $T_{\text{rec}} = T_{\text{Earth}}$, the heat $\dot{Q}_{\text{H}}$ is maximum, accompanied by the minimum radiation 'losses' emitted from the receiver, but the Carnot efficiency approaches zero.

Figure 4.9 displays the Mueser efficiencies for a variety of concentration factors C as a function of the receiver temperature T_{rec}. The maximum conversion efficiency $\eta_{\text{Mues}} = 0.86$ for Earth-based devices is thus achieved at maximum light concentration with an optimum receiver temperature $T_{\text{rec, opt}} \approx 2{,}450\,\text{K}$.

A representation of a device for which $\Omega_{\text{in}} = \Omega_{\text{out}}$ [6] resembling a Mueser engine is schematically depicted in Fig. 4.10. The receiver is surrounded by an ideal mirror with reflection factor unity and held at a temperature $T = 0$, with an aperture size A such that the receiver only sees the Sun or itself via the mirror. The receiver is connected to a Carnot engine which is to be supplied by heat at T_{rec}. The low temperature side of the Carnot engine is connected to the environment at T_{Earth}. Using the above equations, the corresponding output work reads

$$\dot{W} = \left(\Omega_{\text{in}}\varepsilon_{\text{Sun}}\sigma_{\text{STB}}T_{\text{Sun}}^4\alpha_{\text{rec}} - \Omega_{\text{out}}\varepsilon_{\text{rec}}\sigma_{\text{STB}}T_{\text{rec}}^4\right)\left(1 - \frac{T_{\text{Earth}}}{T_{\text{rec}}}\right) . \tag{4.33}$$

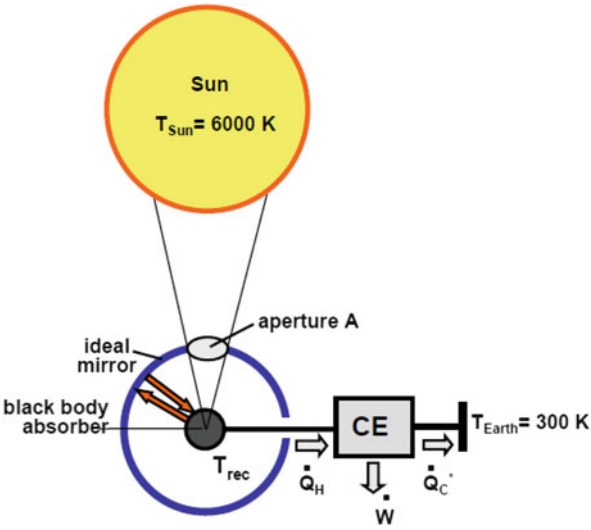

Fig. 4.10 Schematic realization of a Mueser engine. A black receiver is surrounded by an 'ideal' mirror with aperture A, so that the receiver only sees the Sun or itself (implying maximum concentration of solar light to the absorber) [6]. The receiver at temperature T_{rec} is connected to a Carnot engine (CE) which is attached to the Earth at the low temperature side ($T_{Earth} = 300$ K)

Again with $\varepsilon_{Sun} = \varepsilon_{rec} = \alpha_{rec} = 1$, and $\Omega_{in} = \Omega_{out}$

$$\dot{W} = \Omega_{in}\sigma_{STB}T_{Sun}^4\left(1-\left(\frac{T_{rec}}{T_{sun}}\right)^4\right)\left(1-\frac{T_{Earth}}{T_{rec}}\right), \tag{4.34}$$

we get the efficiency $\eta = (\dot{W})/(\Omega_{in}\sigma_{STB}T_{Sun}^4)$ of this device

$$\eta = \left[1-\left(\frac{T_{rec}}{T_{Sun}}\right)^4\right]\left(1-\frac{T_{Earth}}{T_{rec}}\right). \tag{4.35}$$

This relation also obviously consists of the term describing the 'effectiveness' of the photon transport from the Sun at T_{Sun} to a receiver at T_{rec}, this being weighted by the Carnot efficiency which is also governed by the receiver temperature T_{rec}.

4.1.5 Temperatures and Limits of Efficiency for Planets of the Solar System

Analogously with the radiative balance outlined in Sect. 3.3, the temperature of objects orbiting around the Sun as a function of distance d_{SP} (orbital radius) and hence the performance for solar light conversion by a Mueser engine in such a solar orbit can be estimated (see also [3]). For a rough approximation, to be applied to the different planets in our solar System, one once again assumes ideal 'black'

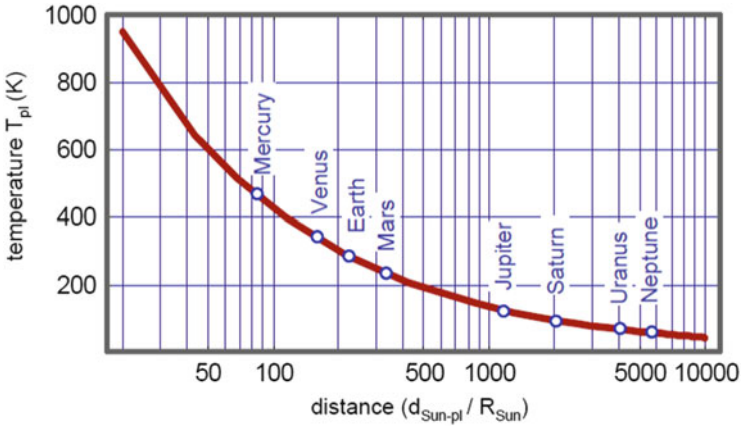

Fig. 4.11 Temperature of ideal black (spherical) receivers/emitters versus distance from the Sun. Positions of planets of the solar system are indicated, although some of them, particularly those in the outer orbits, do not behave as black bodies

receiver/emitter properties and writes the respective temperature[6] $T_P(d_{SP})$ as a function of their distance from the Sun (see Fig. 4.11)[7]:

$$T_P \approx \sqrt[4]{\frac{1}{4}\left(\frac{R_{Sun}}{d_{SP}}\right)^2 T_{Sun}^4 + \left[1 - \left(\frac{1}{4}\right)\left(\frac{R_{Sun}}{d_{SP}}\right)^2\right] T_{Univ}^4}\,. \tag{4.36}$$

Figure 4.12 shows the Mueser engine efficiencies for non-concentrated sunlight versus the temperature that could be associated to distances d_{SP} of planets from the Sun listed above in Fig. 4.11. On the first view it seems amazing that the maximum Mueser engine efficiency does not depend on the distance d_{SP} of the respective planet, but, since the increasing dilution of solar light versus distance from the source and the corresponding decrease in maximum temperature of the hot side of the Mueser engine is just compensated by the analogous decrease of temperature of the "cold" side of the Carnot engine attached to the planet.

[6]The true planetary temperatures can depart substantially from those estimated here with the assumption of ideal 'black' receivers/emitters, due to their individual compositions and spectrally dependent absorptivities and emissivities.

[7]Here the corresponding solid angles for the light input depend on the distance d_{SP} and are replaced by $\Omega_{in}(d_{SP}) = (1/4)\,(R_{Sun}/d_{SP})^2$.

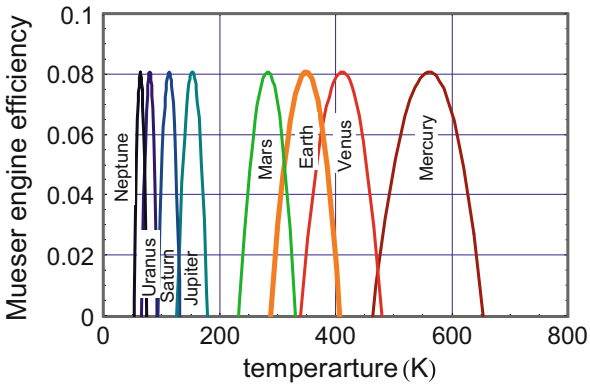

Fig. 4.12 Theoretical efficiency of spherical Mueser engine receivers for unconcentrated sunlight versus temperature for hypothetical black body planets with temperatures according to assumptions in Fig. 4.11

4.1.6 Spectrally Selective Absorbers/Emitters

As already sketched schematically in Sect. 3.4.11, the balance of incoming radiation versus radiation output might be beneficially tuned by high spectral absorption for the incoming light and low spectral emission for the main wavelength regime in which the receiver emits, provided that the temperatures of the source and of the receiver differ considerably from one another (see Fig. 3.16). Thus, with spectral selectivity, which is expressed through the absorptivity $\alpha_{\mathrm{rec}}(\hbar\omega)$ and emissivity $\varepsilon_{\mathrm{rec}}(\hbar\omega)$, the energy flow balance to an engine with a receiver exposed to solar radiation in the solid angle Ω_{in} and emitting via solid angle Ω_{out} when neglecting the contribution from the environment or the Universe resp. writes

$$\Omega_{\mathrm{in}} \frac{1}{c_0^2 4\pi^3 \hbar^3} \int_0^\infty \alpha_{\mathrm{rec}}(\hbar\omega) \frac{(\hbar\omega)^3}{\exp\left(\frac{\hbar\omega}{kT_{\mathrm{Sun}}}\right) - 1} \mathrm{d}(\hbar\omega)$$
$$= \frac{1}{c_0^2 4\pi^3 \hbar^3} 4\pi \int_0^\infty \varepsilon_{\mathrm{rec}}(\hbar\omega) \frac{(\hbar\omega)^3}{\exp\left(\frac{\hbar\omega}{kT_{\mathrm{rec}}}\right) - 1} \mathrm{d}(\hbar\omega) + \dot{Q}_{\mathrm{H}} \,, \tag{4.37}$$

where 4π represents the solid angle for emission and $\alpha_{\mathrm{rec}}(\hbar\omega) = \varepsilon_{\mathrm{rec}}(\hbar\omega)$ is the spectrally strongly varying absorption or emissivity of the receiver.

For an extreme case of a step function in $\alpha_{\mathrm{rec}}(\hbar\omega) = \varepsilon_{\mathrm{rec}}(\hbar\omega)$, viz.,

$$\alpha_{\mathrm{rec}}(0 \le \hbar\omega \le \hbar\omega_{\mathrm{g}}) = 0 \,, \quad \alpha_{\mathrm{rec}}(\hbar\omega_{\mathrm{g}} < \hbar\omega \le \infty) = 1 \,,$$

which allows for absorption only in the high photon energy range in which the solar light is accepted by the receiver, the thermal receiver will not be able to emit a substantial amount of photons due to its lower temperature.

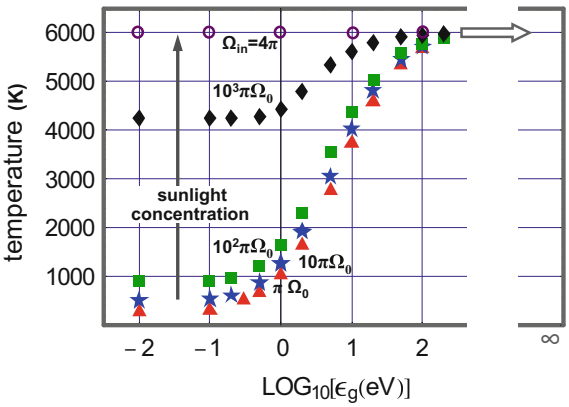

Fig. 4.13 Temperature of a spectrally selective absorber, ideally isolated from the environment and only exposed to a thermal equilibrium radiator like the Sun ($T_{\mathrm{Sun}} = 6{,}000\,\mathrm{K}$) versus optical threshold energy $\epsilon_g = \hbar\omega_g$ for different degrees of solar light concentration

To demonstrate the effect of spectral selectivity, the 'open circuit'-temperature ($\dot{Q}_H = 0$) of a spectrally selective receiver versus optical threshold energy $\epsilon_g = \hbar\omega_g$ is sketched in Fig. 4.13 for different levels of solar light concentration (contributions from the Universe and from the terrestrial environment have been neglected). Against intuition, the receiver temperature T_{rec} for large threshold energies tends asymptotically towards $T_{\mathrm{rec}}(\epsilon_g \to \infty) = T_{\mathrm{Sun}}$, regardless of the light concentration factor $(4\pi/\Omega_{\mathrm{in}})$.

The above balance of radiation and heat supplied to a Carnot engine is modified by the restriction of the integrals to the appropriate photon energy range, viz., $\hbar\omega_g \leq \hbar\omega \leq \infty$, with the result

$$\dot{Q}_H = \Omega_{\mathrm{in}} \frac{1}{c_0^2 4\pi^3\hbar^3} \int_{\hbar\omega_g}^{\infty} \frac{(\hbar\omega)^3}{\exp\left(\dfrac{\hbar\omega}{kT_{\mathrm{Sun}}}\right) - 1} \mathrm{d}(\hbar\omega)$$

$$-\Omega_{\mathrm{out}} \frac{1}{c_0^2 4\pi^3\hbar^3} \int_{\hbar\omega_g}^{\infty} \frac{(\hbar\omega)^3}{\exp\left(\dfrac{\hbar\omega}{kT_{\mathrm{rec}}}\right) - 1} \mathrm{d}\,(\hbar\omega)\ . \tag{4.38}$$

Figures 4.14 displays the output work of an engine in terms of heat $\dot{Q}_H$ times the Carnot efficiency as a function of the photon threshold energy $\hbar\omega_g$ that separates the two regimes of low and high absorption/emission. At high light concentration factors, e.g., $\Omega_{\mathrm{in}} = \Omega_{\mathrm{out}} = 4\pi$, a decrease in T_{rec} starting from $T_{\mathrm{rec}} = T_{\mathrm{Sun}}$ results in a 'walk' along the uppermost curve of the function $\eta_{\mathrm{Mues}}(T_{\mathrm{rec}}/T_{\mathrm{Sun}})$, from left to right. For this maximum solar light concentration, the spectral selectivity of an absorber shows no beneficial effect for the efficiency compared to an ideal 'black' receiver, since the plots clearly show that the threshold energy approaches zero $\hbar\omega_g \to 0$. Under these conditions the receiver only 'sees' the Sun and has to compete in absorption and emission with the solar temperature.

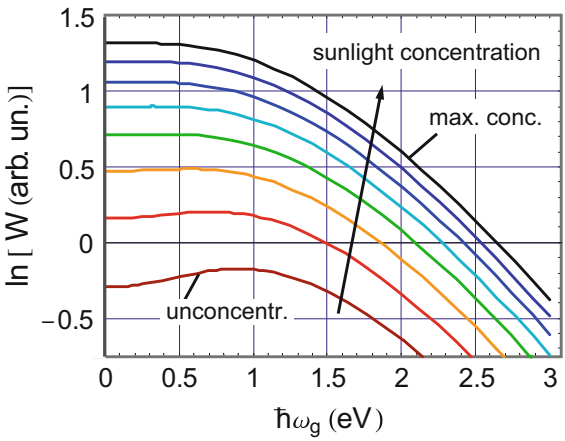

Fig. 4.14 Output work of a Mueser engine versus spectrally selective optical threshold $\hbar\omega_g$ for different levels of sunlight concentration

For lower concentration factors, as indicated in Fig. 4.12, the spectral separation of photon energy regimes with high absorption from those with low emissivity provides for decent benefits in engine efficiency $\eta_{\mathrm{Mues}}(\hbar\omega_g)$, obviously emerging in Fig. 4.14 in the output work W versus $\hbar\omega_g$ for unconcentrated sunlight.

4.1.7 Multispectral Solar Light Conversion

An extension of the approach of spectrally selective absorption of solar light consists of the individual use of photons of different spectral regimes of the solar light, known as "spectrum splitting". This strategy is also named 'multi-spectral' solar energy conversion and it can be realized for instance by n individual spectrally selective absorbers, arranged optically in series with its particular receiver temperature $T_{\mathrm{H},i}$ and each of them connected to its own Carnot engine (Fig. 4.15) [3].

The balance of energy fluxes to and from the receiver system amongst those from source Sun and environment (Earth) has to take into account also the exchange of photons between one receiver and its neighbors. This means that, in order to formulate the respective flows, the geometrical configuration of the receivers has to be given, e.g., flat receivers arranged optically in series and sunlight under normal incidence. Furthermore, for photon exchange between the receivers in particular configurations, multilayer optics may have to be applied. The radiative balance of one receiver (numbered i) from which the relevant heat $\dot{Q}_{\mathrm{H,i}}$ is fed to the high temperature side of the Carnot engine (CE) contains the contribution from the Sun and from its neighbors at upper and lower positions numbered $(i-1)$ and $(i+1)$,

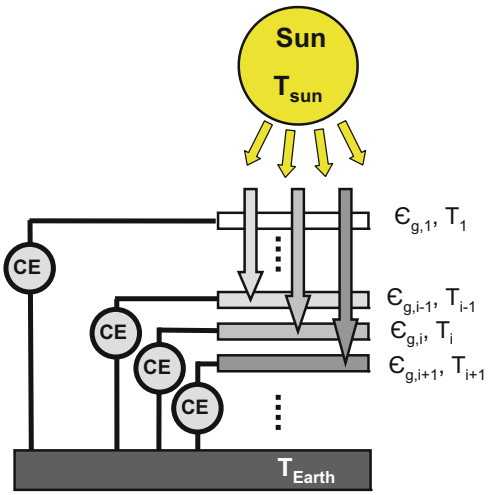

Fig. 4.15 Schematic design of a multispectral thermal solar energy converter. Each of the Carnot engines (*CE*) is supplied by a particular spectral section of the solar radiation [3]

respectively, and of course includes the part that is emitted:

$$\begin{aligned}\dot{Q}_{\mathrm{H},i} = \Omega_{\mathrm{in}} \frac{1}{c_0^2 4\pi^3 \hbar^3} \int_{\hbar\omega_{\mathrm{g},i}}^{\hbar\omega_{\mathrm{g},i-1}} \alpha_i\,(\hbar\omega)\, \frac{(\hbar\omega)^3}{\exp\left(\dfrac{\hbar\omega}{kT_{\mathrm{Sun}}}\right) - 1} \mathrm{d}(\hbar\omega) \\ + 2\pi \frac{1}{c_0^2 4\pi^3 \hbar^3} \int_{\hbar\omega_{\mathrm{g},i-1}}^{\infty} \alpha_i\,(\hbar\omega)\, \varepsilon_{i-1}(\hbar\omega) \frac{(\hbar\omega)^3}{\exp\left(\dfrac{\hbar\omega}{kT_{i-1}}\right) - 1} \mathrm{d}(\hbar\omega) \\ + 2\pi \frac{1}{c_0^2 4\pi^3 \hbar^3} \int_{\hbar\omega_{\mathrm{g},i+1}}^{\infty} \alpha_i\,(\hbar\omega)\, \varepsilon_{i+1}(\hbar\omega) \frac{(\hbar\omega)^3}{\exp\left(\dfrac{\hbar\omega}{kT_{i+1}}\right) - 1} \mathrm{d}(\hbar\omega) \\ - 4\pi \frac{1}{c_0^2 4\pi^3 \hbar^3} \int_{\hbar\omega_{\mathrm{g},i}}^{\infty} \varepsilon_i(\hbar\omega) \frac{(\hbar\omega)^3}{\exp\left(\dfrac{\hbar\omega}{kT_i}\right) - 1} \mathrm{d}(\hbar\omega)\,. \end{aligned} \tag{4.39}$$

In order to determine the efficiency as a function of the number of spectrally selective absorbers, as sketched in Fig. 4.16, we have assumed a multilayer stack with solar light input in the solid angles $\Omega_{\mathrm{in}} = \Omega_{\mathrm{Sun}}$ as well as $\Omega_{\mathrm{in}} = 4\pi$. Each layer (i) emits towards front and towards rear side in the solid angle $\Omega_{\mathrm{i,out}} = 2\pi$ by equal flux upward towards the layer $(i-1)$ and downwards towards the neighbor $(i+1)$. The lower neighbor $(i+1)$ emits photons in the range $\hbar\omega_{i+1} \le \hbar\omega \le \infty$, but its upper neighbor only emits and sees those in $\hbar\omega_{i-1} \le \hbar\omega \le \infty$, this being represented by the absorption $\alpha_{i-1}\,(\hbar\omega_{i-1} \le \hbar\omega \le \infty) \ge 0$.

In the latter balance, neither reflection from the surface of the single layers nor incomplete absorption within the relevant range $\hbar\omega_{i-1} \le \hbar\omega \le \hbar\omega_i$ has been

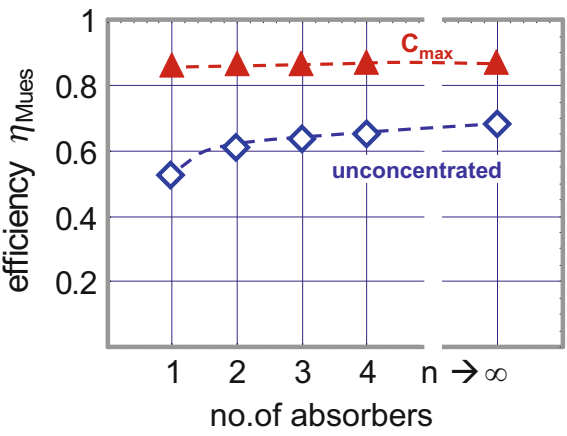

Fig. 4.16 Efficiency of a multispectral thermal solar energy converter based on Mueser engines versus number of individual spectrally selective absorbers [3]; unconcentrated sunlight corresponds to $\Omega_{in} = \pi\,\Omega_0 = \pi\,(R_{Sun}/d_{SE})^2$, maximum concentration relates to $\Omega_{in} = 4\pi$

taken into account. This refinement would require inclusion of overnext nearest neighbor emission and absorption, and in the end, one would have to couple each layer optically to all others.

4.2 Electronic Band Systems for Solar Light Conversion

The photons from the Sun as electromagnetic wave packages with particular energies in the few eV-range mainly couple to the electron system of solids. The electrons in solids may occupy only specific regimes in the energy scale called bands which result from the overlap of wave functions of weakly bound electrons in the potential of an ion lattice formed by atoms or molecules. Figure 4.17 shows the schematic development of energy bands from discrete energy levels by their mutual interaction through the reduction of their spatial separation. This band behavior of the electrons is commonly derived from solutions of the stationary Schrödinger equation for electrons in a periodic potential provided by the positively charged ions. In many materials, including most semiconductors, the interaction between electrons can be neglected (independent-electron picture).[8]

[8] An intuitive way to understand the formation of energetic regimes allowed for electron occupation is to consider a one-dimensional periodic arrangement of potential wells at a certain distance from one another. In an isolated single well of limited depth exist a certain finite number m of discrete energy levels, whereas in an arrangement of n such wells each of the m levels of one of the wells interferes with the companion levels of type m of the other $n - 1$ wells to form an ensemble of levels that are energetically split. The total energy separation of this splitting converges towards a particular value, even for an infinite number of wells $n \to \infty$. The behavior of such an infinite one-dimensional arrangement of potential wells is formulated by the Kronig–Penney model [7, 8] which can be solved analytically showing the formation of individual energy bands for the electrons.

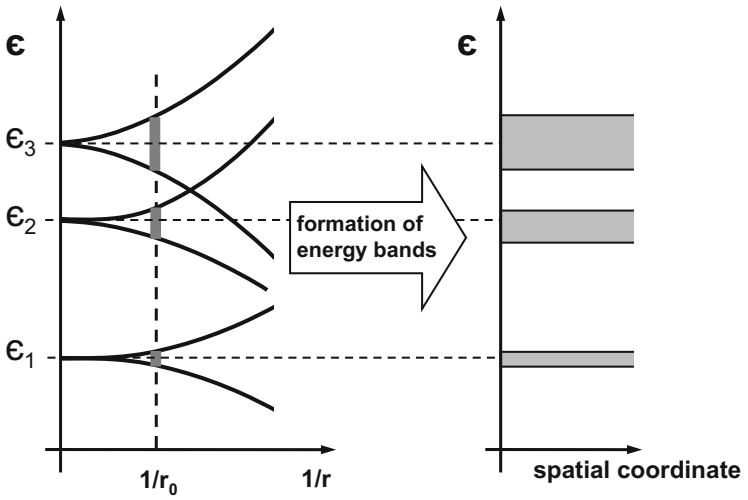

Fig. 4.17 Schematic formation of energy bands by increasing overlap of electron-wave functions of individual atoms (levels ϵ_1, ϵ_2, ϵ_3) with decreasing inter-atomic distance (equilibrium next-neighbor distance r_0)

In thermal equilibrium at a temperature T, the probability that a state of energy ϵ is occupied is given by the Fermi–Dirac distribution function[9]

$$f_{\mathrm{F}}(\epsilon) = \left(\exp\left(\frac{\epsilon - \epsilon_{\mathrm{F}}}{kT}\right) + 1\right)^{-1} .$$

Here,[10] ϵ_{F} designates the Fermi energy. The excitation of electrons in solids such insulators or semiconductors by solar light may initiate an occupation of the electronic levels that substantially departs from the thermal equilibrium distribution. The ability of the photoexcited electron ensemble to deliver electric power to the outside strongly depends on how well the photo-excited state, without return to the thermal equilibrium, can be conserved and be transported to the borders of the light absorber with its electric contacts.

[9] As the solid absorbers of solar light are commonly operated in the neighborhood of $T_{\mathrm{Earth}} = 300\,\mathrm{K}$ boson behavior of electrons characterizing super conductivity is excluded.

[10] In the Fermi–Dirac distribution function the Fermi energy ϵ_{F} designates for moderate temperatures the energetic position of the transition of the occupation probability from high ($f_{\mathrm{F}} > 0.5$) to low ($f_{\mathrm{F}} < 0.5$), and in the particular case of $T \to 0$, the kink in the step-like distribution function represents ϵ_{F}.

4.2.1 Electronic Band System in Thermal Equilibrium

Our exemplary electronic system that is to be exposed to solar radiation consists of two energy bands, a lower one named valence (VB) and an upper one named conduction band (CB) with corresponding densities of states $D_{\mathrm{VB}}(\epsilon)$, and $D_{\mathrm{CB}}(\epsilon)$, equivalently as the bands in an undoped semiconductor.[11] These two bands are separated by an energy gap ϵ_{g} exhibiting in our approach a value which corresponds to photon energies frequently available in the solar spectrum. For the further formulation by convention we name the energy of the upper edge of the valence band ϵ_{V}, and equivalently the lower edge of the conduction band ϵ_{C}; accordingly the band gap reads $\epsilon_{\mathrm{g}} = (\epsilon_{\mathrm{C}} - \epsilon_{\mathrm{V}})$.

In thermal equilibrium in undoped semiconductors the entire number of electrons in the respective volume element is conserved, and in other words the entire carrier concentrations in the excited states, i.e., electrons in CB and empty states in VB, called holes[12] are identical. The total concentrations are found by integrating the energy dependent concentrations $n\,(\epsilon)$ and $p\,(\epsilon)$ over the relevant energy range, these being formulated as the product of the density of states and the respective energy distribution function. As an example, for the electrons in the conduction band with lower band edge ϵ_{C},[13]

$$n_{\mathrm{CB}} = \int_{\epsilon_{\mathrm{C}}}^{\infty} D_{\mathrm{CB}}\,(\epsilon)\; f_{\mathrm{n}}\,(\epsilon)\,\mathrm{d}\epsilon\ .$$

In thermal equilibrium, $f_{\mathrm{n}}\,(\epsilon)$ is given by the Fermi–Dirac distribution function

$$f_{\mathrm{F}}(\epsilon) = \left(\exp\left(\frac{\epsilon - \epsilon_{\mathrm{F}}}{kT}\right) + 1\right)^{-1}\ ,$$

[11] Undoped means except the electrons in VB and CB no additional charges introduced by impurities in the lattice exist. In undoped semiconductors and insulators for the temperature $T \to 0$ states in the valence band ($D_{\mathrm{VB}}(\epsilon)$) are completely occupied by electrons whereas conduction band states are completely unoccupied.

[12] Basically in the semiclassical approach free electrons provide for transport of charges. Their contribution to the electric current density in terms of velocity $\mathbf{v}$ and wave vector $\mathbf{k}$ reads $\mathbf{j} = ((-e)(1/(4\pi)))\int_{\text{occup.}} \mathbf{v}(\mathbf{k})d\mathbf{k}$ with integration over all occupied states in the respective band. The contribution of unoccupied states in this band can be formulated by the integral of a completely occupied band which is vanishing $((1/(4\pi))\int_{\text{all states}} \mathbf{v}(\mathbf{k})d\mathbf{k} = 0)$ subtracting the supply of the unoccupied states $\mathbf{j} = ((+e)(1/(4\pi)))\int_{\text{unoccup.}} \mathbf{v}(\mathbf{k})d\mathbf{k}$; accordingly the current density can be formulated by the unoccupied states with apparent particles of positive elementary charge (holes) moving in opposite direction compared to electrons (see Fig. 4.19 and [7]).

[13] For the sake of simplicity, in order to be able to evaluate the integral analytically, the upper limit of the integral is commonly taken to be $\epsilon \to \infty$ rather than the upper edge of CB, the vacuum level ϵ_{vac}, and for typical temperatures, the Fermi distribution function reduces the contribution of $\epsilon > \epsilon_{\mathrm{vac}}$ to n_{CB} to negligible values. An analogous simplification is applied for the lower boundary value of the integral for holes $\epsilon \to -\infty$.

and we get the charge neutrality condition for an undoped semiconductor

$$\begin{aligned} n_{\mathrm{CB}} &= \int_{\epsilon_{\mathrm{C}}}^{\infty} D_{\mathrm{CB}}(\epsilon)\, \frac{1}{\exp\left(\dfrac{\epsilon-\epsilon_{\mathrm{F}}}{kT}\right)+1}\mathrm{d}\epsilon \\ &= p_{\mathrm{VB}} = \int_{-\infty}^{\epsilon_{\mathrm{V}}} D_{\mathrm{VB}}(\epsilon)\left(1-\frac{1}{\exp\left(\dfrac{\epsilon-\epsilon_{\mathrm{F}}}{kT}\right)+1}\right)\mathrm{d}\epsilon \\ &= \int_{-\infty}^{\epsilon_{\mathrm{V}}} D_{\mathrm{VB}}(\epsilon)\, \frac{1}{1+\exp\left(-\dfrac{\epsilon-\epsilon_{\mathrm{F}}}{kT}\right)}\mathrm{d}\epsilon\,, \end{aligned} \tag{4.40}$$

which serves for the determination of the position of the Fermi energy, ϵ_{F}. In the parabolic band approximation[14] the densities of states in the three-dimensional space are given by

$$D_{\mathrm{CB}}(\epsilon) = \left(\frac{2m_{\mathrm{n}}^*}{\hbar^2}\right)^{3/2} \frac{1}{2\pi^2}\sqrt{\epsilon-\epsilon_{\mathrm{C}}} \tag{4.41}$$

and

$$D_{\mathrm{VB}}(\epsilon) = \left(\frac{2m_{\mathrm{p}}^*}{\hbar^2}\right)^{3/2} \frac{1}{2\pi^2}\sqrt{-\epsilon+\epsilon_{\mathrm{V}}}\,, \tag{4.42}$$

(see Fig. 4.18) where m_{n}^* and m_{p}^* denote the effective masses of electrons in the conduction band and of holes in the valence band.[15]

[14] At the minima and maxima of $\epsilon = \epsilon(\mathbf{k})$ that correspond to the top of the valence band $\epsilon = \epsilon_{\mathrm{V}}$ and the bottom of the conduction band $\epsilon = \epsilon_{\mathrm{C}}$, the energy of electrons or holes depends to a good approximation quadratically on the wave vector $\epsilon \sim k^2$. Using this dependence for a three-dimensional solid, the density of states, again in the vicinity of ϵ_{V} and ϵ_{C}, yields $D \sim \sqrt{\epsilon}$.

[15] The effective mass represents the effect of the periodic potential of the crystal on the motion of electrons (and holes) in externally applied electric fields, and it is derived from the dispersion relation $\epsilon = \epsilon(\mathbf{k})$ for the electrons [9] by

$$\frac{1}{m^*} = \frac{1}{\hbar^2}\begin{pmatrix} \dfrac{\partial^2\epsilon}{\partial k_x^2} & \dfrac{\partial^2\epsilon}{\partial k_x \partial k_y} & \dfrac{\partial^2\epsilon}{\partial k_x \partial k_z} \\ \dfrac{\partial^2\epsilon}{\partial k_y \partial k_x} & \dfrac{\partial^2\epsilon}{\partial k_y^2} & \dfrac{\partial^2\epsilon}{\partial k_y \partial k_z} \\ \dfrac{\partial^2\epsilon}{\partial k_z \partial k_x} & \dfrac{\partial^2\epsilon}{\partial k_z \partial k_y} & \dfrac{\partial^2\epsilon}{\partial k_z^2} \end{pmatrix}.$$

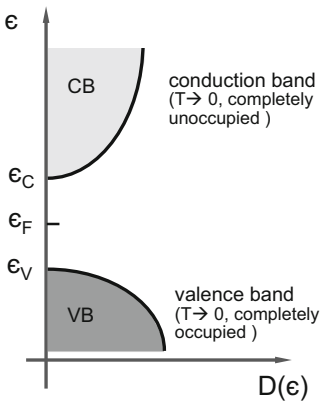

Fig. 4.18 Density of states $D(\epsilon)$ for valence and conduction band in an undoped three-dimensional semiconductor with directional isotropy, so-called parabolic bands, in which the approximation of quasi-free electrons and holes is satisfied with $\epsilon \sim k^2$ resulting in $D(\epsilon) \sim \sqrt{\epsilon}$

With the above approximation and with Boltzmann energy distribution substituting the Fermi distribution function, the thermal equilibrium concentration of electrons in the conduction band is

$$n_0 = 2\left(\frac{m_n^* kT}{2\pi\hbar^2}\right)^{3/2} \exp\left(-\frac{\epsilon_C - \epsilon_F}{kT}\right) = N_C \exp\left(-\frac{\epsilon_C - \epsilon_F}{kT}\right) \tag{4.43}$$

and that of holes in the valence band analogously writes

$$p_0 = 2\left(\frac{m_p^* kT}{2\pi\hbar^2}\right)^{3/2} \exp\left(-\frac{\epsilon_F - \epsilon_V}{kT}\right) = N_V \exp\left(-\frac{\epsilon_F - \epsilon_V}{kT}\right) . \tag{4.44}$$

For charge neutrality $n_0 = p_0$, these are combined to determine the thermal equilibrium position of the Fermi level as

$$\epsilon_F = \frac{\epsilon_C + \epsilon_V}{2} + \frac{1}{2}kT \ln\left[\frac{N_V}{N_C}\right] = \left(\frac{\epsilon_C + \epsilon_V}{2}\right) + \frac{3}{4}kT \ln\left[\frac{m_p^*}{m_n^*}\right], \tag{4.45}$$

which says that the Fermi level ϵ_F is located somewhere midway between the two levels ϵ_C and ϵ_V[16] and slightly shifted towards the band with the lower effective mass[17] (see Fig. 4.19).

[16]For the Fermi energy ϵ_F sufficiently separated from VB- and CB-edge, explicitly $(\epsilon_C - \epsilon_F) > 3kT$ and $(\epsilon_F - \epsilon_V) > 3kT$, the Boltzmann-energy distribution function is a reasonable approximation of the Fermi distribution function.

[17]The effective masses in the upper relation may be regarded as an abbreviation of the respective density of states.

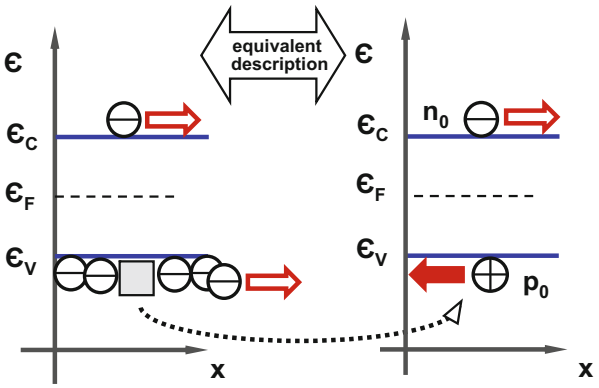

Fig. 4.19 Hole concept. Representation of unoccupied electron states in the lower band (valence band) by holes with thermal equilibrium density p_0 moving in opposite direction compared to electrons

4.2.2 *Quasi-Fermi Levels in Electronic Band Systems*

The thermal equilibrium occupation of electronic bands can be altered substantially by excitation with photons of appropriate energy (in semiconductors one needs $\hbar\omega \geq \epsilon_g = (\epsilon_C - \epsilon_V)$), and in consequence the electron and hole densities n_0 and p_0 get modified by additional Δn and Δp respectively. Here, we consider those in the excited states, that is, electrons at energy $\epsilon \geq \epsilon_C$ and holes at $\epsilon \leq \epsilon_V$:

$$n_{CB} = n_0 + \Delta n = \int_{\epsilon_C}^{\infty} D_{CB} f_n^*(\epsilon) d\epsilon \,, \tag{4.46}$$

$$p_{VB} = p_0 + \Delta p = \int_{\epsilon_V}^{-\infty} D_{VB} f_p^*(\epsilon) d\epsilon \,. \tag{4.47}$$

where the non-equilibrium distribution functions of electrons in the conduction band $f_n^*(\epsilon)$ and of holes in the valence band $f_p^*(\epsilon)$ in general have to be expressed by a complete set of transition rates from and to the respective energy levels in each of the involved bands.

In the particular case of stationary excitation by photons, and of fast energy (ϵ) and wave vector ($\mathbf{k}$) relaxation of electrons and holes in the bands (intraband relaxation times τ_ϵ and $\tau_\mathbf{k}$ are usually much smaller than the interband relaxation time, called recombination life time τ_{rec}) the electron and hole ensembles obey distributions with most likely probability, which means with the maximum number of respective micro-states. This in turn justifies introducing the scalar magnitude 'temperature'.

In inorganic semiconductors this condition of fast intraband relaxation[18] after excitation, compared to recombination life times is easily met with $\tau_\mathbf{k}$ and τ_ϵ

[18]Due to the $\epsilon(\mathbf{k})$ relation in crystals, wave-vector and energy relaxation times are in general not equal, $\tau_k \neq \tau_\epsilon$.

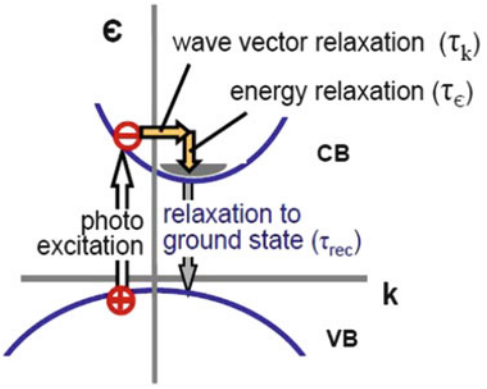

Fig. 4.20 Schematic energy–wave vector diagram $\epsilon = \epsilon(k)$ with relaxation of 'hot' photo excited electrons within relaxation times τ_ϵ for energy and τ_k wave vector. As a consequence of general behavior of $\epsilon = \epsilon(k) \neq \hbar^2 k^2/2m^*$, relaxation times for energy and wave vector are different $\tau_\epsilon \neq \tau_k$. An analogous consideration is valid for 'hot' holes in the valence band

of the order of $(10^{-12} - 10^{-13})$ s [8, 10, 11] whereas, dependent on the type of semiconductor, recombination life times[19] usually $\tau_{\text{rec}} > 10^{-9}$ s (see Fig. 4.20). In other words, electrons in CB and holes in VB exchange wave vector and energy comparatively fast by scattering with their 'companions' and with the lattice (phonons), so that their distributions can be formulated with a single temperature, valid for electrons, for holes, and for phonons. The description of electron and hole concentrations under these conditions, departing from thermal equilibrium, bases upon Fermi statistics with individual Fermi levels for the charges in the respective bands of the excited states, such as electrons in CB and holes in VB.[20]

We calculate the position of quasi-Fermi levels of electrons ϵ_{Fn} and of holes ϵ_{Fp} from their entire concentrations in the conduction and in the valence band; since the energetic regime of the occupation in the bands ($\sim 3kT$) is small compared to the width of the bands (some eV) we may approximate the densities of state $D_{\text{CB}}(\epsilon)$ and $D_{\text{VB}}(\epsilon)$ by the respective square root dependence on energy and moreover replace the Fermi distribution by the classical Boltzmann energy distribution function valid

[19]For recombination lifetimes as small as the intraband relaxation times, we do not need to consider such semiconductors for photovoltaic applications since the photoexcited state is not conserved sufficiently long and thus the splitting of the quasi-Fermi levels becomes negligible.

[20]Whereas the densities of electrons in CB and of holes in VB are formulated with quasi-Fermi distribution functions, their counterparts, the electrons in VB and the holes in CB are derived via conservation of states $n_{\text{VB}}(\epsilon) = D_{\text{VB}}(\epsilon)\left[1 - f_{\text{p}}(\epsilon, \epsilon_{\text{Fp}})\right]$, and $p_{\text{CB}}(\epsilon) = D_{\text{CB}}(\epsilon)\left[1 - f_{\text{n}}(\epsilon, \epsilon_{\text{Fn}})\right]$.

for the low-density limit

$$
\begin{aligned}
n_{\mathrm{CB}} = n_0 + \Delta n &= \int_{\epsilon_{\mathrm{C}}}^{\infty} D_{\mathrm{CB}}(\epsilon)\, \frac{1}{\exp\left(\frac{\epsilon - \epsilon_{\mathrm{Fn}}}{kT}\right) + 1} \mathrm{d}\epsilon \\
&= \int_{\epsilon_{\mathrm{C}}}^{\infty} \left(\frac{2m_n^*}{\hbar^2}\right)^{3/2} \frac{1}{2\pi^2} \sqrt{\epsilon - \epsilon_{\mathrm{C}}} \left[\exp\left(-\frac{\epsilon - \epsilon_{\mathrm{F}}}{kT}\right) \exp\left(-\frac{\epsilon_{\mathrm{F}} - \epsilon_{\mathrm{Fn}}}{kT}\right)\right] d\epsilon \\
&= N_{\mathrm{C}} \exp\left(-\frac{\epsilon_{\mathrm{C}} - \epsilon_{\mathrm{F}}}{kT}\right) \exp\left(-\frac{\epsilon_{\mathrm{F}} - \epsilon_{\mathrm{Fn}}}{kT}\right) \\
&= n_0 \exp\left(\frac{\epsilon_{\mathrm{Fn}} - \epsilon_{\mathrm{F}}}{kT}\right) , \qquad (4.48)
\end{aligned}
$$

together with

$$
\begin{aligned}
p_{\mathrm{VB}} = p_0 + \Delta p &= \int_{-\infty}^{\epsilon_{\mathrm{V}}} D_{\mathrm{VB}}(\epsilon)\, \frac{1}{1 + \exp\left(-\frac{\epsilon - \epsilon_{\mathrm{Fp}}}{kT}\right)} \mathrm{d}\epsilon \\
&= \int_{-\infty}^{\epsilon_{\mathrm{V}}} \left(\frac{2m_p^*}{\hbar^2}\right)^{3/2} \frac{1}{2\pi^2} \sqrt{\epsilon_{\mathrm{V}} - \epsilon} \left[\exp\left(\frac{\epsilon - \epsilon_{\mathrm{F}}}{kT}\right) \exp\left(\frac{\epsilon_{\mathrm{F}} - \epsilon_{\mathrm{Fp}}}{kT}\right)\right] d\epsilon \\
&= N_{\mathrm{V}} \exp\left(-\frac{\epsilon_{\mathrm{F}} - \epsilon_{\mathrm{V}}}{kT}\right) \exp\left(\frac{\epsilon_{\mathrm{F}} - \epsilon_{\mathrm{Fp}}}{kT}\right) \\
&= p_0 \exp\left(\frac{\epsilon_{\mathrm{F}} - \epsilon_{\mathrm{Fp}}}{kT}\right) , \qquad (4.49)
\end{aligned}
$$

and hence

$$
\epsilon_{\mathrm{Fn}} = \epsilon_{\mathrm{F}} + kT \ln\left[\frac{n_{\mathrm{CB}}}{n_0}\right] . \qquad (4.50)
$$

Equivalently,

$$
\epsilon_{\mathrm{Fp}} = \epsilon_{\mathrm{F}} + kT \ln\left[\frac{\mathrm{p}_0}{p_{\mathrm{VB}}}\right] = \epsilon_{\mathrm{F}} - kT \ln\left[\frac{\mathrm{p}_{\mathrm{VB}}}{p_0}\right] , \qquad (4.51)
$$

which leads to the splitting of the quasi-Fermi levels, indicating the usable work to be delivered from the electron–hole system, viz., the chemical potential μ_{np} of this ensemble

$$
\epsilon_{\mathrm{Fn}} - \epsilon_{\mathrm{Fp}} = \Delta\epsilon_{\mathrm{F}} = \mu_{\mathrm{np}} = kT \ln\left[\frac{n_{\mathrm{CB}}\, p_{\mathrm{VB}}}{n_0\, p_0}\right] = kT \ln\left[1 + \frac{\Delta n\, \Delta p}{n_0\, p_0}\right] . \qquad (4.52)
$$

Of course, for a thermal equilibrium occupation of valence and conduction band, one obtains

$$\mu_{\mathrm{np},0} = kT \ln \left[\frac{n_0 p_0}{n_0 p_0} \right] = 0 \, .$$

Commonly n_{CB} and p_{VB} both increase with photo excitation where Δn and Δp may depend on some power ξ of the light flux $\Phi(\Delta n \Delta p \sim \Phi^{\xi})$ where ξ is indicating the type of recombination kinetics.

4.2.3 *Electronic Band System Exposed to Solar Radiation*

We expose an ideal electronic band system, kept at temperature $T_{\mathrm{abs}} = T_{\mathrm{Earth}}$ and electrically completely isolated, to sunlight. Due to the system's ideal properties only radiative transitions for excitation as well as for recombination of charge carriers between VB and CB are allowed as shown schematically in Fig. 4.21. Since charges are neither removed from the absorbing system nor injected into it, this operation[21] represents in terms of stationary carrier concentrations in the bands the maximum departure from thermal equilibrium, or in other words the highest level of photo excitation.

With complete intraband carrier relaxation after photo excitation we express the balance of the solar photons sent to the absorber and the photons emitted from the absorber as a consequence of the radiative recombination. Solar photons with energy beyond the band gap $\hbar\omega \geq (\epsilon_{\mathrm{C}} - \epsilon_{\mathrm{V}}) = \epsilon_{\mathrm{g}}$, are completely absorbed, reflection of these photons is excluded. The photoexcited stationary state of the electron–hole ensemble is characterized by its chemical potential $\mu_{\mathrm{np}} = (\epsilon_{\mathrm{Fn}} - \epsilon_{\mathrm{Fp}})$ (see Sect. 3.4.9) that equals the chemical potential of the radiation emitted by the

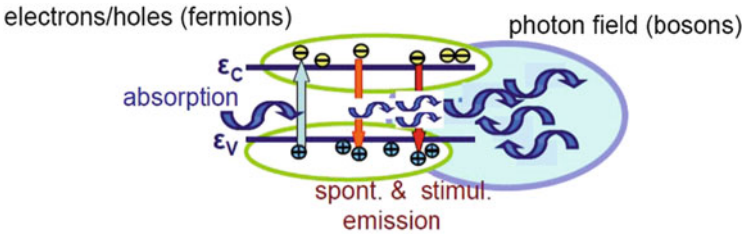

Fig. 4.21 Electronic two-band system in which fermions (electrons and holes) and bosons (photons) are coupled via rate equations for absorption and emission, from which a stationary state for level occupation and the photon density are derived

[21] This mode of operation is called "open circuit".

absorber $\mu_\gamma = \mu_{\mathrm{np}}$. The photon flux from such an excited electron–hole-ensemble may be formulated by the generalization of Planck's radiation equation which expresses the emission of photons [12] by a non-vanishing chemical potential. Accordingly we obtain the photon flux from Sun and Universe into as well as from the absorber to its environment.

$$\frac{\Omega_{\mathrm{in}}}{c_0^2 4\pi^3\hbar^3}\int_{\epsilon_{\mathrm{g}}}^{\infty}\frac{(\hbar\omega)^2}{\exp\left(\dfrac{\hbar\omega}{kT_{\mathrm{Sun}}}\right)-1}\mathrm{d}(\hbar\omega)+\frac{(4\pi-\Omega_{\mathrm{in}})}{c_0^2 4\pi^3\hbar^3}\int_{\epsilon_g}^{\infty}\frac{(\hbar\omega)^2}{\exp\left(\dfrac{\hbar\omega}{kT_{\mathrm{Univ}}}\right)-1}\mathrm{d}(\hbar\omega)$$
$$=\frac{4\pi}{c_0^2 4\pi^3\hbar^3}\int_{\epsilon_{\mathrm{g}}}^{\infty}\frac{(\hbar\omega)^2}{\exp\left(\dfrac{\hbar\omega-\mu_{\mathrm{np,oc}}}{kT_{\mathrm{Earth}}}\right)-1}\mathrm{d}(\hbar\omega)\ . \tag{4.53}$$

This relation introduces the light from the Sun, seen under solid angle Ω_{in}, already containing eventual solar light concentration ($\Omega_{\mathrm{in}} \geq \pi\Omega_0$), the radiation from the Universe, almost always negligible, and the light generated in the band system emitted here into the solid angle $\Omega_{\mathrm{out}} = 4\pi$. The entire radiation emitted by the absorber with $T_{\mathrm{abs}} = T_{\mathrm{Earth}} \ll T_{\mathrm{Sun}}$ has to equalize the photon input from the Sun which goes with T_{Sun}^4. The particular increase of the emission of the absorber by the according factor of $(T_{\mathrm{Sun}}/T_{\mathrm{Earth}})^4 = (20)^4 = 1.6\times10^5$ is formally provided (in the denominator of the exponential function of the integral on the right hand side above) by the chemical potential of the electron–hole system $\mu_{\mathrm{np,oc}}$.

In an attempt to visualize the conservation of the particle fluxes, we introduce the photon flux $\Gamma_{\gamma,\mathrm{in}}(T_{\mathrm{Sun}})$ from the Sun into a volume element $\mathrm{d}V$ of the absorber,[22] the photon flux emitted from the absorber $\Gamma_{\gamma,\mathrm{out}}(T_{\mathrm{abs}},\mu)$. In open-circuit conditions any charge flux from or to the absorber, maintained by electrons and/or holes and resulting in an electric current density Γ_{el} is ruled out. The conservation of photon fluxes sketched schematically in Fig. 4.22 then reads:

$$\Gamma_{\gamma,\mathrm{in}} = \Gamma_{\gamma,\mathrm{out}}\ . \tag{4.54}$$

For this flow balance, the conservation of the etendue ε_i (radiance) [13] of the photon flows [14] is not necessarily conserved ($\Omega_{\mathrm{in}} < \Omega_{\mathrm{out}}$).

Although not mentioned explicitly, the excess energy of solar photons transferred to electrons and holes and converted into heat during fast relaxation has to be removed from the absorber in order to keep it at constant ambient temperature $T_{\mathrm{abs}} = T_{\mathrm{Earth}}$.

[22] Here it is assumed that each photon with energy beyond the threshold for absorption, viz., $\hbar\omega \geq \epsilon_{\mathrm{g}} = \epsilon_{\mathrm{C}} - \epsilon_{\mathrm{V}}$, generates one electron–hole pair, which recombines after a certain time and creates one photon. Any nonlinear generation and/or recombination process, such as impact ionization and Auger recombination, is neglected.

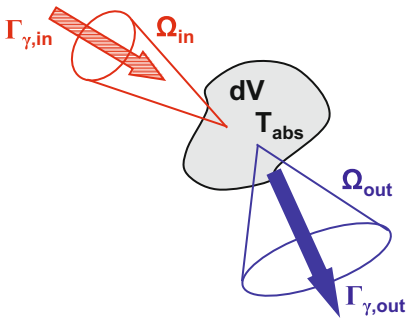

Fig. 4.22 Conservation of the photon fluxes $\Gamma_{\gamma,\mathrm{in}} = \Gamma_{\gamma,\mathrm{out}}$ in an ideal electronic band system operated in open circuit

The last integral equation (Eq. (4.53)) serves to determine $\mu_{\mathrm{np,\,oc}}$, as a function of the band gap ϵ_g and of the solar light concentration (Ω_{in}, Ω_{out}), because each of the other variables is in principle given. An approximation[23] for sufficiently large band gaps in comparison with $kT_\mathrm{abs}(300\,\mathrm{K}) = 0.026\,\mathrm{eV}$ and with above all $kT_\mathrm{Sun} = 0.52\,\mathrm{eV}$, hence for $\epsilon_\mathrm{g} \geq 0.5\,\mathrm{eV}$, yields [15]

$$\mu_{\mathrm{np,\,oc}} = \Delta\varepsilon_{\mathrm{F,oc}} = \epsilon_\mathrm{g}\left(1 - \frac{T_\mathrm{abs}}{T_\mathrm{Sun}}\right) + kT_\mathrm{abs}\ln\left[\frac{T_\mathrm{Sun}}{T_\mathrm{abs}}\right] - kT_\mathrm{abs}\ln\left[\frac{\Omega_\mathrm{out}}{\Omega_\mathrm{in}}\right] . \qquad (4.55)$$

[23]The above approximation is based upon neglecting the contribution of photons from the Universe. Despite the large solid angle from which the absorbers might receive such photons, $(4\pi - \Omega_\mathrm{in})$, the low background temperature of the Universe $T_\mathrm{Univ} = 3\,\mathrm{K}$ makes this part negligible. The marginal contribution of photons from stars and the Moon are also neglected. The modified balance after replacing the Bose–Einstein distribution function by the Boltzmann energy distribution and assuming the solid angle for emission $\Omega_\mathrm{out} = 4\pi$ becomes

$$\Omega_\mathrm{in}\int_{\epsilon_\mathrm{g}}^{\infty}(\hbar\omega)^2\exp\left(-\frac{\hbar\omega}{kT_\mathrm{Sun}}\right)\mathrm{d}(\hbar\omega)$$
$$= 4\pi\int_{\epsilon_\mathrm{g}}^{\infty}(\hbar\omega)^2\exp\left(-\frac{\hbar\omega - \mu_{\mathrm{np,oc}}}{kT_\mathrm{abs}}\right)\mathrm{d}(\hbar\omega) .$$

Introducing the analytical solution of

$$\int x^2\exp(\beta x)\mathrm{d}x = \left(\frac{x^2}{\beta} + \frac{2x}{\beta^2} + \frac{2}{\beta^3}\right)\exp(\beta x) ,$$

one arrives at

$$\exp\left(\frac{\mu_{\mathrm{np,oc}}}{kT_\mathrm{abs}}\right) = \left(\frac{\Omega_\mathrm{in}}{4\pi}\right)\left(\frac{\epsilon_\mathrm{g}^2 kT_\mathrm{Sun} + 2\epsilon_\mathrm{g}(kT_\mathrm{Sun})^2 + 2(kT_\mathrm{Sun})^3}{\epsilon_\mathrm{g}^2 kT_\mathrm{abs} + 2\epsilon_\mathrm{g}(kT_\mathrm{abs})^2 + 2(kT_\mathrm{abs})^3}\right)\left(\exp\left(-\frac{\epsilon_\mathrm{g}}{kT_\mathrm{Sun}} + \frac{\epsilon_\mathrm{g}}{kT_\mathrm{abs}}\right)\right) ,$$

and finally one obtains

$$\mu_{\mathrm{np,oc}} = kT_\mathrm{abs}\ln\left[\frac{\Omega_\mathrm{in}}{4\pi}\frac{kT_\mathrm{Sun}}{kT_\mathrm{abs}}\exp\left(-\frac{\epsilon_\mathrm{g}}{kT_\mathrm{Sun}} + \frac{\epsilon_\mathrm{g}}{kT_\mathrm{abs}}\right)\right] .$$

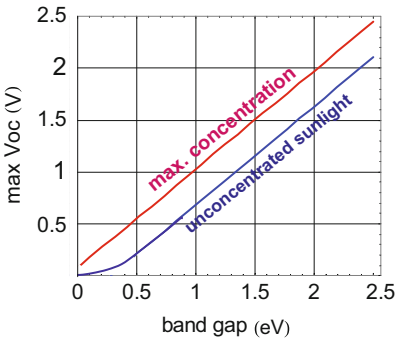

Fig. 4.23 Maximum achievable electron–hole chemical potential μ_{np} indicating maximum achievable open-circuit voltage $eV_{oc} \leq \mu_{np}$ versus optical threshold energy (band gap) under solar radiation without and with maximum concentration (ideal electronic band system at $T = 300\,\mathrm{K}$)

The above result represents the chemical potential, or the splitting of the Fermi levels in a spatially homogeneous volume element without carrier extraction or injection, and consequently describes the behavior in open-circuit operation (subscript oc).

The first term of the relation contains the optical band gap ϵ_g, which is modified by a sort of Carnot factor. Numerically, for $T_{abs} = T_{Earth} = 300\,\mathrm{K}$, it yields $0.95\epsilon_g$. The second term relates to the kinetic energies of the carriers that adds to ϵ_C and to ϵ_V resp., while the third and last term reflects the light flux in and vanishes for maximum solar light concentration $\Omega_{in} = \Omega_{out} = 4\pi$; it becomes negative for any lower concentration $\Omega_{in} < \Omega_{out}$. For no concentration of sunlight we get $\Omega_{in} = \pi\Omega_0 = 6.67 \times 10^{-5}$ and $\Omega_{out} = 4\pi$; and finally we arrive with $-kT_{abs} \ln[\Omega_{out}/\Omega_{in}] = -0.382\,\mathrm{eV}$. The numerical solution of $\Delta\epsilon_F = \Delta\epsilon_F\left(\epsilon_g, T_{abs} = 300\,\mathrm{K},\ T_{Sun} = 6{,}000\,\mathrm{K}\right)$ is displayed in Fig. 4.23 for the two extreme situations, sunlight without and with maximum concentration.

4.2.4 *Carrier Extraction From an Illuminated Electronic Band System*

The extraction of charges from an illuminated band system causes a drop in the internal excess densities, which in turn reduces the chemical potential $\mu_{np} = (\epsilon_{Fn} - \epsilon_{Fp})$ of the electron–hole ensemble. As the chemical potential μ_{np} depends logarithmically on the excess carrier concentration, the rate of the extracted excess charges, say the current density depends exponentially on μ_{np}. On the other hand, the chemical potential of the electron–hole-ensemble representing the 'work' the carriers are able to perform may be interpreted likewise as product of elementary charge and voltage, $e \cdot V$, establishing at ideal contacts of the system.

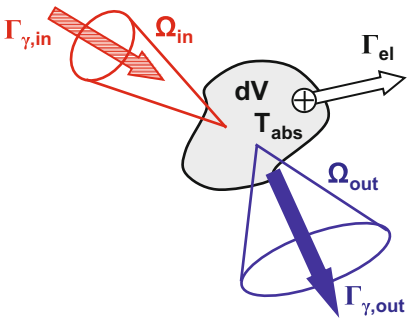

Fig. 4.24 Fluxes of photons and charges to and from a volume element of an ideal absorber in the radiative limit

A convincingly easy derivation of the dependence of the electric output current density (flux of charges) versus voltage of an ideal photovoltaic converter [24] is based upon the balance of fluxes of photons and charges. We assume an input photon flux from the Sun $\Gamma_{\gamma,\mathrm{in}}(T_{\mathrm{Sun}})$, an output photon flux emitted from the photo excited band system $\Gamma_{\gamma,\mathrm{out}}(T_{\mathrm{abs}}, \mu_{\mathrm{np}})$, and a charge flux (electric current density) $\Gamma_{\mathrm{el}}(\mu_{\mathrm{np}})$. The photon fluxes $\Gamma_{\gamma,\mathrm{in}}(T_{\mathrm{Sun}})$, $\Gamma_{\gamma,\mathrm{out}}(T_{\mathrm{abs}}, \mu_{\mathrm{np}})$, of course, depend on the corresponding solid angles for coupling light in and out, Ω_{in}, Ω_{out}.

The flux balance of this radiative limit schematically displayed in Fig. 4.24 reads

$$\Gamma_{\gamma,\mathrm{in}}(T_{\mathrm{Sun}}) = \Gamma_{\gamma,\mathrm{out}}(T_{\mathrm{abs}}, \mu_{\mathrm{np}}) + \Gamma_{\mathrm{el}}(\mu_{\mathrm{np}}) \tag{4.56}$$

In our approach the particle flux balance is met whereas the energy fluxes do not balance since the solar photons are substantially 'hotter' than the photons emitted from the absorber ($T_{\mathrm{Sun}} \gg T_{\mathrm{abs}}$).

We express the solar photon flux as thermal equilibrium radiation hitting the absorber in the solid angle Ω_{in} [25]

$$\Gamma_{\gamma,\mathrm{in}}(T_{\mathrm{Sun}}) = \left(\frac{\Omega_{\mathrm{in}}}{c_0^2 4\pi^3\hbar^3}\right)\int_{\epsilon_{\mathrm{g}}}^{\infty} \frac{(\hbar\omega)^2}{\exp\left(\frac{\hbar\omega}{kT_{\mathrm{Sun}}}\right) - 1} d\,(\hbar\omega) \tag{4.57}$$

as well as the photons emitted by the absorber into the solid angle Ω_{out}

$$\Gamma_{\gamma,\mathrm{out}}(T_{\mathrm{abs}}, \mu_{\mathrm{np}}) = \left(\frac{\Omega_{\mathrm{out}}}{c_0^2 4\pi^3\hbar^3}\right)\int_{\epsilon_{\mathrm{g}}}^{\infty} \frac{(\hbar\omega)^2}{\exp\left(\frac{\hbar\omega - \mu_{\mathrm{np}}}{kT_{\mathrm{abs}}}\right) - 1} d\,(\hbar\omega) \tag{4.58}$$

[24] Ideal here means that all solar photons arriving at the absorber are absorbed (no reflection of solar light); absorption of one photon generates one electron–hole pair and vice versa for recombination and light emission.

[25] Here we have again neglected the photon contribution from the environment/Universe.

and the electric charge leaving the absorber

$$\Gamma_{\mathrm{el}}(\mu_{\mathrm{np}}) = \frac{1}{e} j_{\mathrm{el}}^{*}(\mu_{\mathrm{np}}) \tag{4.59}$$

with $j_{\mathrm{el}}^{*}(\mu_{\mathrm{np}})$ designating the electric output current density of the absorber and elementary charge $e = 1.6 \times 10^{-19}\mathrm{As}$.

After rearranging the relation of the flux balance we arrive at an explicit relation for

$$\begin{aligned}\Gamma_{\mathrm{el}}(\mu_{\mathrm{np}}) = &\left[\left(\frac{\Omega_{\mathrm{in}}}{c_0^2 4\pi^3\hbar^3}\right)\int_{\epsilon_{\mathrm{g}}}^{\infty}\frac{(\hbar\omega)^2}{\exp\left(\frac{\hbar\omega}{kT_{\mathrm{Sun}}}\right)-1}d\,(\hbar\omega)\right] \\ &-\left[\left(\frac{\Omega_{\mathrm{out}}}{c_0^2 4\pi^3\hbar^3}\right)\int_{\epsilon_{\mathrm{g}}}^{\infty}\frac{(\hbar\omega)^2}{\exp\left(\frac{\hbar\omega-\mu_{\mathrm{np}}}{kT_{\mathrm{abs}}}\right)-1}d\,(\hbar\omega)\right]\end{aligned} \tag{4.60}$$

The first term on the right side of this relation represents the solar light input and is given with the adjustable solid angle Ω_{in} and the parameter, optical band gap ϵ_{g}; we abbreviate this term by $A(\Omega_{\mathrm{in}}, \epsilon_{\mathrm{g}})$:

$$A = \left(\frac{\Omega_{\mathrm{in}}}{c_0^2 4\pi^3\hbar^3}\right)\int_{\epsilon_{\mathrm{g}}}^{\infty}\frac{(\hbar\omega)^2}{\exp\left(\frac{\hbar\omega}{kT_{\mathrm{Sun}}}\right)-1}d\,(\hbar\omega)\,.$$

The second term contains the only variable, the chemical potential μ_{np} of the electron–hole ensemble. With approximation of the Boltzmann-energy distribution this term simplifies

$$\begin{aligned}&\left(\frac{\Omega_{\mathrm{out}}}{c_0^2 4\pi^3\hbar^3}\right)\int_{\epsilon_{\mathrm{g}}}^{\infty}\frac{(\hbar\omega)^2}{\exp\left(\frac{\hbar\omega-\mu_{\mathrm{np}}}{kT_{\mathrm{abs}}}\right)-1}d\,(\hbar\omega) \\ &\approx\left(\exp\left(\frac{\mu_{\mathrm{np}}}{kT_{\mathrm{abs}}}\right)\right)\left(\frac{\Omega_{\mathrm{out}}}{c_0^2 4\pi^3\hbar^3}\right)\int_{\epsilon_{\mathrm{g}}}^{\infty}(\hbar\omega)^2\exp\left(-\frac{\hbar\omega}{kT_{\mathrm{abs}}}\right)d\,(\hbar\omega) \\ &= B\exp\left(\frac{\mu_{\mathrm{np}}}{kT_{\mathrm{abs}}}\right)\end{aligned} \tag{4.61}$$

to arrive at

$$j_{\mathrm{el}}^{*}(\mu_{\mathrm{np}}) = e\left[A - B\exp\left(\frac{\mu_{\mathrm{np}}}{kT_{\mathrm{abs}}}\right) - 1\right]. \tag{4.62}$$

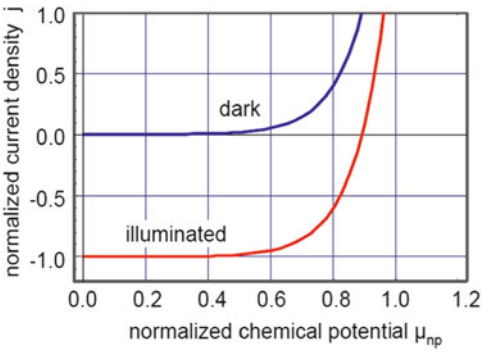

Fig. 4.25 Current density–voltage (j–V) relation for illuminated and non-illuminated ideal electronic band system at $T = 300\,\mathrm{K}$

We keep in mind that $B = B(\epsilon_\mathrm{g})$ and rewrite the upper equation and approximate[26]

$$\begin{aligned} j^*_\mathrm{el}(\mu_\mathrm{np}) &= -e\left[B\left(\exp\left(\frac{\mu_\mathrm{np}}{kT_\mathrm{abs}}\right)-1\right)-(A-B)\right] \\ &\approx -e\left[B\left(\exp\left(\frac{\mu_\mathrm{np}}{kT_\mathrm{abs}}\right)-1\right)-A\right]. \end{aligned} \tag{4.63}$$

Commonly such band systems like all electronic devices are formally treated as consuming elements with current input by convention defined positive. In order to align to this description we finally write the **input** electric current density $j(\mu_\mathrm{np})$

$$j(\mu_\mathrm{np}) = -j^*_\mathrm{el}(\mu_\mathrm{np}) = e\left[B\left(\exp\left(\frac{\mu_\mathrm{np}}{kT_\mathrm{abs}}\right)-1\right)-A\right]. \tag{4.64}$$

The comparison of the latter equation with the well known current density-voltage relation of an illuminated ideal diode, displayed in Fig. 4.25, which reads

$$j = j_0\left[\exp\left(\frac{eV}{kT}\right)-1\right]-j_\mathrm{phot} \tag{4.65}$$

shows the identity of both relations. Here, j_0 and j_phot are reverse saturation and photo current density, resulting from the minority carriers in the dark (j_0) and from those under light (j_phot). In our case the magnitude B represents the rate of the radiative recombinations in the dark at vanishing μ_np, being associated with the thermal equilibrium density of the minority carriers, whereas A contains the entire rate of transitions of the absorption under sunlight which equals the rate of the extracted charges in short circuit operation (subscript *sc*), where the current $j_\mathrm{sc} = -j_\mathrm{phot}$.

[26] We approximate $-(A-B) \approx -A$ since $A \gg B$.

It is worthwhile noting that this relation for an illuminated ideal photovoltaic converter has been derived on the basis of the balance of photons and electric charges in an electronic band system without any ingredients of semiconductor device physics.

The curved shape of the j–μ_{np} relation is exclusively determined by the temperature of the absorber T_{abs}, implying that the resulting function is purely governed by thermodynamic and statistical physics considerations.

Furthermore, by the ansatz that the current density j_{el} is formulated in terms of rates for absorption of photons/generation of electrons and holes, and of recombination rates, it has been implicitly assumed that the current instantaneously responds to carrier generation and thus that excess carriers leave the system instantaneously, which would require infinite mobilities or diffusion coefficients. The gradient in chemical potential needed for charge transport under these conditions thus fades away, and in consequence, for sufficient reverse bias, the slope $\mathrm{d}j/\mathrm{d}\mu_{\mathrm{np}} \to 0$.

4.2.5 Ideal Photovoltaic Converter

4.2.5.1 Electronic Design of an Ideal Photovoltaic Converter

An ideal photovoltaic converter meets the condition of exclusively radiative transitions of charges from the relevant excited state to the ground state. This is called the radiative limit. In two-band systems, these processes are transitions of electrons from the conduction band CB to the valence band VB, which are equivalent to transitions of holes from the valence band into conduction band states. The best option for photon receivers in this respect, at variance with doped semiconductors, are intrinsic absorbers [15], which in the ideal case show zero density of states between valence and conduction band[27] (Fig. 4.26). These intrinsic absorbers should be equipped with 'entropy-free' leads (called membranes) [15] which simultaneously provide photoexcited excess electrons and holes moving in opposite directions.

The idealized leads may be imagined as a high band gap n-type semiconductor at the electron exit, perfectly aligning the edge of the conduction band and an analogous p-type one at the hole exit, likewise aligning ideally the valence band edge (Fig. 4.27). These leads are assumed to conduct the entire splitting of the quasi-Fermi levels $\mu_{\mathrm{np}} = \epsilon_{\mathrm{Fn}} - \epsilon_{\mathrm{Fp}}$ to the outside, so that the difference in electrical potential at the borders of the absorber, say the output voltage reads $\epsilon_{\mathrm{Fn}} - \epsilon_{\mathrm{Fp}} = e \cdot V$.

The 'no-entrance' condition may be realized by appropriately high barriers for electrons $\Delta\epsilon_{\mathrm{C}}$ at the hole exit and for holes $\Delta\epsilon_{\mathrm{V}}$ the electron exit. Due to the

[27] Here we neglect the fact that, for thermodynamic reasons, any crystal at temperature $T > 0$ will contain a certain amount of defects, such as point defects, dislocations, interstitial site occupation, etc., not to mention unavoidable chemical impurities.

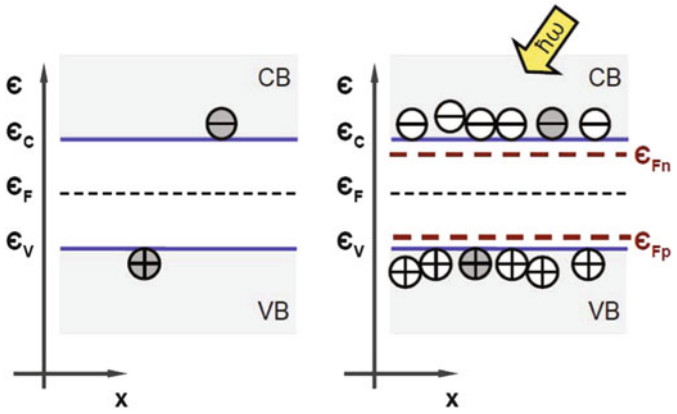

Fig. 4.26 Band diagram of an intrinsic ideal electronic two-band absorber with schematically displayed carrier concentrations in CB and VB in dark *(left)* and under illumination with photogenerated carrier densities leading to splitting of quasi-Fermi levels $\epsilon_{Fn} - \epsilon_{Fp}$ *(right)*

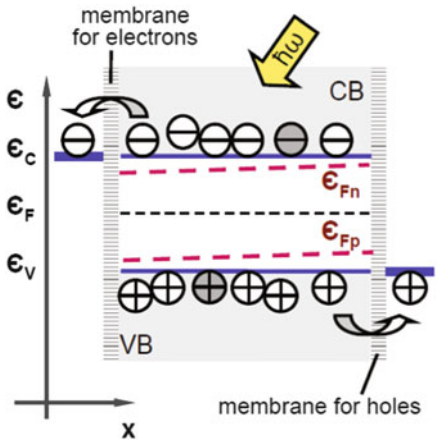

Fig. 4.27 Band diagram of illuminated two-band system with ideal leads for electron (*left side*) and hole extraction (*right side*). The respective transfer to the leads and the according separation of charges is provided by ideal membranes for electrons (at the level of the conduction band edge, ϵ_C) and for holes (at the level of the valence band edge, ϵ_V) (the function of the membranes might be imagined by appropriately doped high-band gap semiconductors (n-type on the *left* and p-type on the *right side*)

resulting comparatively large band gap of the leads, photogeneration is negligible and thus the leads form sinks for the corresponding excess carriers generated in the absorber. Furthermore, the recombination in both sinks is assumed also exclusively radiative, since we have not introduced any defects in these perfect leads.

For charge transport in the absorber, assumed ideally as well, we would need no gradients in quasi-Fermi levels, whereas in reality for transport with scattering of

carriers (and subsequent momentum and wave vector relaxation and corresponding energy dissipation), a gradient in quasi-Fermi levels is required, whence the external splitting of the quasi-Fermi levels detectable as an external voltage V is reduced (schematically indicated by weak slopes of ϵ_{Fn} and ϵ_{Fp} in Fig. 4.27).

The idealized leads produce another set of beneficial effects on the excess carrier densities, in particular, separating the absorption regime from unavoidable metal contacts and thereby preventing the photogenerated charges from 'feeling' the vanishing lifetime in the metal ($\tau_{\mathrm{intraband}} \approx 10^{-13}\,\mathrm{s}$), which commonly attracts excess carriers for recombination and in turn causes the splitting of the absorber quasi-Fermi level to suffer from surface recombination. On the other hand, in the absorber and the leads also infinite carrier mobilities/diffusion coefficients are assumed to rule out gradients of the quasi-Fermi levels commonly needed for charge transport.

4.2.5.2 Output Power and Efficiency Limit of an Ideal Photovoltaic Converter

The determination of the upper limit of the efficiency of a photovoltaic converter published by Shockley and Queisser [16] and attempted in a somewhat simpler form even earlier by Trivich and Flinn [17] relates the maximum of the electric output power density

$$p_{\mathrm{el}} = \frac{\mu_{\mathrm{np}}}{e} j(\mu_{\mathrm{np}}) = V \cdot j(V) \tag{4.66}$$

to the power of the solar light $\Gamma_{\epsilon,\mathrm{Sun}}$ fed to the converter

$$\Gamma_{\epsilon,\mathrm{Sun}} = \frac{\Omega_{\mathrm{in}}}{c_0^2 4\pi^3\hbar^3} \int_{\epsilon_{\mathrm{g}}}^{\infty} \frac{(\hbar\omega)^3}{\exp\left(\dfrac{\hbar\omega}{kT_{\mathrm{Sun}}}\right) - 1} \mathrm{d}(\hbar\omega)\ .$$

Of course, the chemical potential $\mu_{\mathrm{np}} = \mu_{\mathrm{np}}(j)$ as well as the electric output current density j are dependent on the optical band gap ϵ_{g} of the absorber.

The electrical output current density j is nonlinearly related to the voltage ($V = \mu_{\mathrm{np}}(j)/e$) as implicitly given in Sect. 4.2.4 particularly in Eq. (4.61), and the electric output power in addition competes via μ_{np} with the radiation emitted by the absorber due to radiative recombination of excess carriers. The maximum electric current density to be supplied by the absorber to the outside corresponds to the entirely absorbed solar photon flux (abbreviated by term $A(\epsilon_{\mathrm{g}})$) and elementary charge e

$$j_{\mathrm{max}} = e \frac{\Omega_{\mathrm{in}}}{c_0^2 4\pi^3\hbar^3} \int_{\epsilon_{\mathrm{g}}}^{\infty} \frac{(\hbar\omega)^2}{\exp\left(\dfrac{\hbar\omega}{kT_{\mathrm{Sun}}}\right) - 1} \mathrm{d}(\hbar\omega)\ .$$

This maximum current density is associated with vanishing difference in chemical potential, accordingly also with vanishing radiative recombination of excess carriers,[28] and in the language of the $j - V$-curve of the illuminated system is named short-circuit current density

$$j(V = 0) = j_{\mathrm{sc}} = -j_{\mathrm{phot}}.$$

We remember the ingredients we have made use of for this formal procedure:

- independent electron picture (no interaction between electrons),
- temperature of absorber is strongly coupled to a large and stable temperature reservoir, here $T = T_{\mathrm{Earth}} = 300\,\mathrm{K}$,
- stationary state, implying no transient effects, e.g., for 'hot' carrier extraction,
- complete absorption of photons with energy above band gap ($\hbar\omega \geq \epsilon_{\mathrm{g}}$),
- each absorbed photon generates an electron–hole pair that is separated appropriately and both, electron and hole contribute to the photocurrent with unit probability (collection efficiency),
- depth profile of photogenerated charges is neglected (flat/homogeneous excess density),
- the assumed ideal collection of photo generated electrons and holes requires infinite mobility/infinite diffusion coefficient,
- ideal leads to the absorber (no influence of contacts to initiate recombination at lead/contact interface),

and furthermore some simplifications of minor importance, such as

- pressure of photons (in terms of wave vectors) has not been included in the balance,
- no red- or blueshift of photons escaping from the solar, or entering the terrestrial gravitational field.

This upper limit for the efficiency of photovoltaic conversion (η, here named η_{SQ}) has been derived by Shockley and Queisser [16] in an equivalent approach like ours above, on the basis of the detailed balance of flows of photons and charges.

Figure 4.28 depicts this efficiency η_{SQ} versus the optical band gap for different factors of sunlight concentration $C = 1$; $C = 400$; and $C = C_{\mathrm{max}} = 1.88 \times 10^5$ (corresponding to $\Omega_{\mathrm{in}} = \pi\Omega_0 = 6.67 \times 10^{-5}$; 2.67×10^{-2}; and 4π, while for the emission we select $\Omega_{\mathrm{out}} = 4\pi$) as derived from

$$\eta_{\mathrm{SQ}} = \frac{\mu_{\mathrm{np}}(j)\, j_0 \left[\exp\left(\dfrac{\mu_{\mathrm{np}}(j)}{kT_{\mathrm{abs}}}\right) - 1\right]}{\dfrac{\Omega_{\mathrm{in}}}{c_0^2 4\pi^3\hbar^3}\displaystyle\int_{\epsilon_{\mathrm{g}}}^{\infty} \frac{(\hbar\omega)^3}{\exp\dfrac{\hbar\omega}{kT_{\mathrm{Sun}}} - 1}\,\mathrm{d}(\hbar\omega)}\,. \tag{4.67}$$

[28] In this mode of operation the absorber only emits thermal equilibrium radiation, as it is kept at ambient temperature by an appropriate heat reservoir.

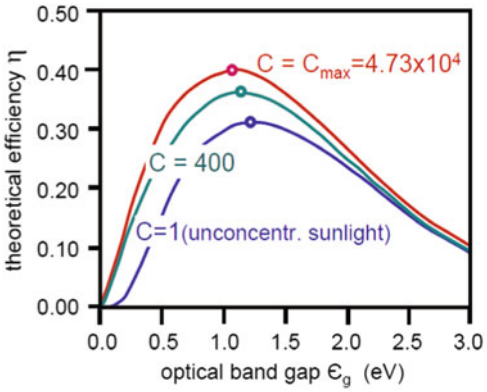

Fig. 4.28 Theoretical efficiency for photovoltaic solar energy conversion with absorber kept at $T = 300\,\mathrm{K}$ versus optical band gap for different levels of solar light concentration C. The solar insolation here refers to AM0 spectral and total light flux. The reader should not be confused when finding different maximum theoretical efficiency numbers. These are due to different spectral and total light fluxes, such as the recently introduced artificial AM1.5 spectrum of the National Renewable Energy Lab (NREL), a US governmental institution in Golden, CO

After replacing the reverse saturation current density j_0 by the thermal equilibrium photon flux of the absorber, viz.,

$$j_0 = \left(\frac{\Omega_{\mathrm{out}}}{c_0^2 4\pi^3 \hbar^3}\right) \int_{\epsilon_\mathrm{g}}^{\infty} (\hbar\omega)^2 \exp\left(-\frac{\hbar\omega}{kT_{\mathrm{abs}}}\right) d\,(\hbar\omega)$$

and introducing the implicitly expressed $\mu_{\mathrm{np}}(j)$ (Sect. 4.2.4, Eq. (4.61)) one obtains the numerical solution for

$$\eta_{\mathrm{SQ}} = \eta_{\mathrm{SQ}}\left(\epsilon_\mathrm{g}, \Omega_{\mathrm{in}}, T_{\mathrm{abs}}\right) \ . \tag{4.68}$$

This radiative limit with efficiency η_{SQ} takes into account:

- the loss of photon excess energies $\hbar\omega > \epsilon_\mathrm{g}$, which are transferred to the electron–hole ensemble as a consequence of the extremely short relaxation times to be deposited as heat in the lattice, from which it has to be removed instantaneously to keep the absorber at environmental temperature (T_{Earth}).
- the lack of energy of photons not absorbed with $\hbar\omega < \epsilon_\mathrm{g}$.
- the considerable departure of the product of current and 'voltage' $j \cdot V$, even at its maximum (maximum power point), from maximum achievable $V = V_{\mathrm{oc}}$ times maximum achievable $j = j_{\mathrm{sc}}$ due to the bending of the j–V curve resulting from absorber temperatures $T > 0$.

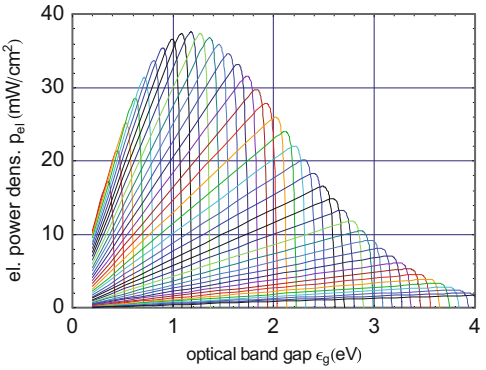

Fig. 4.29 Electric power density $p_{\mathrm{el}} = j_{\mathrm{el}} \cdot V$ (product of current density and voltage) as a function of the band gap ϵ_{g} of an AM0-illuminated ideal photovoltaic converter at $T = 300\,\mathrm{K}$. The envelope curve gives the respective maxima of electric output power density for varying 'voltages' (μ_{np}), while the ratio $p_{\mathrm{el}}/p_{\mathrm{Sun}}$ yields the efficiency η. The maximum theoretical efficiency of a single-absorber structure at illumination with non-concentrated sunlight (AM0) is $\eta_{\mathrm{max,AM0}} = \eta(\epsilon_{\mathrm{g}} \approx 1.25\,\mathrm{eV}) = 0.29$

Figure 4.29 shows the electric output power density p_{el} at $T = 300\,\mathrm{K}$ and under AM0 insolation[29] as a function of the band gap ϵ_{g} for varying output chemical potentials $\mu_{\mathrm{np}} = e \cdot V$; the envelope of the individual curves represents the maximum output power density. The division of the respective output power by the radiation input power translates the number into the maximum achievable efficiency of a one-absorber system in the radiative limit. In particular, for terrestrial conditions (300 K, non-concentrated sunlight) and an absorber with a band gap $\epsilon_{\mathrm{g}} \approx 1.25\,\mathrm{eV}$ one gets $\eta_{\mathrm{SQ,opt}} = 0.29$.

4.2.5.3 Characteristic Magnitudes of the j–μ Relation

The above j–V relation reveals three specific modes for operating a photovoltaic converter running as a power generator, i.e., in the fourth quadrant of Fig. 4.25:

- at maximum (negative) output current density $j(V = 0) = j_{\mathrm{sc}} = -j_{\mathrm{phot}}$ (called the short-circuit current density), where each of the photogenerated carriers is extracted from the absorber 'instantaneously' after generation and the internal carrier density consists solely of the thermal equilibrium concentration. In this mode of operation, the electrical output power collapses and this short-circuit current density $j_{\mathrm{sc}} = -j_{\mathrm{phot}}$ varies linearly with the light flux $\Gamma_{\gamma,\mathrm{in}} \sim j_{\mathrm{sc}}$.

[29] AM0 relates to non-concentrated sunlight at the Earth's position without the influence of the atmosphere on the spectral distribution, such as photon energy dependent scattering, absorption, and reflection.

- at vanishing output current density, with $V(j = 0) = V_{oc}$ (open-circuit conditions), a situation in which each photogenerated carrier recombines radiatively in the absorber, the output power disappears once again. The open-circuit voltage derived from the j–V relation for vanishing output current density, viz.,

$$V(j = 0) = V_{oc} = (1/e)(kT) \ln \left[\frac{j_{phot}}{j_0} + 1 \right] ,$$

  for sufficient illumination, rises logarithmically with the light flux $\Gamma_{\gamma,in} \sim j_{phot}$.
- at a particular j–V combination $0 < j < j_{sc}$ or $V_{oc} > V > 0$, the product $j \cdot V$ becomes maximal.[30] The according ratio of the maximum power output $p_{mpp} = j_{mpp} V_{mpp}$ and $j_{sc} V_{oc}$ is called the filling factor:

$$FF = \frac{j_{mpp} V_{mpp}}{j_{sc} V_{oc}} .$$

Maximum power values might be estimated from the derivative of the jV product via

$$p_{el} = jV = \left[j_0 \left(\exp\left(\frac{eV}{kT} \right) - 1 \right) - j_{phot} \right] V , \tag{4.69}$$

with $\mathrm{d}(jV)/\mathrm{d}V = 0$, we get

$$j_0 \left(\exp\left(\frac{eV}{kT} \right) - 1 \right) - j_{phot} + j_0 \frac{eV}{kT} \exp\left(\frac{eV}{kT} \right) =^{!} 0 . \tag{4.70}$$

Recalling that

$$\ln \left[\frac{j_{phot}}{j_0} + 1 \right] = \frac{eV_{oc}}{kT} ,$$

one obtains

$$\exp\left(\frac{eV}{kT} \right) - \exp\left(\frac{eV_{oc}}{kT} \right) + \frac{eV}{kT} \exp\left(\frac{eV}{kT} \right) = 0 ,$$

or

$$\left(\frac{eV}{kT} + 1 \right) \exp\left(\frac{eV}{kT} \right) = \exp\left(\frac{eV_{oc}}{kT} \right) . \tag{4.71}$$

[30] This mode of operation is called 'maximum power point' (mpp).

Finally, we write $V = V_{\mathrm{opt}}$ for maximum power output and arrive at

$$\frac{eV_{\mathrm{opt}}}{kT} + \ln\left[1 + \frac{eV_{\mathrm{opt}}}{kT}\right] = \frac{eV_{\mathrm{oc}}}{kT} \,.$$

Instead of $\ln\left[1 + eV_{\mathrm{opt}}/kT\right]$, we approximate by the 'worst case' condition

$$\ln\left[1 + \frac{eV_{\mathrm{oc}}}{kT}\right] \geq \ln\left[1 + \frac{eV_{\mathrm{opt}}}{kT}\right] \,,$$

and obtain

$$V_{\mathrm{opt}} \geq V_{\mathrm{oc}} - (1/e)\, kT \ln\left[1 + \frac{eV_{\mathrm{oc}}}{kT}\right] \,. \tag{4.72}$$

With common solar cells at $T = 300\,\mathrm{K}$ corresponding to $k \cdot 300\,\mathrm{K} \approx 0.026\,\mathrm{eV}$ and under AM0 illumination, one gets $eV_{\mathrm{oc}} = (0.5 \ldots 1)\,\mathrm{eV}$ and for the natural logarithm $\ln[1 + (20 \ldots 40)] \approx 3$, whence the maximum power point V_{mpp} reads

$$V_{\mathrm{mpp}} = V_{\mathrm{opt}} \approx V_{\mathrm{oc}} - (3kT)/e \,. \tag{4.73}$$

4.2.5.4 Theoretical Efficiency Versus Light Flux

The electric power output of such an ideal configuration is based upon the product of the current density $j(V)$ and the voltage V. Indicating the maximum value of this product with 'maximum power point' (the subscript mpp), this output power reads $p = \mu_{\mathrm{mpp}} j_{\mathrm{mpp}}/e$. The link with the characteristic magnitudes of the open-circuit voltage V_{oc} and the short-circuit current density j_{sc} is commonly provided by another characteristic magnitude called the filling factor, defined above by which quantifies how well the rectangle spanned by V_{mpp} and j_{mpp} is filling out the j–V curve with V_{oc} and j_{sc} (see the sketch in Fig. 4.30).

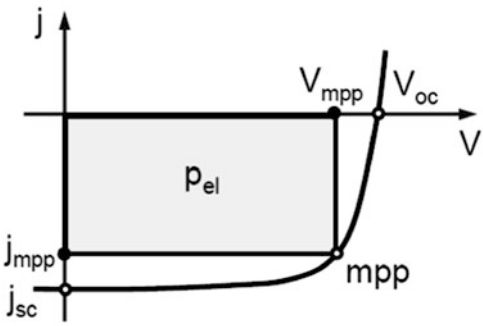

Fig. 4.30 Current density–voltage curve of an illuminated ideal photovoltaic solar energy converter showing characteristic magnitudes like short-circuit current density j_{sc}, open-circuit voltage V_{oc}, and maximum power point mpp. The ratio $p_{\mathrm{max,el}}/j_{\mathrm{sc}}V_{\mathrm{oc}} = j_{\mathrm{mpp}}V_{\mathrm{mpp}}/j_{\mathrm{sc}}V_{\mathrm{oc}} = \mathrm{FF}$ is called the filling factor

The output power versus the light flux $\Gamma_{\gamma,\mathrm{in}}$ rises stronger than linearly, since $j_{\mathrm{sc}} \sim \Gamma_{\gamma,\mathrm{in}}$ and $V_{\mathrm{oc}} \sim \ln \Gamma_{\gamma,\mathrm{in}}$, so that the efficiency also rises with light flux:

$$\eta \sim \frac{j_{\mathrm{mpp}} V_{\mathrm{mpp}}}{\Gamma_{\gamma,\mathrm{in}}} = \frac{j_{\mathrm{sc}} V_{\mathrm{oc}} \mathrm{FF}}{\Gamma_{\gamma,\mathrm{in}}} \sim \frac{\Gamma_{\gamma,\mathrm{in}} \ln\left[\Gamma_{\gamma,\mathrm{in}}\right] \mathrm{FF}\left(\Gamma_{\gamma,\mathrm{in}}\right)}{\Gamma_{\gamma,\mathrm{in}}} \sim \ln\left[\Gamma_{\gamma,\mathrm{in}}\right] \mathrm{FF}\left(\Gamma_{\gamma,\mathrm{in}}\right) \ . \tag{4.74}$$

The dependence of the filling factor on the light flux $\Gamma_{\gamma,\mathrm{in}}$ of our ideal device can be estimated from the above approximation

$$V_{\mathrm{mpp}} \approx V_{\mathrm{oc}} - 3kT \ , \tag{4.75}$$

and the corresponding current density

$$j_{\mathrm{mpp}} = j_0 \left(\exp\left(\frac{V_{\mathrm{oc}} - 3kT}{kT} \right) - 1 \right) - j_{\mathrm{phot}} \ . \tag{4.76}$$

Substituting in $V_{\mathrm{oc}} = kT \ln\left(j_{\mathrm{phot}}/j_0 + 1\right)$ and $j_{\mathrm{phot}} = -j_{\mathrm{sc}}$, we arrive at

$$\mathrm{FF} = \frac{j_{\mathrm{mpp}} V_{\mathrm{mpp}}}{-j_{\mathrm{phot}} V_{\mathrm{oc}}} = -\frac{V_{\mathrm{oc}} - 3kT}{V_{\mathrm{oc}}} \left[\frac{j_0}{j_{\mathrm{phot}}} \left(\exp\left(\frac{V_{\mathrm{oc}} - 3kT}{kT} \right) - 1 \right) - 1 \right] \tag{4.77}$$

and hence,

$$\mathrm{FF} = -\frac{kT \ln\left[\frac{j_{\mathrm{phot}}}{j_0} + 1\right] - 3kT}{kT \ln\left[\frac{j_{\mathrm{phot}}}{j_0} + 1\right]} \left[\frac{j_0}{j_{\mathrm{phot}}} \left(\exp\left(\frac{kT \ln\left[\frac{j_{\mathrm{phot}}}{j_0} + 1\right] - 3kT}{kT} \right) - 1 \right) - 1 \right] . \tag{4.78}$$

With the abbreviation $j_{\mathrm{phot}}/j_0 = \xi$ and approximating $\ln(\xi + 1) \approx \ln \xi$, because (e.g., for c-Si cells with $\epsilon_{\mathrm{g}} = 1.1\,\mathrm{eV}$) $\xi \geq 5 \times 10^8$, we get

$$\mathrm{FF} = -\left(1 - \frac{3}{\ln[\xi]}\right) \left[\frac{1}{\xi} \left(\exp(\ln[\xi] - 3) - 1 \right) - 1 \right] . \tag{4.79}$$

Figure 4.31 exemplifies the dependence of the filling factor $\mathrm{FF}(\xi)$ for a hypothetic ideal 1- eV band-gap device with $(j_{\mathrm{phot\,(AM0)}})/j_0 \approx 5 \times 10^8$ whereas the corresponding maximum achievable solar light concentration yields

$$j_{\mathrm{phot}}(1.88 \times 10^5 \mathrm{AM0})/\mathrm{j}_0 \approx 10^{14} \ .$$

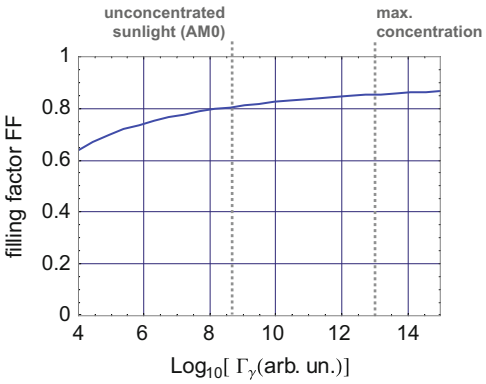

Fig. 4.31 Filling factor FF versus light flux calculated for an ideal two-band system with band gap $\epsilon_g = 1.0\,\mathrm{eV}$ and at $T = 300\,\mathrm{K}$

4.2.5.5 Temperature Dependence of the Chemical Potential of Electron–Hole Ensembles

In the low-temperature limit $T \rightarrow 0$, the excited states for electrons $D(\epsilon_C)$ and for holes $D(\epsilon_V)$ in thermal equilibrium are not occupied, so photogeneration of carriers, e.g., even of a single electron in CB and a single hole in VB, will shift the corresponding quasi-Fermi levels to the band edges $\epsilon_{Fn} \rightarrow \epsilon_C$ and $\epsilon_{Fp} \rightarrow \epsilon_V$. For the analytical treatment, we start with the relation for the chemical potential of electrons and holes approximated with the Boltzmann energy distribution , writing

$$eV_{oc,max} \leq \mu_{np} = \mu_n + \mu_p \approx kT \ln\left[\frac{np}{n_0 p_0}\right]$$
$$= kT \ln\Big[\,(\Delta n + n_0)\,(\Delta p + p_0)\,\Big] - kT \ln\left[(n_0 p_0\right] \ .$$

For moderate temperatures, the thermal equilibrium densities $n_0 \ll \Delta n$ and $p_0 \ll \Delta p$, and we set

$$n_0 = N_{0C} \exp\left(-\frac{\epsilon_C - \epsilon_F}{kT}\right)$$

and analogously

$$p_0 = N_{0V} \exp\left(-\frac{\epsilon_F - \epsilon_V}{kT}\right) \ .$$

Accordingly, we get

$$\mu_{np} \approx kT \ln\left[\Delta n \Delta p\right] - kT \ln\left[\exp\left(\frac{-\left(\epsilon_C - \epsilon_F\right)}{kT}\right)\right] - kT \ln\left[N_{0C}\right]$$
$$-kT \ln\left[\exp\left(\frac{-\left(\epsilon_F - \epsilon_V\right)}{kT}\right)\right] - kT \ln\left[N_{0V}\right] \ ,$$

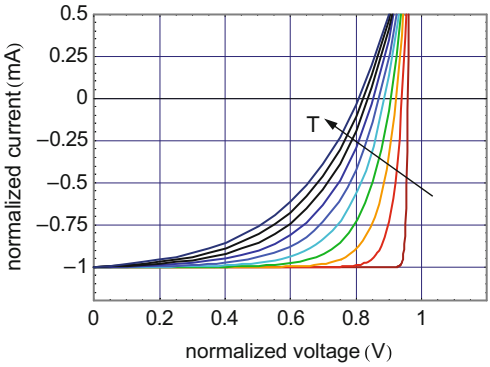

Fig. 4.32 Normalized current density–voltage curves of an ideal photovoltaic solar energy converter for different absorber temperatures. The bending of the curves results solely from the absorber temperature $T > 0$

and finally arrive at

$$\mu_{\mathrm{np}}\,(T \to 0) \approx -kT\left(\frac{-(\epsilon_{\mathrm{C}} - \epsilon_{\mathrm{F}})}{kT}\right) - kT\left(\frac{-(\epsilon_{\mathrm{F}} - \epsilon_{\mathrm{V}})}{kT}\right) = (\epsilon_{\mathrm{C}} - \epsilon_{\mathrm{V}}) = \epsilon_{\mathrm{g}}\ .$$

Figure 4.32 shows the temperature dependence by current density-voltage curves. As eV_{oc} approaches the band gap, the curves with decreasing temperature get increasingly edge-like, with filling factor FF $\to 1$, i.e., the difference in quasi-Fermi levels $(\epsilon_{\mathrm{Fn}} - \epsilon_{\mathrm{Fp}})$ corresponds to the energy gap.[31]

From a thermodynamic point of view, the lower the temperature of the absorber (as low temperature 'heat reservoir') the higher the efficiency of conversion, or, the more approaches the current density-voltage curve the rectangular shape and the product $j_{\mathrm{mpp}} \cdot V_{\mathrm{mpp}} \to j_{\mathrm{sc}} \cdot V_{\mathrm{oc}}$. On the other hand, for increasing departures from $T = 0$, say for $T > 0$, the photoexcited electrons and holes have more and more to compete with their thermally excited companions in order to generate a substantial degree of thermal non-equilibrium state.

4.2.6 Optical Absorption in Band Systems

4.2.6.1 Initial to Final States Transitions

The optical absorption in two-band systems is based on electron transitions from initial states indexed by i (in the valence band with density of states $D_{\mathrm{V}}(\epsilon)$) to final states f (in the conduction band with $D_{\mathrm{C}}(\epsilon)$) (see Fig. 4.33) with respect to their individual occupation. Hence, only for sufficiently low temperatures ($T \to 0$) and

[31] For $T \to 0$ and corresponding $(\epsilon_{\mathrm{Fn}} - \epsilon_{\mathrm{Fp}}) \to \epsilon_{\mathrm{g}}$ we have neglected inversion and the respective transition to lasing; in addition we did not consider that doping by incorporation of impurities for $T \to 0$ will not work.

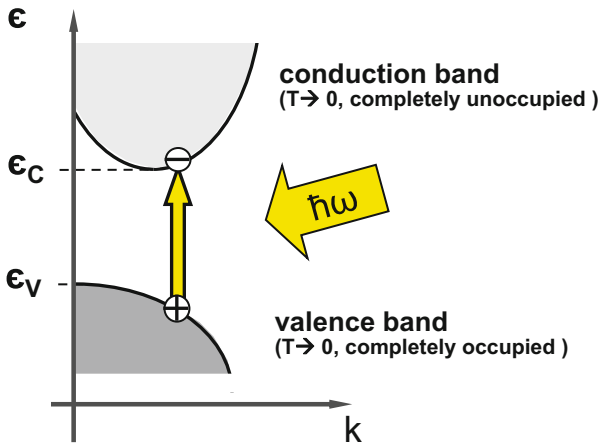

Fig. 4.33 Transition of electron from valence to conduction band by absorption of a photon having energy $\hbar\omega > \epsilon_g$, with conservation of total energy and wave vector; the wave vector of photons with energies of a few eV is negligible in comparison to lattice wave vectors in the first Brillouin zone

negligible perturbation by light are the initial states completely occupied and the final states completely unoccupied the probability for photon absorption and the absorption coefficient are independent of the light flux ($\Gamma_{\gamma,\mathrm{in}}$) initiating transition rates from initial to final states $r_{\mathrm{if}} \sim \Gamma_{\gamma,\mathrm{in}}$.

The absorption coefficient α defines the spatial decay of the photon flux ($-d\Gamma_\gamma/dx$) commonly written as ($-\mathrm{d}\Phi/\mathrm{d}x$) in many cases given by a linear relation such that

$$-\frac{\mathrm{d}\Phi\,(x)}{\mathrm{d}x} = \alpha\Phi(x)\ , \tag{4.80}$$

which is known as the Lambert–Beer law. This local decay of the flux through an area A along the length element $\mathrm{d}x$ yielding $-\mathrm{d}\Phi/\mathrm{d}x$ arises from the transitions of electrons from VB to CB in the volume element $A \cdot \mathrm{d}x$ and within the time slot $\mathrm{d}t$, which leads to the rate $r_{\mathrm{if}} = -\mathrm{d}\Phi/\mathrm{d}x$ and finally to the equation

$$\alpha\Phi = n_{\mathrm{i}}\, p_{\mathrm{f}} A_{\mathrm{if}} \Phi \tag{4.81}$$

where n_{i}, p_{f}, A_{if}, and Φ designate for electrons the densities of initial (i, occupied) and final states (f, unoccupied), the transition coefficient, and the photon flux, respectively.

Under any other conditions, such as increased temperature or under strong photoexcitation of the system, the states in the energy bands CB and VB involved in the transition are partially occupied or unoccupied, respectively. Accordingly, the

rate of transitions due to photon absorption

$$r_{\mathrm{if}} = n_{\mathrm{i}}\, p_{\mathrm{f}} A_{\mathrm{if}} \Phi \ , \tag{4.82}$$

varies with the actual occupation of states.

We then have for the absorption coefficient of a two-band system α given by

$$\alpha = n_{\mathrm{i}}(\Phi)\, p_{\mathrm{f}}(\Phi) A_{\mathrm{if}} \ . \tag{4.83}$$

Introducing the individual carrier concentrations, i.e., n_i for electrons in VB and p_f for holes in CB, we get

$$n_{\mathrm{i}} = n_{\mathrm{V}} = D_{\mathrm{VB}}\, f_{\mathrm{n}}\,(\epsilon) = D_{\mathrm{VB}} \left(1 - \frac{1}{\exp\left(\frac{\epsilon_{\mathrm{Fp}} - \epsilon_{\mathrm{V}}}{kT} \right) + 1} \right) = \frac{D_{\mathrm{VB}}}{\exp\left(-\frac{\epsilon_{\mathrm{Fp}} - \epsilon_{\mathrm{V}}}{kT} \right) + 1} \ , \tag{4.84}$$

together with

$$p_{\mathrm{f}} = p_{\mathrm{C}} = D_{\mathrm{CB}}\, f_{\mathrm{p}}\,(\epsilon) = D_{\mathrm{CB}} \left(1 - \frac{1}{\exp\left(\frac{\epsilon_{\mathrm{C}} - \epsilon_{\mathrm{Fn}}}{kT} \right) + 1} \right) = \frac{D_{\mathrm{CB}}}{\exp\left(-\frac{\epsilon_{\mathrm{C}} - \epsilon_{\mathrm{Fn}}}{kT} \right) + 1} \ . \tag{4.85}$$

We substitute these relations into the above equation to obtain α as a function of the occupation expressed by the quasi-Fermi energies of electrons and holes

$$\alpha = A_{\mathrm{if}} D_{\mathrm{VB}} D_{\mathrm{CB}} \left(\frac{1}{\exp\left(-\frac{\epsilon_{\mathrm{Fp}} - \epsilon_{\mathrm{V}}}{kT} \right) + 1} \right) \left(\frac{1}{\exp\left(-\frac{\epsilon_{\mathrm{C}} - \epsilon_{\mathrm{Fn}}}{kT} \right) + 1} \right) \ . \tag{4.86}$$

If the quasi-Fermi levels in an ideal two-band system are sufficiently far away from the respective band edges, i.e., $(\epsilon_{\mathrm{C}} - \epsilon_{\mathrm{Fn}}) \geq 3kT$ and $(\epsilon_{\mathrm{Fp}} - \epsilon_{\mathrm{V}}) \geq 3kT$ (with $\epsilon_{\mathrm{Fn}} \approx \epsilon_{\mathrm{Fp}} \approx \epsilon_{\mathrm{F}}$ the two exponential terms get extremely small) and we find $\alpha = A_{\mathrm{if}} D_{\mathrm{VB}} D_{\mathrm{CB}} = \text{const}$. However, for a significant departure from this situation for sufficiently high photoexcitation or carrier injection, the densities of initial and final states (n_{i} and p_{f}) may be significantly depleted (associated with the quasi-Fermi levels approaching the band edges) with the consequence of a decrease of the absorption rate. Figure 4.34 shows the influence of the depletion of the initial and final states on the absorption rate in terms of occupation functions governed by the separation of the quasi-Fermi levels with respect to the band gap energy.[32]

[32] In an ideal two-band system, the depletion of the initial state (electrons in the VB) corresponds directly to the depletion of the final state (holes in CB).

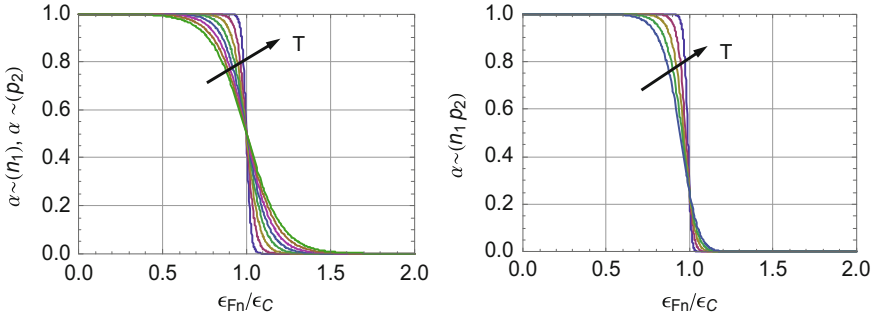

Fig. 4.34 Influence of depletion of initial (n_i) and final (p_f) state carrier concentrations on absorption in terms of occupation function $\left(\exp\left(-\frac{\epsilon_{\mathrm{Fp}}-\epsilon_{\mathrm{V}}}{kT}\right)+1\right)^{-1}$ and $\left(\exp\left(-\frac{\epsilon_{\mathrm{C}}-\epsilon_{\mathrm{Fn}}}{kT}\right)+1\right)^{-1}$ which enter the absorption coefficient α

It is obvious that, with increasing depletion not only the absorption rate drops but likewise stimulated emission has to be considered in the entire balance of the rates of absorption and emission. For $(\epsilon_{\mathrm{Fn}}-\epsilon_{\mathrm{Fp}}) \geq (\epsilon_{\mathrm{C}}-\epsilon_{\mathrm{V}})$, the formal condition of 'inversion' is met which signals lasing behavior with the absorption coefficient being no longer a meaningful magnitude.

4.2.6.2 Direct and Indirect Semiconductors

In crystals the translational periodic arrangement of ionic potentials leads to the stationary state solution of the Schrödinger equation with the independent-electron ansatz to relations between the electron energy ϵ and electron wave vector $\mathbf{k}$, referred to as $\epsilon(\mathbf{k})$-diagrams (dispersion relation). The energetic regimes allowed for the occupation by the electrons, called bands are separated from one another by forbidden regimes, or band gaps. At low temperatures $(T \rightarrow 0)$ the highest energy completely occupied regime (valence band) is separated from the next higher energies (conduction band) by the band gap ϵ_{g}. If the highest occupied band[33] is only partially 'filled' at $T \rightarrow 0$ by electrons, the crystal shows metallic behavior.

The local arrangement and the electronic details of the ionic potentials also determine whether, in the $\epsilon(\mathbf{k})$ relation of semiconductors or insulators, the maximum of the valence band (VB) at energy $\epsilon = \epsilon_{\mathrm{V}}$ and minimum of the conduction band (CB) at energy $\epsilon = \epsilon_{\mathrm{C}}$ are located at identical wave vectors in the Brillouin zone (direct semiconductor) or at different $\mathbf{k}$ values separated by $\Delta\mathbf{k}$ (indirect semiconductors), as shown schematically in Fig. 4.35 for GaAs and c-Si respectively.

[33] In metals there are often several bands overlapping each other and crossing ϵ_{F}.

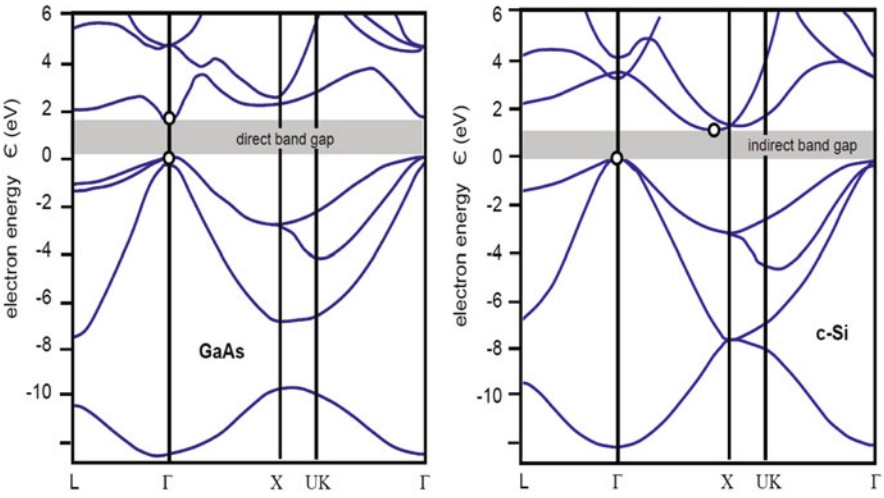

Fig. 4.35 Energy–wave vector diagram $\epsilon = \epsilon(k)$ of a typical direct (GaAs) *(left)* and an indirect semiconductor (c-Si) *(right)*

As a consequence, the transition of electrons from VB to CB by photoexcitation with minimum photon energy $\hbar\omega = \epsilon_g = \epsilon_C - \epsilon_V$ in an indirect semiconductor, requires the participation of a lattice vibration (phonon) with a wave vector $\Delta\mathbf{k}$ in order to meet the condition of wave vector conservation, because the wave vectors of photons in the visible spectral range are negligible compared to wave vectors on the scale of the first Brillouin zone of crystals.[34]

The phonon is either generated by the incoming photon in optical interaction with the lattice (optical phonon), or already available in the lattice (thermally generated) and absorbed to meet momentum conservation. Of course, the phonon wave vector is associated with the phonon energy via the particular dispersion relation $\hbar\omega_{\text{phon}}(\mathbf{k})$ of lattice vibrations. The participation of a third particle like a phonon for light absorption, along with the photon and electron, makes the probability for absorption substantially lower than that of a direct electronic transition from VB to CB.

[34]For a typical lattice constant of 0.3 nm, the first Brillouin zone spans from

$$-\frac{\pi}{0.3\,\text{nm}} \leq k \leq \frac{\pi}{0.3\,\text{nm}},$$

whereas photon wave vectors, e.g., for $\hbar\omega = 2\,\text{eV}$, correspond to $\lambda \approx 600\,\text{nm}$ and relate to wave vectors

$$k_{\text{phot},2\,\text{eV}} \approx \frac{2\pi}{600\,\text{nm}} \approx 0.01(1/\text{nm}) \ll k\ .$$

4.2.6.3 Absorption in Direct Semiconductors

For direct optical transitions of electrons between valence and conduction band as a consequence of photon absorption, as well as the process in the opposite direction (CB to VB-transitions for light emission), momentum and energy conservation laws in the independent-electron picture with negligible photon momentum $k_{\text{phot}} \approx 0$ read:

$$\mathbf{k_{e,\,VB}} + \mathbf{k_{phot}} \approx \mathbf{k_{e,\,VB}} = \mathbf{k_{h,\,VB}} = \mathbf{k_{e,\,CB}} \,, \tag{4.87}$$

$$\epsilon_{\text{phot}} = \hbar\omega = \epsilon_{\text{g}} + \epsilon_{\text{kin,\,h}} + \epsilon_{\text{kin,\,e}} \,. \tag{4.88}$$

Assuming three-dimensional isotropic dispersion of electrons (CB) and holes (VB) close to the band edges

$$\epsilon(k) = \frac{\hbar^2 k^2}{2m^*} \,,$$

we rewrite energy conservation with regard of the wave vector balance $\mathbf{k_{h,\,VB}} - \mathbf{k_{e,\,CB}} = \Delta\mathbf{k} = 0$ in the form

$$\hbar\omega = \epsilon_{\text{g}} + \frac{\hbar^2 k^2}{2}\left(\frac{1}{m_{\text{h}}^*} + \frac{1}{m_{\text{e}}^*}\right) = \epsilon_{\text{g}} + \frac{\hbar^2 k^2}{2m_{\text{c}}^2} \,. \tag{4.89}$$

The share of the kinetic energies of holes and electrons is expressed by the ratio of the inverse effective masses[35] which are combined to the reduced effective mass m_{c} as $\left(1/m_{\text{h}}^* + 1/m_{\text{e}}^*\right) = \left(1/m_{\text{c}}^*\right)$.

In direct optical transitions from any of the states in the valence band with $\epsilon_{\text{i}}(\mathbf{k})$ electrons by the interaction with a photon of $\hbar\omega$ are solely transferred to their 'companion states' in CB with identical wave vector (see Fig. 4.36).

The density of states in the parabolic band approximation (VB, CB) varies with $\sim \sqrt{\epsilon}$ for energies of the band edge and deeper in the respective band,

$$D_{\text{VB}}(\epsilon) = \frac{(2m_{\text{h}})^{3/2}}{2\pi^2\hbar^3}\sqrt{-\epsilon},$$

$$D_{\text{CB}}(\epsilon) = \frac{(2m_{\text{e}})^{3/2}}{2\pi^2\hbar^3}\sqrt{\epsilon - \epsilon_{\text{g}}},$$

[35] Remember that the effective mass m^* may be interpreted as an abbreviation for the density of states in the parabolic band approximation. This abbreviation is usually applied for the density of states in the valence D_{VB} and in the conduction band D_{CB} as well as for their combined density of states D_{c}.

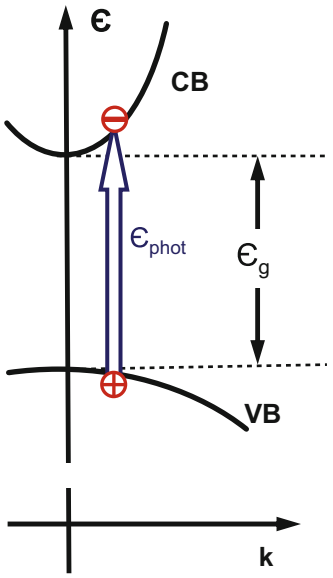

Fig. 4.36 Transition of electron from valence to conduction band in a direct semiconductor by absorption of a photon with energy $\hbar\omega > \epsilon_g$, with conservation of the electron wave vector $\mathbf{k}_{el}(\mathrm{VB}) = \mathbf{k}_{el}(\mathrm{CB})$; remember that the wave vector of photons with energies of a few eV is negligible in comparison to lattice wave vectors in the first Brillouin zone

and also likewise the combined density of states

$$D_c(\epsilon) = \frac{(2m_c)^{3/2}}{2\pi^2\hbar^3}\sqrt{\epsilon - \epsilon_g}.$$

The absorption coefficient comprises the transition coefficient A_{if} that couples the electron wave function to the electromagnetic field, and the initial and final density of states expressed in the combined density of states. Accordingly we get the absorption coefficient of direct transitions (see Eq. (B.4)) as a function of the energy of photons $\epsilon = \hbar\omega$

$$\alpha(\hbar\omega) = A_{if}\frac{(2m_c)^{3/2}}{2\pi^2\hbar^3}\sqrt{\hbar\omega - \epsilon_g}. \tag{4.90}$$

For this derivation we have once more assumed the valence band to be entirely occupied by electrons and the conduction band respectively to be entirely unoccupied.

The typical representation of the absorption coefficient α of a direct transition versus photon energy, as long as it remains in the vicinity of the band gap, is a plot

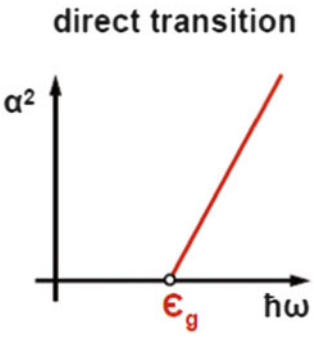

Fig. 4.37 Representation of absorption coefficient $\alpha(\hbar\omega)$ of a direct semiconductor in terms of α^2 versus photon energy $\hbar\omega$ to show the linear relation of $\alpha^2 \sim (\hbar\omega - \epsilon_g)$

called the Tauc plot[36] (see Fig. 4.37).

$$[\alpha(\hbar\omega)]^2 \sim \hbar\omega - \epsilon_g \ .$$

Due to the linear relation of α^2 versus photon energy $\hbar\omega$, the band gap is easily identified as the intercept with the $\hbar\omega$-axis.

4.2.6.4 Absorption in Indirect Semiconductors

As a consequence of the participation of a phonon to be either absorbed or emitted/generated in indirect transitions, energy and momentum conservation laws read

$$\mathbf{k}_{\mathbf{e,\,VB}} + \mathbf{k}_{\mathbf{phot}} \approx \mathbf{k}_{\mathbf{e,\,VB}} = \mathbf{k}_{\mathbf{e,\,CB}} \pm \mathbf{k}_{\mathbf{phon}} \ , \tag{4.91}$$

$$\epsilon_{\mathrm{phot}} = \hbar\omega = \epsilon_{\mathrm{f}} - \epsilon_{\mathrm{i}} \pm \epsilon_{\mathrm{phon}} \ , \tag{4.92}$$

with initial and final state energies ϵ_{i} and ϵ_{f}. We replace $\epsilon_{\mathrm{f}} = \epsilon_{\mathrm{g}} + \epsilon_{\mathrm{kin,\,e}}$, and $-\epsilon_{\mathrm{i}} = \epsilon_{\mathrm{kin,\,h}}$ and get

$$\hbar\omega = \epsilon_{\mathrm{g}} + \epsilon_{\mathrm{kin,\,e}} + \epsilon_{\mathrm{kin,\,h}} \pm \epsilon_{\mathrm{phon}} \ . \tag{4.93}$$

[36] In amorphous and microcrystalline semiconductors, such as a-Ge:H, a-Si:H, μc-Si etc., the spectral absorption for low absorption coefficients is strongly governed by states in band tails and at midgap. Due to the contribution of these states it is difficult to determine the pseudo-optical band gap from experimental absorption coefficients $\alpha(\hbar\omega)$; a more appropriate evaluation of the pseudo-band gap according to the proposal of Tauc [18] is derived when plotting α^2 versus $\hbar\omega$ for direct, or equivalently $\sqrt{\alpha}$ versus $\hbar\omega$ for indirect semiconductors; in these plots the linear extrapolation of α^2, or $\sqrt{\alpha}$ respectively at sufficiently high photon energies resulting from band-to band transitions yields consistent values for the pseudo-band gaps by the intercept with the photon-energy axis.

Once again for three-dimensional isotropic bands in the independent-electron picture we continue with the densities of states in the valence and conduction band

$$N_\mathrm{i} = N\left(\epsilon_\mathrm{i}\right) = \frac{\left(2m_\mathrm{h}^*\right)^{3/2}}{2\pi^2\hbar^3}\sqrt{-\epsilon_\mathrm{i}}\,, \tag{4.94}$$

$$N_\mathrm{f} = N\left(\epsilon_\mathrm{f}\right) = \frac{\left(2m_\mathrm{n}^*\right)^{3/2}}{2\pi^2\hbar^3}\sqrt{\epsilon_\mathrm{f}-\epsilon_\mathrm{g}}\,. \tag{4.95}$$

and introduce the energy balance from above, to find for the final states

$$N_\mathrm{f} = \frac{\left(2m_\mathrm{n}^*\right)^{3/2}}{2\pi^2\hbar^3}\sqrt{\hbar\omega-\epsilon_\mathrm{g}+\epsilon_\mathrm{i}\mp\epsilon_\mathrm{phon}}\,. \tag{4.96}$$

Since we consider transitions from each of the available initial states to any final state, irrespective of their accompanying wave vector $\mathbf{k}$, where energy conservation is met with the contribution of absorption or emission of a suitable phonon with $\hbar\omega_\mathrm{phon}$ (see Fig. 4.38), we express the combined density of states D_c^* by the respective numbers of initial and final states $N_\mathrm{i}N_\mathrm{f} = N_\mathrm{c}$, within the energy interval $\mathrm{d}\epsilon_\mathrm{i}$

$$\begin{aligned} D_\mathrm{c}^* &= \int N_\mathrm{i}N_\mathrm{f}d\epsilon_\mathrm{i} = \int N_\mathrm{c}d\epsilon_\mathrm{i} \\ &= \frac{\left(2m_\mathrm{n}^*\right)^{3/2}\left(2m_\mathrm{p}^*\right)^{3/2}}{\left(2\pi\hbar^3\right)^2}\int_{-\left(\hbar\omega-\epsilon_\mathrm{g}\mp\epsilon_\mathrm{phon}\right)}^{0}\sqrt{\epsilon_\mathrm{i}}\sqrt{\hbar\omega+\epsilon_\mathrm{i}-\epsilon_\mathrm{g}\mp\epsilon_\mathrm{phon}}\,\mathrm{d}\epsilon_\mathrm{i}\,. \end{aligned} \tag{4.97}$$

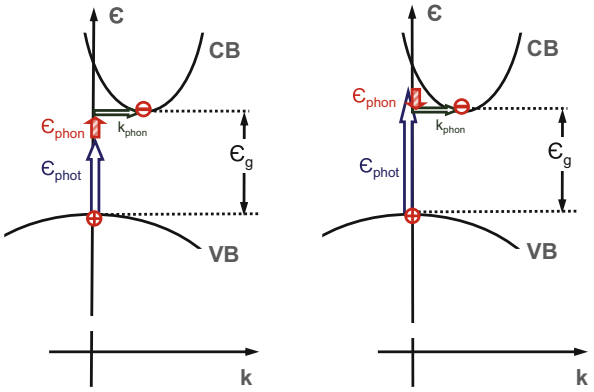

Fig. 4.38 Transition of electron from valence to conduction band in an indirect semiconductor by absorption of a photon having energy $\hbar\omega < \epsilon_\mathrm{g}$, with conservation of total energy and wave vector accompanied by phonon absorption (*left*) and with phonon generation ($\hbar\omega > \epsilon_\mathrm{g}$) (*right*). The wave vector of photons with energies of a few eV is negligible in comparison to lattice wave vectors in the first Brillouin zone; energies are not to scale, since $\epsilon_\mathrm{phon} << \epsilon_\mathrm{g}$

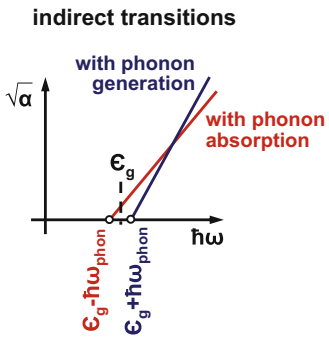

Fig. 4.39 Representation of absorption coefficient $\alpha(\hbar\omega)$ of an indirect semiconductor in terms of $\sqrt{\alpha}$ versus photon energy $\hbar\omega$ to show the linear relation of $\sqrt{\alpha} \sim \hbar\omega - (\epsilon_g \pm \hbar\omega_{phon})$

The absorption coefficient $\alpha(\hbar\omega)$ of indirect transitions contains the probability P_{phon} of generating or absorbing a phonon, an effect depending on the temperature and quantified by the Bose–Einstein distribution function, and the phonon dispersion relation $\omega = \omega(\mathbf{k})$. Moreover $\alpha(\hbar\omega)$ includes the combined density of states and the optical matrix element, which is assumed to be independent of photon energy in the vicinity of $\hbar\omega \approx \epsilon_g$. Hence, finally,

$$\alpha(\hbar\omega) \sim P_{phon} \frac{\left(2m_n^*\right)^{3/2}\left(2m_p^*\right)^{3/2}}{\left(2\pi\hbar^3\right)^2}\left(\hbar\omega - \epsilon_g \pm \epsilon_{phon}\right)^2 . \tag{4.98}$$

Here, we distinguish between the probabilities $P_{phon,\,em}$ and $P_{phon,\,abs}$ for phonon emission and absorption. An equivalent Tauc plot with $\sqrt{\alpha(\hbar\omega)} \sim \left(\hbar\omega - \epsilon_g\right)$ is used for the visualization of indirect transitions, allowing for the experimental determination of the band gap ϵ_g. A schematic example is displayed in Fig. 4.39.

4.2.7 Reversal of Photon and Carrier Fluxes

Absorption and emission of photons in and from matter are coupled by the excitation of electrons and their radiative return to the ground state (see Sect. 4.2.3 and Fig. 4.21). In the radiative limit a stationary state of an absorber is achieved by balancing the rate of absorbed photons (r_{abs}) by the rate of emitted photons, where the emission is composed of spontaneous ($r_{em,spon}$) and stimulated optical transitions ($r_{em,stim}$) and by the rate of carriers such as electrons and holes extracted from the absorber (r_{el}).[37] For moderate absorption rates, such as those caused by solar

[37]The rate of carriers extracted from the absorber is composed of electrons and holes moving in opposite directions and thus contribution by particular fractions to the entire electrical output current.

light fluxes, even when concentrated, the stimulated emission is negligible and the balance of the rates becomes $r_{\mathrm{abs}} \approx r_{\mathrm{em,spon}} + r_{\mathrm{el}}$.

In a similar way, the removal of carriers from photoexcited absorber as electrical current (photocurrent) can be reversed by inverting directions of fluxes, such as the injection of carriers and the emission of photons by radiative transitions of carriers in the excited state to the ground state. In this sense of reversal of fluxes (reciprocity principle [19, 20]), solar cells and luminescence diodes are equivalent structures.

4.2.7.1 Reciprocity and Flux Balance for Photovoltaic Converters

In the radiative limit of photovoltaic structures, by definition, we find complete reciprocity, since each of the absorbed photons is assumed to create one electron–hole pair, and the generated charges are either extracted as output current with probability (charge collection efficiency) unity, or will recombine radiatively in spontaneous or stimulated transitions and thus create an appropriate number of photons. Consequently, in any mode of operation, the balance of the fluxes of photons $\Gamma_{\gamma,\mathrm{in}}$ and $\Gamma_{\gamma,\mathrm{out}}$ and of charges (electrical output current) Γ_{el} is satisfied (outlined exemplarily in Fig. 4.24):

$$\Gamma_{\gamma,\mathrm{in}} - \Gamma_{\gamma,\mathrm{out}} = \Gamma_{\mathrm{el}} \ .$$

For incoming and emitted photons, we regard the fluxes in the according solid angle, and we do not care about an eventual increase in etendue $\Delta\varepsilon = \varepsilon_{\mathrm{out}} - \varepsilon_{\mathrm{in}} > 0$, which is not necessarily conserved. Moreover, we accept that the incoming photons usually possess much higher energy reflecting the temperature of the Sun's surface (6,000 K) compared to those of $\Gamma_{\gamma,\mathrm{out}}(T_{\mathrm{abs}} = 300\,\mathrm{K})$. Without saying, the radiative output $\Gamma_{\gamma,\mathrm{out}}$ contains the contributions of the photoexcited state dependent on chemical potential μ_{np} and temperature T_{abs} which includes, of course, the contribution of the thermal radiation. The temperature T_{abs} is kept intentionally constant by the contact to an external heat reservoir such as the global environment ($T_{\mathrm{Earth}} = 300\,\mathrm{K}$), and this is assumed to be independent of what the receiver does with the absorbed solar photons (already mentioned in Sect. 3.3).

If the absorbed photons generate excitons, i.e., bound states between an electron in CB and a hole in VB, instead of free carriers in the bands, we assume the excitons to recombine and in turn contribute to the emitted photon flux, or be dissociated and be extracted from the absorber as charges.

In the ideal open circuit mode (V_{oc}) no carriers leave or enter the absorber, and in the radiative limit the input photon flux is converted by exclusively radiative recombination into an output photon flux. The absorber having established its individual temperature T_{abs} due to contact to its environment is thus emitting due to its chemical potential $\mu_{\mathrm{np,abs}}$ and its temperature T_{abs}, so that $\Gamma_{\gamma,\mathrm{in}} = \Gamma_{\gamma,\mathrm{out}}$ In this case, the emitted flux $\Gamma_{\gamma,\mathrm{out}}$ due to the non-vanishing chemical potential contains the excess photons and the thermal equilibrium photons. (Remember that the entire flux is formulated by Planck's generalized law and we do **not** distinguish between photons resulting from one or the other origin.)

In short-circuit mode (j_{sc}) of the radiative limit, each of the photons taking the absorber out of thermal equilibrium is 'converted' into electron–hole pairs and leaves the absorber as output current, so the balance can be expressed by $\Gamma_{\gamma,\,in} = \Gamma_{el} + \Gamma_{\gamma,0}$, where the last term $\Gamma_{\gamma,0}$ denotes the thermal equilibrium radiation. In this ideal approach, the excess carriers generated in the absorber are extracted instantaneously (with infinite diffusion coefficients and/or infinite mobilities) to the boundaries of the absorber, so only the thermal equilibrium carrier density is present in the band system.

In any mode $0 < V < V_{oc}$, equivalent to $j_{sc} > j > 0$, the incoming photon flux $\Gamma_{\gamma,\,in}$ is balanced by the superposition of output photon and output carrier flux, expressed by $\Gamma_{\gamma,\,in} = \Gamma_{el} + \Gamma_{\gamma,\,out}$. Here the share of output of photons and carriers obeys the $j - V$ relation of the ideal diode (see Sect. 4.2.4) in which the voltage represents the chemical potential appearing in the denominator of the spectral photon flux equation (Sect. 4.2.3) $e \cdot V = \mu_{np}$.

In the trivial case of a non-illuminated absorber kept at constant temperature no photons are available for the excitation of the electron system, and accordingly no extra photons exceeding thermal equilibrium radiation are emitted, and thus the carrier output vanishes.[38]

In real solar cells, however, departures from reciprocity are unavoidable and are due to

- incomplete conversion of absorbed photons into electron–hole pairs,
- incomplete radiative recombination, which means additional non-radiative decay of the concentration of photoexcited carriers, and
- incomplete charge collection.

Consequently, the general flux balance is modified to $\Gamma_{\gamma,\,in} > \Gamma_{el} + \Gamma_{\gamma,\,out}$.

4.2.7.2 Reciprocity and Flux Balance for Light Emitters

When operating the band system as light-emitting device equivalently to a luminescence diode, the direction of fluxes, except that of the thermal equilibrium radiation, is inverted.

In open-circuit, the input current density vanishes and the absorber radiates in accordance with the chemical potential of its electron–hole system, which corresponds to the splitting of the quasi-Fermi levels. To arrive at this state, we switch on a current through the diode ($\Gamma_{el} < 0$) and establish the respective photon field and splitting of the quasi-Fermi levels. Now, the diode emits with its chemical potential of the electron system. We turn that radiation back to the diode by an ideal mirror and the photon emission rate equals the absorption rate. Further on we switch off the current supply and the diode illuminates itself in a way that

[38] Note, that the free energy of those thermal equilibrium photons with respect to a converter at identical temperature disappears.

satisfies reciprocity, such that the rates of emission and absorption are equal, i.e., $\Gamma_{\gamma,\mathrm{out}}(\hbar\omega) = \Gamma_{\gamma,\in}(\hbar\omega)$, even with identical spectral distributions and solid angles. This operation resembles the open-circuit mode in solar cells, with the exception that, in solar cells in the radiative limit, the solid angles (or etendues) are not necessarily conserved.

In steady state short-circuit mode, by injection of carriers, the diode again creates a photon field which illuminates the diode itself, while the further flux of charges injected initiates the photons emitted to the environment according to the relation $-\Gamma_{\mathrm{el}} = \Gamma_{\gamma,\mathrm{out}} - \Gamma_{\gamma,0}$; note, that the thermal part $\Gamma_{\gamma,0}$ is separately supplied by the heat source which keeps the band system at constant temperature.

Operation at $0 \leq V \leq V_{\mathrm{oc}}$ and $j_{\mathrm{sc}} \geq j \geq 0$ again reflects a mixture between both states, for which the net output photon flux in accordance with the j–V curve of an ideal illuminated diode, in which charge injection balances the photon emission $-\Gamma_{\mathrm{el}}(V) = \Gamma_{\gamma,\mathrm{out}}(V) - \Gamma_{\gamma,0}$.

4.2.8 Irreversibilities in Solar Light Conversion

The reception and the conversion of solar photons is associated with several irreversible processes, by which the free energy either of photons or of the electron–hole ensemble may substantially be reduced and thus the efficiency of conversion. Amongst the usual imperfections of the absorbers, such as sites for additional non-radiative recombination decreasing the life times of excited carriers, like defects or interface and surface states, non-perfect barriers, limited carrier transport properties, here, some more fundamental effects are summarized which are discussed in terms of entropy generation and according drop of performance of solar light conversion.

4.2.8.1 Cooling of Solar Photons

We draft the generation of heat, as a fundamental irreversible process, by cooling of solar photons in an ideal electronic band system exemplarily operated at open circuit. The input into the system consists of the solar photon flux $\Gamma_{\gamma,\mathrm{Sun}} = \Gamma_{\gamma,\mathrm{in}}$, is exactly balanced in open circuit by the output flux $\Gamma_{\gamma,\mathrm{abs}} = \Gamma_{\gamma,\mathrm{out}} = \Gamma_{\gamma,\mathrm{in}}$ when the exchange of charges is forbidden. Neglecting light from the environment and from the Universe the flux balance reads:

$$\begin{aligned}\Gamma_{\mathrm{Sun}} = \Gamma_{\gamma,\mathrm{in}} &= \frac{\Omega_{\mathrm{in}}}{c_0^2 4\pi^3\hbar^3}\int_{\epsilon_{\mathrm{g}}}^{\infty}\frac{(\hbar\omega)^2}{\exp\left(\dfrac{\hbar\omega}{kT_{\mathrm{Sun}}}\right)-1}\mathrm{d}(\hbar\omega)\\ &= \Gamma_{\mathrm{abs}} = \Gamma_{\gamma,\mathrm{out}}\frac{\Omega_{\mathrm{out}}}{c_0^2 4\pi^3\hbar^3}\int_{\epsilon_{\mathrm{g}}}^{\infty}\frac{(\hbar\omega)^2}{\exp\left(\dfrac{\hbar\omega-\mu_{\mathrm{np}}}{kT_{\mathrm{abs}}}\right)-1}\mathrm{d}(\hbar\omega)\,. \qquad (4.99)\end{aligned}$$

While these photon fluxes are ideally balanced, the energy fluxes $\Gamma_{\epsilon,\mathrm{Sun}} = \Gamma_{\epsilon,\mathrm{in}}$, $\Gamma_{\epsilon,\mathrm{abs}} = \Gamma_{\epsilon,\mathrm{in}}$ are not [21], since solar photons, corresponding to $T_{\mathrm{Sun}} = 6{,}000\,\mathrm{K}$, on the average possess much higher energies than photons emitted by the absorber at $T_{\mathrm{abs}} = 300\,\mathrm{K}$. Thus the energy fluxes in the inequality relation below read:

$$\Gamma_{\epsilon,\,\mathrm{Sun}} = \Gamma_{\epsilon,\,\mathrm{in}} = \frac{\Omega_{\mathrm{in}}}{c_0^2 4\pi^3\hbar^3}\int_{\epsilon_\mathrm{g}}^{\infty}\frac{(\hbar\omega)^3}{\exp\left(\dfrac{\hbar\omega}{kT_{\mathrm{Sun}}}\right)-1}\mathrm{d}(\hbar\omega)$$

$$> (!)\,\Gamma_{\epsilon,\,\mathrm{absorber}} = \Gamma_{\epsilon,\,\mathrm{out}} = \frac{\Omega_{\mathrm{out}}}{c_0^2 4\pi^3\hbar^3}\int_{\epsilon_\mathrm{g}}^{\infty}\frac{(\hbar\omega)^3}{\exp\left(\dfrac{\hbar\omega-\mu_{\mathrm{np}}}{kT_{\mathrm{abs}}}\right)-1}\mathrm{d}(\hbar\omega)\,. \tag{4.100}$$

The chemical potential μ_{np} in the exponential function in the denominator of the above balance compensates for the comparatively low T_{abs}. The photon fluxes $\Gamma_{\gamma,\mathrm{in}}$, $\Gamma_{\gamma,\mathrm{out}}$ (having $(\hbar\omega)^2$ in the numerator of the integral) compensate each other, whereas the energy fluxes $\Gamma_{\epsilon,\mathrm{in}}$, $\Gamma_{\epsilon,\mathrm{out}}$ (with $(\hbar\omega)^3$ in the numerator) of course do not balance. Thus, the energy flux from the Sun substantially exceed that emitted from the electronic band system.

We treat the behavior of our band system in the radiative limit and in open circuit (no carrier extraction or injection). Figure 4.40 (left) shows the absorbed solar energy flux and the one emitted by the absorber in the radiative limit in open circuit for various solar light concentration factors (Ω_{out}) as a function of the band gap ϵ_g. This clearly confirms the absorbed energy per unit time from the Sun to be much greater than the energy emitted by the absorber.

In Fig. 4.40 (right), the difference of these two energy fluxes (energy fluxes from Sun minus those from the absorber in Fig. 4.40, (left)), which coincides with the heat generation $\Delta\dot{q}$ in the absorber by 'cooling' highly photo-excited electrons and holes,[39] is displayed as a function of the band gap and with the solar light concentration factor as parameter. With increasing band gap, the difference gets smaller, and in the limit of the band gap approaching infinity, it will vanish. This effect of vanishing generation of heat and entropy, however, is not very helpful because, when dealing with matter of zero absorptivity and emissivity, solar light can neither be absorbed nor can radiation from this matter be emitted.

To achieve full reversibility in the process of harvesting solar photons, one would need completely reversible individual processes. Since the complete conversion of solar light into electric power with an absorber at $T > 0\,\mathrm{K}$ is not possible (see Sect. 4.1.3), the only remaining option of full reversibility is open-circuit operation with emission of photons with the same spectral shape as the incoming solar light,

[39]This heat $\Delta\dot{q}$ (generated by fast relaxation of 'hot' photoexcited electrons and holes which subsequently recombine with emission of photons with lower energy) may easily be translated into an entropy density term by $(1/T_{\mathrm{abs}})\dot{q} = \dot{s}$.

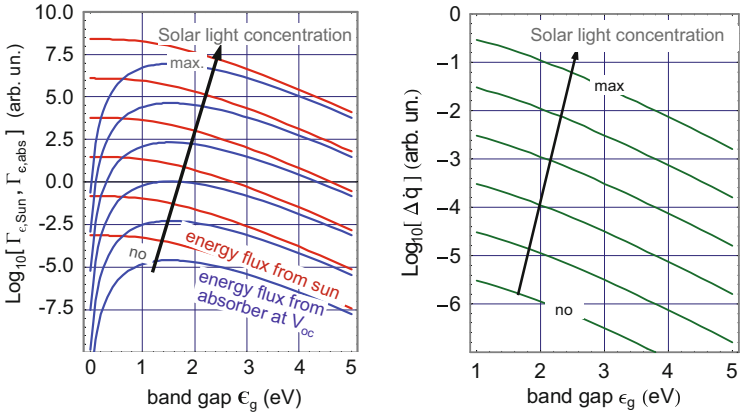

Fig. 4.40 Radiative energy fluxes from the Sun $\Gamma_{\epsilon,\mathrm{Sun}}$ to an electronic two-band absorber (AM0, $T_{\mathrm{abs}} = 300\,\mathrm{K}$) and flux $\Gamma_{\epsilon,\mathrm{abs}}$ from the receiver in the radiative limit in open-circuit voltage mode versus optical threshold energy (band gap) for different levels of solar light concentration *(left)*; heat generation ($\Gamma_{\epsilon,\mathrm{Sun}}$-$\Gamma_{\epsilon,\mathrm{abs}}$) in an electronic two-band absorber at $T_{\mathrm{abs}} = 300\,\mathrm{K}$) in the radiative limit in open-circuit voltage mode versus optical threshold energy (band gap) for different levels of solar light concentration *(right)*

which means absorption in an ideal multispectral absorber being composed of an infinite number of individual band gaps. In addition, the etendue of the incoming solar photon flux must not be enlarged for the emission (solid angle for light in and out to be identical). In essence, this hypothetical system is equivalent to an ideal mirror at $T_{\mathrm{mirr}} = 0$ which reflects each of the solar photons back to the Sun, regardless of its respective energy/frequency, and takes no energy from the solar radiation.

For the operation of an electronic band system at maximum power in the energy flux balance, the amount of emitted light in comparison to $\mu_{\mathrm{np}} = e \cdot V_{\mathrm{oc}}$ gets reduced according to $\mu_{\mathrm{np}} \approx (e \cdot V_{\mathrm{oc}} - 3kT)$, but the entropy free amount of the electric output power $p_{\mathrm{el}} = (j_{\mathrm{mpp}} V_{\mathrm{mpp}})$ substantially diminishes the rate of heat production. In the mode of short circuit, incidentally, the radiative output is restricted to thermal equilibrium radiation and to vanishing electric output power, so that the entire radiative energy from the source is converted into heat.

4.2.8.2 Etendue of Solar Radiation Versus Etendu of Light Emission

The solar light flux is coupled in to an appropriate absorber under a particular solid angle that determines the entire input of photons which in turn generate the photoexcited state. The geometrical configuration of solid angles for light input and light output determine the fraction of solar energy that is convertible. After the first step of entropy generation upon solar light absorption ("cooling" of solar photons), the emission of radiation by the absorber into a solid angle larger than the solid

angle of the light input represents a further reduction of the conversion of solar light (remember the dependence of the maximum achievable open circuit voltage on the ratio of the solid angles ($\Omega_{\mathrm{out}}/\Omega_{\mathrm{in}}$) in Eq. (4.55)). Furthermore, the random emission into a larger solid angle than that of the light input by light scattering in the absorber or at its rough surface, which cannot be reversed by "passive" optical elements, increases the entropy of the photons as well, even when elastically scattered.[40]

For the formulation of the entropy production as a function of light fluxes, studied quantitatively by Markvart [21], the chemical potential of the photon field $\mu_{\mathrm{abs}}(\hbar\omega_0)$ of a small spectral part $\hbar\omega_0$ emitted in the radiative limit from an absorber at T_{abs} and illuminated by the Sun explicitly contains, amongst other terms, the contribution for the etendue of the photon fluxes in $\varepsilon_{\mathrm{Sun}}$ and out $\varepsilon_{\mathrm{abs}}$ in the third term of the equation below (which is identical to Eq. (4.55), when replacing $\hbar\omega_0$ by ϵ_{g} and interpreting $\gamma(T)$ as mean kinetic energy of the particular photo-excited species):

$$\mu_{\mathrm{abs}}(\hbar\omega_0) = \left(1 - \frac{T_{\mathrm{abs}}}{T_{\mathrm{Sun}}}\right)\hbar\omega_0 + kT_{\mathrm{abs}} \ln\left[\frac{\gamma(T_{\mathrm{Sun}})}{\gamma(T_{\mathrm{abs}})}\right] - kT_{\mathrm{abs}} \ln\left[\frac{\varepsilon_{\mathrm{abs}}}{\varepsilon_{\mathrm{Sun}}}\right]. \tag{4.101}$$

As the etendue in the best case (for reversible effects) is conserved and in irreversible steps always increases, the chemical potential of the photon field of the absorber decreases if the absorber increases the incoming etendue: $\varepsilon_{\mathrm{in}} < \varepsilon_{\mathrm{out}}$.

4.2.8.3 Entropy Production by Diffusion of Photoexcited Species in Absorbers

According to the Lambert–Beer law, the carrier generation profile $g(z)$ exhibits an exponential decay along the absorption path z, of the form $g(z) \sim \exp(-\alpha z)$, where α denotes the optical absorption coefficient, which might include the increase in absorption by scattering at rough surfaces, i.e., $\alpha \sim (2n)^2$ [22]. Due to diffusion, the exponential-like photoexcitation profile will smear out across the absorber thickness d and establish a flatter profile. For a quantitative estimate of this effect we compare

[40]The directional dispersion of light is commonly treated by the difference in the etendue of the propagating light before and after the interaction with matter. The etendue ε describes the "radiance" of the light beam, which is conserved in non-scattering, non-absorbing media, where

$$\delta\varepsilon = n^2 \cos\theta \delta\Omega \delta A,$$

with angle θ to the normal to the area element δA, solid angle for emission $\delta\Omega$, and refractive index n of the matter [16]. By scattering of photons and/or by absorption and subsequent emission with Stokes shift into a larger solid angle than that of the incoming photon flux, due to the lower photon flux density of the 'bundle' of rays in the 'beam', the ability of the photon gas to perform valuable work is reduced. In the language of statistical physics, it is the increase in etendue that reduces the free energy of the photons.

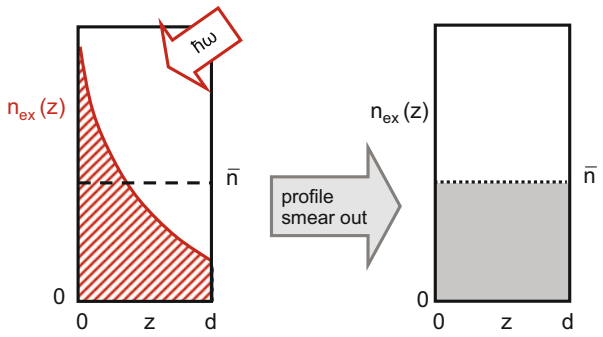

Fig. 4.41 Profile of photogenerated excess carriers according to the profile of photogeneration $n_{ex}(z)$ (*left*) and hypothetic completely flat excess carrier distribution $\bar{n} = \text{const.}$ (*right*)

a profile of excess carriers (e.g., electrons as minority carriers) according to the generation profile[41]

$$n_1 = n(z) = \Gamma_0 \alpha \tau \exp(-\alpha z)$$

with an entirely flat profile

$$n_2 = \overline{n} = \text{const.}$$

which for negligible surface recombination at the rear and front and for density-independent lifetime τ in a hypothetically assumed extreme case would establish (see Fig. 4.41).

The average constant profile $\overline{n}$ is obtained by

$$\overline{n} = \frac{1}{d}\int_0^d g(z)\tau \mathrm{d}z = \frac{1}{d}\int_0^d \Gamma_0 \alpha \tau \exp(-\alpha z)\,\mathrm{d}z = \frac{\Gamma_0 \tau}{d}\left[1 - \exp(-\alpha d)\right]. \tag{4.102}$$

The chemical potential of these electrons with densities n in the approximation of the Boltzmann energy distribution is given by

$$\mu_n = kT \ln\left[\frac{\Delta n + n_0}{n_0}\right], \tag{4.103}$$

where $\Delta n(z)$ might be a function of the spatial coordinate z rendering the chemical potential $\mu = \mu(z)$ dependent on z as well. For sufficient departure of Δn from

[41]For the sake of simplicity we use a flat profile and assume moreover negligible surface recombination at the rear and front as well as density-independent carrier lifetimes τ.

thermal equilibrium densities n_0, i.e., $\Delta n \gg n_0$ or $\Delta n + n_0 \approx \Delta n$, we may approximate by

$$\mu_{\mathrm{n}} \approx kT \ln\left[\frac{\Delta n}{n_0}\right] . \tag{4.104}$$

We write the density of excess carriers according to the generation profile (1) assuming the carriers do not move due to gradients in concentration and as well as the density of a hypothetic completely flat excess carrier profile (2), and we get the corresponding local chemical potentials of the electrons $\mu_{\mathrm{n},1}$ and $\mu_{\mathrm{n},2}$

$$\mu_{\mathrm{n},1}(z) = kT \ln\left[\frac{\Delta n}{n_0}\right] = kT \ln\left[\tau \Gamma_0 \alpha \exp\left(-\alpha z\right)\right] - kT \ln n_0 , \tag{4.105}$$

or equivalently,

$$\mu_{\mathrm{n},1}(z) = kT \ln\left[\tau \Gamma_0 \alpha\right] - kT\alpha z - kT \ln\left[n_0\right] , \tag{4.106}$$

and analogously, for the spatially constant excess density, we write

$$\begin{aligned} \mu_{\mathrm{n},2} &= kT \ln\left[\frac{\tau \Gamma_0}{d}\left[1 - \exp\left(-\alpha d\right)\right]\right] - kT \ln\left[n_0\right] \\ &= kT \ln\left[\frac{\tau \Gamma_0}{d}\right] + kT \ln\left[1 - \exp\left(-\alpha d\right)\right] - kT \ln\left[n_0\right] . \end{aligned} \tag{4.107}$$

The difference in the chemical potential of the two situations thus becomes

$$\begin{aligned} \mu_{\mathrm{n},1}(z) - \mu_{\mathrm{n},2} = \Delta\mu(z) = kT \Bigg\{ & \ln\left[\tau \Gamma_0 \alpha\right] - \alpha z - \ln\left[n_0\right] - \ln\left[\frac{\tau \Gamma_0}{d}\right] \\ & - \ln\left[1 - \exp\left(-\alpha d\right)\right] + \ln\left[n_0\right] \Bigg\} , \end{aligned} \tag{4.108}$$

and we arrive at

$$\Delta\mu(z) = kT \left\{ \ln\left[\frac{\tau \Gamma_0 \alpha}{\tau \Gamma_0 / d}\right] - \alpha z - \ln\left[1 - \exp\left(-\alpha d\right)\right] \right\} . \tag{4.109}$$

Finally, we may write

$$\Delta\mu(z) = kT \ln\left[\frac{\alpha d \exp\left(-\alpha z\right)}{1 - \exp(-\alpha d)}\right] . \tag{4.110}$$

Integrating $\Delta\mu(z)$ across the length d and normalizing with respect to d yields the difference in chemical potential per unit length:

$$\begin{aligned}\frac{\Delta\mu_{\text{tot}}}{d} &= \frac{kT}{d}\int_0^d \ln\left[\frac{\alpha d\,\exp(-\alpha z)}{1-\exp(-\alpha d)}\right]\mathrm{d}z \\ &= \frac{kT}{d}\int_0^d \Big\{\ln[\alpha d]-\alpha z-\ln\left[1-\exp\left(-\alpha d\right)\right]\Big\}\mathrm{d}z \\ &= \frac{kT}{d}\Big\{d\ln[\alpha d]-\frac{\alpha}{2}d^2-d\ln\left[1-\exp\left(-\alpha d\right)\right]\Big\} \\ &= kT\Big\{\ln[\alpha d]-\frac{\alpha}{2}d-\ln\left[1-\exp\left(-\alpha d\right)\right]\Big\}\ . \end{aligned} \tag{4.111}$$

A detailed inspection of the above relation shows that the chemical potential $\mu_{\text{n},1}$ of the system in the initial state, with excess carrier distribution having an exponential spatial decay, is greater than after relaxation to a flat excess carrier profile with $(\mu_{\text{n},2})$. Consequently, the entropy difference between the initial state and the final state, viz.,

$$\frac{\Delta s}{d} = \frac{1}{T}\frac{\Delta\mu_{\text{tot}}}{d}\ ,$$

is negative.[42] Conversely, the entropy is increased by smearing-out a carrier profile:

$$\frac{1}{d}\left(s_2-s_1\right) = \Delta s_{1\to 2} = k\left\{-\ln[\alpha d]+\frac{1}{2}\alpha d+\ln\left[1-\exp(-\alpha d)\right]\right\} > 0\ . \tag{4.112}$$

Figure 4.42 shows schematically the entropy increase upon smearing out a carrier profile versus absorption coefficient times absorption length αd.

[42] Starting from the fundamental relation of thermodynamics

$$\mathrm{d}U = T\mathrm{d}S - p\mathrm{d}V + \mu_i\mathrm{d}N_i\ ,$$

where U, T, S, p, V, μ, N are the internal energy, temperature, entropy, pressure, volume, chemical potential of a particular species, and number $N_i = N_i(z)$, for spatial rearrangement of particles with no change in total internal energy $\mathrm{d}U = 0$, constant temperature T = constant, no volume change $\mathrm{d}V = 0$, and solely an exchange of the chemical potential of particles/species at particular locations, we get in essence

$$\mathrm{d}S = \frac{1}{T}\left(\mathrm{d}U + p\mathrm{d}V - \mu_i\mathrm{d}N_i\right) = -\frac{\mu_i}{T}\mathrm{d}N_i\ .$$

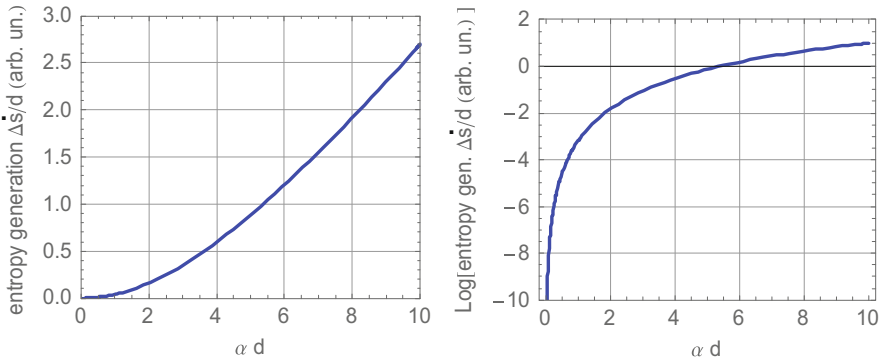

Fig. 4.42 Qualitative entropy production with smearing-out the original carrier generation profile (as sketched in Fig. 4.40) in linear *(left)* and log representation *(right)* versus absorption coefficient times absorber thickness

4.2.8.4 Entropy Production of an Ideal Solar Cell in Different Modes of Operation

The three characteristic modes for the operation of an ideal solar cell, are examined with respect to entropy production. We simplify the problem and avoid the discussion of the photon cooling effect by—in our gedankenexperiment—illumination of the ideal band system with photons of a source like a thermal equilibrium radiator (T_{source}), with a spectral distribution identical with that the absorber emits ($T_{\text{abs}} = T_{\text{source}}$); the total flux from the source to the band system is, of course, much higher than the thermal-equilibrium radiation of the system to provide for a substantial departure of it from thermal equilibrium.[43]

- In open circuit mode remember that there is no electric power delivered to outside) the band system emits photons of the same 'quality' (spectral distribution) and of the same amount as it gets from the source; we even may think of identical solid angles for light in and light out and consequently the entropy generation term in this particular case vanishes ($\dot{S}_{\text{oc}} = 0$).
- The situation in maximum power point can be extrapolated from the V_{oc}-mode: the output radiation is reduced by a factor of about $\exp(3) \approx 20$ (due to the decrease of the chemical potential from $\mu_{\text{np,oc}} = eV_{\text{oc}}$ to $\mu_{\text{np,mpp}} = eV_{\text{oc}} - 3kT$).[44] The electric output power density ($p_{\text{el}} = V_{\text{mpp}} \cdot j_{\text{mpp}}$) is free of entropy and the difference in carrier flux $j_{\text{sc}} - j_{\text{mpp}}$ is considered in the reduction of the photon flux according to μ_{mpp}. The difference of chemical potentials $\mu_{\text{np,oc}} - \mu_{\text{np,mpp}}$

[43] Since the electron system of the absorber has no memory, how the excitation to the excess carrier concentration has been performed, the excitation state also could have been established by the very same photon flux for $\hbar\omega \geq \epsilon_{\text{g}}$ from the Sun.

[44] We approximate the radiation out

that excited carriers have to endure results from the fact that the $j - V$-curve is bending for $T > 0$ or, in other words that the access to excited carriers is limited by the presence of thermally excited ones (the photoexcited carriers have to compete with the thermally excited ones; similarly to the situation in an ideal gas where there is only limited access to the internal energy of species in terms of $F = U - TS$).

- In the ideal short-circuit mode (sc) we are not able to extract electrical power from the device and each of the photogenerated carriers escapes instantaneously from the absorber (recall that we are here assuming infinite mobility/diffusion coefficients, as explained in Sect. 4.2.5). Consequently only the thermal-equilibrium carrier densities are present, whence the absorber only emits thermal equilibrium radiation. In this situation the entire solar radiation input is converted into heat at T_{abs}.

4.2.9 Gradients in Quasi-Fermi Levels for Charge Transport

Amongst the asymmetric behavior implemented into solar light absorbers by junctions or by particular contacts, the separation of charges is governed by specific features for their transport:

The motion of charge carriers, is generally described in the quasi-classical approach by the Boltzmann transport equation (see Appendix F). Particularly in semiconductors the generalized driving force for the carrier motion under small perturbation can be derived on the basis of their spatial distribution, here

$$\frac{\Omega_{\mathrm{out}}}{c_0^2 4\pi^3 \hbar^3} \int_{\epsilon_{\mathrm{g}}}^{\infty} \frac{(\hbar\omega)^3}{\exp\left(\dfrac{\hbar\omega - \mu}{kT_{\mathrm{abs}}}\right) - 1} \mathrm{d}(\hbar\omega)$$

by

$$\frac{\Omega_{\mathrm{out}}}{c_0^2 4\pi^3 \hbar^3} \int_{\epsilon_{\mathrm{g}}}^{\infty} (\hbar\omega)^3 \exp\left(\frac{\hbar\omega - \mu}{kT_{\mathrm{abs}}}\right) \mathrm{d}(\hbar\omega)$$

and get the fraction

$$(\Gamma_{\epsilon,\mathrm{out}}(oc))/(\Gamma_{\epsilon,\mathrm{out}}(mpp)) = \frac{\int_{\epsilon_{\mathrm{g}}}^{\infty} (\hbar\omega)^3 \exp\left(-\dfrac{\hbar\omega - \mu_{\mathrm{oc}}}{kT_{\mathrm{abs}}}\right) \mathrm{d}(\hbar\omega)}{\int_{\epsilon_{\mathrm{g}}}^{\infty} (\hbar\omega)^3 \exp\left(-\dfrac{\hbar\omega - (\mu_{\mathrm{oc}} - 3kT_{\mathrm{abs}})}{kT_{\mathrm{abs}}}\right) \mathrm{d}(\hbar\omega)},$$

which simplifies to

$$\exp\left(\frac{\mu_{\mathrm{oc}}}{kT_{\mathrm{abs}}}\right) / \exp\left(\frac{(\mu_{\mathrm{oc}} - 3kT_{\mathrm{abs}})}{kT_{\mathrm{abs}}}\right) = \exp\left(\frac{3kT_{\mathrm{abs}}}{kT_{\mathrm{abs}}}\right) = \exp(3)\,.$$

formulated for "free" electrons with local concentration $n(\mathbf{x})$; the "free" electrons in semiconductors allowing for transport are those in the conduction band where their transport level is close to the band edge $\epsilon = \epsilon_C$. The electron density, assumed to be only weakly varying in space,[45] writes

$$n(\mathbf{x}) = N_C f_{\text{Fermi, el}} = N_C \frac{1}{\exp\left(\dfrac{\epsilon_C(\mathbf{x}) - \epsilon_{Fn}(\mathbf{x})}{kT(\mathbf{x})}\right) + 1} . \tag{4.113}$$

The relevant magnitudes $\epsilon_C(\mathbf{x})$, $\epsilon_{Fn}(\mathbf{x})$, and $T(\mathbf{x})$ are spatially dependent; N_C designates the effective density of states in the conduction band. In the particular case of thermal equilibrium, the quasi-Fermi level for electrons approaches $\epsilon_{Fn} = \epsilon_F$. For holes, the equivalent description introduces their transport energy, the valence band edge E_V, the distribution function $f_{\text{Fermi, hole}}$, and the effective density of states:

$$p(\mathbf{x}) = N_V f_{\text{Fermi, hole}} = N_V \frac{1}{\exp\left(\dfrac{\epsilon_{Fp}(\mathbf{x}) - \epsilon_V(\mathbf{x})}{kT(\mathbf{x})}\right) + 1} . \tag{4.114}$$

Forming the spatial derivatives of the above equation for the electron part, we obtain

$$\frac{1}{N_C}\nabla_{\mathbf{x}}\left[n(\mathbf{x})\right] \tag{4.115}$$

$$= \left(\frac{1}{kT}\right) \frac{\exp\left(\dfrac{\epsilon_C - \epsilon_{Fn}}{kT}\right)}{\left(\exp\left(\dfrac{\epsilon_C - \epsilon_{Fn}}{kT}\right) + 1\right)^2} \left\{\nabla_{\mathbf{x}}\left[\epsilon_C(\mathbf{x})\right] - \nabla_{\mathbf{x}}\left[\epsilon_{Fn}(\mathbf{x})\right] + \left(\frac{\epsilon_C - \epsilon_F}{T}\right)\nabla_{\mathbf{x}}\left[T(\mathbf{x})\right]\right\} .$$

Introducing the abbreviation

$$\beta^* = \frac{\exp\left(\dfrac{\epsilon_C - \epsilon_{Fn}}{kT}\right)}{\exp\left(\dfrac{\epsilon_C - \epsilon_{Fn}}{kT}\right) + 1} ,$$

[45] Only a weak dependence of $\epsilon_C(\mathbf{x})$, $\epsilon_{Fn}(\mathbf{x})$, and $T(\mathbf{x})$ is assumed, justifying the idea that only the gradients are spatial functions, while the temperature dependence of the effective density N_C of electrons in the conduction band is also neglected (N_C = constant).

we get the gradient of the quasi-Fermi level of the electrons that contains each of the quantities contributing to electron transport

$$\nabla_{\mathbf{x}}\left[\epsilon_{\mathrm{Fn}}(\mathbf{x})\right] = \nabla_{\mathbf{x}}\left[\epsilon_{\mathrm{C}}(\mathbf{x})\right] - \frac{kT}{N_{\mathrm{C}}}\left(\exp\left(\frac{\epsilon_{\mathrm{C}} - \epsilon_{\mathrm{Fn}}}{kT}\right) + 1\right)\frac{1}{\beta^*}\nabla_{\mathbf{x}}\left[n(\mathbf{x})\right] + \left(\frac{\epsilon_{\mathrm{C}} - \epsilon_{\mathrm{Fn}}}{T}\right)\nabla_{\mathbf{x}}\left[T(\mathbf{x})\right] . \tag{4.116}$$

Recognizing that

$$\frac{1}{N_{\mathrm{C}}}\left[\exp\left(\frac{\epsilon_{\mathrm{C}}(\mathbf{x}) - \epsilon(\mathbf{x})}{kT(\mathbf{x})}\right) + 1\right] = \frac{1}{n(\mathbf{x})} ,$$

one arrives at

$$\nabla_{\mathbf{x}}\left[\epsilon_{\mathrm{Fn}}(\mathbf{x})\right] = \nabla_{\mathbf{x}}\left[\epsilon_{\mathrm{C}}(\mathbf{x})\right] - kT\frac{1}{n(\mathbf{x})}\frac{\exp\left(\frac{\epsilon_{\mathrm{C}} - \epsilon_{\mathrm{Fn}}}{kT}\right)}{\exp\left(\frac{\epsilon_{\mathrm{C}} - \epsilon_{\mathrm{Fn}}}{kT}\right) + 1}\nabla_{\mathbf{x}}\left[n(\mathbf{x})\right] + \left(\frac{\epsilon_{\mathrm{C}} - \epsilon_{\mathrm{Fn}}}{T}\right)\nabla_{\mathbf{x}}\left[T(\mathbf{x})\right] . \tag{4.117}$$

A detailed inspection of the factor β^* reveals its almost constant behavior $\beta^* \to 1$ for sufficiently large difference $\epsilon_{\mathrm{C}} - \epsilon_{\mathrm{Fn}} \geq 3kT$, shown in Fig. 4.43 as a function of $(\epsilon_{\mathrm{Fn}}/\epsilon_{\mathrm{C}})$ for different values of kT with $kT \ll \epsilon_{\mathrm{C}}$. This treatment leads to a result similar to the approximation by the Boltzmann-energy distribution of the above relation for $n(\mathbf{x})$.

Furthermore we may extend the gradients towards fluxes in particular for the electron contribution to the electrical current density by multiplication of left- and

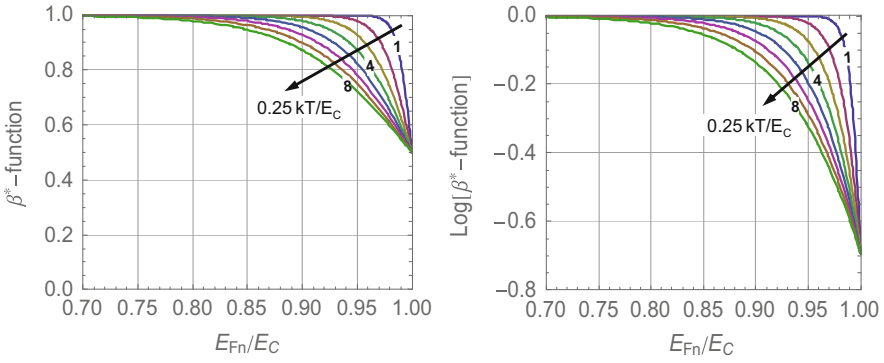

Fig. 4.43 β^*-Function which modifies (only marginally) the Fermi–Dirac distribution function in the transport approach, justifying the approximation $\beta^* \approx 1$ in $0 \leq \epsilon_{\mathrm{Fn}} \leq \epsilon_{\mathrm{C}}$, ($kT = 26\,\mathrm{meV}$; $\epsilon_{\mathrm{C}} = 1\,\mathrm{eV}$, $\epsilon_{\mathrm{V}} = 0\,\mathrm{eV}$)

right-hand sides of the relation above with the electron mobility[46] μ_{n}^{*} and by the concentration $n(\mathbf{x})$ to get

$$\mu_{\mathrm{n}}^{*} n(\mathbf{x}) \nabla_{\mathbf{x}}\big[\epsilon_{\mathrm{Fn}}(\mathbf{x})\big] = \mu_{\mathrm{n}}^{*} n(\mathbf{x}) \nabla_{\mathbf{x}}\big[\epsilon_{\mathrm{C}}(\mathbf{x})\big] - \mu_{\mathrm{n}}^{*} n(\mathbf{x}) \frac{kT}{\beta^{*} n(\mathbf{x})} \nabla_{\mathbf{x}}\big[n(\mathbf{x})\big] + \mu_{\mathrm{n}}^{*} n(\mathbf{x}) \left(\frac{\epsilon_{\mathrm{C}} - \epsilon_{\mathrm{Fn}}}{T}\right) \nabla_{\mathbf{x}}\big[T(\mathbf{x})\big] \,. \tag{4.118}$$

Substituting the gradient of the conduction band level ϵ_{C} by the electric field

$$\nabla_{\mathbf{x}}(\epsilon_{\mathrm{C}}) = \nabla_{\mathbf{x}}\big[-e\varphi(\mathbf{x})\big] = e\mathbf{E}(\mathbf{x})$$

in the first term, and setting $\beta^{*} \approx 1$ as well as replacing the mobility μ_{n}^{*} by the diffusion coefficient D_{n} via the Einstein relation

$$\mu^{*} = \frac{e}{kT} D$$

in the second term, the above equation evidently reads as a contribution of electrons to the electric current density $j_{\mathrm{n}}(\mathbf{x})$:

$$\mu_{\mathrm{n}}^{*} n(\mathbf{x}) \nabla_{\mathbf{x}}\big[\epsilon_{\mathrm{Fn}}(\mathbf{x})\big] = e\mu_{\mathrm{n}}^{*} n(\mathbf{x}) \mathbf{E}(\mathbf{x}) - eD_{\mathrm{n}} \nabla_{\mathbf{x}}\big[n(\mathbf{x})\big] + \mu_{\mathrm{n}}^{*} n(\mathbf{x}) \left(\frac{\epsilon_{\mathrm{C}} - \epsilon_{\mathrm{Fn}}}{T}\right) \nabla_{x}\big[T(\mathbf{x})\big] = j_{\mathrm{n}}(\mathbf{x}) \,, \tag{4.119}$$

where the first term represents carrier drift, the second describes carrier diffusion, and the last term details the contribution due to a thermal gradient that in turn leads to thermal conduction and to thermoelectric effects. Evidently, for a comprehensive and consistent formulation of the current in photovoltaic cells we only need to regard the gradient in the quasi-Fermi energy of the respective carriers.

References

1. M. Rubin, Phys. Rev. A **19**, 1272 (1979)
2. F. Curzon, B. Ahlborn, Am. J. Phys. **43**, 22 (1975)
3. A. deVos, *Endoreversible Thermodynamics for Solar Energy Conversion* (Oxford University Press, Oxford, 1992); *Thermodynamics of Solar Energy Conversion* (Wiley-VCH, Weinheim, 2008)
4. P.T. Landsberg, J. Appl. Phys. **54**, 2841 (1983)
5. H. Müser, Zeitschr. f. Phys. **148**, 380 (1957)
6. P. Würfel, Physica E **14**, 18 (2002)

[46] The electron mobility is represented here by the asterixed μ_{n}^{*} and might not be confused with the electron chemical potential μ_{n}.

7. N.W.Ashcroft, N.D. Mermin, *Solid State Physics/Int. Edition* (W.B. Saunders Company, Philadelphia, 1976)
8. K-.H. Seeger, *Semiconductor Physics* (Springer, Berlin, 2010)
9. P.Y. Yu, M. Cardona, *Fundamentals of Semiconductors, Physics and Material Properties* (Springer, Berlin, 1996)
10. Z.G. Yu et al., Phys. Rev. B **71**, 245312 (2005)
11. P.H. Song et al., Phys. Rev. B **66**, 035205 (2003)
12. P. Würfel, J. Phys. C Solid State Phys. **15**, 3967 (1982)
13. W.T. Welford, R. Winston, *The Optics of Non-imaging Concentrators* (Academic, New York, 1978)
14. T. Markvart, J. Opt. A: Pure Appl. Opt. **10**, 015008 (2008)
15. P. Würfel, *Physics of Solar Cells* (Wiley-VCH, Weinheim, 2009)
16. W. Shockley, H.-J. Queisser, J. Appl. Phys. **32**, 510 (1961)
17. D. Trivich, P.A. Flinn, in *Solar Energy Research*, ed. by F. Daniels, J. Duffie (Thames & Hudson, London, 1955)
18. J. Tauc, Mater. Res. Soc. Bull. **3**, 37 (1968)
19. C. Donolato, Appl. Phys. Lett. **46**, 270 (1985); J. Appl. Phys. **66**, 4524 (1989)
20. U. Rau, Phys. Rev. B **76**, 08503 (2007)
21. T. Markvart, Appl. Phys. Lett. **91**, 064102 (2007)
22. E. Yablonovitch, J. Opt. Soc. Am. **72**, 899 (1982)

Chapter 5
Real Photovoltaic Converters

Real photovoltaic converters (solar cells), consisting of molecular, liquid, or solid state structures of various types, exhibit particular departures from the ideal converter presented in Chap. 4. These departures concern for example:

- Incomplete absorption of solar photons with energies above the optical threshold energy.
- Considerable rates of non-radiative transitions from excited states to the ground states, commonly introduced by defects, dopants, impurities, surface states, and interface states.
- Limitations of transport of charge carriers or excitonic compounds that move the photoexcited states to the boundaries of the absorber and connect them to leads to the outside.

A prominent set of such converters is presented here and discussed in terms of the parameters and effects explained in Sect. 4 and hence recognized as relevant for the function of solar light conversion.

The majority of today's solar cells are made up of inorganic matter, explicitly semiconductors, with various optical band gaps and electronic properties, such as densities of states, type of optical transitions (direct/indirect), absorption coefficients, type of doping, and carrier mobilities. These properties can be moderately well understood qualitatively in terms of stationary state solutions of the Schrödinger equation in an infinitely extended three-dimensional periodic potential, applying the independent-electron picture. For inorganic absorbers, the currently important types of barrier structures are discussed in detail in Sects. 5.1–5.4. This allows the formulation of the state of electrons and their counterpart, the holes, in thermal equilibrium and under photoexcitation under certain conditions of sufficiently fast intraband relaxation on the basis of Fermi statistics.

The excitation of molecular species, such as organic absorbers and dye molecules in several matrices, equipped again with majority-carrier barriers, are then examined.

G.H. Bauer, *Photovoltaic Solar Energy Conversion*, Lecture Notes in Physics 901,
DOI 10.1007/978-3-662-46684-1_5

5.1 Homogeneous *pn*-Junctions

One of the conceptually simplest device options for photovoltaic cells is a homogeneous semiconductor *pn*-junction (homogeneous *pn*-diode). The junction between *p*- and *n*-type doped region creates an asymmetry for the transport of differently charged carriers, such as electrons and holes and thus provides source and sink for the relevant excess species. The source of photoexcited electrons is the *p*-doped region where the electrons are minority carriers, and their sink is the *n*-doped layer where they adopt majority carrier behavior. The photoexcited holes originate analogously as minority carriers from the *n*-doped region, while their sink is the *p*-type regime. The concentrations of photoexcited majority carriers, holes in the *p*-doped region and electrons in the *n*-doped region, even at maximum solar light concentration, are extremely low in comparison with the respective thermal equilibrium concentrations and do not contribute significantly to the resulting photocurrents.

As the treatment of other types of junctions is conceptually identical to that of a homogeneous barrier, we explain how they work and derive the relevant equations here in some detail (see also textbooks on semiconductor physics such as [1–4]).

5.1.1 Space-Charge Region

The combination of two differently doped regimes of one type of semiconductor leads at their interface to a diffusion of electrons and holes which establishes a regime of depleted majority carriers, with a deficit of electrons at the *n*-side and of holes at the *p*-side. A space-charge regime $\rho(x)$ thus forms, originating from the locally arrested negatively charged acceptor ions (n_{A}^{-}) in the *p*-regime and the positively charged donor ions (n_{D}^{+}) in the *n*-regime (see Fig. 5.1).[1]

The twofold (indefinite) spatial integration of this space charge $\rho(x)$ results in a spatially dependent electrostatic potential

$$\varphi(x) = \varepsilon\varepsilon_0 \int \left(\int \rho(x)\mathrm{d}x \right) \mathrm{d}x \ ,$$

which is translated into the electron energy $\epsilon_{\mathrm{electron}}(x) = e\varphi(x)$ by multiplication with the electron charge $-e = -1.6 \times 10^{-19}$ A s.

The spatially dependent function $\epsilon_{\mathrm{electron}}(x) \sim \varphi(x)$ modifies the electron (and hole) energy levels in the neighborhood of the space-charge region which separates the two differently doped parts of the *pn*-configuration. Hence, the vacuum level

[1] For infinite *p*- and *n*-type doped layers, it is assumed that the finite number of electrons and holes having moved across the junction are distributed within the infinite layer lengths without increasing the overall initial thermal-equilibrium majority carrier concentrations.

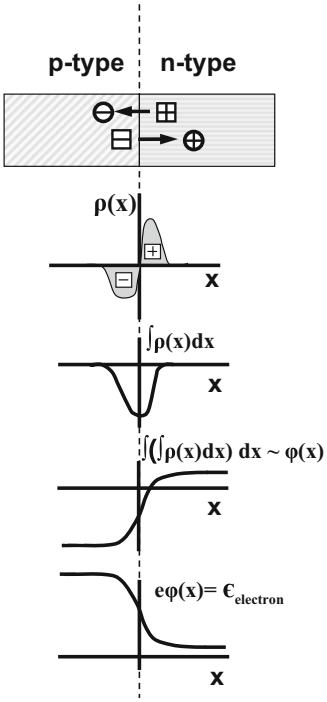

Fig. 5.1 Formation of space-charge region (SCR) in a homogeneous *pn*-junction by exchange of electrons and holes across the interface. The transition from the local space-charge $\rho(x)$ to the local electron energy level distribution $\epsilon(x)$ is established qualitatively derived by applying Poisson's equation

ϵ_{vac}, the edge of the conduction band ϵ_{C}, and the edge of the valence band ϵ_{V} become spatially dependent, and this local behavior enters into the band diagram of the junction as an energy barrier for transport of the majority carriers (see Figs. 5.1 and 5.2).[2]

An analytical formulation of this space-charge effect and its consequences on electronic levels by assuming an abrupt spatial regime of positively and negatively charged dopants is displayed in Fig. 5.3.

For the sake of algebraic simplicity, we calculate the electrostatic potential $\varphi(x)$ with help of Poisson's equation in a one-dimensional representation, for the abrupt space-charge region (Fig. 5.3):

$$\frac{\mathrm{d}^2\varphi(x)}{\mathrm{d}x^2} = -\frac{e}{\varepsilon_0\varepsilon}\left[n_{\mathrm{A}}^{-}(x) - n_{\mathrm{D}}^{+}(x)\right] . \tag{5.1}$$

For these p-type ($-x_{\mathrm{p}} \leq x \leq 0$) and n-type ($0 \leq x \leq x_{\mathrm{n}}$) doped regimes, we get the corresponding derivative ($\mathrm{d}\varphi(x)/\mathrm{d}x$) of the electrostatic potential and the potential $\varphi(x)$ itself. In the above relation, e, ε_0, ε, n_{A}^{-}, and n_{D}^{+} denote elementary charge,

[2]Each of the core levels of the atoms in the p- and n-type doped regimes are spatially modulated by this potential function $\varphi(x)$.

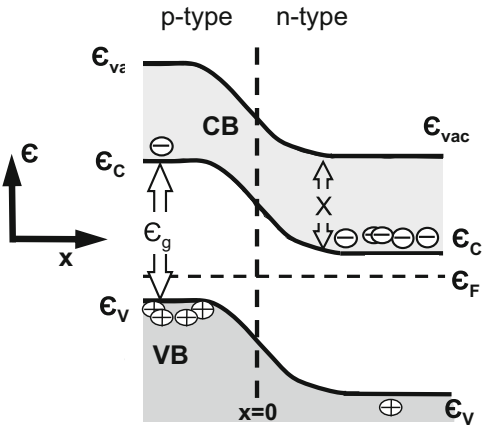

Fig. 5.2 Schematic band diagram of a homogeneous *pn*-junction in thermal equilibrium with zero applied voltage (Fermi level ϵ_F is horizontal) with majority carriers (electrons in the *n*-type and holes in the *p*-type doped regimes) and minority charges (electrons in the *p*-type and holes in the *n*-type doped regimes). Also in the space-charge regime, carrier concentrations $n(x)$ and $p(x)$ are determined by Fermi statistics

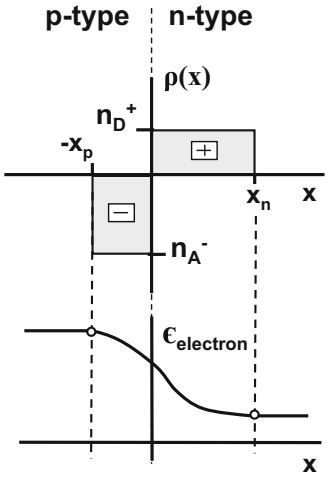

Fig. 5.3 Space-charge region of an abrupt *pn*-junction and qualitative electron energy level, e.g., conduction band. This approach allows for an easy analytical treatment of the junction properties

vacuum dielectric constant, dielectric susceptibility of the particular semiconductor, density of negatively charged acceptors, and density of positively charged donors. Moreover, we assume completely ionized acceptor and donor states, which means that each of the incorporated impurities, acceptors N_A and donors N_D, contribute to the space charge: $n_A^- = N_A$, and $n_D^+ = N_D$ (the individual magnitudes in the respective regions are indexed by p and n).

For relatively low temperatures in the neighborhood of $T = 300\,\mathrm{K}$ and below, the Fermi distribution can be approximated by a step function. The bending of the bands, e.g., the 'upward' bending of ϵ_C and of the donor level ϵ_D in the *n*-regime close to the interface crosses the Fermi level ϵ_F, and for $\epsilon_D > \epsilon_F$, the energy level of the donor is to a good approximation unoccupied, with donor state n_D^+. The acceptor

impurities for the downward bending of ϵ_V and of the acceptor level ϵ_A are occupied by electrons since $\epsilon_A < \epsilon_F$, and accordingly the acceptor states are n_A^-.

For these parts of p- and n-regions we thus get with integration constants C and C' by applying Poisson's equation:

$$-\frac{d^2\varphi(x)}{dx^2} = \frac{e}{\varepsilon_0\varepsilon}\big(-N_A\big)\,, \tag{5.2}$$

$$-\frac{d\varphi(x)}{dx} = -\frac{e}{\varepsilon_0\varepsilon}N_A x + C\,, \tag{5.3}$$

$$-\frac{d^2\varphi(x)}{dx^2} = \frac{e}{\varepsilon_0\varepsilon}N_D\,, \tag{5.4}$$

$$-\frac{d\varphi(x)}{dx} = \frac{e}{\varepsilon_0\varepsilon}N_D x + C'\,. \tag{5.5}$$

Left- and right-hand side boundary conditions are

$$\frac{d\varphi(x=-x_p)}{dx} = 0 = \frac{d\varphi(x=x_n)}{dx} \tag{5.6}$$

and

$$\varepsilon_{p\text{-side}}\frac{d\varphi(x=0)}{dx} = \varepsilon_{n\text{-side}}\frac{d\varphi(x=0)}{dx}\,. \tag{5.7}$$

In a homogeneous junction, where the dielectric susceptibilities are identical on the left- and right-hand sides, i.e., $\varepsilon_{p\text{-side}} = \varepsilon_{n\text{-side}} = \varepsilon$, we get for the p-side

$$\frac{d\varphi(x)}{dx} = -\frac{e}{\varepsilon_0\varepsilon}N_A(x + x_p)\,, \tag{5.8}$$

and for the n-side

$$\frac{d\varphi(x)}{dx} = \frac{e}{\varepsilon_0\varepsilon}N_D(x - x_n)\,. \tag{5.9}$$

At $x = 0$, the requirement of continuous normal components of the dielectric displacement, viz., $\varepsilon_{p\text{-side}}\mathbf{E}_{\text{normal, }p\text{-side}} = \varepsilon_{n\text{-side}}\mathbf{E}_{\text{normal, }n\text{-side}}$, implies that

$$\frac{d\varphi(x=0)}{dx} = -\frac{e}{\varepsilon_0\varepsilon}N_A x_p = -\frac{e}{\varepsilon_0\varepsilon}N_D x_n\,. \tag{5.10}$$

The equality $N_A x_p = N_D x_n$ announces charge neutrality for the entire width of the *pn*-junction, across $-x_p \le x \le x_n$.

A further spatial integration leads to the electrostatic potential $\varphi(x)$. With $\varphi_\mathrm{p}(x)$ for the p-side and $\varphi_\mathrm{n}(x)$ for the n-side, we thus have, for $-x_\mathrm{p} \leq x \leq 0$,

$$\varphi_\mathrm{p} = V(x) = -\int \frac{-e}{\varepsilon_0 \varepsilon} N_\mathrm{A}(x + x_\mathrm{p})\mathrm{d}x = \frac{e}{\varepsilon_0 \varepsilon} N_\mathrm{A} \left(\frac{x^2}{2} + x_\mathrm{p} x \right) + C_1 \,, \tag{5.11}$$

and for $0 \leq x \leq x_\mathrm{n}$,

$$\varphi_\mathrm{n} = \varphi(x) = -\int \frac{-e}{\varepsilon_0 \varepsilon} N_\mathrm{D}(x - x_\mathrm{n})\mathrm{d}x = -\frac{e}{\varepsilon_0 \varepsilon} N_\mathrm{D} \left(\frac{x^2}{2} - x_\mathrm{n} x \right) + C_2 \,. \tag{5.12}$$

The boundary conditions introduce $\varphi_\mathrm{p}(x = 0) = \varphi_\mathrm{n}(x = 0)$, resulting in $C_1 = C_2$, and arbitrarily selected $\varphi_\mathrm{p}(-x_\mathrm{p}) = 0$ and $\varphi_\mathrm{n}(x_\mathrm{n}) = V_\mathrm{bi}$, called the built-in potential. We finally obtain

$$\varphi_\mathrm{p}(x) = \frac{e}{2\varepsilon_0 \varepsilon} N_\mathrm{A}(x + x_\mathrm{p})^2 \tag{5.13}$$

and

$$\varphi_\mathrm{n}(x) = \frac{e}{2\varepsilon_0 \varepsilon} N_\mathrm{D} \left(-x^2 + 2x x_\mathrm{n} + \frac{N_\mathrm{A}}{N_\mathrm{D}} x_\mathrm{p}^2 \right) \,. \tag{5.14}$$

We thus arrive at the built-in potential

$$V_\mathrm{bi} = \varphi_\mathrm{n}(x_\mathrm{n}) = \frac{e}{2\varepsilon_0 \varepsilon} \left(N_\mathrm{A} x_\mathrm{p}^2 + N_\mathrm{D} x_\mathrm{n}^2 \right) \,. \tag{5.15}$$

From this built-in potential and with the condition of charge neutrality $N_\mathrm{A} x_\mathrm{p} = N_\mathrm{D} x_\mathrm{n}$, we calculate the total width $w = x_\mathrm{n} + x_\mathrm{p}$ of this regime in which charge neutrality is violated, and which is thus referred to as the space-charge region (SCR):

$$w = x_\mathrm{n} + x_\mathrm{p} = \sqrt{\frac{2\varepsilon_0 \varepsilon V_\mathrm{bi}}{e N_\mathrm{A} N_\mathrm{D}} (N_\mathrm{A} + N_\mathrm{D})} = \sqrt{\frac{2\varepsilon_0 \varepsilon V_\mathrm{bi}}{e} \left(\frac{1}{N_\mathrm{A}} + \frac{1}{N_\mathrm{D}} \right)} \,. \tag{5.16}$$

The built-in potential V_bi represents the energy shift in thermal equilibrium between the vacuum level of p-doped and n-doped regimes, far away from the junction. In a homogeneous junction where p- and n-type layers consist of the same basic material differing solely in the type of doping, V_bi can be determined by the optical band gap ϵ_g and the energy differences of the Fermi levels from the majority band edges, e.g., $\epsilon_\mathrm{F} - \epsilon_{\mathrm{V},\, p\text{-side}}$ and $\epsilon_{\mathrm{C},\, n\text{-side}} - \epsilon_\mathrm{F}$. We therefore obtain

$$eV_\mathrm{bi} = \epsilon_\mathrm{g} - \left(\epsilon_\mathrm{F} - \epsilon_{\mathrm{V},\, p\text{-side}} \right) - \left(\epsilon_{\mathrm{C},\, n\text{-side}} - \epsilon_\mathrm{F} \right) \,. \tag{5.17}$$

Of course, in the two equations above, the expressions for V_{bi} are consistent with one another since the dopant concentrations N_{A} and N_{D} govern the position of the respective Fermi levels.

Furthermore, we see that the higher the concentrations N_{A} and N_{D} of dopants, the smaller the width of the corresponding space-charge region at the p- and n-sides, together with their sum. This width is necessary to establish the appropriate amount of charges at the junction, resulting from the 'reaction' of the majority carriers on each side, to reach chemical equilibrium.

An exemplary estimate of the spatial extension of the space-charge width in crystalline silicon, with medium dopand concentrations representative of typical electronic or optoelectronic devices, viz., $N_{\mathrm{A}} = N_{\mathrm{D}} = 10^{16}\,\mathrm{cm}^{-3}$, dielectric susceptibility $\varepsilon_{\mathrm{Si}} = 12$, and $V_{\mathrm{bi}} = 1.0\,\mathrm{V}$, yields $w \approx 0.5\,\mu\mathrm{m}$. This is considerably smaller than the common thickness of c-Si wafers[3] of about $d_{\text{c-Si}} = 200\text{–}400\,\mu\mathrm{m}$.

Here we have to recognize that, in the space-charge region, the potential has a non-vanishing gradient $\nabla\varphi(\mathbf{x}) \neq 0$, accompanied by $\nabla\epsilon_{\mathrm{C}}(\mathbf{x}) \neq 0$ and $\nabla\epsilon_{\mathrm{V}}(\mathbf{x}) \neq 0$, which is often called an electric field. However, these gradients definitely do not induce carriers to move 'downhill'. For this reason, we refrain from referring to these gradients as electric fields and rather keep the original expression of gradients of the electrostatic potential $\nabla_{\mathbf{x}}\varphi(\mathbf{x})$, or gradients of the conduction or valence band energy.[4]

5.1.2 Current Density–Voltage Relation of a Homogeneous pn-Diode

An externally applied voltage V_{ext} at a non-illuminated *pn*-junction leads to a perturbation of the thermal equilibrium and thus to a departure from $V_{\mathrm{ext}} = 0$ and $j = 0$, a condition that allows for a non-vanishing current density $j(V_{\mathrm{ext}} \neq 0) \neq 0$.

In the idealized formulation of the current density, we assume:

- Carrier transport from the contacts to the junction requires negligible voltage drops, which means negligible $\nabla_{\mathbf{x}}\epsilon_{\mathrm{Fn}} \approx \nabla_{\mathbf{x}}\epsilon_{\mathrm{C}}$ for electrons in the n-doped layer and also negligible $\nabla_{\mathbf{x}}\epsilon_{\mathrm{Fp}} \approx \nabla_{\mathbf{x}}\epsilon_{\mathrm{V}}$ for holes in the p-doped region—both conditions are met by hypothetic high (infinite) carrier mobilities/diffusion coefficients.

[3] If the thickness of the semiconductor is less than the width of the space-charge region, the surplus of charges needed for chemical equilibrium is located in the outer metal contacts of the device.

[4] Regardless of its mode of operation (except for particularly extreme cases which are irrelevant for our purposes), the space-charge region of a diode exhibits spatial gradients in the conduction and valence bands. These gradients also exist in thermal equilibrium (no illumination, no applied voltage, etc.), where—in accordance with the second law of thermodynamics—definitely no current can flow. Here we do not discuss Brownian motion, which does not contribute to stationary carrier flows.

- Accordingly, the externally applied voltage only drops within the space-charge region of the junction, modifying the widths of those regimes at the n- and the p-side, and thereby changing the built-in voltage towards $V_{bi} - V_{ext}$.
- The p- and n-doped regimes are infinitely extended (p-side within $-\infty \leq x \leq 0$, and n-side within $0 \leq x \leq \infty$).
- The supply of majority and minority carriers to contribute to the resulting current density is provided by thermal generation. Due to the assumption of infinitely extended n- and p-layers, there is no limitation to their total generation rates. Figure 5.4 shows zero applied voltage, forward bias, and reverse bias conditions.

With these assumptions, under forward bias voltage, carriers from the majority-carrier side, electrons from the n-type and holes from the p-type region, are injected across the interface into the adjacent layers. In the space-charge region, the majority carriers govern the entire current density. Therefore, this current density in forward bias is comparatively high (Fig. 5.4 center).

In reverse bias, electron and hole minority carriers determine the current density across the barrier regime (Fig. 5.4 lower part), resulting in an extremely low total

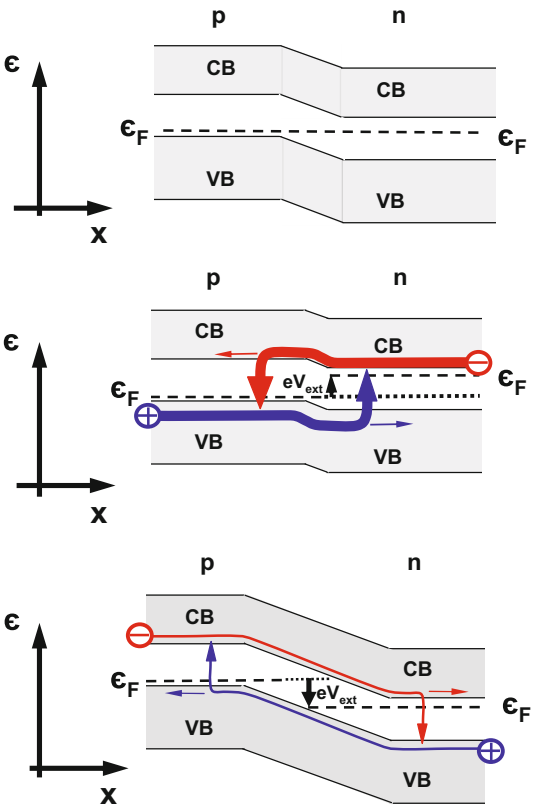

Fig. 5.4 Schematic band diagrams of a homogeneous *pn*-junction under zero applied voltage (*upper*), under forward bias voltage $V_{ext} > 0$ (*center*), and under reverse bias voltage $V_{ext} < 0$ (*lower*). *Arrows* indicate major current contributions across the barrier. Recombination in the space-charge region has been excluded by definition

current density. The excess carrier concentrations in the layer adjacent to the reservoirs from which they have been injected, be they majority (forward bias) or minority carriers (reverse bias), are exhausted by recombination, which is assumed in the simple model to occur only outside the space-charge regime.

For the analytical formulation of current densities in a *pn*-junction, we shall neglect effects in the spatial extent of the space-charge region. We explore the probability for transport in this artificial step-like energy configuration by comparing the carrier concentrations left and right side of the junction at their respective transport levels; the lowest energetic level for transport of electrons across the barrier is the conduction band edge of the p-doped regime ($\epsilon_{\mathrm{C,p\text{-}side}}$), for holes the highest level is correspondingly the valence band edge ($\epsilon_{\mathrm{V,n\text{-}side}}$) of the n-type doped semiconductor.[5]

The concentration of carriers in the bands, here discussed for electrons in the conduction band, and the relevant number of those above a particular energy, such as above the potential step, is expressed through the density of states in the band, and their occupation is described by Fermi-Dirac statistics (Fermi or quasi-Fermi distributions).

The electron concentration in the conduction band of the p-side is

$$n_{\mathrm{CB},\,p\text{-side}}(\epsilon) = D_{\mathrm{CB}}(\epsilon)\frac{1}{\exp\left(\dfrac{\epsilon_{p\text{-side}} - \epsilon_{\mathrm{F}}}{kT}\right) + 1}\,, \tag{5.18}$$

whereas the electron concentration at the n-side amounts to

$$n_{\mathrm{CB},\,n\text{-side}}(\epsilon) = D_{\mathrm{CB}}(\epsilon)\frac{1}{\exp\left(\dfrac{\epsilon_{n\text{-side}} - \epsilon_{\mathrm{F}}}{kT}\right) + 1}\,. \tag{5.19}$$

The level $\epsilon_{\mathrm{C},\,p\text{-side}}$ as the edge of the conduction band in the p-type doped region in thermal equilibrium corresponds to the level $\epsilon_{\mathrm{C},\,p\text{-side}} = \epsilon_{\mathrm{C},\,n\text{-side}} + eV_{\mathrm{bi}}$ in the n-doped region, where the very same electron density appears, since the Fermi level in thermal equilibrium is 'horizontal' (see band diagram in the upper part of Fig. 5.4). So the entire concentration of electrons for energies $\epsilon \geq \epsilon_{\mathrm{C},\,p\text{-side}} = \epsilon_{\mathrm{C},\,n\text{-side}} + eV_{\mathrm{bi}}$ is then

$$\begin{aligned} n_{\mathrm{CB},\,p\text{-side}} &= \int_{\epsilon_{\mathrm{C},\,p\text{-side}}}^{\infty} D_{\mathrm{CB}}(\epsilon)\frac{1}{\exp\left(\dfrac{\epsilon - \epsilon_{\mathrm{F}}}{kT}\right) + 1}\mathrm{d}\epsilon \\ &= \int_{\epsilon_{\mathrm{C},\,n\text{-side}}+eV_{\mathrm{bi}}}^{\infty} D_{\mathrm{CB}}(\epsilon)\frac{1}{\exp\left(\dfrac{\epsilon - \epsilon_{\mathrm{F}}}{kT}\right) + 1}\mathrm{d}\epsilon = n^{*}_{\mathrm{CB},\,n\text{-side}}\,, \end{aligned} \tag{5.20}$$

and is identical for thermal equilibrium.

[5] We may also regard the extension of the electron and hole-wave functions which are extended infinitely in the infinite device for energies $\epsilon \geq \epsilon_{\mathrm{C,p\text{-}side}}$ for electrons and $\epsilon \leq \epsilon_{\mathrm{V,n\text{-}side}}$ for holes.

For a departure from thermal equilibrium due to an applied voltage V_{ext}, either forward or reverse bias (see Fig. 5.4 center and lower part), the electron concentration at the level $\epsilon_{\text{trans}} = \epsilon_{\text{CB, }p\text{-side}}$ allowing for transport in $-\infty \leq x \leq +\infty$ is no longer identical on the left- and right-hand sides of the junction, since the applied voltage shifts the bands relative to one another: the n-side goes up with respect to the p-side for forward bias, and down for reverse bias. In other words, the term of the built-in potential in thermal equilibrium eV_{bi} is now modified by the externally applied voltage and writes $(eV_{\text{bi}} - eV_{\text{ext}})$.

With the approximation of the Maxwell–Boltzmann statistics, we get the electron density in the n-region (right-hand side of the junction) at the transport energy level:

$$n_{\text{CB, }n\text{-side}} = n^*_{\text{CB, }n\text{-side}} \exp\left(\frac{eV_{\text{ext}}}{kT}\right) . \tag{5.21}$$

This now departs from the value on the left-hand side, which reads

$$n_{\text{CB, }p\text{-side}} = n^*_{\text{CB, }n\text{-side}} \tag{5.22}$$

by the factor $\exp\left(\frac{eV_{\text{ext}}}{kT}\right)$. The difference in concentration of electrons available for transport at the junction will lead to an exchange across the interface between the p- and n-type regions ($x = 0$, see Fig. 5.5), to be formulated by diffusion.[6]

[6]Diffusion of a particular species originates from the spatial gradient of their concentration $n(\mathbf{x})$. The resulting flux Γ reads $\boldsymbol{\Gamma}(\mathbf{x}) = D\big[-\nabla n(\mathbf{x})\big]$, where D is the diffusion coefficient. The spatial density $n(\mathbf{x})$ is derived by solving the steady-state continuity equation

$$\nabla\cdot\big[n(\mathbf{x})\mathbf{u}(\mathbf{x})\big] = \nabla\cdot\boldsymbol{\Gamma}\,(\mathbf{x}) = g(\mathbf{x}) - r(\mathbf{x}) .$$

With carrier velocity $\mathbf{u}(\mathbf{x})$ generation rate $g(\mathbf{x}) = 0$ and recombination rate given by the quotient of the density $n(\mathbf{x})$ and the lifetime τ, viz., $r(\mathbf{x}) = n(\mathbf{x})/\tau$, we arrive at the second order differential equation

$$\nabla\cdot\big[-D\nabla n(\mathbf{x})\big] = -D\Delta n(\mathbf{x}) = -\frac{n(\mathbf{x})}{\tau} .$$

In one dimension, this has the general solution

$$n(x) = A\exp\left(+\frac{x}{\sqrt{D\tau}}\right) + B\exp\left(-\frac{x}{\sqrt{D\tau}}\right) .$$

The length $\sqrt{D\tau} = L$ is called the diffusion length. In the case considered here, for infinite extension of the p-type regime (towards $x \to -\infty$) and n-type region (towards $x \to +\infty$), only one of the terms of the solution meets the boundary condition of density n approaching zero at infinite distances from the junction, and we arrive at $n(x)$ decaying purely exponentially either in $x < 0$, or in $x > 0$.

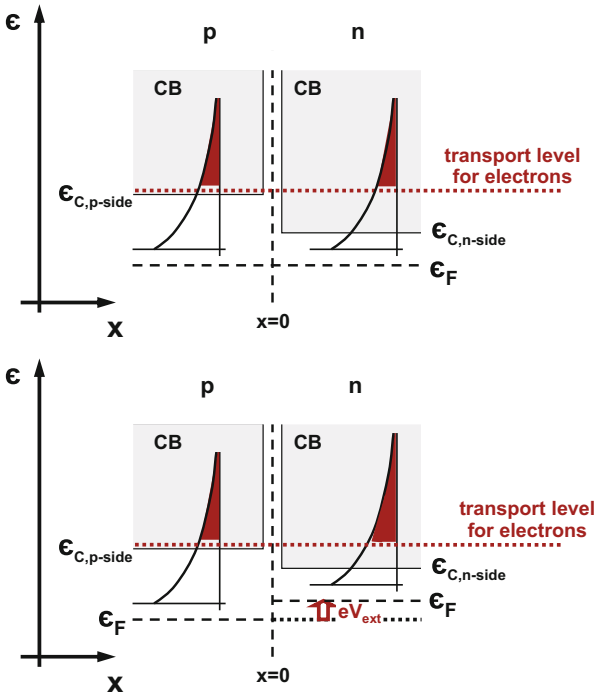

Fig. 5.5 Abrupt homogeneous *pn*-junction with schematic carrier distribution functions left and right side of the junction in thermal equilibrium (*upper part*) and under forward bias voltage ($eV_{\text{ext}} > 0$) demonstrating the larger electron concentration at the transport level $\epsilon_{\text{C,p-side}}$ in the n-type doped part of the junction (*lower part*)

This diffusion current density is written for the position of abrupt $p-n$-interface where we have disregarded the space-charge region and where no recombination of carriers has occurred. The electron contribution (j_{n}) to the total diffusion current density is

$$j_{\text{n}}(x=0) = eD_{\text{n}}\nabla n\,(x=0) = eD_{\text{n}}\left(\frac{n_{\text{CB, }p\text{-side}} - n^{*}_{\text{CB, }n\text{-side}}}{L_{\text{n}}}\right)$$
$$= e\frac{D_{\text{n}}}{L_{\text{n}}} n_{\text{CB, }p\text{-side}}\left(\exp\left(\frac{eV_{\text{ext}}}{kT}\right) - 1\right), \tag{5.23}$$

where $n_{\text{CB, }p\text{-side}} = n_{\text{p0}}$ represents the thermal equilibrium electron concentration (minorities) in the conduction band of the p-type region. At the interface the entire electron current density in the p-type region is caused by electrons in the CB, whereas with increasing distance from the interface towards $x < 0$, both electrons and holes contribute to the current. Due to the infinite length of the diode resulting in a single exponential decay of the excess electrons in the p-regime, the gradient $\nabla n(x)$ in the above relation can be written comparatively simply as

$$\nabla n\,(x=0) = \frac{n_{\text{CB, }p\text{-side}} - n^{*}_{\text{CB, }n\text{-side}}}{L_{\text{n}}}\,.$$

The contribution of holes in the valence band is formulated equivalently, because the factor between the hole concentration in the minority and the majority region

amounts to $\exp\left(\frac{eV_{\text{ext}}}{kT}\right)$ as well:

$$j_{\text{p}}(x=0) = eD_{\text{p}}\nabla p\,(x=0) = e\frac{D_{\text{p}}}{L_{\text{p}}}p_{\text{VB},\,n\text{-side}}\left(\exp\left(\frac{eV_{\text{ext}}}{kT}\right)-1\right)\,, \tag{5.24}$$

where $p_{\text{VB},\,n\text{-side}} = p_{\text{n0}}$ denotes the thermal-equilibrium hole concentration, these being once again the minority carriers in the valence band in the n-type doped regime. Of course, in our one-dimensional steady-state approach, the total current density of a non-illuminated diode with an externally applied voltage adds up the contributions of both carrier types, so that finally,

$$\begin{aligned} j &= j_{\text{n}} + j_{\text{p}} = e\left(\frac{n_{\text{p0}}D_{\text{n}}}{L_{\text{n}}} + \frac{p_{\text{n0}}D_{\text{p}}}{L_{\text{p}}}\right)\left(\exp\left(\frac{eV_{\text{ext}}}{kT}\right)-1\right) \\ &= j_0\left(\exp\left(\frac{eV_{\text{ext}}}{kT}\right)-1\right)\,, \end{aligned} \tag{5.25}$$

where

$$j_0 = e\left(\frac{n_{\text{p0}}D_{\text{n}}}{L_{\text{n}}} + \frac{p_{\text{n0}}D_{\text{p}}}{L_{\text{p}}}\right)$$

is called 'reverse saturation' current density originating from both thermal-equilibrium minority carrier densities.

5.1.3 Illuminated Homogeneous pn-Diode

The illumination of a diode with photons of appropriate energy $\hbar\omega \geq \epsilon_{\text{g}}$ (ϵ_{g} denotes the optical band gap) leads to a perturbation of the thermal equilibrium state by additionally photogenerated carriers (electrons in CB and holes in VB). Under regular sunlight, even if concentrated by a factor of several hundred compared to one-Sun-illumination, the increase in majority-carrier density by illumination is negligible, whereas the increase in minority density is considerable. The current density $j(V_{\text{ext}})$ of non-illuminated diodes is modified by the contribution of photogenerated minority carriers which add up to a negative flux of charges, $(-j_{\text{phot}})$. Neglecting the contribution of photogenerated majority carriers the current density of the illuminated diode is then

$$\begin{aligned} j_{\text{illum}} &= e\left(\frac{n_{\text{p0}}D_{\text{n}}}{L_{\text{n}}} + \frac{p_{\text{n0}}D_{\text{p}}}{L_{\text{p}}}\right)\left(\exp\left(\frac{eV_{\text{ext}}}{kT}\right)-1\right) - j_{\text{phot}} \\ &= j_0\left(\exp\left(\frac{eV_{\text{ext}}}{kT}\right)-1\right) - j_{\text{phot}}\,, \end{aligned} \tag{5.26}$$

which coincides qualitatively with the relation of the ideal two-band system presented in Sect. 4.2.4. (A detailed description of the behavior of dark and illuminated pn-diodes in the language of semiconductor devices has been given, i.e., by Wagemann and Eschrich [5].)

5.1.4 Comparison of Homogeneous pn-Junctions with the Ideal Converter

In the ideal converter, which consists of an undoped (intrinsic) electronic two-band system (Sect. 4.2.5), the splitting $\epsilon_{\mathrm{Fn}} - \epsilon_{\mathrm{Fp}}$ of the quasi-Fermi levels under illumination is limited exclusively by radiative recombination. In the approximation with Maxwell–Boltzmann statistics, we write

$$\epsilon_{\mathrm{Fn}} - \epsilon_{\mathrm{Fp}} = \epsilon_{\mathrm{F}} + kT \ln\left[\frac{n}{n_0}\right] - \left(\epsilon_{\mathrm{F}} - kT \ln\left[\frac{p}{p_0}\right]\right) . \tag{5.27}$$

Moreover, we introduce the carrier concentrations (composed of thermal equilibrium densities, n_0, p_0, and photogenerated excess concentration Δn, Δp) in the upper and lower energy levels, namely electrons in CB and holes in VB:

$$n = n_0 + \Delta n, \qquad p = p_0 + \Delta p ,$$

and arrive at

$$\begin{aligned}(\epsilon_{\mathrm{Fn}} - \epsilon_{\mathrm{Fp}}) &= kT \ln\left[\frac{\Delta n + n_0}{n_0}\right] + kT \ln\left[\frac{\Delta p + p_0}{p_0}\right] \\ &= kT \ln\left[\frac{n_0 p_0 + \Delta n\,(n_0 + p_0) + \Delta n^2}{n_0 p_0}\right] = kT \ln\left[\frac{np}{n_0 p_0}\right],\end{aligned} \tag{5.28}$$

assuming that $\Delta n = \Delta p$, and remembering that $n_0 p_0 = n_{\mathrm{i}}^2$.

In a homogeneous *pn*-diode (a frequent example of this type of diode is a crystalline silicon junction), with very same band gap and at equal temperature, the separation of the quasi-Fermi levels is achieved in both the p-type and n-type regions (see Fig. 5.6). Provided the splitting is identical in both parts of the absorber (symmetric behavior in the p- and n-regimes), we find

$$\left(\epsilon_{\mathrm{Fn}} - \epsilon_{\mathrm{Fp}}\right)\big|_{p\text{-type}} = \left(\epsilon_{\mathrm{Fn}} - \epsilon_{\mathrm{Fp}}\right)\big|_{n\text{-type}} .$$

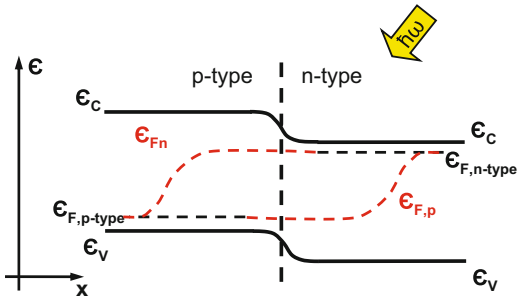

Fig. 5.6 Schematic band diagram of an illuminated homogeneous *pn*-junction with splitting of quasi-Fermi levels, assuming that the quasi-Fermi levels of majority carriers do not depart from their thermal equilibrium position, i.e., $\epsilon_{\mathrm{Fp}} = \epsilon_{\mathrm{F},\,p\text{-type}}$ and $\epsilon_{\mathrm{Fn}} = \epsilon_{\mathrm{F},\,n\text{-type}}$; note that the splitting of the quasi-Fermi levels decays with increasing distance from the junction due to recombination of the injected minority carriers

Although the contribution to $\epsilon_{\mathrm{Fn}} - \epsilon_{\mathrm{Fp}}$ in the p-type doped absorber results mainly from the shift of ϵ_{Fn}, and in the n-type regime from the shift of ϵ_{Fp}, the total contribution is,

$$(\epsilon_{\mathrm{Fn}} - \epsilon_{\mathrm{Fp}}) = kT \ln\left[\frac{np}{n_0 p_0}\right] = kT \ln\left[\frac{np}{n_i^2}\right] . \tag{5.29}$$

Obviously in our hypothetic undoped two-band system the splitting of quasi-Fermi levels does not depend on the position of the Fermi level ϵ_{F}. The excess carrier densities Δn and Δp hence, under illumination are governed by the recombination lifetimes τ, and by generation rate g, which enters into $\Delta n = g_{\mathrm{n}}\tau_{\mathrm{n}}$ and $\Delta p = g_{\mathrm{p}}\tau_{\mathrm{p}}$.

In doped electronic band systems, however, the impurity levels have to be considered for recombination as well which in addition to the ideal undoped band system, only allowing for radiative transitions, will increase the total recombination rate and thus reduce the actual recombination lifetimes and hence also the excess carrier density and the splitting $(\epsilon_{\mathrm{F}} - \epsilon_{\mathrm{Fp}})$.[7] Consequently, the separation of the quasi-Fermi levels in illuminated *pn*-diodes is reduced below that of the ideal absorber device of Sect. 4.2.4.

In comparison with undoped absorbers, in doped ones the thermal equilibrium concentrations of majority carriers (here designated by primes) are increased $n_0^* > n_0$ and $p_0^* > p_0$, and since these act as partners for recombination of photo excited minority carriers, the respective recombination rates are increased furthermore. In essence, by this effect of doping for identical optical generation, the photogenerated

[7] See, for example, the recombination in a 3-level system, as discussed in detail in [6].

steady-state concentrations in the *pn*-diode get again lower than that in the ideal undoped device:

$$\Delta n^* < \Delta n \ , \qquad \Delta p^* < \Delta p \ .$$

For doped regimes the numerator in the argument of the logarithm in Eq. (5.28) gets smaller, whereas the denominator keeps unchanged; with

$$\Delta n^* = \xi \Delta n \ , \qquad \Delta p^* = \xi \Delta p \ .$$

and $\xi < 1$ we easily find[8]

$$\frac{\epsilon_{Fn}(\Delta n^*) - \epsilon_{Fp}(\Delta n^*)}{\epsilon_{Fn}(\Delta n) - \epsilon_{Fp}(\Delta n)} = \frac{\ln\left[\xi \Delta n (n_0 + p_0) + \xi^2 (\Delta n)^2\right]}{\ln\left[\Delta n (n_0 + p_0) + (\Delta n)^2\right]} < 1. \tag{5.30}$$

5.1.5 *Upper Limits of the Open-Circuit Voltage Achievable in pn-Junctions*

The open-circuit voltage in junctions is governed by the splitting of the quasi-Fermi energies ($\epsilon_{\mathrm{Fn}} - \epsilon_{\mathrm{Fp}}$) which increases monotonically with the degree of photoexcitation (light flux). For sufficient departures from thermal equilibrium we may approximate $(\epsilon_{\mathrm{Fn}} - \epsilon_{\mathrm{Fp}}) = kT \ln\left[\frac{np}{n_0 p_0}\right]$. For an excitation with fluxes far beyond that achieved with solar photons—even at maximum solar light concentration—the Fermi energies approach the bands ($\epsilon_{\mathrm{Fn}} \rightarrow \epsilon_{\mathrm{C}}$) and ($\epsilon_{\mathrm{Fp}} \rightarrow \epsilon_{\mathrm{V}}$) and consequently stimulated transitions are no longer negligible, means, the system will undergo the transition to 'inversion' and lasing.

In junctions, commonly used for charge separation, there exists another effect limiting the open-circuit voltage: It results from the competition between photogenerated minority and their counterpart the photogenerated majority carriers. Here we exemplarily examine the balance of conduction band electrons as minority carriers (in the *p*-doped regime) and majority carriers (in the *n*-doped regime) of a *pn*-junction, as in Fig. 5.4 when $V_{\mathrm{ect}} = V_{\mathrm{oc}}$. Assuming that the quasi-Fermi level approach is again applicable, we balance the *p*- and *n*-side electrons without

[8] We immediately recognize with $\xi < 1$ for the arguments in the *ln*-functions $\left[\xi \Delta n (n_0 + p_0) + \xi^2 (\Delta n)^2\right] < \left[\Delta n (n_0 + p_0) + (\Delta n)^2\right]$, and remember the natural logarithm to be a monotonous function to find the ratio of the respective ln-functions.

consideration of an eventual influence of the space-charge layer (recombination therein), writing

$$n_{\mathrm{p0}} + \Delta n = (n_{\mathrm{n0}} + \Delta n) \exp\left(-\frac{\epsilon_{\mathrm{g}} - eV_{\mathrm{oc}}}{kT}\right) . \tag{5.31}$$

We assume the Fermi levels in the p- and n-regime to be close to the band edges ($\epsilon_{\mathrm{F},\,p\text{-type}} = \epsilon_{\mathrm{V},\,p\text{-type}}$ and $\epsilon_{\mathrm{F},\,n\text{-type}} = \epsilon_{\mathrm{C},\,n\text{-type}}$). We also assume that generation rates and lifetimes in the p- and n-regions are identical ($\Delta n = \Delta p$). From thermal equilibrium, we know that $n_{\mathrm{n0}} = n_{\mathrm{p0}} \exp\left(-\epsilon_{\mathrm{g}}/kT\right)$, whence

$$n_{\mathrm{p0}} + \Delta n = \left(n_{\mathrm{p0}} \exp\left(\frac{\epsilon_{\mathrm{g}}}{kT}\right) + \Delta n\right) \exp\left(-\frac{\epsilon_{\mathrm{g}} - eV_{\mathrm{oc}}}{kT}\right) , \tag{5.32}$$

or

$$eV_{\mathrm{oc}} = kT \ln\left[\frac{1 + \Delta n/n_{\mathrm{p0}}}{1 + \dfrac{\Delta n}{n_{\mathrm{p0}}} \exp\left(-\dfrac{\epsilon_{\mathrm{g}}}{kT}\right)}\right] . \tag{5.33}$$

Figure 5.7 shows the increase in eV_{oc} versus generation rate of minority and majority carriers $\Delta n/n_{\mathrm{p0}}$, saturating at respective band gaps when the photogenerated carrier concentration approaches the thermal equilibrium majority carrier density.

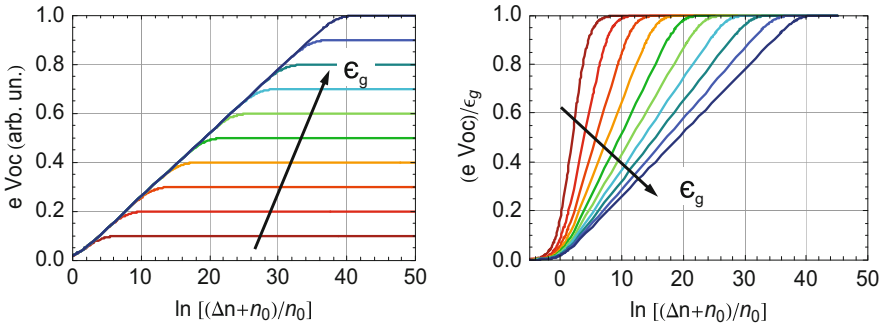

Fig. 5.7 Schematic dependence of the maximum achievable open circuit voltage V_{oc} derived from splitting of quasi-Fermi levels in a homogeneous pn-junction versus carrier density $n = n_0 + \Delta n$. The splitting ($\epsilon_{\mathrm{Fn}} - \epsilon_{\mathrm{Fp}}$) saturates when the photoexcited excess minority density approaches the thermal equilibrium majority concentration (exemplarily chosen ϵ_{g} from 0.1 to 1.0 eV in 0.1-eV steps, $kT = 0.026$ eV)

5.1.6 *Ideality Factor of Diodes*

The current-density–voltage curve $j = j(V)$ was derived for the ideal converter in Sect. 4.2.4, and for a *pn*-junction with ideal properties in Sect. 5.1.3, where the excess charges injected across the junction recombine exclusively in the respective opposite regimes outside the space-charge region. This assumption results in a relation $j = j(V)$ containing the exponential term $\exp(eV_{\text{ext}}/kT)$. The denominator kT in the argument of the exponential expression reflects the linear recombination kinetics of excess electrons injected from the n-side into the conduction band of the p-side where they recombine with majority carriers, the holes. The corresponding spatiotemporal relation for motion and recombination of electrons in the p-doped regime, the continuity equation, is

$$\frac{1}{e}\nabla\mathbf{j} = D_{\text{n}}\Delta\big(n_{\text{p}}(\mathbf{x})\cdot\mathbf{u}(\mathbf{x})\big) = g - r = -\frac{n_{\text{p}}(\mathbf{x})}{\tau_{\text{n}}}\ , \tag{5.34}$$

where n, g and $\mathbf{u}$ are carrier concentration available for transport, generation rate, and carrier velocity. The recombination rate r depends on the spatially dependent density $n_{\text{p}}(\mathbf{x})$ and its final state counterpart, the holes $p_{\text{p}}(\mathbf{x})$, which in the p-type semiconductor represent the majority carriers and are taken as independent of the spatial position, that is, $p_{\text{p}}(\mathbf{x}) = p_{\text{p0}} = \text{constant}$.

When recombination occurs mainly in the space-charge regime [7] where the densities of both conduction-band electrons and valence-band holes are spatially dependent, the recombination rate depends on $n(\mathbf{x})\cdot p(\mathbf{x})$. The product governing the recombination rate

$$\begin{aligned} n(\epsilon)\cdot p(\epsilon) &= D_{\text{CB}}(\epsilon)\, f_{\text{F}}(\epsilon_{\text{Fn}})\, D_{\text{VB}}(\epsilon)\, f_{\text{F}}(\epsilon_{\text{Fp}}) \\ &= D_{\text{CB}}(\epsilon) D_{\text{VB}}(\epsilon) \left(\frac{1}{\exp\left(\dfrac{\epsilon_{\text{e}}-\epsilon_{\text{Fn}}}{kT}\right)+1}\right)\left(\frac{1}{\exp\left(\dfrac{\epsilon_{\text{Fp}}-\epsilon_{\text{h}}}{kT}\right)+1}\right) \end{aligned} \tag{5.35}$$

(Here, ϵ_{e} and ϵ_{h} designate the individual energies of electrons (in CB) and holes (in VB).) In a symmetric configuration with identical densities of states in VB and CB and same doping of n- and p-regions, the $n(\epsilon)p(\epsilon)$-product peaks at $\epsilon = (\epsilon_{\text{C}} - \epsilon_{\text{V}})/2$, reflecting the major recombination rates at energies around half the gap value[9] (see Fig. 5.8).

In this particular approach, the carriers moving across the interface are assumed to recombine exclusively in the space charge region regardless whether these are

[9] When looking at the peak of the *np*-product more closely, we have neglected the contribution of the comparatively weak dependence of the densities of states on energy ($D(\epsilon) \sim \sqrt{\epsilon}$.

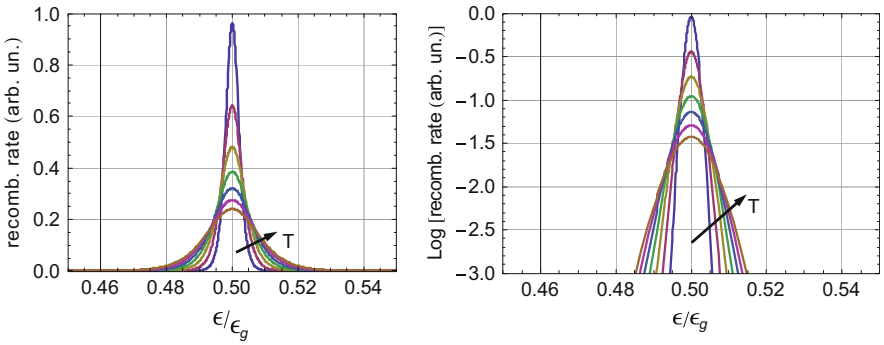

Fig. 5.8 Qualitative recombination rate in the middle of the space charge region of a symmetrically doped *pn*-junction derived from the product $f_{\text{Fermi}}(1 - f_{\text{Fermi}})$ versus energy $(\epsilon/\epsilon_{\text{g}})$. The maximum recombination rate appears at the position of ϵ_{F}, here, due to the symmetric doping, at midgap position (temperature range $6.5\,\text{K} \leq T \leq 52\,\text{K}$; 6.5 K-steps; $\epsilon_{\text{g}} = 1\,\text{eV}$)

minority (reverse current), or majority carriers (forward current), and independent of in the dark or under illumination. Accordingly the current density is governed by recombination with a net rate $U = R - G_0$, where R is a total recombination rate and G_0 a thermal generation rate. In symmetric junctions, as assumed above, recombination lifetimes of electrons and holes are identical, $\tau_{\text{n}} = \tau_{\text{p}} = \tau_{\text{rec}}$, and we have equal thermal-equilibrium concentrations $n_0 = p_0$. For forward bias voltage with

$$np = n_0 p_0 \exp\left(\frac{eV_{\text{ext}}}{kT}\right) = n_i^2 \exp\left(\frac{eV_{\text{ext}}}{kT}\right) ,$$

the net recombination rate (SRH ansatz) is then [6]

$$U = \frac{n_i^2 \exp\left(\dfrac{eV_{\text{ext}}}{kT}\right)}{\tau_{\text{rec}}\,(n + p + 2n_i)} . \tag{5.36}$$

For sufficiently large departures from thermal equilibrium, i.e., $n \gg n_i$ and $p \gg p_i$, and $p_i = n_i$, we simplify the denominator and write

$$U \approx \frac{n_i^2 \exp\left(\dfrac{eV_{\text{ext}}}{kT}\right)}{\tau_{\text{rec}}\,(n + p)} = \frac{n_i^2 \exp\left(\dfrac{eV_{\text{ext}}}{kT}\right)}{\tau_{\text{rec}}\,(n + p)} = \frac{n_i^2 \exp\left(\dfrac{eV_{\text{ext}}}{kT}\right)}{\tau_{\text{rec}} 2n_i \sqrt{\exp\left(\dfrac{eV_{\text{ext}}}{kT}\right)}}$$

$$= \frac{n_i^2 \exp\left(\dfrac{eV_{\text{ext}}}{kT}\right)}{\tau_{\text{rec}} 2n_i \exp\left(\dfrac{1}{2}\dfrac{eV_{\text{ext}}}{kT}\right)} . \tag{5.37}$$

Since the major recombination rate $U \approx U_{\text{peak}}$ is maximal at the midpoint of the junction,[10] we arrive at

$$U \approx U_{\text{peak}} \sim \frac{\exp\left(\frac{eV_{\text{ext}}}{kT}\right)}{\exp\left(\frac{eV_{\text{ext}}}{2kT}\right)} = \exp\left(\frac{eV_{\text{ext}}}{2kT}\right) . \tag{5.38}$$

The recombination current density in the forward direction integrates spatially across the recombination region, a small regime with U_{peak}, and exhibits the very same dependence on the external voltage:

$$j_{\text{forward}} \sim \exp\left(\frac{eV_{\text{ext}}}{2kT}\right) . \tag{5.39}$$

This modifies the total current density in the dark diode to

$$j = j_{\text{forward}} + j_{\text{reverse}} = j_0 \left(\exp\left(\frac{eV_{\text{ext}}}{2kT}\right) - 1\right) . \tag{5.40}$$

Analogously, for the illuminated diode, we get

$$j_{\text{illum}} = j_0 \left(\exp\left(\frac{eV_{\text{ext}}}{2kT}\right) - 1\right) - j_{\text{photo}} , \tag{5.41}$$

where j_{phot} represents the photo-current density corresponding to the rate of the entirely absorbed photon flux (see Sect. 4.2.4).

In real diode devices there might be a mixture of both types of recombination processes, in the space-charge regime and outside, resulting in the so-called diode ideality factor n with $1 \leq n \leq 2$.

Another, more phenomenological approach consists of a parallel arrangement of diodes [8] with different ideality factors. For example, in a two-diode model, we may formulate the total current density under illumination by

$$j_{\text{illum}} = j_{0,i} \left(\exp\left(\frac{eV_{\text{ext}}}{n_i kT}\right) - 1\right) + j_{0,j} \left(\exp\left(\frac{eV_{\text{ext}}}{n_j kT}\right) - 1\right) - j_{\text{photo}} . \tag{5.42}$$

In our general thermodynamic view, the diode ideality factor n might be introduced into the temperature as $nT = T^*$, and with $n > 1$, we see that $T^* > T$, and consequently the device works formally at a higher temperature than the nominal

[10] In this approach (named SHR-approach after Shockley, Read, and Hall) the recombination rate depends on the carrier concentrations in the bands $U \backsim np$ and accordingly the transition is radiative.

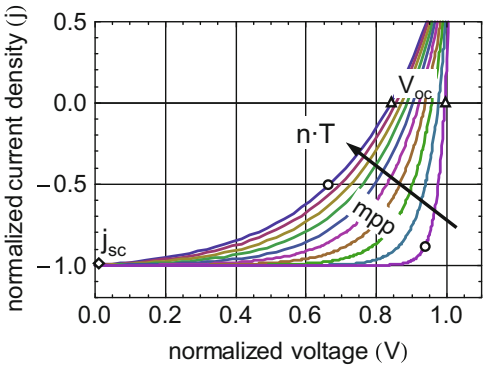

Fig. 5.9 j–V curve and characteristic magnitudes V_{oc} and mpp of a *pn*-junction for different temperatures $n \cdot T$, imitating the effect of the diode factor n when it departs from the ideal $n = 1$ towards $n > 1$

temperature, e.g., 300 K environmental temperature. As a consequence of the higher effective Temperature $nT = T^* > T$ of the heat sink the efficiency of the device drops with increasing diode ideality factor n.

In the semiconductor device picture outlined schematically in Fig. 5.9, an increase in temperature will decrease the open-circuit voltage V_{oc} of the illuminated diode as well as its filling factor FF, and hence also the complete conversion efficiency.

Moreover it is even confusing that $j - V$ curves of real solar cells with various types of non-ideal behavior (non-radiative recombination, limited transport, interface effects, etc.) are commonly used to be reproduced with diode factors[11] $n > 1$, where the diode factor in the denominator of the argument of the exponential function describes the behavior of very ideal diodes only operated at (modified) temperature, $T^* = n \cdot T$.

5.1.7 *Relevance of Space Charge Region for Charge Separation*

The space charge region in diodes effectively provides for an asymmetry in terms of source and sink of photogenerated carriers. The gradients in the energy levels, such as $\nabla_{\mathbf{x}}(\epsilon_C(\mathbf{x}))$ and $\nabla_{\mathbf{x}}(\epsilon_V(\mathbf{x}))$ are definitively not the origin of carrier motion and charge separation, because such gradients also exist in thermal equilibrium, where apart from Brownian motion, no charge flow exists (for electrons see Fig. 5.10 left part, where $\nabla_{\mathbf{x}}(\epsilon_C(\mathbf{x})) \neq 0$, and $\nabla_{\mathbf{x}}(\epsilon_{Fn}(\mathbf{x})) = 0$).

From semiclassical transport theory the driving force of a species n_i is the spatial gradient of its chemical potential $\mu_i(\mathbf{x})$, which constitutes of quantities,

[11]Diode factors $n > 1$ by all appearances are usually interpreted to reflect losses of additional irreversible effects in recombination and transport.

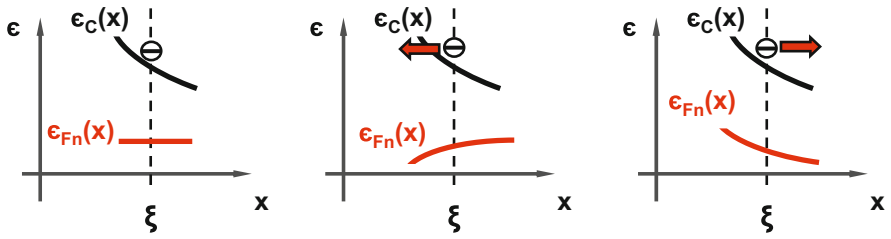

Fig. 5.10 Conduction band edge $\epsilon_C(x)$ and electron quasi-Fermi level $\epsilon_{Fn}(x)$ versus spatial coordinate x indifferent situations; *left*, $\nabla\epsilon_{Fn}(\xi) = 0$, no electron motion; *center*, $\nabla\epsilon_{Fn}(\xi) > 0$, electron motion to the left; *right*, $\nabla\epsilon_{Fn}(\xi) > 0$ electron motion to the right

such as external electric fields (drift), gradients of species concentration (diffusion), temperature gradients (thermoelectric effects, etc.). Provided the energy distribution of the particular species may be formulated by Fermi statistics, the chemical potential μ_i can be substituted by the respective quasi-Fermi level, e.g, for electrons by ϵ_{Fn} (see Fig. 5.10).

The relevance, not to say the irrelevance, of the gradients in the band edges for charge transport across the space-charge region in a diode can be easily demonstrated by an analytical procedure:

We select a position ξ in the space-charge region, where we regard the electron density $n(\xi)$ as a function of the Fermi level $\epsilon_F(\xi)$ or quasi-Fermi level $\epsilon_{Fn}(\xi)$, the temperature $T(\xi)$, the externally applied voltage V_{ext}, as well as their spatial gradients (see Fig. 5.10).[12]

We start with the electron concentration in the conduction band $n(\xi)$ at position ξ in the space-charge region:

$$n(\xi) = N_0 \frac{1}{\exp\left(\dfrac{\epsilon_C(\xi) - \epsilon_{Fn}(\xi)}{kT(\xi)}\right) + 1}\,, \tag{5.43}$$

and write $n(\xi) = n_0(\xi) + \Delta n(\xi)$, where $\Delta n(\xi) = g_0^* \tau^*$ is the general expression for the local excess electron density.[13] The corresponding regions carry subscripts p and n. For a symmetric homogeneous junction with identical dopand concentration, we get the splitting

$$\epsilon_C(\xi) - \epsilon_{Fn}(\xi) = kT \ln\left[\frac{N_0}{n(\xi)} - 1\right] = kT \ln\left[\frac{N_0}{n_0(\xi) + \Delta n(\xi)} - 1\right]\,, \tag{5.44}$$

[12] In this analytical approach for the determination of the $\nabla\epsilon_{Fn}$, we only require information about the local behavior of $\epsilon_C(\xi)$ and $\epsilon_{Fn}(\xi)$. Of course, we gain no knowledge of the 'outer' magnitudes of the device, such as current density, applied voltage, etc.

[13] Of course, the local excess concentration $\Delta n(\xi) = g_0^* \tau^*$ results from photogeneration, and respective motion and recombination of electrons; however, we neither need to know, nor we are interested in the details of its development.

and

$$\epsilon_{\mathrm{C}}(\xi) - \epsilon_{\mathrm{Fn}}(\xi) = kT \ln \left\{ \frac{N_0}{N_0 \left[\exp\left(\frac{\epsilon_{\mathrm{C}}(\xi) - \epsilon_{\mathrm{F}}(\xi)}{kT(\xi)} \right) + 1 \right]^{-1} + \Delta n} - 1 \right\} , \tag{5.45}$$

which we abbreviate to

$$\epsilon_{\mathrm{C}}(\xi) - \epsilon_{\mathrm{Fn}}(\xi) = kT \ln \beta \ . \tag{5.46}$$

We form the spatial gradient of the quasi-Fermi level $\epsilon_{\mathrm{Fn}}(\xi)$ which delivers the general driving force for electrons:

$$\nabla \epsilon_{\mathrm{Fn}}(\xi) = \nabla \epsilon_{\mathrm{C}}(\xi) - \nabla \big(kT \ln \beta \big) \ . \tag{5.47}$$

We immediately see that the driving force for the motion of electrons (here, in the space-charge region) is not the so-called 'electric field' derived from the gradient $\nabla \epsilon_{\mathrm{C}}$, but rather is significantly modified by contributions resulting from the gradients of the Fermi level $\epsilon_{\mathrm{F}}(\xi)$, of the temperature $T(\xi)$, and of the excess electron density $\Delta n(\xi)$. Only for particularly extreme and in fact non-realistic cases such as $T \to 0$ does the driving force reduce to $\nabla \epsilon_{\mathrm{C}}$.

The full algebraic relation of the gradient of the quasi-Fermi level for spatially constant temperature T is given by

$$\nabla \epsilon_{\mathrm{Fn}}(\xi) = \nabla \epsilon_{\mathrm{C}}(\xi) \left[1 - \frac{\exp\left(-\frac{\epsilon_{\mathrm{C}}(\xi) - \epsilon_{\mathrm{F}}(\xi)}{kT} \right)}{\Xi^*} \right] - \nabla \epsilon_{\mathrm{F}}(\xi) \left[1 - \frac{\exp\left(-\frac{\epsilon_{\mathrm{C}}(\xi) - \epsilon_{\mathrm{F}}(\xi)}{kT} \right)}{\Xi^*} \right] , \tag{5.48}$$

with denominator Ξ^*

$$\begin{aligned} \Xi^* = & \left[\exp\left(\frac{\epsilon_{\mathrm{C}}(\xi) - \epsilon_{\mathrm{F}}(\xi)}{kT} \right) + 1 \right]^2 \left\{ \left[\exp\left(\frac{\epsilon_{\mathrm{C}}(\xi) - \epsilon_{\mathrm{F}}(\xi)}{kT} \right) + 1 \right]^{-1} + \frac{\Delta n}{N_0} \right\}^2 \\ & \times \left(\left\{ \left[\exp\left(\frac{\epsilon_{\mathrm{C}}(\xi) - \epsilon_{\mathrm{F}}(\xi)}{kT} \right) + 1 \right]^{-1} + \frac{\Delta n}{N_0} \right\}^{-1} - 1 \right) \end{aligned} \tag{5.49}$$

Figure 5.11 shows the ratio of $\nabla \epsilon_{\mathrm{Fn}} / \nabla \epsilon_{\mathrm{C}}$ versus excess carrier concentration $\Delta n / n_0$ for applied voltage $V_{\mathrm{ext}} = 0$ (representing short-circuit conditions) and

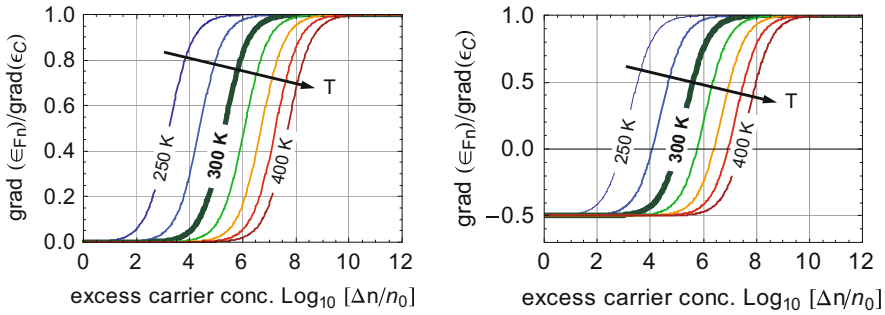

Fig. 5.11 Ratio of $\nabla\epsilon_{\mathrm{Fn}}/\nabla\epsilon_{\mathrm{C}}$ in a hypothetical electronic two-level diode system ($\epsilon_{\mathrm{C}} = 1\,\mathrm{eV}$, $\epsilon_{\mathrm{F}} = 0.5\,\mathrm{eV}$, $N_0 = 10^{10}\,\mathrm{cm}^{-3}$) versus normalized excess carrier concentration $\Delta n/n_0$ at $T = 300\,\mathrm{K}$. *Left*: vanishing externally applied voltage $V_{\mathrm{ext}} = 0\,\mathrm{V}$ (corresponds to short circuit); *right*: applied voltage $V_{\mathrm{ext}} = +0.5\,\mathrm{V}$. Light fluxes are associated with $4 \leq \log_{10}[\Delta n/n_0] \leq 7$

$V_{\mathrm{ext}} = +0.5$ V (forward bias)[14] for different temperatures. It is clear that the driving force for electron motion, the gradient in chemical potential $\nabla\epsilon_{\mathrm{Fn}}$, is hardly expressed by the 'electric field' derived as $\nabla\epsilon_{\mathrm{C}}$. Even under short-circuit conditions, where the entire internally generated gradient of the chemical potential accounts for carrier transport, the gradient of the electron quasi-Fermi level departs substantially from the gradient of the conduction band edge, viz., $\nabla\epsilon_{\mathrm{Fn}} \leq \nabla\epsilon_{\mathrm{C}}$.

5.1.8 So-Called Back Surface Field

At the rear end of an absorber is a lead out of the device which generally consists of a metal contact. The excess lifetime (wave vector relaxation time) of carriers in excited states in metals is extremely short, lying somewhere near 10^{-13} s. Thus, by strong recombination, the metal contact collects the excess carriers from the rear end of the absorber and may affect the excess carrier density, thereby squeezing the splitting of the quasi-Fermi levels which depend on diffusion properties deep within the bulk of the absorber.

For preventing losses like these, a so-called 'back surface field' (BSF) is introduced at the absorber rear side in order to 'repel' excess minority carriers from the rear contact. However, in terms of transport, the BSF acts rather as a doping profile governing the chemical potential of minorities than as an 'electric field'. Here, the very same argument for transport is applied, namely the gradient in chemical potential, as in the space charge region of *pn*-junctions, which likewise

[14] As the voltage in the short circuit mode (V_{bi}) and under bias, e.g. forward bias ($V_{\mathrm{ext}} > 0$) drops across the space charge region, we may qualitatively compare V_{bi} and V_{ext} instead of $\nabla\epsilon_{\mathrm{C}}$ and $\nabla\epsilon_{\mathrm{Fn}}$.

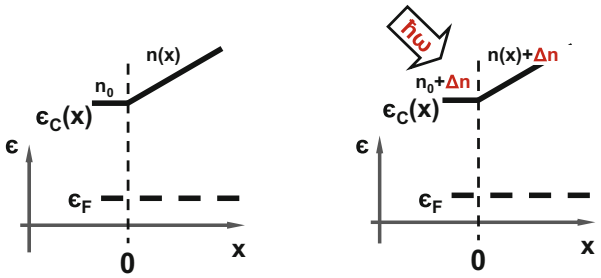

Fig. 5.12 Band diagram of the linearly graded conduction band ($x > 0$) as example of the 'so-called back surface field' for minority carriers (electrons) in a p-type absorber

exhibits a gradient of conduction and valence band energy with no relevance for carrier motion (Sect. 5.1.7).

We express this shift of the conduction band energy versus depth $\epsilon_C = \epsilon_C(x)$ which basically modifies the thermal-equilibrium concentration of the electrons in the conduction band of a p-doped absorber, where $n(x < 0) = n_0$ and $n(x)$ represent the minority concentration (see Fig. 5.12).[15]

For the sake of simplicity, we assume a linear increase $\epsilon_C(x) = \epsilon_{C0} + x\delta$, with gradient $\nabla_x \epsilon_c = \delta$ ($\delta > 0$). The total carrier concentration is composed of an excess density $\Delta n = const$, assumed initially to be independent of local position and also of the thermal equilibrium density

$$n(x) = n\big(\epsilon_C(x)\big) = n_0 \left(\frac{1}{\exp\left(\dfrac{(\epsilon_{C0} + x\delta) - \epsilon_F}{kT} \right) + 1} \right) .$$

We thus arrive at

$$n(x) + \Delta n = n_0 \left(\frac{1}{\exp\left(\dfrac{(\epsilon_{C0} + x\delta) - \epsilon_F}{kT} \right) + 1} \right) + \Delta n \ . \tag{5.50}$$

Since we have accepted that the motion (spatial displacement versus time) of any species is based on the gradient of its chemical potential (in general cases the gradient of the electrochemical potential), which is represented here by the gradient of the electron quasi-Fermi level, we calculate this gradient with the approximation

[15]The thermal equilibrium concentration n is the 'enemy' of the excited state characterized by an excess density Δn when entering into the chemical potential

$$\mu = kT \ln \left[\frac{\Delta n + n}{n} \right] .$$

of the Boltzmann energy distribution neglecting the contribution of the holes, i.e., $\Delta p \ll p(x)$:

$$\begin{aligned}\epsilon_{\mathrm{Fn}} - \epsilon_{\mathrm{Fp}} &= kT \ln\left[\frac{[n(x)+\Delta n][p(x)+\Delta p]}{n(x)\,p(x)}\right] \\ &\approx kT \ln\left\{1 + \frac{\Delta n}{n_0}\left[\exp\left(\frac{(\epsilon_{\mathrm{C0}} + x\delta) - \epsilon_{\mathrm{F}}}{kT}\right) + 1\right]\right\} \quad . \end{aligned} \tag{5.51}$$

The corresponding gradient of the electron quasi-Fermi level now reads

$$\nabla_x\left(\epsilon_{\mathrm{Fn}}\right) = kT\nabla_x\left(\ln\left\{\frac{\Delta n}{n_0}\left[\exp\left(\frac{(\epsilon_{\mathrm{C0}} + x\delta) - \epsilon_{\mathrm{F}}}{kT}\right) + 1\right] + 1\right\}\right) \tag{5.52}$$

and

$$\nabla_x\left(\epsilon_{\mathrm{Fn}}\right) = \delta \frac{\left(\exp\left(\frac{\epsilon_{\mathrm{C}} - \epsilon_{\mathrm{F}} + x\delta}{kT}\right)\right)}{\left(1 + \frac{\Delta n}{n_0}\left(1 + \exp\left(\frac{\epsilon_{\mathrm{C}} - \epsilon_{\mathrm{F}} + x\delta}{kT}\right)\right)\right)} \quad . \tag{5.53}$$

The ratio $\left(\nabla_x\left(\epsilon_{\mathrm{Fn}}\right)/\nabla_x\left(\epsilon_{\mathrm{C}}\right)\right)$ finally shows that the slope $\delta = \nabla_x\left(\epsilon_{\mathrm{C}}\right)$ in the conduction band is not correct as a solution for $\bigtriangledown\epsilon_{\mathrm{Fn}}$, and only yields a quantitative expression for the effect of repelling minority carriers from the rear contact (see Fig. 5.13):

$$\frac{\nabla_x(\epsilon_{\mathrm{Fn}})}{\nabla_x(\epsilon_{\mathrm{C}})} = \frac{\left(\exp\left(\left(\frac{\epsilon_{\mathrm{C}} - \epsilon_{\mathrm{F}} + x\delta}{kT}\right)\right)\right)}{\left(1 + \frac{\Delta n}{n_0}\left(1 + \exp\left(\frac{\epsilon_{\mathrm{C}} - \epsilon_{\mathrm{F}} + x\delta}{kT}\right)\right)\right)} \quad . \tag{5.54}$$

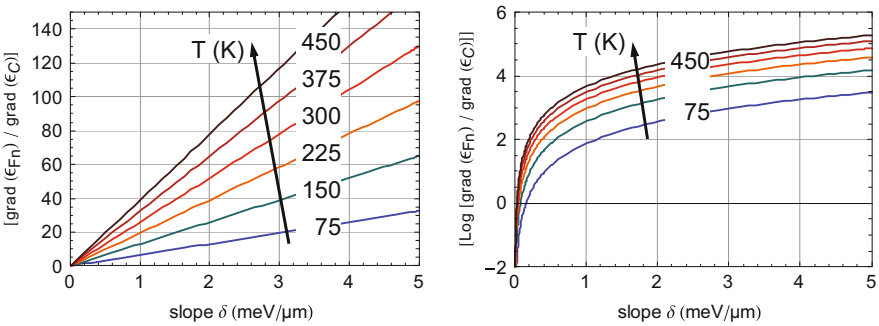

Fig. 5.13 Ratio of $\nabla_x(\epsilon_{\mathrm{Fn}})/\nabla_x(\epsilon_{\mathrm{C}})$ versus slope δ [in linear (*left*) and logarithmic representation (*right*)] to show the departure of the correct driving force $\nabla_x(\epsilon_{\mathrm{Fn}})$ versus $\nabla_x(\epsilon_{\mathrm{C}}) = \delta$. For the calculation: $\epsilon_{\mathrm{C}}(x < 0) - \epsilon_{\mathrm{F}} = 1.0\,\mathrm{eV}$, $\delta = 1\,\mathrm{meV/\mu m}$, and $n_0 = 10^7\,\mathrm{cm}^{-3}$, $\Delta n = 10^{13}\,\mathrm{cm}^{-3}$

5.2 Heterojunctions

5.2.1 Concept of Heterojunctions

The absorption of electromagnetic radiation in electronic band systems generates free charges according to the law of Lambert–Beer. As a consequence of this relation the photon flux in matter decays exponentially with propagation length. Thus the maximum rate of excess carriers introduced by solar photons is generated at the light entrance side of the absorber, where strong recombination due to surface states may substantially lower the steady-state concentration of excess charges and thereby considerably reduce the exploitation of the solar light.

Figure 5.14 (left) displays excess-carrier depth profiles for various front surface velocities 10^0 cm/s $\leq S_0 \leq 10^6$ cm/s and an extremely high rear surface recombination velocity $S_d = 10^6$ cm/s, representing a metallic contact, while Fig. 5.14 (right) shows the total excess density versus absorber thickness (integral over thickness d of curves in Fig. 5.14 left) for the different surface recombination velocities. For large absorber thicknesses, the influence of the front surface gets weaker, since above a certain depth exceeding the diffusion length the excess density will no longer 'feel' the eventually disadvantageous effect of the surface in terms of surface recombination.

The concept of a heterojunction consists of an optically highly transparent window layer in front of the absorber, transferring the high-absorption regime into the internal device and thereby avoiding the high rate of front surface recombination (see Fig. 5.15) [9]. An additional benefit of the heterojunction emerges from the high band-gap window, with lower thermal-equilibrium density of the minority carriers.

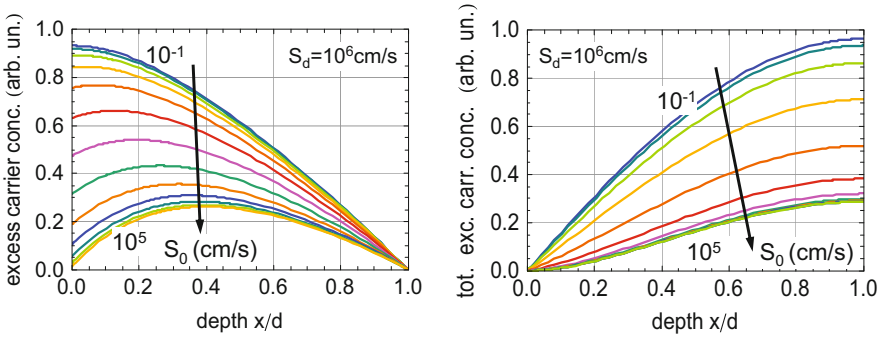

Fig. 5.14 Excess carrier concentration versus depth of absorber for comparatively high rear surface recombination velocity ($S_\mathrm{d} = 10^6$ cm/s) and different front surface recombination velocities $S_0 = (10^{-1}, 3 \times 10^{-1}, 10^{-1}, \ldots, 10^5)$ cm/s (*left*); total excess carrier concentration (integral of data on the left) versus spatial depth x/d for identical set of surface recombination velocities S_0 and S_d (*right*) with $\alpha = 2/d$, $L = 0.7d$, $D = 10\,\mathrm{cm}^2/\mathrm{s}$

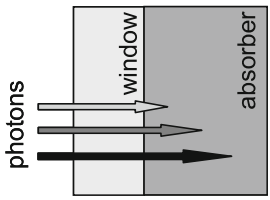

Fig. 5.15 Geometrical design of a heterojunction with high-band gap window layer at the light entrance side and a lower band gap absorber

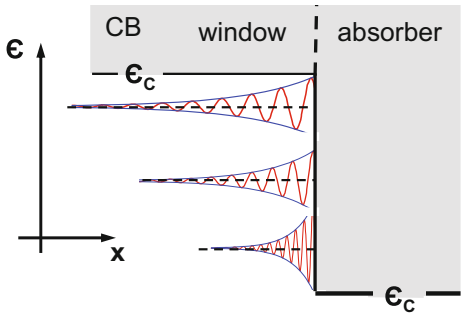

Fig. 5.16 Spatial decay of the electron wave function at the band offset of a low gap absorber (*right part*) towards a high band gap window semiconductor (*left part*). This concept announces electronic states in the gap at the interface, although chemical interface passivation seems to be perfect

In principle, this reduction by the contribution of the window minority carriers results in a considerable reduction of the reverse saturation current density, which in turn is beneficial for the open-circuit voltage.

However, these advantages are in reality often jeopardized by the influence of defect states at the interface between window and absorber, which allow the transition of majority carriers to their respective 'minority-carrier side' by tunneling and subsequent recombination. This effect disadvantageously initiates an increase in the reverse saturation current density and provides for additional recombination paths lowering the density of photogenerated minority carriers.

Interface states primarily arise from differences in structural properties between window layer and absorber, including different crystallographic structures, different crystal orientations, and/or different lattice constants. Secondly, an electronic contribution to interface states originates from the difference in the $\epsilon = \epsilon(\mathbf{k})$ relations of the window and absorber and introduces electronic states in the window layer through the exponentially decaying wave functions of electrons and holes in the absorber (see schematic energy step at the interface in Fig. 5.16).

In strongly absorbing direct semiconductors only few microns for efficient solar light absorption are needed. Accordingly in those thin absorbers the negative effect of recombination particularly of the front surface has to be suppressed by protecting the light entrance side with a window layer to form a heterodiode. These are commonly prepared with so-called 'thin film absorbers', such as polycrystalline chalcogenides CdTe, CdSe, CuS, etc., chalcopyrites $Cu(In,Ga)(S,Se)_2$, or kesterides $Cu_2ZnSn(S,Se)_4$.

5.2.2 *Electronic Properties of Heterojunctions*

The electronic properties of heterojunctions are qualitatively the same as those of homogeneous junctions. The vacuum levels of the p- and n-side have to be aligned similarly (with a continuous vacuum level), and the band diagram (see Fig. 5.17) is formed in an analogous way, except that at the interface between window and absorber the normal components of the dielectric displacement functions instead of the normal components of the electric field are continuous.

Due to the difference in optical band gap between window and absorber ($\epsilon_{g,wind} > \epsilon_{g,abs}$), and due also to the generally different electron affinities ($\chi_{wind} \neq \chi_{abs}$), discontinuities occurs in the conduction and valence bands, and this usually creates spikes and/or cliffs strongly affecting charge flow across the junction and once again supporting recombination at the interface.[16]

The main relation $j = j(V_{ext})$ remains unchanged, although the respective magnitudes j_0 and the diode ideality factor n may differ from those in idealized homogeneous junctions, where $n = 1$. In the illuminated diode, absorption in the ideal situation is only performed in the absorber, providing for the entire photocurrent. The total photogenerated carrier density in the absorber needed to establish the splitting of the quasi-Fermi levels ($\epsilon_{Fn} - \epsilon_{Fp}$) is counteracted by the reverse saturation current density. The competition between photogenerated and thermally generated carriers for the desired high values of ($\epsilon_{Fn} - \epsilon_{Fp}$) is thus almost exclusively carried out in the absorber.

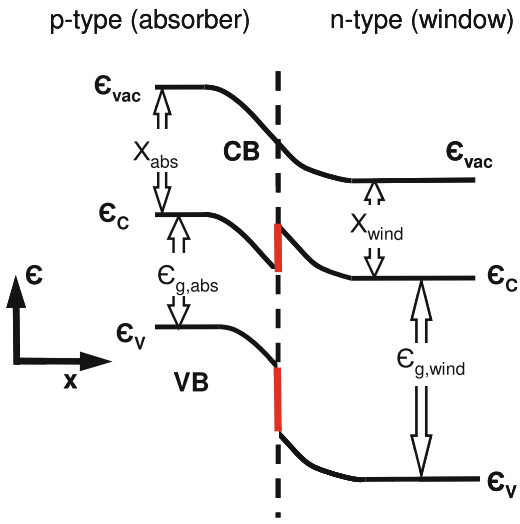

Fig. 5.17 Typical band diagram of a heterojunction. Band offsets occur as a consequence of continuous vacuum level and differences in electron affinities (χ_i) and in band gaps ($\epsilon_{g,i}$) of the absorber and the window layer

[16] For the correct reproduction of a heterojunction band diagram, and in particular for the band behavior at the interface, the different dielectric functions of the individual layers have to be considered.

5.3 pin Diodes

5.3.1 Concept of pin Diodes

The concept of *pin* diodes basically results from optical detectors in which, in reverse bias at sufficiently high applied voltages, photogenerated carriers are collected at the contacts. Since the degree of carrier collection determines the response of the detectors, a homogeneously distributed driving force across the entire thickness of the absorbing layers is desired for the photogenerated charges. Instead of using a *pn*-junction, where the distribution of the 'driving force' is substantially inhomogeneous, *pin* diodes have been developed, with extremely thin *p*- and *n*-doped layers sandwiching an undoped (intrinsic) absorber layer of much larger thickness (see the schematic band diagrams in Fig. 5.18).

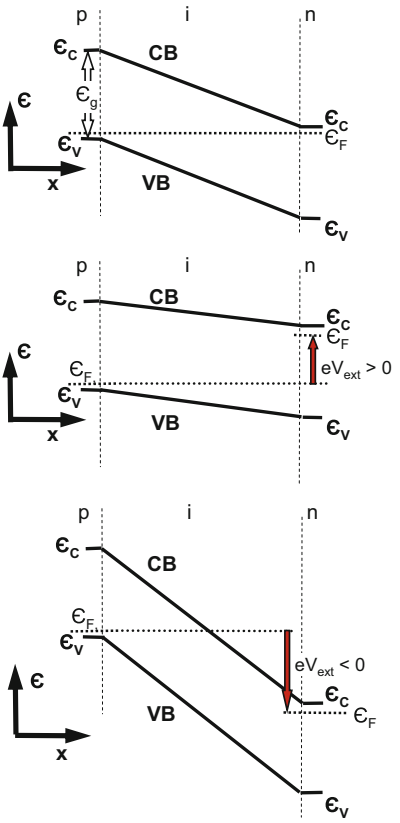

Fig. 5.18 Highly simplified band diagram of a pin junction in short-circuit situation (*top*), in forward bias (*center*), and in reverse bias (*bottom*)

In particular, for semiconductors with low diffusion lengths and low carrier mobilities,[17] this *pin* design has been also used for solar cells.

5.3.2 Space-Charge Region in Real pin Diodes

In disordered semiconductors like in a-Si:H, due to the lack of translational symmetry, the density of states at the band edges shows localized tail states and a specific density of dangling-bond states deep within the pseudogap. Consequently, in the intrinsic region, the charges in the p- (negatively charged acceptors) and in the n-doped overlayer (positively charged donors) will be at least partially compensated. This compensating charge substantially modifies the band diagram of an ideal *pin* diode with originally desired constant gradients in the conduction and in the valence band.

We estimate the influence of the space charge in the i-layer, originating mainly from carriers trapped in tail and deep defect states, and assume exemplarily a triangular distribution with a slope a as sketched in Fig. 5.19 for thermal equilibrium.

In addition to the constant gradients in the conduction- and valence-band edges resulting from the negatively charged p-layer and the positively charged n-side, the band structure is modified by space charges

$$\rho(x) = -\frac{ea}{\varepsilon_0 \varepsilon} x \ ,$$

which integrates to

$$E_{\mathrm{sc}}(x) = \int_{-w/2}^{w/2} \rho(x)\mathrm{d}x = -\frac{ea}{2\varepsilon_0 \varepsilon}\left[x^2 - \left(\frac{w}{2}\right)^2\right] \ , \tag{5.55}$$

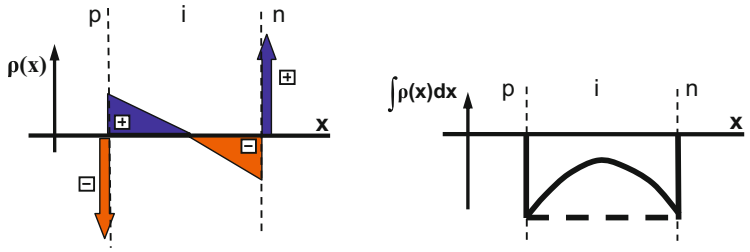

Fig. 5.19 Schematic space-charge distribution $\rho(x)$ in a *pin* diode and corresponding integral $\int \rho(x)\mathrm{d}x$ derived qualitatively via Poisson's equation

[17] Semiconductors with significantly disturbed translational symmetry, such as amorphous or microcrystalline silicon thin films (a-Si:H, μc-Si:H) and their corresponding alloys with other group IV elements like Si-Ge- and Si-C-alloys show such low mobility and low diffusion lengths.

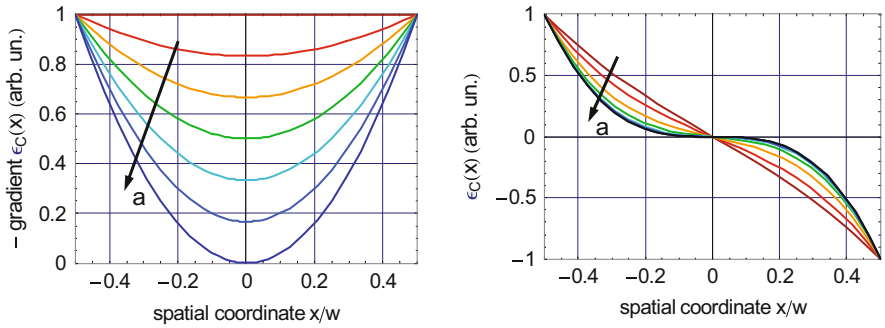

Fig. 5.20 Effect of triangular-shaped space charges in a *pin* diode on the gradient of conduction band $-\nabla\epsilon_C(x)$ (*left*) (some call it the internal field) and on the local distribution of the conduction band edge $\epsilon_C(x)$ (*right*)

sketched in Fig. 5.20 (left). Furthermore, after a second spatial integration, we find

$$-eV_{sc}(x) = -(-e)\int E_{sc}(x)\mathrm{d}x = \frac{e^2 a}{2\varepsilon_0\varepsilon}\left[\frac{1}{3}x^3 - \left(\frac{w}{2}\right)^2 x\right] + C\ . \tag{5.56}$$

This energy eV_{sc} is superimposed on the linear spatial dependence of the bands without internal charges. The integration constant C is chosen intentionally to align the bands on the right-hand side of the space-charge region with zero ($a = 0$) (Fig. 5.20).

We immediately see that the 'electric field'[18] is substantially modified by the space charge, and can even vanish, e.g., in the center ($x = 0$), for a specific choice of parameters.

5.3.3 *Charge Separation by Gradients of Quasi-Fermi Levels*

Once again, the real driving force for the motion of carriers, either injected by light or emanating from the contacts under an applied voltage, are the gradients of the quasi-Fermi levels of holes and electrons, as generally formulated in Sect. 4.2.9.

In *pin* diodes, the detailed expressions for local electron $n_{CB}(x)$ and hole $p_{VB}(x)$ concentrations—in the dark or under illumination—are much more complicated, since in the i-layer both carrier types are 'minorities' and contribute to the photocurrent, and their concentrations are coupled by Poisson's equation. Needless to say, $n_{CB}(x)$ and $p_{VB}(x)$ consist of charges in the bands and are trapped in any tail or defect states, as they occur in amorphous or microcrystalline hydrogenated

[18] We have to keep in mind that the quantity 'electric field' $E_x = -\int \rho(x)\mathrm{d}x$ does not represent the correct driving force for charge carriers.

group-IV semiconductors. Roughly speaking, the *pin* diode behaves qualitatively like a *pn*-diode with a considerably extended space charge region.

The only beneficial effect for charge separation in *pin* solar cells is the longer lifetime of photoexcited carriers, here electrons and holes, in the undoped i-region, compared with the much lower lifetime of the relevant minority carriers in the doped regimes.

In the terminology of Sect. 4.1, the i-region where most of the solar light absorption occurs, constitutes the source for excess charges in the form of both, electrons and holes, whereas the n-regime acts as a sink for the excess electrons and the p-type layer forms the sink for the photogenerated holes.

5.4 Schottky Diodes

Conceptually, metal–semiconductor junctions (Schottky diodes) are the simplest rectifying devices [1, 10, 11]. Analogously with *pn*- and *pin* diodes, the majority carriers see an energy barrier as a result of the contact between a specifically doped semiconductor and a metal with appropriate work function ϕ_{m}.

5.4.1 Space-Charge Region and Band Diagram

We construct a rectifying junction between an n-type semiconductor and a metal with a barrier for the conduction band electrons against transfer to the metal. Let us say that the metal shows a comparatively high work function $\phi_{\mathrm{m,n}}$. For a p-type doped semiconductor, we need the barrier for the holes, with a relatively low metal work function $\phi_{\mathrm{m,p}}$ (see Fig. 5.21).

The local space charge and the corresponding band diagram in the space-charge regime are derived here as an example for the metal/n-type semiconductor junction, where the position $x = 0$ indicates the interface between metal and semiconductor. The formal height of the barriers yields, in the metal/n-type barrier,

$$\phi_{\mathrm{b,n}} = \phi_{\mathrm{m,n}} - \chi_{\mathrm{n}} - (\epsilon_{\mathrm{C}} - \epsilon_{\mathrm{F}}) \ , \tag{5.57}$$

and accordingly for the metal/p-type junction,

$$\phi_{\mathrm{b,p}} = \chi_{\mathrm{p}} + \epsilon_{\mathrm{g}} - (\epsilon_{\mathrm{F}} - \epsilon_{\mathrm{V}}) - \phi_{\mathrm{m,p}}, \tag{5.58}$$

with $\epsilon_{\mathrm{g}} = (\epsilon_{\mathrm{C}} - \epsilon_{\mathrm{V}})$ and electron affinities χ_{n}, χ_{p} as difference of energetic position of the vacuum level ϵ_{vac} and the conduction band edge ϵ_{C}.

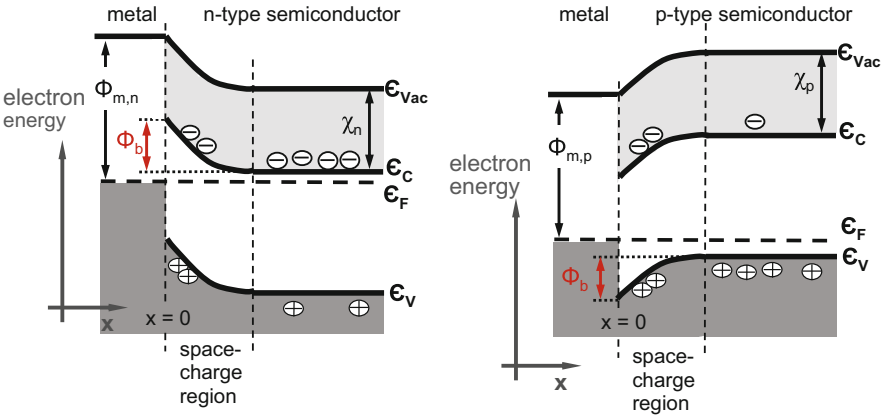

Fig. 5.21 Band diagrams of metal–semiconductor rectifying junctions ($V_{ext} = 0$). *Left*: Comparatively high-work-function metal/*n*-type semiconductor ($\Phi_{m,n}$). *Right*: Comparatively low-work-function metal/*p*-type semiconductor ($\Phi_{m,p}$)

The local space charge $\rho(x)$ results from holes in the valence band $p_{VB}(x)$, electrons in the conduction band $n_{CB}(x)$, and positively charged donors n_D^+. With the approximation of Maxwell–Boltzmann statistics, we have

$$\rho(x) = e\left\{n_D^+(x) + N_V \exp\left(-\frac{\epsilon_F - \epsilon_V(x)}{kT}\right) - N_C \exp\left(-\frac{\epsilon_C(x) - \epsilon_F}{kT}\right)\right\} . \tag{5.59}$$

The band bending in the space charge region with potential $\psi(x)$ governed by $\rho(x)$ reads

$$\epsilon_C(x) - \epsilon_F = \epsilon_{C,0} - \epsilon_F + e\psi(x) \tag{5.60}$$

and

$$\epsilon_F - \epsilon_V(x) = \epsilon_F - \epsilon_{V,0} + e\psi(x) . \tag{5.61}$$

Using Poisson's equation in one dimension, we get

$$\frac{d^2\psi(x)}{dx^2} = -\frac{\rho(x)}{\varepsilon_0\varepsilon} = -\frac{e}{\varepsilon_0\varepsilon}\left\{n_D^+ + p_{n0}\exp\left(\frac{e\psi(x)}{kT}\right) - n_{n0}\exp\left(-\frac{e\psi(x)}{kT}\right)\right\} , \tag{5.62}$$

where n_{n0} and p_{n0} are the thermal-equilibrium electron and hole densities in the *n*-doped semiconductor. In general, the concentration of positively charged donors also depends on the spatial coordinate x. However, we shall assume complete ionization $n_D^+ = N_D$ to begin with, because the assumption $n_D^+ = N_D \approx n_{n0}$ is

sufficiently well justified since the Fermi level in the space-charge region towards the metal contact shifts even further away from the conduction band edge ϵ_C, resulting in correspondingly low probability of donors being neutral.

Rewriting Poisson's equation to formulate it with an integrating factor, we get

$$\frac{\mathrm{d}^2\psi(x)}{\mathrm{d}x^2} = \frac{\mathrm{d}}{\mathrm{d}x}\left[\frac{\mathrm{d}\psi(x)}{\mathrm{d}x}\right] = \frac{\mathrm{d}\psi'(x)}{\mathrm{d}x} = F(x)\ . \tag{5.63}$$

The integration reads

$$\psi'\mathrm{d}\psi' = F\big(\psi(x)\big)\psi'\mathrm{d}x = F\big(\psi(x)\big)\frac{\mathrm{d}\psi}{\mathrm{d}x}\mathrm{d}x = F(\psi)\mathrm{d}\psi\ , \tag{5.64}$$

and thus

$$\int \psi'\mathrm{d}\psi' = \int F(\psi)\mathrm{d}\psi\ . \tag{5.65}$$

After a first integration, we find

$$\frac{1}{2}\left(\psi'\right)^2 = \int F(\varphi)\mathrm{d}\varphi + \frac{1}{2}\mathrm{const.}\ , \tag{5.66}$$

and

$$\psi' = \sqrt{\left[2\int F(\psi)\mathrm{d}\psi + \mathrm{const.}\right]}\ . \tag{5.67}$$

From Poisson's equation above, we have

$$\frac{\mathrm{d}^2\psi}{\mathrm{d}x^2} = \frac{e}{\varepsilon_0\varepsilon}n_{\mathrm{n0}}\left[1 + \frac{p_{\mathrm{n0}}}{n_{\mathrm{n0}}}\exp\left(\frac{e\psi}{kT}\right) - \exp\left(-\frac{e\psi}{kT}\right)\right]\ , \tag{5.68}$$

whence we derive

$$\frac{\mathrm{d}\psi}{\mathrm{d}x} = \psi' = \sqrt{2\frac{en_{\mathrm{n0}}}{\varepsilon_0\varepsilon}}\sqrt{\psi + \frac{p_{\mathrm{n0}}}{n_{\mathrm{n0}}}\frac{kT}{e}\exp\left(\frac{e\psi}{kT}\right) + \frac{kT}{e}\exp\left(-\frac{e\psi}{kT}\right) + C_1}\ . \tag{5.69}$$

The next step is to write

$$\frac{\mathrm{d}\psi}{\sqrt{2\frac{n_{\mathrm{n0}}e}{\varepsilon_0\varepsilon}}\sqrt{\psi + \frac{p_{\mathrm{n0}}}{n_{\mathrm{n0}}}\frac{kT}{e}\exp\left(\frac{e\psi}{kT}\right) + \frac{kT}{e}\exp\left(-\frac{e\psi}{kT}\right) + C_1}} = \mathrm{d}x\ , \tag{5.70}$$

and so to arrive at

$$\int \frac{1}{\sqrt{2\dfrac{en_{\mathrm{n0}}}{\varepsilon_0\varepsilon}}} \frac{\mathrm{d}\psi}{\sqrt{\psi + \dfrac{p_{\mathrm{n0}}}{n_{\mathrm{n0}}}\dfrac{kT}{e}\exp\left(\dfrac{e\psi}{kT}\right) + \dfrac{kT}{e}\exp\left(-\dfrac{e\psi}{kT}\right) + C_1}} = \int \mathrm{d}x = x + C_2 \,, \tag{5.71}$$

which requires a numerical procedure for solution.

As a reasonable approximation, we may neglect the term containing the ratio of the thermal-equilibrium carrier concentrations, since in an n-type semiconductor $p_{\mathrm{n0}}/n_{\mathrm{n0}} \ll 1$. Furthermore, for sufficiently large band bending $\mid -e\psi(x) \mid /kT > 3$, which means substantial depletion of electrons in the conduction band, we can neglect the term $\exp(-e\psi/kT)$ to arrive at a simple integral of type

$$\int \frac{\mathrm{d}\psi}{\sqrt{\beta}\sqrt{\psi + C_1}} = \int \mathrm{d}x = x + C_2 \,, \tag{5.72}$$

using the abbreviation $\beta = 2en_{\mathrm{n0}}/\varepsilon_0\varepsilon$. In the range $0 \le x \le w$, this yields

$$\frac{2}{\sqrt{\beta}}\sqrt{\psi + C_1} = x + C_2 \,. \tag{5.73}$$

Finally, we solve for the potential

$$\psi(x) = (x + C_2)^2 \frac{\beta}{4} - C_1 \,. \tag{5.74}$$

The space-charge region and the band bending in the semiconductor decay towards $x > 0$, and at a distance $x = w$ from the metal–semiconductor interface, which is located at $x = 0$, we assume band bending to be terminated. The relevant boundary conditions thus get

$$\psi'(x = w) = 0 = 2\,(w + C_2)\,\frac{\beta}{4} \tag{5.75}$$

and

$$\psi(x = w) = 0 = (w + C_2)^2 \frac{\beta}{4} - C_1 \,. \tag{5.76}$$

From the first condition, we immediately find

$$C_2 = -w \,, \tag{5.77}$$

and introducing this into $\psi'(x = w)$, we determine

$$C_1 = 0 \,. \tag{5.78}$$

This leads to

$$\psi(x) = (x - w)^2 \frac{\beta}{4} = (x - w)^2 \frac{e n_{\mathrm{n0}}}{2\varepsilon_0 \varepsilon} \,, \tag{5.79}$$

and

$$\psi'(x) = (x - w) \frac{\beta}{2} = (x - w) \frac{e n_{\mathrm{n0}}}{\varepsilon_0 \varepsilon} \,. \tag{5.80}$$

With the above approximation, the linear spatial decay of $\psi'(x)$ in $0 \leq x \leq w$ translates into a parabolic decay of $\varphi(x)$ versus spatial coordinate x, and resembles the result for an abrupt space charge distribution $\rho = e n_{\mathrm{n0}} = \text{const.}$ in $0 \leq x \leq w$, with $\rho = 0$ for $x > w$ (see Fig. 5.22). The behavior of the band bending of the n-type semiconductor is qualitatively and quantitatively equivalent to the n-type part of the abrupt homogeneous junction in Sect. 5.1.1.

At the metal–semiconductor interface $x = 0$, we additionally get the so-called electric field $\psi'(x = 0) = -(w e n_{\mathrm{n0}})/(\varepsilon_0 \varepsilon)$, and the offset in the bending of the conduction band designating the barrier height for the majority carriers (electrons):

$$\phi_{\mathrm{B,\,Sch}} = e\psi(x = 0) = w^2 \frac{e^2 n_{\mathrm{n0}}}{2\varepsilon_0 \varepsilon} \,.$$

In comparison with the homogeneous pn-junction, the barrier height in the Schottky diode amounts to only a fraction of this value. In turn, the width of the space charge is only a fraction of the width in the homogeneous pn-junction, as the contribution from the metal due to its extremely high electron density is negligible. The width w of the space-charge region is established in accordance with the concentration of

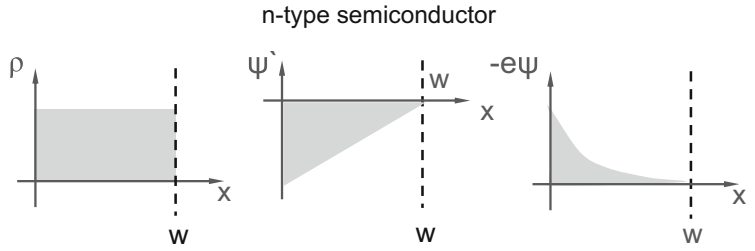

Fig. 5.22 Qualitative space charge, 'electric field', and electron energy (e.g., conduction band edge) of a metal-n-type semiconductor junction using the approximate analytical treatment above (Sect. 5.4.1)

dopants (here donors $N_D \approx n_D^+$) in such a way that the vacuum level of the n-type semiconductor and metal meet at $x = 0$ as already shown in Fig. 5.21.

5.4.2 *Illuminated Schottky Diode*

The light-entrance side of a Schottky diode is usually the semiconductor, with an appropriate thickness to provide for sufficient absorption of photons and at the same time with appropriate lifetime to allow for adequate minority carrier collection. The metal serves as rear contact and acts in addition as an optical mirror for low-energy photons.[19]

The source of the photogenerated minority carriers, in our example holes in the valence band, is the semiconductor, whereas the sink for the photogenerated holes is the metal, where they recombine with electrons at $\epsilon \leq \epsilon_{F,\,metal}$. This spatial configuration provides for the asymmetry necessary for 'separation' of the photoexcited charges, here solely the holes in the valence band.

The driving force for carriers leading to the total current composed of contributions of electrons and holes is of course supplied by the gradients in the respective quasi-Fermi levels, sketched as an example for the holes in an illuminated Schottky diode in short circuit in Fig. 5.23.

The splitting of the quasi-Fermi levels, and the splitting for no net carrier extraction, which represents the situation of maximum achievable external voltage

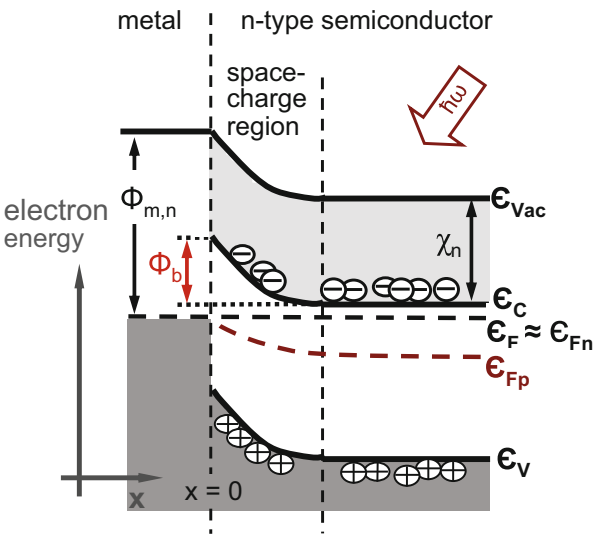

Fig. 5.23 Band diagram of a metal/n-type semiconductor junction with qualitatively indicated quasi-Fermi levels for electrons (majority carriers) and holes (minority carriers) in the short- circuit mode ($V_{ext} = 0$)

[19] For the complete device on needs, of course, a transparent front contact.

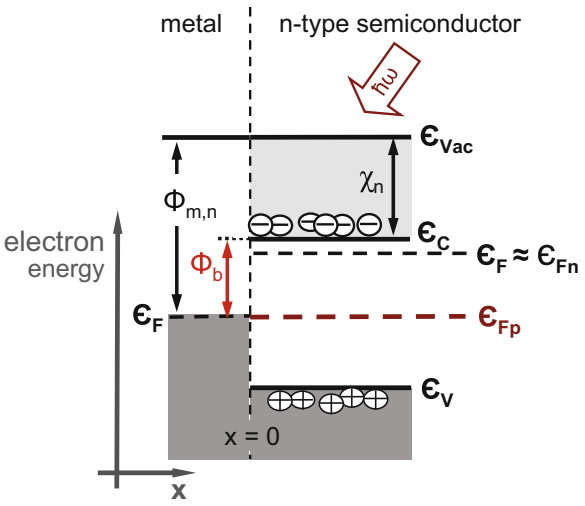

Fig. 5.24 Band diagram for a metal/*n*-type semiconductor junction in open circuit for the idealized condition of maximum achievable open-circuit voltage

(V_{oc}), is not limited in Schottky diodes by the optical band gap of ideal absorbers, but rather by the height of the barrier $\phi_b = \phi_{m,n} - \chi_n - (\epsilon_C - \epsilon_{F,n\text{-type}})$, which acts on the majority carriers in the absorbing medium, here the *n*-type semiconductor.

The maximum shift of the Fermi level $\epsilon_F \approx \epsilon_{Fn}$ in the semiconductor for arbitrarily high excitation—but below the lasing level—in the vicinity of the junction leads to a flat alignment of ϵ_{Fp} at the metal Fermi level, together with flat ϵ_{Fn} and accordingly flat ϵ_C and ϵ_V (space charge width disappears). The vanishing gradients in the electron and hole quasi-Fermi levels for each component rule out carrier transport ($j = 0$), and we would get open-circuit conditions (see Fig. 5.24).

5.4.2.1 Effective Barrier Heights in Schottky Diodes

In metal–semiconductor junctions, the doping of the semiconductor exclusively governs the width of the space-charge region and thus determines amongst width also the shape of the barrier. For spatially homogeneously doped absorbers $N_D \neq N_D(x)$, the high-energy part of the spike-like barrier may be approximated by an upward step with discontinuity ϕ_b and a linear decay. This spiky potential allows for electron tunneling in the forward direction of the diode at energies $\phi_{b\,tunnel}$ below the formal barrier height $\phi_b > \phi_{b\,tunnel}$ (see Fig. 5.25). This tunnel barrier height changes with the external voltage.[20]

[20]The tunneling probability through barriers that are linearly dependent on spatial coordinates is represented by solutions of the two branches of the Airy-type differential equation.

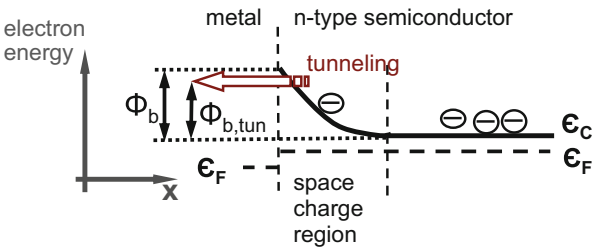

Fig. 5.25 Effective barrier height for majority carriers (electrons) $\Phi_{b,tun} < \Phi_b$ as a consequence of tunneling through a sufficiently thin energy barrier (diode in forward bias; $V_{ext} > 0$)

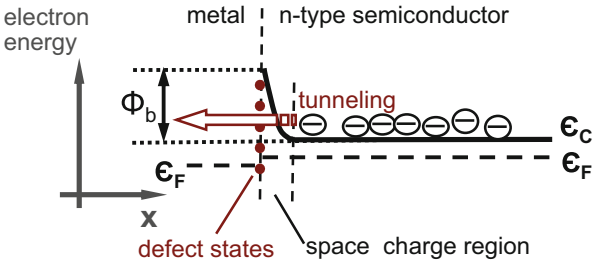

Fig. 5.26 Extreme decrease in effective barrier height for majority carriers (electrons) in a heavily doped n-type semiconductor with extremely small space charge region [diode under forward bias ($V_{ext} > 0$)]

Here, the optical threshold energy for photoexcitation of charges, the semiconductor band gap $\epsilon_g = \epsilon_C - \epsilon_F$ is much larger than the electronic threshold ϕ_b, which limits the maximum achievable splitting of the quasi-Fermi levels.

5.4.2.2 Further Drawbacks in Real Schottky Diodes

In real Schottky diodes during preparation of the rear contact, the semiconductor surface is exposed to metal atoms, possibly under extreme conditions such as vacuum, high temperatures, and presence of radical species. During those processes, an intermixing of components of the absorber and of contact materials, such as interdiffusion of elements is unavoidable. Unfortunately, the incorporation of metal atoms into a semiconductor generally creates deep defect states for electrons in the gap, which act as recombination centers for photoexcited carriers and, moreover, depending on the position of the Fermi or quasi-Fermi levels, are occupied by charges which contribute to the space-charge region of the junction. In this way, the average spatial separation of positively and negatively charged sites is decreased (shrinking of space-charge width) which in turn reduces the total energy of the system.

A thinner space-charge region leads to a more spiky potential for the majority carriers and thus lowers their effective barrier height for tunneling. Accordingly the higher tunnel probability leads to a higher reverse saturation current of then illuminated diode and affects the photovoltaic performance (see Fig. 5.26).

In addition to the detrimental effect of a reduced effective barrier in real devices, the interface defects introduced by metals and/or by the preparation technology are not at all distributed laterally in a homogeneous way. This commonly results

in a substantial lateral fluctuation of barrier heights. Consequently, the majority electrons will find the lowest barriers and deteriorate furthermore the photovoltaic function of the diode.

5.4.2.3 Metal–Insulator–Semiconductor Diodes

In order to establish reproducible and adjustable barrier heights in Schottky diodes an insulating layer (I-layer) with appropriate thickness allowing for electron tunneling may be incorporated between metal and semiconductor (MIS diode). The thickness of these I-layers amounts to only a few nanometers (1–2 nm) and the lateral area of constant insulator thickness corresponds to some tens or hundreds of square centimeters (think of $10 \times 10\,\mathrm{cm}^2$). The relative accuracy of 0.1-nm fluctuation within 0.1 m lateral extension corresponds to $\Delta d_\mathrm{I}/l_\mathrm{I} \geq 10^{-9}$, a ratio which one might not even think to be technologically easily achievable.

In conclusion, metal–semiconductor barriers have been treated here for completeness rather than to argue for their actual technical relevance in solar light conversion devices.

5.5 Excitons and Subsequent Charge Transfer in Organic Absorbers

The use of organic absorbers for solar light conversion [12–15] requires a substantial deviation from the concepts of inorganic semiconducting matter. Organic absorbers are made of molecules of different geometrical sizes, commonly classified according to their weight, from a few thousand (small molecules) to several tens of thousands of atomic mass units (polymers). The intermediate mass range has recently been represented by dendrimers. The fundamental optical, electronic, and optoelectronic properties of these organic absorbers are qualitatively similar, irrespective of their size.

In contrast to semiconductor properties which are governed by electron wave functions resulting from a hypothetic infinitely extended periodic arrangement of atomic potentials, in organic matter the electron wave functions are determined by molecular orbits with wave functions that do not extend infinitely and exhibit comparatively weak overlap to neighbor sites. Weak overlap to adjacent sites, however, deteriorates charge transport often performed by tunneling. The low coordination of molecular structures compared to crystal structures, in addition, usually causes polaron effects, which result in a distortion and/or a rearrangement of the molecular structure when an electron is excited from the ground state. In the excited state in molecules, due to the shrinking of its wave function in an environment of comparatively low dielectric susceptibility, the electron is still bound to the positive charge and thus forms an exciton.

5.5.1 General Aspects of Light Absorption and Generation of Excited States

In organic absorbers the photoexcitation mainly generates bound electron hole states, called excitons, which are dissociated to free electrons and holes at particular sites. These sites providing for an individual transport level for the electrons and analogous ones for the holes, represent the asymmetry needed for the subsequent charge separation (see Fig. 5.27). The charge separation is commonly facilitated by a reduction of the energetic separation of electrons and holes originally established by the optical threshold that represents the energy difference between the lowest unoccupied molecular level (LUMO) and the highest occupied one (HOMO)

$$\Delta\epsilon_{\text{opt. thresh.}} = \epsilon_{\text{LUMO}} - \epsilon_{\text{HOMO}}$$

to the level difference

$$\Delta\epsilon_{\text{el. thresh.}} = \epsilon_{\text{LUMO}} - \epsilon_{\text{HOMO}} - (\Delta_{\text{L}} + \Delta_{\text{H}}) \ .$$

This principle is used in almost all devices based on organic absorbers, such as molecular dyes in conjunction with conductive matrices or in polymer absorbers.

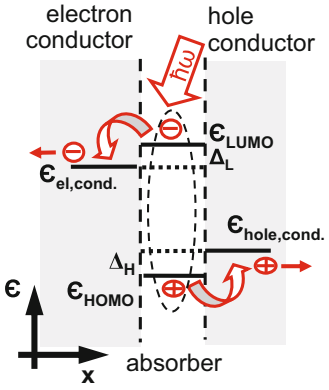

Fig. 5.27 Band/energy diagram of an exciton-generating molecule sandwiched between an electron (*left*) and a hole conductor (*right*). At appropriate energy position of the HOMO (highest occupied molecular orbit) and LUMO (lowest unoccupied molecular orbit) with respect to transport levels $\epsilon_{\text{electron}}$ and ϵ_{hole}, exciton dissociation and generation of free electron–hole pairs is achieved

After optical generation the ensemble of electrons and holes undergo the total energy relaxation[21] of $\Delta_\mathrm{L} + \Delta_\mathrm{H}$ and establish a correspondingly lower chemical potential.

In the steady state, the system resumes a stationary electron and hole occupation in the conductors and also a stationary occupation of the Coulomb-coupled electrons and holes (excitons) in the absorber, regardless of any rates for transitions between the relevant energy levels. Provided the electron and hole conductors are spatially separated, and electrons and holes do not interact, there will be no recombination of excess carriers. Accordingly, no excess radiation resulting from recombination in the leads will be emitted apart from their thermal-equilibrium photons. However, due to the law of Kirchhoff, which states that spectral emission equals spectral absorption, the absorber emits photons with a spectral distribution corresponding to its excited state and its temperature. In the radiative limit, by analogy with solid-state absorbers, the radiative balance in open circuit (without carrier extraction at the contacts, and with omission of the photon contribution from the Universe, stars, and Moon) is given by (see Sect. 4.2.3):

$$\Omega_\mathrm{in} \int_{\epsilon_\mathrm{g}^*}^{\infty} \frac{A\hbar\omega}{c_0^2 4\pi^3\hbar^3} \frac{(\hbar\omega)^2}{\exp\dfrac{\hbar\omega}{kT_\mathrm{Sun}} - 1} \mathrm{d}(\hbar\omega) = 4\pi \int_{\epsilon_\mathrm{g}^*}^{\infty} S_\mathrm{oc}(\hbar\omega)\mathrm{d}(\hbar\omega) \; . \tag{5.81}$$

The general term $S_\mathrm{oc}(\hbar\omega)$ represents the spectral photon flux emitted from the absorber into the solid angle 4π. The expression above contains the spectral emissivity (which equals the spectral absorption, including a possible Stokes shift) and the occupation and transition probabilities of initial and final states of each of the involved levels. The optical threshold energy ϵ_g^* for absorption/emission defines the lower limit of the photon energy, whereas the upper limit for contributions to the spectral flux $S(\hbar\omega \to \infty)$ is included in the spectral absorption/emission and its decay with increasing photon energy.

Our approach resembles the one used for the radiative limit in Chap. 4 for an ideal semiconductor absorber, and it would yield the same result for the maximum splitting of the quasi-Fermi levels, provided that the independent-electron picture and the stationary-state quasi-Fermi level ansatz were valid.

In organic absorbers, be it molecular dyes or extended polymers, in contrast to inorganic ones, electrons are often correlated and the comprehensive formulation of their behavior is much more complicated. Even for only two electrons, it does not allow for an analytical solution like the quasi-Fermi approach (see [16]).

Compared with the ideal electronic band absorber in which the optical threshold ϵ_g simultaneously acts as the electronic threshold, in the organic absorber–lead

[21] In order to avoid immediate recombination of excited electrons and holes in the absorber molecule, electrons and holes are transferred with energetic relaxation, Δ_L (for electrons from the LUMO level) and Δ_H (for holes from the HOMO level) to their respective transport levels ($\epsilon_\mathrm{el,cond}$, $\epsilon_\mathrm{hole,cond}$).

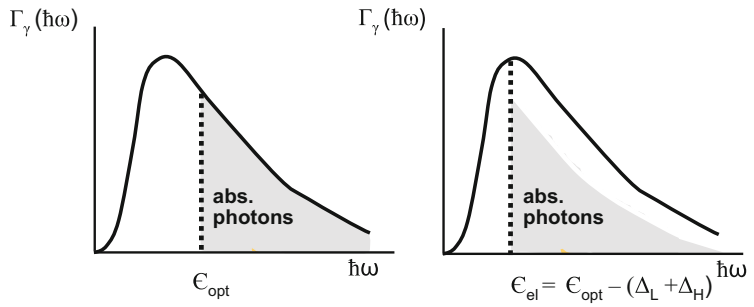

Fig. 5.28 Maximum amount of usable solar photons with optical threshold of energy ϵ_{opt} and same amount after Stokes down-shifting by $(\Delta_H + \Delta_L)$ to ϵ_{el}

system, the optical threshold also governs the absorption of solar photons, but the generated photoexcited species are transferred to a substantially lower electronic level that enters into their chemical potential. The system behaves like a small-band-gap system illuminated with the lower total photon flux $\Gamma_\gamma(\hbar\omega \geq \epsilon_{opt})$ of an absorber with corresponding higher band gap ϵ_{opt} (Fig. 5.28).

5.5.2 Barriers with Organic Absorbers

5.5.2.1 Dye-Sensitized Solar Cells

A typical example of a solar cell composed of a molecular absorber and appropriate conductors for electrons and holes, is the dye-sensitized diode shown schematically in Fig. 5.29 [17, 18]. The absorber consists of dye molecules attached to the surface of an optically transparent and extremely porous metal oxide. This highly fractal configuration with a huge surface area (up to a factor of 10^3 larger than the size of the corresponding planar surface) provides for sufficient total concentration of the dye absorber and equivalent high absorption.

The large-band-gap porous metal oxide (e.g., TiO_2) is strongly *n*-doped with negligible hole contribution to charge transport, and serves as electron conductor to the front contact. Its fractal structure is, of course, beneficial for the loading of the system with a suitable concentration of absorber molecules. The electron transport, however, is limited in the porous network by percolation.

As a hole conductor nicely penetrating the porous network and giving holes electronic access to dye molecules, an electrolyte (redox system) is commonly chosen, in which the exchange of photoexcited holes from the absorbing dye is achieved by a 'reduction' of the electrolyte. The corresponding 'oxidation' of the electrolyte is accomplished by injection of electrons from the metal rear contact.

This type of solar cell may also be classified as a photo-electrochemical solar cell, due to the fact that a liquid conductor is involved (see Sect. 5.6) [19].

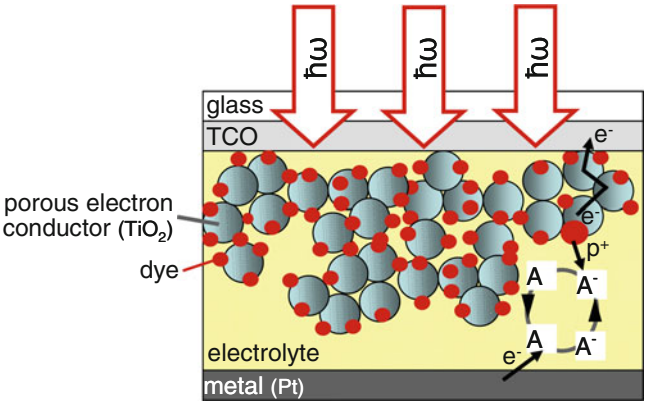

Fig. 5.29 Schematic structural design of a dye-sensitized solar cell. Behind the transparent electrode at the light entrance side, an electron conductor (high band gap) is 'doped' with a dye that absorbs the solar photons, creates a photoexcited state (exciton), and transfers the excited electron and the excited hole to the respective conductors across which they are transported to the front (electron) and rear contact (hole)

5.5.2.2 Organic Bulk Junction Cells

The simplest organic bulk diode contains one type of absorber sandwiched between two metal contacts with different work functions to attain the necessary asymmetric behavior. In organic matrices, in contrast to inorganic semiconductors, the incoming photons do not usually generate free electrons and holes, but rather create excitons [20]. These excitons either decay geminately,[22] or in non-radiative transitions or, after been dissociated, contribute as free electrons and holes to a current towards the boundaries of the absorber, where contacts provide access to the ensemble in terms of the chemical potential of electrons and holes.

For dissociation of the excitons, the dissociation energy of this Coulomb-bound quasi-particle, with the aim of getting a free electron and a free hole, is provided by a reduction in their energy separation and is hence accompanied by a lowering of the quality of the excited state.

Here, we consider the dissociation of an exciton by tunneling in the presence of extreme gradients in the conduction and valence band ($\nabla\epsilon_C$, $\nabla\epsilon_V$). In forward direction, the mode in which solar cells operate, this effect reduces to a large extent the photoinduced splitting of the quasi-Fermi levels. Moreover, only in short-circuit mode where maximal gradients in CB and VB occur, and the output power vanishes, does this approach based on tunneling work (see Fig. 5.30).

Another option for using organic bulk absorbers is based on the mixture of two different bulk materials A and B, one with *p*-type, the other with *n*-

[22]Geminate recombination refers to the 'immediate' back reaction of species, e.g., weakly bound photogenerated electrons and holes (excitons) in terms of a radiative transition to the ground state.

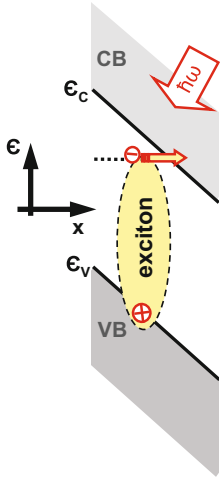

Fig. 5.30 Charge transfer from an excited molecule (exciton) to the conduction (CB) and valence band (VB) of a semiconductor, both showing extremely large gradients

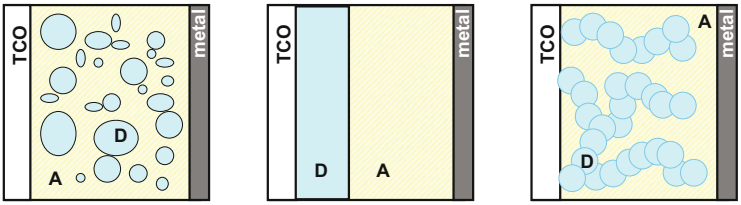

Fig. 5.31 Geometrical arrangement of organic solar light absorbers with donor and acceptor behavior. Mixture of comparatively small-scale clusters (*left*), bilayer arrangement (*center*), and interpenetrating network composed of two different absorbers with optimized transport properties for electrons and holes (*right*)

type behavior. Needless to say, the *p*- and the *n*-type regimes enable hole and electron transport. The geometrical arrangements of such mixed structures, called hetero-bulk absorbers, can be designed in three different types [21]: a mixture of small-scale regimes (dual molecule approach), a bilayer configuration (a sequence of two homogeneous absorber layers connected in optical series, each with its own individual band gap), and an interpenetrating network of the two different absorbers (see Fig. 5.31).

At each of the interfaces between bulk A and bulk B, a heterojunction is formed at which exciton dissociation occurs in conjunction with the energetic relaxation of the originally photo excited state. Depending on the lateral extent of the phases and the corresponding doping levels, the space-charge region is fully or only partially developed.

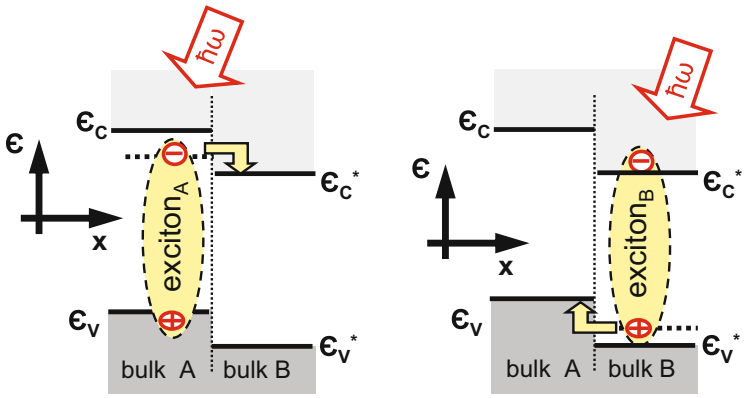

Fig. 5.32 Schematic dissociation of excitons and charge separation (injection) in the presence of a bulk material with appropriate energy level of the given transport path

Figure 5.32 shows a section of the band diagram at the interface of two bulk regions with the options for exciton dissociation by relaxation of electrons at the step-down of the conduction band or holes at the step-up of the valence band. However, it is questionable to treat these processes using a traditional band diagram since in polymers and in molecular matter the independent-electron picture often cannot be applied.

In the course of solar-light conversion to electrical output power in organic devices, several restrictions arise with regard to the ideal processes. Due to molecular behavior, the absorption of solar photons and the resulting generation of photoexcited states (excitons) is not only limited by the thickness of the absorbing medium [the necessary thickness is $d_{\mathrm{abs}} \geq 1/\alpha(\hbar\omega)$] but also by the decrease in the absorption coefficient for photon energies sufficiently higher than the optical threshold.

The collection of photoexcited excitons is governed by their diffusion length $L_{\mathrm{D,exc}}$, which is usually considerably smaller than the necessary thickness for photon absorption.[23] Consequently, excited states generated beyond the regime of the diffusion length are hardly collected.

The conversion of excitons (dissociation) to mobile charges requires a downward energy step, and the subsequent transport of electrons and holes in terms of mobilities is reduced due to low wave-function overlap in molecular structures. In addition, the transport paths turns out to be percolative. Both, the latter two effects require a non-negligible drop in chemical potential of the electron–hole ensemble.

[23] Although the absorption coefficient of molecular dyes generally may exceed those of semiconductors the effective thickness of dye layers—due to low exciton diffusion lengths—is usually chosen much lower so that full absorption $A \rightarrow 1$ might not be achieved.

5.5.2.3 Summary for Organic Solar Light Converters

Illuminated organic diodes are somewhat analogous to inorganic solar cells. They are characterized by their relation of current density versus voltage, showing the characteristic features in the fourth quadrant of an I–V curve. Similar quantities, such as open-circuit voltage, short-circuit current density, filling factor, and maximum power point efficiency can be determined. In contrast to inorganic devices, an analytic derivation of the j–V relation for organic diodes is not available so far. Here we only have discussed the qualitative similarity to the inorganic representatives.

5.6 Photo-Electrochemical and Photochemical Cells

Devices combining absorbers with liquids are generally included among photochemical and photo-electrochemical cells. In these devices the function of 'direct' solar light conversion is based on only one type of majority, namely photogenerated holes, for which a suitable sink is formed by the liquid. In the language of chemists, the injection of holes into the liquid (identical with the extraction of electrons) reduces the electrolyte.

The advantages of liquid conductors are their excellent suitability for penetrating practically any type of absorber geometric network. Handicaps may arise from incomplete wetting of the surface, from necessary overpotentials[24] for appropriate current densities at the absorber–liquid interface, and from stability issues of the electrolyte in conjunction with the absorber.

5.6.1 Photo-Electrochemical Cells

A schematic energy diagram of a photo-electrochemical diode is given in Fig. 5.33. With this scheme, we may also explain the processes in a dye-sensitized solar cell (see Sect. 5.5.2 and in particular p. 151).

The transition of a photoexcited hole from the valence band of the n-type absorber to the electrolyte level where the conversion of the hypothetical species $S^- \rightarrow S$ occurs requires an overpotential $\Delta 1$ for non-negligible current densities. Analogously, on the metal side, where an electron from the metal (often Pt with a beneficial catalytic effect) flops to the electrolyte level $S \rightarrow S^-$, another overpotential $\Delta 2$ is established. The transport of species S^- from their point of generation (source), namely at the interface of the illuminated semiconducting absorber with

[24] Overpotential (Δ_i) designates the departure of the potentials of an electrode system from its chemical equilibrium value. Such a departure is required to create a net chemical reaction; the larger (Δ_i) the larger the reaction rate.

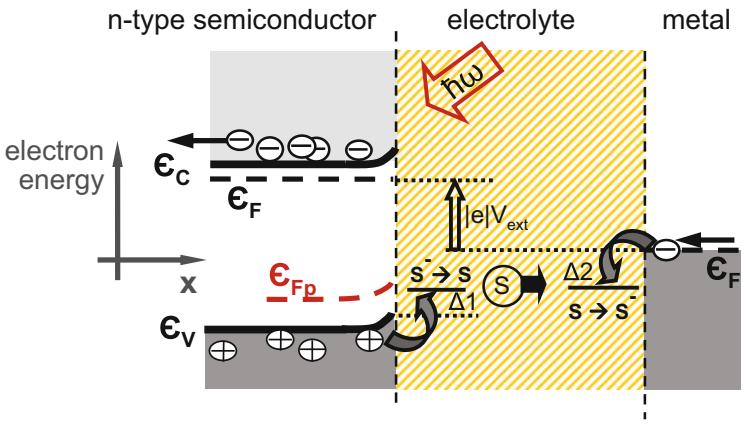

Fig. 5.33 Schematic band/energy level diagram of an electrochemical cell. Illumination of the semiconductor provides for the injection of holes into the electrolyte (equivalent to electron transition from a level in the electrolyte to the valence band of the semiconductor), the transport of a hypothetical species (S) from the semiconducting anode towards the metal cathode by diffusion (gradient in concentration of S), and subsequent 'oxidation' of S at the cathode by transition of an electron from the metal ($S + e^- \rightarrow S^-$)

the liquid, towards the metal electrode occurs by diffusion. Frequently, the transport of these ions requires a gradient of their concentration and thus a drop in chemical potential of the species S^- which adds to the two overpotentials $\Delta 1$ and $\Delta 2$ to produce an internal loss that reduces the achievable splitting in Fermi levels on the right- and left-hand sides at the outer electrical contacts (loss in the external difference of the electrochemical potential eV_{ext}).

5.6.2 *Photochemical Cells*

The working principle of photochemical cells is identical to that of photo-electrochemical cells except that they are operated in short-circuit mode, supplying the complete achievable photogenerated difference in chemical potential to excited species for the production of chemically stable products, one type at the semiconductor side (called the anode) and its counterpart at the metal side (called the cathode). To separate the two species in order to avoid the back-reaction, the two sides of the electrolyte are separated by a diaphragm. (A tremendous bottleneck for technical operation of this scheme is the competition between rates for hole transfer from the absorber to the liquid and the rates of decomposition of the absorbing semiconductor. So far, for water splitting by absorbers with reasonable band gaps the decomposition has always been the predominant effect.)

5.7 Optical Absorption in Real Systems

5.7.1 Absorption Coefficient and Lambert–Beer Law

The spectral coefficient $\alpha(\hbar\omega)$ for absorption of photons in solid matter describes the attenuation of the photon flux $\Gamma_\gamma(x)$ along the propagation length x in the linear approach

$$-\frac{\mathrm{d}\Gamma_\gamma(x)}{\mathrm{d}x} = \alpha\Gamma_\gamma(x) \tag{5.82}$$

known as the Lambert–Beer law (see Sect. 4.2.6.1). The absorption coefficient $\alpha(\hbar\omega)$ can be derived from Maxwell's equations in terms of material properties such as the dielectric function $\varepsilon(\omega)$, magnetic permeability $\mu(\omega)$, and electrical conductivity $\sigma(\omega)$, independently of the amplitudes of the electric and magnetic field strengths $\mathbf{E}$ and $\mathbf{H}$. The combination of the two equations for the formulation of the spatiotemporal behavior of $\mathbf{E}(\mathbf{x}, t)$ and $\mathbf{H}(\mathbf{x}, t)$, e.g., for the electric field strength, yields

$$\nabla \times (\nabla \times \mathbf{E}) = \nabla\,(\nabla \cdot \mathbf{E}) - \Delta\mathbf{E} = -\varepsilon_0\varepsilon\mu_0\mu\frac{\mathrm{d}^2\mathbf{E}}{\mathrm{d}t^2} - \mu_0\mu\sigma\frac{\mathrm{d}\mathbf{E}}{\mathrm{d}t}\,. \tag{5.83}$$

The solution for harmonic filed strengths is a complex $\tilde{\mathbf{E}}(\mathbf{x}, t)$ whose imaginary part

$$\frac{1}{2}\omega\sqrt{\varepsilon_0\mu_0}\varepsilon\left[\sqrt{1+\left(\frac{\sigma}{\omega\varepsilon_0\varepsilon}\right)^2} - 1\right] = \alpha^*;$$

α^* is the attenuation factor for the amplitude as a function of $\mathbf{x}$ (see Appendix A.1 for details). The square of the electric field corresponds to the photon flux and accordingly the optical absorption coefficient $\alpha(\omega) = 2\alpha^*(\omega)$, given by

$$\alpha(\omega) = \omega\sqrt{\varepsilon_0\mu_0}\varepsilon\left[\sqrt{1+\left(\frac{\sigma}{\omega\varepsilon_0\varepsilon}\right)^2} - 1\right]\,. \tag{5.84}$$

The solution of the Lambert–Beer relation for the local photon flux $\Gamma_\gamma(x)$, here in a one-dimensional representation with x denoting the direction of photon propagation, is related to the flux $\Gamma_0 = \Gamma_\gamma(x = 0)$ coupled in at the entrance of the absorbing medium by

$$\Gamma_\gamma(x) = \Gamma_0 \exp\big[-\alpha(\omega)x\big]\,. \tag{5.85}$$

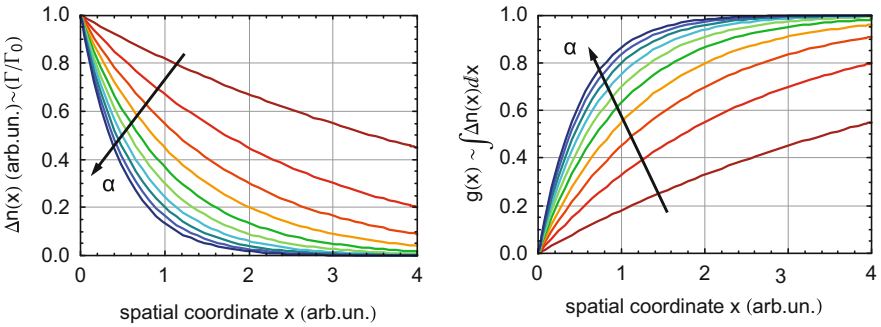

Fig. 5.34 Decay of a monochromatic photon flux $\Gamma(x)/\Gamma_0$ generating the spatial excess density $\Delta n(x)$ versus depth x of propagation into an absorber for different absorption coefficients α (*left*) and integrated absorption of monochromatic photons $\int \Delta n(x)dx$ versus absorber thickness x (*right*) reflecting the optical generation rate $g(x) \sim j_{sc}$, as well as short-circuit current density j_{sc}

The local rate for generation of photoexcited species results from the spatial decay of the flux $\Gamma_\gamma(x)$ within the area A oriented perpendicularly to the propagation:

$$g(x) = -A\frac{\mathrm{d}\Gamma_\gamma(x)}{\mathrm{d}x} = A\alpha(\omega)\Gamma_\gamma(x)\ . \tag{5.86}$$

We get the total number of generated species (total generation rate) in the volume $V = Ad$ from the above relation by integrating over the thickness d:

$$\begin{aligned} g(d) &= \int_0^d g(x)\mathrm{d}x = A\int_0^d \alpha(\omega)\Gamma_\gamma(x)\mathrm{d}x \\ &= A\int_0^d \alpha(\omega)\Gamma_0 \exp\big[-\alpha(\omega)x\big]\mathrm{d}x = A\Gamma_0\Big\{1-\exp\big[-\alpha(\omega)d\big]\Big\}. \end{aligned} \tag{5.87}$$

This gives the total rate of generation $g(x)$ of photoexcited species, such as electron–hole pairs or excitons (see Fig. 5.34).

5.7.2 Optimum Thickness of Absorber Layers

As a consequence of the thickness-dependent total photogeneration of electron–hole pairs in a solar-cell absorber, an optimum value d^* exists for which the product of the short-circuit current density j_{sc} (equivalent to the photocurrent density j_{photo})

and the open-circuit voltage V_{oc} reaches a maximum value. The product $j_{\mathrm{sc}} V_{\mathrm{oc}}$ contains the total rate of photogenerated charges. The short-circuit current density is

$$j_{\mathrm{sc}} \sim \int_0^d \left[1 - \exp(-\alpha x)\right] \mathrm{d}x \ , \tag{5.88}$$

whereas in the ideal case of negligible surface recombination at the front and rear sides, the open-circuit voltage reads

$$V_{\mathrm{oc}} = kT \ln\left[\frac{np}{n_0 p_0}\right] \ , \tag{5.89}$$

where the actual densities under illumination are assumed to distribute by sufficiently efficient diffusion across the entire absorber thickness (here, normalized), and we get the averaged excess carrier density

$$(n - n_0) = \Delta n \sim \int_0^d \frac{1}{d}\left[1 - \exp(-\alpha x)\right] \mathrm{d}x \ .$$

The short-circuit current density $j_{\mathrm{sc}}(d)$ saturates for large thicknesses d, and the open-circuit voltage $V_{\mathrm{oc}}(d)$ vanishes for large d because the finite number of excess charges are hypothetically smeared out across an infinite length, thereby decreasing $\Delta n(d \to \infty) = 0$. Here we have chosen $p = p_0$. The individual magnitudes j_{sc} and $\ln(np/n_0 p_0) \sim V_{\mathrm{oc}}$ versus absorption length represented by the thickness d of the absorber are displayed in Fig. 5.35, where we have chosen $np = 10^6 n_0 p_0$.

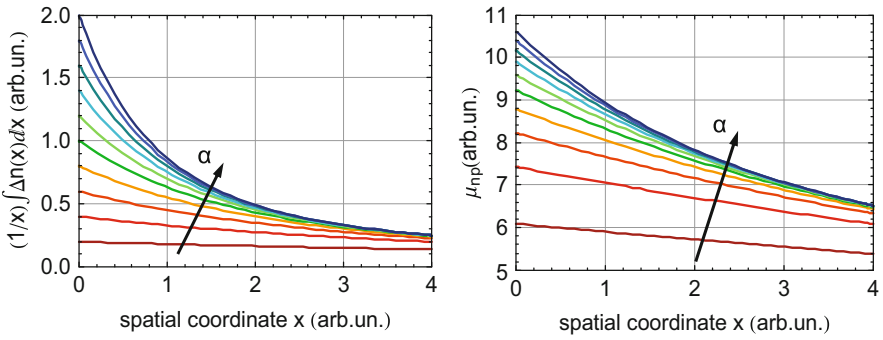

Fig. 5.35 Averaged excess carrier density $(1/x) \int \Delta n(x) dx \sim (\epsilon_{\mathrm{Fn}}(x) - \epsilon_{\mathrm{F}}) = \mu_{\mathrm{n}}(x)$ (*left*) and logarithm of product of electrons and holes $\ln\left(np/n_0 p_0\right) \sim \mu_{\mathrm{np}}(x)$, representing the behavior of the open-circuit voltage, versus absorber depth x (*right*). As the short-circuit current increases with the number of absorbed photons, the open-circuit voltage (for ideally passivated front and rear surfaces) decreases as a consequence of the increase in the volume/length across which the photogenerated excess carriers are distributed

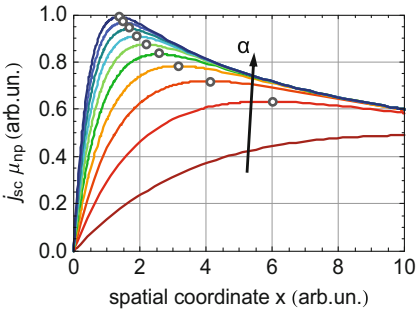

Fig. 5.36 Product of short-circuit current and open-circuit voltage in terms of electron-hole chemical potential μ_{np} (in arbitrary units) which qualitatively represents output power (efficiency) of an ideal solar cell versus absorber thickness for different absorption coefficients α. Each value of α requires a particular optimum absorber thickness (*circles*)

The product

$$j_{sc} kT \ln\left[\frac{np}{n_0 p_0}\right] = j_{sc} V_{oc} \ ,$$

which is proportional to the electric output power density of a solar cell, assuming for the sake of simplicity that the filling factor remains unchanged, is shown in arbitrary units in Fig. 5.36. Here we observe the optimum thickness $d_{opt} = d_{opt}(\alpha)$ as a function of the absorption coefficient $\alpha(\omega)$ for which we get the maximum output power.

If we allow for non-negligible front- and rear-surface recombination, the behavior of an optimum absorber thickness is qualitatively conserved. The quantitative behavior depends on the resulting excess carrier profile which itself is governed by the generation profile, surface recombination velocities, and minority-carrier diffusion length.

5.7.3 *Absorption of Semiconductors Versus Molecules or Atoms*

The absorption of photons in matter arises from transitions between occupied initial electronic states and unoccupied final ones. The driving force for those transitions is the electromagnetic field expressed as a vector potential that couples the wave functions of the relevant states via the optical matrix element (for details see [22]).

In densely packed bulk solid matter, like semiconductors, and in contrast to the situation for atoms or molecules, the steady-state solution of the energy eigenstates of electrons yields energy bands with width of a few eV, whereas in atoms or

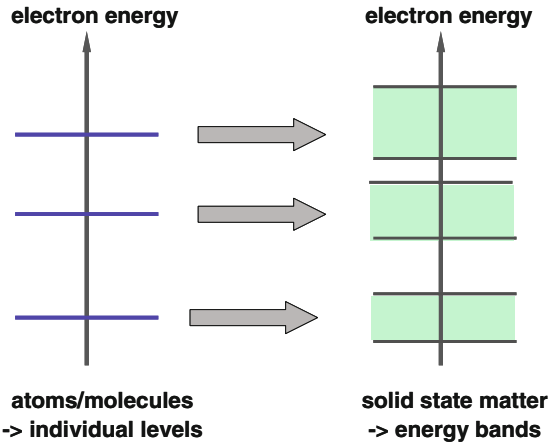

Fig. 5.37 Qualitative transition from discrete energy levels in atoms to energy bands in condensed matter by 'interference' of electron wave functions

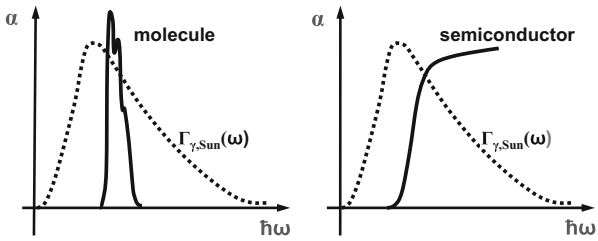

Fig. 5.38 Schematic spectral absorption coefficient α (*bold lines*) of molecules (dyes) (*left*) and semiconductors (*right*) together with the spectral photon flux $\Gamma_{\gamma,\mathrm{Sun}}$ from the Sun (*dotted lines*)

molecules, due to the much lower number of individual sites, more or less discrete energy levels exist for the electrons (see Fig. 5.37).

As a consequence of bands in dielectrics and semiconductors the energy regime for the combined density of states spans a much broader energy scale than for atoms and small enough molecules, such as those of commonly used dyes (see the schematic representation in Fig. 5.38). By the Lambert–Beer law, the absorption $A(\hbar\omega)$ depends on the absorption coefficient $\alpha(\hbar\omega)$ according to $A(\hbar\omega) = 1 - \exp\left[-\alpha(\hbar\omega)d\right]$. For solar light conversion, the absorption of appropriately thick semiconductors in photon energy regimes sufficiently higher than the band gap ϵ_g, reaches unity, i.e., $A\left(\hbar\omega \gg \epsilon_\mathrm{g}\right) \rightarrow 1$, whereas in molecules, the absorption for photon energies well above the LUMO–HOMO transition energy $\epsilon_{\mathrm{LUMO\text{–}HOMO}}$ decays to zero, i.e., $A\left(\hbar\omega \gg \epsilon_{\mathrm{LUMO\text{–}HOMO}}\right) \rightarrow 0$.

In addition, in semiconductors and dielectrics, due to the well-defined relation of energy and wave vector, $\epsilon = \epsilon(\mathbf{k})$, electronic transitions initiated by photons occur without or with change of electron/hole wave vectors, which are called direct or indirect transitions respectively. In indirect transitions, the wave vector $\Delta\mathbf{k}$ necessary to fulfill momentum conservation is provided either by phonon absorption or phonon emission. Both effects are controlled by the corresponding phonon energy $\hbar\omega_\mathrm{phon}(\Delta\mathbf{k})$, which we find in the corresponding phonon dispersion

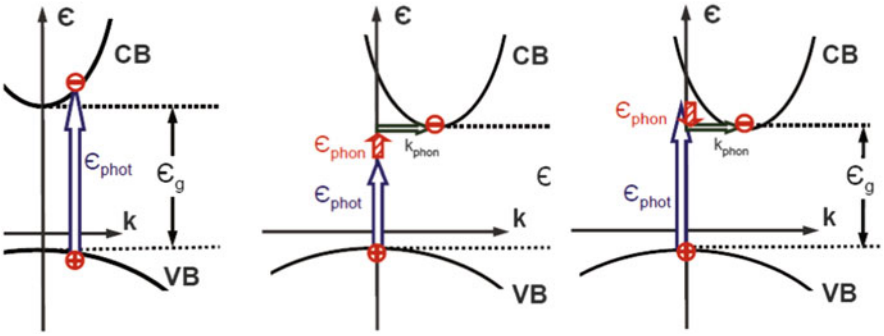

Fig. 5.39 Electronic transition through absorption of a photon with band gap energy in a direct semiconductor (*left*) and in an indirect semiconductor. The transition with band-gap energy in an indirect semiconductor requires the supply of a specific $\Delta\mathbf{k}$ from lattice vibrations (phonons); indirect transition with phonon absorption (*center*), and with phonon emission (*right*)

relation $\omega_{\text{phon}}(\mathbf{k})$. The participation of phonons makes the photon absorption process much less likely than for a direct transition, and the absorption coefficients for direct transitions are thus correspondingly higher than for indirect ones (by a factor of about 10^2).

When the minimum energy separation of the valence and conduction bands, i.e., the energy difference between the top of the valence and the bottom of the conduction band are located at identical wave vector $\mathbf{k}$, the semiconductor is said to be direct. If the positions of VB maximum and CB minimum differ by a wave vector $\Delta\mathbf{k}$, we are dealing with an indirect semiconductor (see Fig. 5.39). The distinction between direct semiconductors with high absorption coefficients and indirect ones with comparatively low absorption coefficients specifies solar-cell technology into thin-film and thick-film approaches.

5.8 Equivalent Circuit of Illuminated Diodes

For reasons of completeness, we consider here the equivalent circuits of an ideal diode and of a diode with losses due to non-radiative recombination of photoexcited carriers (think of defects) and losses due to those initiated by non-ideal transport properties of carriers (e.g., limited mobilities, or in other words, limited diffusion coefficients, non-ideal contacts). The effect of non-radiative recombination in this picture is represented by an additional current, bypassing the ideal diode in which solely radiative recombination is possible. The bypass itself is represented by a parallel resistor r_{p}. This is a highly simplifying assumption, since non-radiative recombination is not linearly associated with the voltage across the junction. The

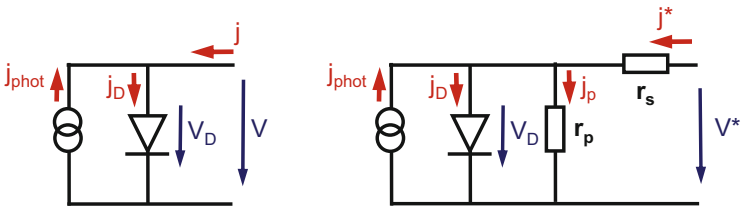

Fig. 5.40 Equivalent circuits of an illuminated ideal diode (*left*) and a diode with parallel and series resistors representing losses by non-radiative recombination (r_p) and non-ideal leads (r_s) (*right*)

transport losses in the leads to the junction correspond to a voltage drop which would be better introduced by means of a series resistor r_s[25] (Fig. 5.40).

The current-density–voltage relation of the illuminated ideal diode including the photo current density j_{phot} is (remember Sect. 4.2.4)

$$j = j_0 \left(\exp \frac{eV}{kT} - 1 \right) - j_{phot} \,, \tag{5.90}$$

where current density j and applied voltage V are externally accessible parameters. The resistors r_p and r_s are to be modified by an appropriate area A to express these quantities in ohms. The external current density for the illuminated diode with the loss terms is modified to

$$j = j_D + j_p - j_{phot} \,. \tag{5.91}$$

Introducing

$$V_D = V - jr_s \,, \qquad j_D = j_0 \left[\exp \left(\frac{e(V - jr_s)}{kT} \right) - 1 \right] \,, \qquad j_p = \frac{V_D}{r_p} = \frac{V - jr_s}{r_p} \,,$$

we arrive at

$$j = j_0 \left[\exp \left(\frac{e(V - jr_s)}{kT} \right) - 1 \right] + \frac{V - jr_s}{r_p} - j_{phot} \,. \tag{5.92}$$

We now examine the effect of the series and parallel resistors for comparatively small departures from the ideal diode for which $r_s \to 0$ and $r_p \to \infty$. In a formal

[25]The 'resistors' r_p and r_s are expressed in terms Ohm cm^2, as in the sketches in Fig. 5.40.

procedure we discuss the derivative $(\mathrm{d}j/\mathrm{d}V)$ for boundary conditions $V(j = 0) = V_{\mathrm{oc}}$ and for $V = 0 = V(j_{\mathrm{sc}})$:

$$1 = j_0 \left(-\frac{er_{\mathrm{s}}}{kT}\right) \exp\left(-\frac{ejr_{\mathrm{s}}}{kT}\right) \exp\left(\frac{eV}{kT}\right) + j_0 \exp\left(-\frac{ejr_{\mathrm{s}}}{kT}\right) \left(\frac{e}{kT}\right) \exp\left(\frac{eV}{kT}\right) \left(\frac{\mathrm{d}V}{\mathrm{d}j}\right) + \frac{1}{r_{\mathrm{p}}} \left(\frac{\mathrm{d}V}{\mathrm{d}j}\right) - \frac{r_{\mathrm{s}}}{r_{\mathrm{p}}} . \tag{5.93}$$

Reorganizing this relation, we get

$$\frac{\mathrm{d}V}{\mathrm{d}j} = r_{\mathrm{s}} + \frac{1}{\dfrac{1}{r_{\mathrm{p}}} + \dfrac{j_0 e}{kT} \exp\left(\dfrac{e\,(V - jr_{\mathrm{s}})}{kT}\right)} . \tag{5.94}$$

For particular boundary conditions, such as open circuit or short circuit, we arrive at

$$\left.\frac{\mathrm{d}V}{\mathrm{d}j}\right|_{j=0/V=V_{\mathrm{oc}}} = r_{\mathrm{s}} + \frac{r_{\mathrm{p}}}{1 + \dfrac{ej_0 r_{\mathrm{p}}}{kT} \exp\left(\dfrac{eV_{\mathrm{oc}}}{kT}\right)} \approx r_{\mathrm{s}} \tag{5.95}$$

or

$$\left.\frac{\mathrm{d}V}{\mathrm{d}j}\right|_{j=j_{\mathrm{sc}}/V=0} = r_{\mathrm{s}} + \frac{r_{\mathrm{p}}}{1 + \dfrac{ej_0 r_{\mathrm{p}}}{kT} \exp\left(-\dfrac{ej_{\mathrm{sc}} r_{\mathrm{s}}}{kT}\right)} \approx r_{\mathrm{s}} + r_{\mathrm{p}} \approx r_{\mathrm{p}} . \tag{5.96}$$

In the j–V relation, provided the departure of the loss resistors from ideal is small, we see as inverse slopes the parallel resistance r_{p} in short-circuit operation and the series resistance r_{s} in open-circuit mode (see Fig. 5.41).

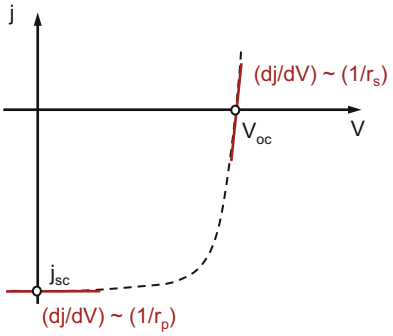

Fig. 5.41 Current density–voltage curve of an illuminated diode with parallel and series resistors r_{p} and r_{s}. Their influence on the j–V curve emerges as derivatives $(\mathrm{d}V/\mathrm{d}j)$ at j_{sc} and V_{oc}, respectively

5.9 Status of Cell and Module Efficiencies

Table 5.1 summarizes the efficiencies of laboratory cells and of modules, to some extent even commercially available (data mainly collated from [23]). This survey lists photovoltaic cells based on crystalline silicon, III–V compounds, inorganic thin-film absorbers, such as thin silicon and polycrystalline compound semiconductors (chalcogenides, chalcopyrites, etc.), as well as organic solar cells and multijunction devices.

Table 5.1 Efficiencies of best solar cells under illumination by global AM1.5 spectral distribution with total 100 mW/cm^2 and ambient temperature $T = 25\,^{\circ}\mathrm{C}$

Type of cell	Area (cm^2)	Efficiency (%)	References
Silicon			
• Monocrystalline Si (Perl cell)	4.0	25.0	[23]
• Monocrystalline Si	1.0	20.4	[23]
• Monocrystalline Si (artificial thin absorber 45 μm)	4.0	16.7	[23]
III–V cells			
• Monocrystalline GaAs	1.0	26.4	[23]
• Multicrystalline GaAs	4.0	18.4	[23]
• Monocrystalline GaAs (thin film)	4.0	28.1	[23]
• Monocrystalline InP	4.0	22.1	[23]
Amorphous or micro-/nanocrystalline silicon			
• a-Si:H (single junction, light soaked)	1.0	10.1	[23]
• Nanocrystalline Si (single junction)	1.2	10.1	[23]
Chalcopyrites/chalogenides			
• $CuInGaSe_2$	0.5	20.3	[24]
• $CuInGaS_2$	0.5	12.6	[25]
• CdTe	1.0	16.7	[23]
• $Cu_2ZnSn(Se,S)_4$	0.43	9.6	[26]
Photochemical cells			
• Dye-sensitized cell	1.0	10.4	[23]
Organic absorber solar cells			
• Organic polymer cell	1.0	8.3	[23]
Multijunction cells			
• GaInP/GaAs	4.0	30.3	[23]
• GaInP/GaAs/Ge	4.0	32.0	[23]
• GaAs/CIS	4.0	25.8	[23]
• a-Si:H/μc-Si	14.0	11.7	[23]
• Organic tandem absorber	1.0	9.8	[27]
• InGaP/GaAs/InGaAs (343 suns concentrated)	1.0	41.3	[23]

References

1. S.M. Sze, *Physics of Semiconductor Devices* (Wiley, New York, 1981)
2. B. Sapoval, C. Hermann, *Physics of Semiconductors* (Springer, Berlin, 2003)
3. R. Enderlin, N.J.M. Horing, *Fundamentals of Semiconductor Physics and Devices* (World Scientific, Singapore, 1997)
4. R. Sauer, *Halbleiterphysik* (Oldenbourg, München, 2009)
5. H.G. Wagemann, H. Eschrich, *Grundlagen der photovoltaischen Energiewandlung* (Teubner, Stuttgart, 2010)
6. W. Shockley, W.T. Read, Phys. Rev. **87**, 835 (1952); R.N. Hall, Phys. Rev. **87**, 387 (1952)
7. J.S. Yuan, J.J. Liou, *Semiconductor Device Physics and Simulation* (Plenum, New York, 1998)
8. P. Würfel, *The Physics of Solar Cells* (Wiley-VCH, Weinheim, 2009)
9. D.V. Morgan, R.H. Williams, *Physics and Technology of Heterojunction Devices* (P. Peregrinus Ltd, London, 1991)
10. W. Schottky, Zeitschr. Physik **118**, 539 (1942)
11. H.K. Henisch, *Semiconductor Contacts* (Clarendon Press, Oxford, 1984)
12. C.W. Tang, Appl. Phys. Lett. **48**, 183 (1986)
13. G. Yu et al., Science **270**, 1789 (1995)
14. M. Granström et al., Nature **395**, 257 (1998)
15. K. Yoshino et al., IEEE Trans. Electron Dev. **44**, 1315 (1997)
16. P. Fulde, *Electron Correlations in Molecules and Solids* (Springer, Berlin, 1995)
17. U. Bach et al., Nature **395**, 583 (1998)
18. M. Graetzel, MRS-Bull. **30**, 23 (2005)
19. J. Kroon, A. Hinsch, Dye-sensitized solar cells, in *Organic Photovoltaics*, ed. by C. Brabec et al. (Springer, Berlin, 2003)
20. B.A. Gregg, J. Appl. Phys. **93**, 3605 (2003)
21. S.R. Forest, MRS-Bull. **30**, 28 (2005)
22. C. Hamaguchi, *Basic Semiconductor Physics* (Springer, Berlin, 2001)
23. M.A. Green, K. Emery, Y. Hishikawa, W. Warta, E.D. Dunlop, Prog. Photovolt. Res. Appl. **19**, 565 (2011)
24. P. Jackson et al., Prog. Photovolt. Res. Appl. **19**, 894 (2011)
25. S. Merdes et al., Sol. Energy Mater. Sol. Cells **95**, 864 (2011)
26. T.K. Todorov et al., Adv. Mater. **22**, E156 (2010)
27. C.L. Uhrich, R. Meersheim, T. Mueller, F. Lindner et al., Proc. SPIE8477, *Organic Photovoltaics XIII*, 847705 (2012)

Chapter 6
Advanced Concepts: Beyond the Shockley–Queisser Limit

The main difference between the theoretical limit of solar energy conversion, like that of a Mueser engine at maximum concentration (see Sect. 4.1.4, where we found $\eta_{\mathrm{Mues}} = 0.86$) and the Shockley–Queisser efficiency, representing the radiative limit of a single-gap absorber illuminated by sunlight without concentration ($\eta_{\mathrm{SQ}} = 0.29$, [1]) results from

- the excess energy of photons $\hbar\omega > \epsilon_{\mathrm{g}}$ which is converted into heat,
- the amount of photons $\hbar\omega < \epsilon_{\mathrm{g}}$ not absorbed,
- the low photon solid angle $\Omega_{\mathrm{in}} = \Omega_{\mathrm{Sun}} = 5.3 \times 10^{-6}$ of non-concentrated sunlight[1] compared to the solid angle for emission Ω_{out} (e.g., for flat absorbers with highly reflecting rear contacts $\Omega_{\mathrm{out}} = 2\pi$)

Accordingly, amongst the many technological attempts to increase the optoelectronic properties of absorber semiconductors, such as reduction of bulk and surface recombination rates, two issues have been regarded as the most promising options for increasing the performance of photovoltaic solar-light conversion:

- Use of photons with energy above the optical band gap ($\hbar\omega > \epsilon_{\mathrm{g}}$).
- Stronger trapping of light in the absorber.

6.1 Concentration of Sunlight

The departure from thermal equilibrium by photoexcitation is commonly formulated using the quasi-Fermi-level approach. This leads to a logarithmic dependence of the chemically usable potential of species versus their concentration, which in

[1] Since the efficiency of ideal photovoltaic converters rises logarithmically with the absorbed photon flux ($\sim \ln[\Gamma_\gamma/\Gamma_{\gamma,0}] \sim \ln[(np)/n_0 p_0]$), the maximum achievable Γ_γ which corresponds to $\Omega_{\mathrm{in}} = \Omega_{\mathrm{out}}$ should be applied to the absorber to get nominally the highest conversion efficiency.

G.H. Bauer, *Photovoltaic Solar Energy Conversion*, Lecture Notes in Physics 901,
DOI 10.1007/978-3-662-46684-1_6

turn depends on the excitation flux fed to the absorber. Thus the harvesting and the performance of conversion of sunlight in an absorbing system depends on the light flux departing the system from thermal equilibrium. The enhancement of the light flux leads to a rise of conversion performance, already exemplified by the logarithmic behavior of the open-circuit voltages versus light flux in traditional solar cells, viz.,

$$V_{\mathrm{oc}} = kT \ln \left[\frac{np}{n_0 p_0} \right] ,$$

as discussed in Sects. 4.2.3 and 5.1.4, where n and p are the steady-state concentrations of photoexcited electrons and holes.

6.1.1 Imaging Concentration of Sunlight

An easy concept for the increase of the flux of sunlight is to focus direct solar radiation by passive optical elements such as lenses or mirrors. It goes without saying that these do not alter the original spectral distribution of photons. Here we distinguish between one- and two-dimensional concentrators ($n = 1$ or $n = 2$), for which we find the maximum theoretical concentration $C_{\mathrm{max,n}}$ by reversion of the spatial dilution of the light propagating from the Sun's surface to the Earth

$$C_{\mathrm{max},\,n} = \left(\frac{d_{\mathrm{SE}}}{R_{\mathrm{Sun}}} \right)^n ,$$

which yields $C_{\mathrm{max}}(n = 1) = 217$ and $C_{\mathrm{max}}(n = 2) = (217)^2 = 4.7 \times 10^4$.

6.1.2 Non-imaging Concentration of Sunlight

Non-imaging concentration of sunlight is based on geometrically simpler, and hence cheaper structures than focussing optical component, namely flat or shaped mirrors, or strongly scattering surfaces at the light entrance side or at the rear surface of the absorber.

One option of a non-imaging concentration, a 'linearly' shaped spherically truncated pyramid which concentrates the incoming photons from area A_{in} into area A_{out} is schematically displayed in Fig. 6.1. On the right-hand side, A_{out}, has been chosen too small to allow all the photons entering A_{in} to pass through. Only those photons within A_{acc} are coupled to the outlet area where an absorber/converter is located. The acceptance area A_{acc} is determined by identifying the contour within which the photons are accepted for guidance through the concentrating device. This is called the edge-ray principle (for further details, see [2]).

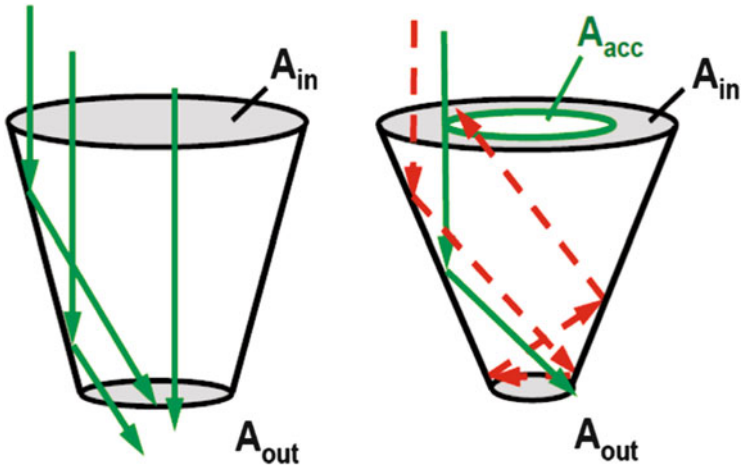

Fig. 6.1 Schematics of non-imaging solar light concentrators. Concentration factor determined by outlet and inlet (*left*) and by acceptance area A_{acc} circumvented by the edge ray line (*right*)

However, non-imaging light concentration generates a spatially inhomogeneous light flux which results in a spatially inhomogeneous generation of excess carriers and similarly in general produces an inhomogeneous excess density. This non-homogeneous distribution is less favorable than a homogeneous one, because the mixing of intensive thermodynamic variables may create additional entropy.[2]

In a simple exemplary approach, we compare the chemical potential of a homogeneous overall excess carrier density $\overline{n}$ with a spatial variation of this density in regions with $\overline{n} + \Delta$ and $\overline{n} - \Delta$. Comparing the chemical potential μ_{nm} of the non-mixing system with the value μ_{m} for the mixing one, we find

$$\mu_{\mathrm{nm}} = kT \ln\left[\frac{\overline{n}}{n_0}\right] , \tag{6.1}$$

whereas

$$\mu_{\mathrm{m}} = \frac{1}{2}kT\left(\ln\left[\frac{\overline{n}+\Delta}{n_0}\right] + \ln\left[\frac{\overline{n}-\Delta}{n_0}\right]\right) = \frac{1}{2}kT \ln\left[\frac{(n+\Delta)\,(n-\Delta)}{n_0^2}\right] , \tag{6.2}$$

[2]In solar thermal collectors, e.g., inhomogeneous light fluxes generate, of course, equivalent inhomogeneous temperature distributions, which in turn lead to a mixture of intensive variables and to generation of entropy.

and hence,

$$\mu_{\mathrm{m}} = kT \ln \left[\sqrt{\frac{\overline{n}^2 - \Delta^2}{n_0^2}} \right] = kT \ln \left[\frac{\overline{n}}{n_0} \left(\sqrt{1 - \frac{\Delta^2}{\overline{n}^2}} \right) \right] < \mu_{\mathrm{nm}} \,. \tag{6.3}$$

For any value Δ, the exploitability of the mixing systems turns out to be lower than that of the homogeneous one.

6.1.3 Non-imaging Concentration with Stokes Shift/Fluorescence Collectors

6.1.3.1 Principle of Light-Trapping and Light-Guiding in Fluorescence Collectors

Solar fluorescence collectors (flucos) [3, 4] are made of absorber molecules (dye) incorporated in a dielectric matrix transparent to most solar radiation (near-UV to near-IR photons). Geometrically, they consist of thin plates with comparatively large areas exposed to the solar radiation and small side surfaces through which the dye-converted radiation may be coupled out orthogonally to the incoming light (see Fig. 6.2).

In the fluco a particular energy regime of the solar photons $\hbar\omega$ is absorbed by the dye and transferred by Stokes shift to fluorescence light $\hbar\omega^*$ with somewhat lower photon energies (see schematic absorption and emission coefficients displayed in Fig. 6.3).

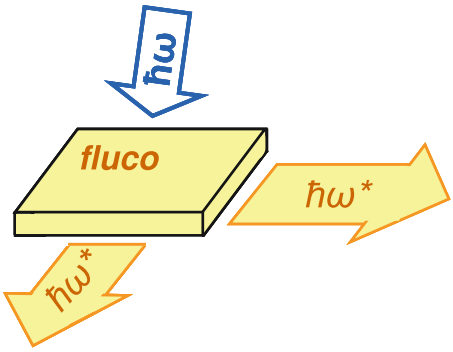

Fig. 6.2 Schematics of a solar fluorescence collector. Photons of a particular energy are absorbed by dye molecules and re-emitted after Stokes shift to lower frequency. The emitted photons—except those propagating in the angle regime of the escape cone (see Fig. 6.4)—are reflected at the upper and lower surface and guided to the edge of the fluco. Photons of energies beyond the absorption regime don't 'feel' the presence of the dye and propagate like in dielectrics (transmission and reflection at surfaces)

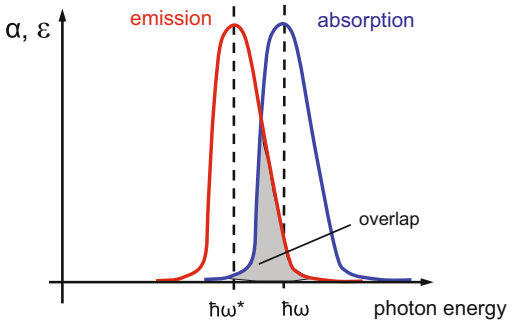

Fig. 6.3 Schematic spectral absorption and Stokes-shifted emission of photons in a fluorescence collector; as a consequence of the overlap of emission and absorption spectrum a particular fraction of the fluorescence photons are re-absorbed on their way to the edge of the collector. Due to the dye's quantum efficiency ($Q_{\mathrm{dye}} < 1$) and because of the probability for re-emitted photons to be scattered into the escape cone another fraction of the re-absorbed photons are lost for the conversion in an externally attached solar cell

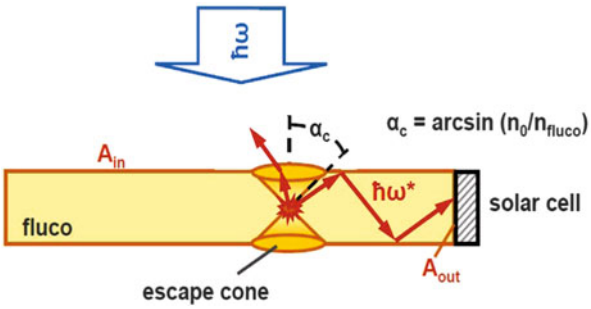

Fig. 6.4 Emission of Stokes-shifted photons in a fluorescence collector (fluco), total reflection of photons at front and rear surface (light entrance area A_{in}), propagation in the angle regime outside the escape cone ($\alpha > \alpha_{\mathrm{c}}$), and guiding to the fluco edge, where these photons are fed to solar cells with comparatively small area A_{out}

Due to the contrast between the refractive indices of the fluco ($\tilde{n}_{\mathrm{fluco}}$) and its environment (in most cases air with $n_{\mathrm{env}} = n_{\mathrm{air}} \approx 1.0$), photons propagating across the interfaces, such as solar photons to be coupled into the fluco, but also fluorescence photons generated in the fluco to be transmitted to a solar cell attached at the edge of the fluorescence collector, suffer from reflections. According to Maxwell's equations, the coefficients for reflection r and transmission t for amplitudes of electric and magnetic field components are given in terms of the (complex) refractive indices $\tilde{n}_i$ of the two adjacent phases by (see Appendix A.2)

$$r = \frac{\tilde{n}_1 - \tilde{n}_2}{\tilde{n}_1 + \tilde{n}_2}\,, \qquad t = \frac{2\tilde{n}_1}{\tilde{n}_1 + \tilde{n}_2}\,.$$

For photon propagation from the dense optical phase, here from the fluco with n_{fluco}, to the lower-refractive phase of the environment, e.g., with n_0, total reflection occurs for angles

$$\varphi \geq \alpha_c = \arcsin\left[\frac{n_0}{n_{\text{fluco}}}\right],$$

where α_c is the critical angle,[3] and this keeps photons propagating within the fluco until they see the angle $\varphi' = 90° - \varphi \leq \alpha_c$, e.g., at the edge perpendicular to the light entrance surface, and escape towards a solar cell (see Fig. 6.4).

6.1.3.2 Performance and Limits for Solar-Light Conversion in Fluorescence Collectors

The spectrally selective fluorescence light emitted from the edge of the fluco and fed to a solar cell with appropriate optical band gap results only from that particular wavelength regime of the solar light in which the dye efficiently absorbs photons. The fluco photons originate from the input of the solar radiation across the area A_{in} much larger than the area A_{out} through which the light is coupled out to the solar cell. This increase in outgoing photon flux against incoming photon flux, which means concentration of light, even diffuse light, is possible by virtue of Stokes shift between incoming and outgoing photons.

The maximum enhancement of the photon flux into the fluco [5, 6] is generally found using a quantum approach which is based upon the balance of photons in the radiative limit; this upper limit results from thermodynamic restrictions and cannot be derived from geometrical optics.

In matter, absorption and emission of photons are strongly coupled to one another.[4] By the principle of reversibility, this coupling allows for the formation of a stationary state of matter under illumination by forward (absorption) and back reactions (emission).

We apply the description already used in Sect. 4.2.3 for emission (into the solid angle $\Omega_{\text{out}} = 4\pi$) of the spectral photon flux $\Gamma_\gamma(\omega)$ from matter and pushed out at

[3] The comprehensive derivation of the total reflection includes the distinction of the direction of photon polarization with respect to the orientation of the reflecting surface.

[4] In molecular systems electrons undergo optical transitions for absorption and emission from and to electronic levels, to which only different vibrational and rotational terms are added. After absorption of a photon the electron in the excited state usually undergoes a relaxation to a lower vibrational energy level from which it may return to the initial electronic level by emission of a photon with lower energy compared to the energy of the absorbed photon.

temperature T_{abs} and governed by the chemical potential μ [6]:

$$\Gamma_\gamma(\omega) = \frac{\Omega_{\text{out}}}{c_0^2 4\pi^3\hbar^3} \frac{(\hbar\omega)^2}{\exp\left(\dfrac{\hbar\omega - \mu}{kT_{\text{abs}}}\right) - 1} = \frac{1}{c_0^2\pi^2\hbar^3} \frac{(\hbar\omega)^2}{\exp\left(\dfrac{\hbar\omega - \mu}{kT_{\text{abs}}}\right) - 1}\,, \tag{6.4}$$

from which we extract the chemical potential

$$\mu = \hbar\omega - kT \ln\left[1 + \frac{(\hbar\omega)^2}{c_0^2\pi^2\hbar^3\Gamma_\gamma(\omega)}\right] = \hbar\omega - kT \ln\left[1 + \frac{(\hbar\omega)^2}{\beta\Gamma_\gamma}\right] \tag{6.5}$$

(with abbreviation $\beta = c_0^2\pi^2\hbar^3$).

We now suppose two hypothetical systems, one operating with optical threshold $\epsilon_1 = \hbar\omega_1$, which we dedicate to the absorption of solar light in the fluco (of course, also for emission) characterized by the flux $\Gamma_{\gamma,1}$, and a second one at the very same temperature T, emitting the flux $\Gamma_{\gamma,2}$ with Stokes-shifted $\epsilon_2 = \hbar\omega_2 < \hbar\omega_1$, and let them interact with one another. In the steady state their chemical potentials are at best equal $\mu_1(\Gamma_{\gamma,1})) = \mu_2(\Gamma_{\gamma,2})$. We express this equality in terms of the equation above to obtain

$$\hbar\omega_1 - kT_0 \ln\left[1 + \frac{(\hbar\omega_1)^2}{\beta\Gamma_{\gamma,1}(\omega)}\right] = \hbar\omega_2 - kT_0 \ln\left[1 + \frac{(\hbar\omega_2)^2}{\beta\Gamma_{\gamma,2}(\omega)}\right]\,. \tag{6.6}$$

We then arrive at

$$\exp\left(\frac{\hbar\omega_1 - \hbar\omega_2}{kT_0}\right) = \frac{1 + \dfrac{(\hbar\omega_1)^2}{\beta\Gamma_{\gamma,1}}(\omega)}{1 + \dfrac{(\hbar\omega_2)^2}{\beta\Gamma_{\gamma,2}}(\omega)}\,.$$

After a little rearrangement and the recognition that the flux emitted from system 1 has to balance the flux from the Sun $\Gamma_{\gamma,1} = \Gamma_{\text{Sun}}$, we finally obtain

$$\begin{aligned} C_{\text{max, fluco}} &= \frac{\Gamma_{\gamma,2}}{\Gamma_{\gamma,1}} \\ &= \left(\frac{\hbar\omega_2}{\hbar\omega_1}\right)^2 \left[1 + \beta\frac{\Gamma_{\gamma,1}}{(\hbar\omega_1)^2}\left(1 - \exp\left(\frac{\hbar\omega_1 - \hbar\omega_2}{kT_0}\right)\right)\right]^{-1} \exp\left(\frac{\hbar\omega_1 - \hbar\omega_2}{kT_0}\right)\,. \end{aligned} \tag{6.7}$$

For regular sunlight fluxes $\Gamma_{\gamma,1} = \Gamma_{\mathrm{Sun}}$, and even for concentrations of sunlight up to about 100 suns equivalent, $\beta\Gamma_{\gamma,1}/\left(\hbar\omega_1\right)^2 < 1$, and we approximate

$$C_{\mathrm{max,\,fluco}} \approx \left(\frac{\hbar\omega_2}{\hbar\omega_1}\right)^2 \exp\left(\frac{\hbar\omega_1 - \hbar\omega_2}{kT_0}\right) = \left(\frac{\hbar\omega_2}{\hbar\omega_1}\right)^2 \exp\left(\frac{\Delta\left(\epsilon_{\mathrm{Stokes\,shift}}\right)}{kT_0}\right) . \tag{6.8}$$

However, in the fluco, the concentrated fluorescence light towards the exit area is additionally modified

- by incomplete absorption of solar photons ($\hbar\omega_1$) as they propagate along the path length d in the fluco, which yields the factor,

$$\left\{1 - \exp\left(-\alpha_{\mathrm{dye}}(\hbar\omega_1)d\right)\right\} < 1 ,$$

- but also by the internal quantum yield of the dye $\eta_\gamma < 1$ for conversion of solar light ($\hbar\omega_1$) into fluorescence photons ($\hbar\omega_2$), by elastic scattering of fluorescence photons originally propagating outside the escape cone back into it, and last but not least by absorption of fluorescence photons by the dye and subsequent non-radiative relaxation of excited dye molecules, which contributes to incomplete 'photon recycling'; those losses can be quantified by a factor η^*:

$$\eta^{**} = \left\{1 - \exp\left(-\alpha_{\mathrm{dye}}(\hbar\omega_2)l\right)\right\}\eta_\gamma\eta^* ,$$

  where l denotes the actual path length of the fluorescence photons 'zigzagging' in the collector.

A theoretical approach for a single-stage fluorescence collector with ideal conversion of solar photons to luminescence photons including the balance of the etendue [7–9] (radiance input and output) yields an efficiency close to the Shockley–Queisser limit (shown in Fig. 6.5 and discussed in Sect. 4.2.5, and [1]).

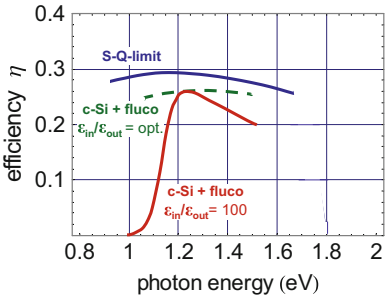

Fig. 6.5 Efficiency η of a fluco coated with c-Si absorber versus photon energy for different ratios of etendue of photons in and out: $\varepsilon_{\mathrm{in}}/\varepsilon_{\mathrm{out}} = $ opt. and $\varepsilon_{\mathrm{in}}/\varepsilon_{\mathrm{out}} = 100$ (see [8, 9] of Chap. 5) compared with the spectral Shockley–Queisser limit [1]

In essence, for the characterization of real flucos where—amongst the beneficial effect of light concentration—we have to consider the particular spectrally selective and incomplete absorption of solar photons. In addition we have to regard the imperfect transformation of the incoming solar light to lower photon energies for the generation of fluorescence light, the elastic as well as inelastic scattering of solar and fluorescence photons by the dye in the dielectric matrix imbedding the dye, and also scattering at imperfect (rough) surfaces of this matrix.

6.1.4 Optical Design for Increase of the Photon Density in Matter

The photon density in matter and likewise the degree of photons available for exploitation is governed not only by incomplete absorption $A = 1 - \exp(\alpha(\hbar\omega)\, d) < 1$ but equivalently by incomplete coupling of photons to the absorber resulting from reflection. As a consequence of the contrast in refractive indices between two media, e.g., air and absorber, a substantial fraction of photons may be reflected unless anti-reflection strategies are applied.

The reflection coefficient for the amplitude (r_{ampl}) of an electromagnetic wave is found by considering the electric field strength propagating across an interface between materials with (complex) refractive indices $\tilde{n}_1$ and $\tilde{n}_2$ (see Appendix A.2 and see footnote 3 in Sect. 6.1.3.2). This leads for perpendicular incidence on the absorber to

$$\tilde{r}_{\mathrm{ampl}} = \frac{\tilde{n}_1 - \tilde{n}_2}{\tilde{n}_1 + \tilde{n}_2}\,,$$

whence the reflection factor for the photon flux will be the square of this magnitude, viz.,

$$r_\gamma = \left(\tilde{r}_{\mathrm{ampl}}\right)^2 = \left(\frac{\tilde{n}_1 - \tilde{n}_2}{\tilde{n}_1 + \tilde{n}_2}\right)^2\,.$$

For a typical absorber like c-Si with real part of the refractive index in the near IR-range $n_2 \approx 3.5$, one gets a reflection factor of the photon flux for normal incident illumination of $r_\gamma = (2.5/4.5)^2 \approx 0.31$, implying that only 69 % of the light incident on the absorber would be coupled in, an entirely unacceptable situation. For this reason, anti-reflective (AR) films are generally used to coat the absorber. These exhibit a particular combination of spectral refractive indices and thicknesses which allows most solar photons with energies above the band gap to be wave-optically fed to the absorber medium.

In addition to AR coatings, specific surface contours are prepared, such as comparatively large scale (mm) 2D regular or random sized pyramids, or inverted pyramids, 1D grooves, etc. to 'scatter' that part of the solar light that is reflected

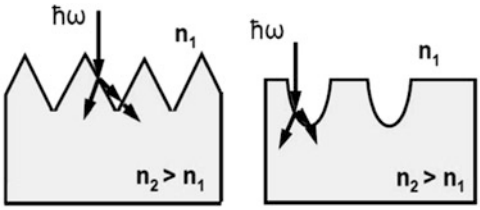

Fig. 6.6 Scattering of solar light at absorber entrance side with rough surfaces. 1D or 2D regular or inverted pyramids (*left*) and 1D or 2D grooves (*right*) increase absorption lengths and decrease reflection losses

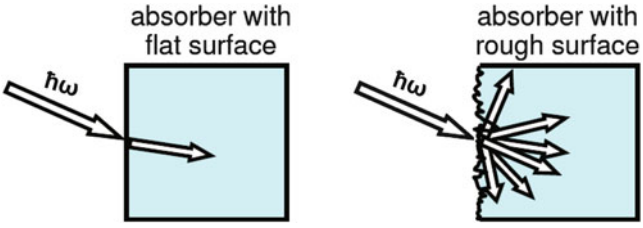

Fig. 6.7 Comparison of propagation of photons (ray picture) coupled into an absorber with ideally flat surface (*left*) and with optimum rough light entrance surface (*right*)

at first contact with the device back towards the surface again in order to provide another opportunity to be coupled in (see Fig. 6.6).

Another artificial increase in photon propagation length at the front and/or rear surface can be obtained by ideally randomized photon scattering into the solid angle of 2π, facilitated by small scale rough surface or interface contours. Due to the absorption of photons, the flux $\Gamma(x)$ and the total rate of photoexcited species $g(d)$, be they electron–hole pairs or excitons, only asymptote towards the maximum achievable values of initial flux Γ_0 and total possible accumulated generation rate g_0

$$\frac{\Gamma(x)}{\Gamma_0} \to 0\ , \quad \text{or } g(d) \to g_0\ ,$$

with a strong dependence on the absorption coefficient $\alpha(\omega)$, and on the length d of the path the photons travel in the absorber. The photon path length d is usually an unambiguous quantity, since we consider only one direction of light propagation in the absorbing medium. However, when front or rear surfaces of the absorber are strongly scattering, photon propagation becomes randomly oriented and the average path length increases, whereupon the accumulated generation rate $g(d)$ also rises (see Fig. 6.7).

From geometrical optics in conjunction with statistics, the upper limit for the increase in effective absorption lengths to be achieved by ideal scattering into the 2π-solid angle (Lambertian type of scattering) at the front as well as at the side amounts to a factor of $4n^2$ (see [10] and Appendix C). In Fig. 6.8, the

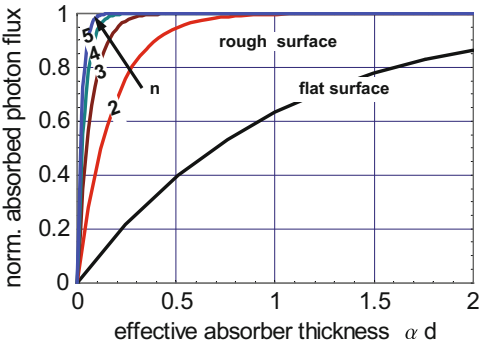

Fig. 6.8 Normalized absorbed photon flux versus absorption length in absorbers with flat and with ideally rough surface (optimum scattering). The increase in effective absorption length is governed by the absorber refractive index n

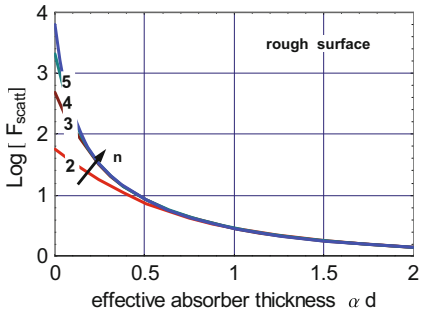

Fig. 6.9 Ratio of absorption of photons in matter with ideally scattering surfaces with $F_{\text{scatt}} = Log[exp(-n^2\alpha d)/exp(-\alpha d)]$ (Lambertian scattering) as compared with a flat surface plotted against absorber thickness for different refractive indices n

accumulated generation rate $g(d)$—equivalent to the absorbed photon flux—for maximum random scattering versus absorber thickness is sketched for different refractive indices $n = 2$–4. For comparison, the absorbed flux is displayed for perpendicular propagation through a flat surface without scattering.

The factor F_{scat} for the increase in total generation by scattering surfaces versus absorber thickness d as compared with a flat surface is shown in Fig. 6.9.

An even greater light-trapping effect has been proposed by combining randomized scattering surfaces and spectrally selective filters [11].

6.1.5 *Photonic Crystal Stop Gaps to Reduce Luminescence Emission*

A further so-called 'third generation' approach aims to reduce the emission of luminescence radiation which, in the Shockley–Queisser limit, balances the incoming and outgoing photon fluxes to establish a steady state, preventing the exit of photons in a particular range of wavelengths and emission angles by placing

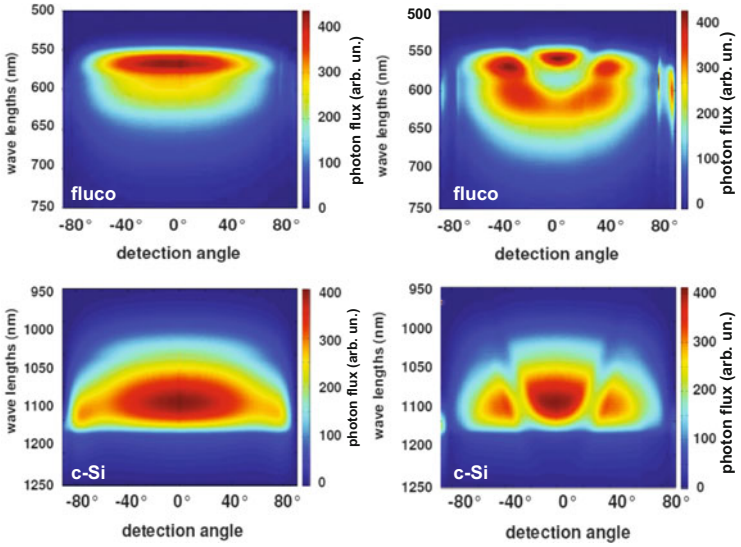

Fig. 6.10 Angle and wavelength dependent light fluxes from photoexcited absorbers. *Upper row*: Rhodamine 6G-doped fluorescence collector; *Lower row*: c-Si, both structures without (*left*) and with overcoating of a particularly designed photonic crystal (*right*) to block light emission through the escape cone

a photonic crystal on top.[5] By appropriately designed photonic crystals [12], the emission of luminescence photons from the excited absorber is suppressed. As a consequence, the photon field in the absorber is enhanced, which might lead to subsequent reabsorption of luminescence photons and thus to a higher photoexcited state of the absorber. Figure 6.10 exemplifies the effect of suppressing luminescence photons from a dye-doped fluorescence collector and from a c-Si absorber by means of suitably designed photonic crystals [13].

[5] A photonic crystal is the analog for photons of an 'electronic' crystal where the periodic arrangement of the ions with their electrostatic potentials determines the electronic band structure, i.e., the energy-wave vector relation $\epsilon(\mathbf{k})$, in matter in general leading to energy gaps between allowed energy bands (see Sect. 4.2). The allowed energy states present solutions to the Schrödinger equation for electrons.

By analogy, for photons whose propagation also obeys differential equations of second order in space and time, the Maxwell equations for $\mathbf{E}(\mathbf{x}, t)$, $\mathbf{H}(\mathbf{x}, t)$, a periodic arrangement of refractive indices have the solution with frequency/energy regimes in which light propagation is not allowed (in fact, the wave vectors become imaginary). These are called stop gaps. In three dimensions, the spatial arrangement of periodic refractive indices controls the energy and angular direction of these stop gaps.

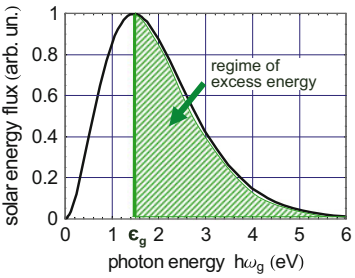

Fig. 6.11 Schematic spectral solar energy flux and cutoff energy ϵ_g to represent the portion of solar energy absorbed (*shaded area*) and converted subsequently into chemical energy of excited species such as electron–hole pairs. Note that the excess photon energy remains largely unused

6.2 Multispectral Conversion

An absorber with a band gap ϵ_g, such as the optical threshold in semiconductors or the HOMO–LUMO gap in molecular absorbers, can be excited only by a specific regime of solar photons which are continuously distributed across the entire energy scale $0 \leq \hbar\omega \leq \infty$. Photons with energies $\hbar\omega < \epsilon_g$ cannot be used, as they are not absorbed. Their companions with $\hbar\omega \geq \epsilon_g$ can in principle be absorbed in semiconductors, but their excess energy[6] $\Delta\epsilon_{exc} = \hbar\omega - \epsilon_g$ is mainly lost by rapid thermalization of the 'hot' carriers. As the probability for generation of more than one excited species (electron–hole pair or exciton) with one solar photon, even with equivalent high energy, is almost negligible in conventional bulk absorbers, a large fraction of solar photons essentially possess either too low or too high an energy to be exploited efficiently (see Fig. 6.11).

6.2.1 Traditional Spectrum Splitting

The subdivision of the solar spectrum into more than one regime and the subsequent conversion of the individual ranges of photon energies in selected absorbers with finely adjusted optical band gaps has been a common approach for several decades. The proposals for reducing the excess photon energies simultaneously decrease the fraction of photons with too low an energy, thus raising the total conversion efficiency. The concept of multispectral use of solar light, in specific setups with two or three different optical threshold energies (as sketched in Fig. 6.12), generally referred to as multispectral solar light conversion, or multicolour conversion, was already proposed in the late 1950s and early 1960s for solar thermal systems

[6]Here, we have neglected the kinetic energy of electrons and holes (each of them amounting to $(3/2kT)$.

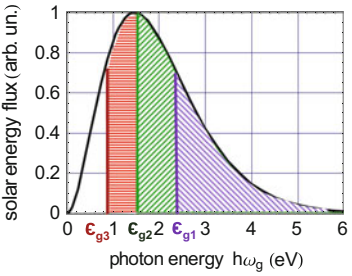

Fig. 6.12 Schematic spectral solar energy flux divided by 'spectrum splitting' into three regimes with appropriate cutoff energies ϵ_{g1}, ϵ_{g2},ϵ_{g3} to reduce losses of photon excess energies and obtain access to lower photon energies as well

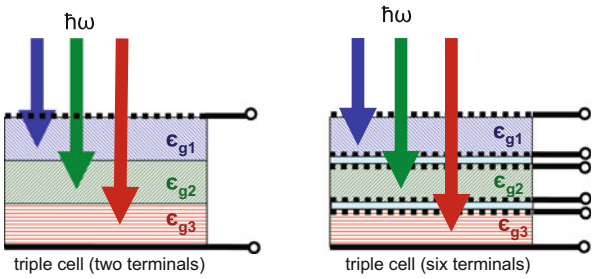

Fig. 6.13 Spectrum splitting by optical series connection of absorbers with different optical band-gap energies (band gaps). *Left*: Electrical series connection, called a two-terminal device with only front and rear contact. *Right*: Electrically separated optically series connected devices, e.g., 6-terminal approach with individual contacts for each cell (for power conditioning of cells in electric series or parallel connection each cell needs two independent leads)

[14, 15], and intensively discussed for photovoltaics in the late 1970s and early 1980s [16, 17]. When this approach was later applied to solar cells, as referred to tandem cells, triple cells, etc., it has been reintroduced in the last 20 years as one of the most promising options for the great breakthrough of photovoltaics.

The optical arrangement of more than one gap cell, e.g., three band gaps in series allows for the two versions of electrical design sketched in Fig. 6.13. The individual optical band gaps are to be optimized with respect to the number of thresholds (cells), the total light flux (concentration), and the spectral distribution, e.g., AM1, AM1.5, etc.[7]

Furthermore, the electronic design of such devices must also be considered, since the connection of the absorbers in optical series might be achieved by connecting electrically in series, which would require ideal current matching of each cell involved, or each cell could be addressed separately by individual contacts,

[7] AMi abbreviation of Air-Mass index designates the attenuation of the solar light flux when travelling through the Earth's atmosphere.

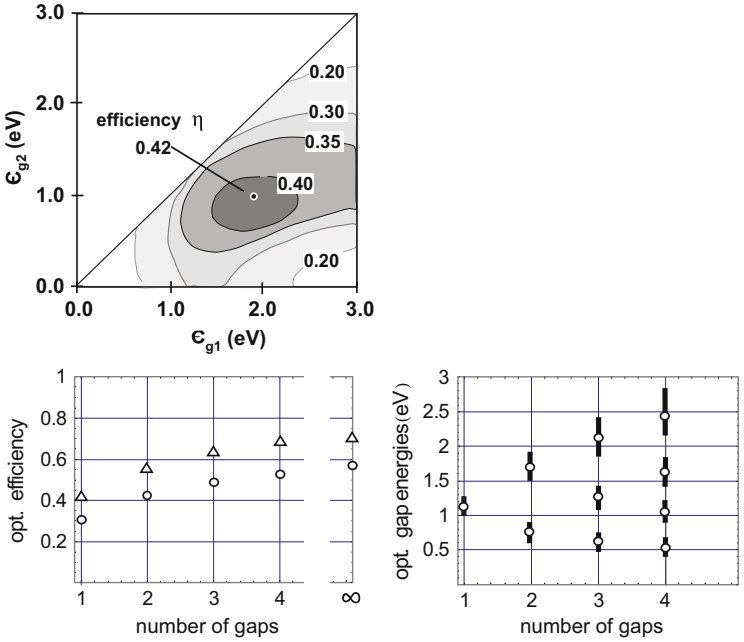

Fig. 6.14 Iso-efficiency lines of an ideal tandem system versus band gas of top (ϵ_{g1}) and bottom cell (ϵ_{g2})[18] (*upper*); theoretical maximum efficiencies of ideal multiband gap systems versus number of optical threshold energies for illumination with unconcentrated sunlight (*circles*) and for maximum concentrated sunlight (*triangles*) (*lower left*), optimum gap energies versus number of band gaps (*lower right*). *Grey bars* indicate the tolerance of gap values to keep variation in optimum efficiency $\Delta\eta \leq 0.01\eta_{\text{opt}}$ [19]

posing the technological challenge of transparent contacts and a substantially greater number of technical steps for preparation.

Figure 6.14 (upper part) displays iso-efficiency lines versus bottom- and top-cell band gaps ϵ_{g1} and ϵ_{g2} of ideal tandem devices for AM0 illumination and absorber temperature $T_0 = 300\,\text{K}$ [18]. The dependence of 300 K-efficiencies versus optimized band gaps and the correspondingly necessary number of optical thresholds is illustrated in Fig. 6.14 (lower part left) for unconcentrated as well as for maximum concentrated sunlight [19]. Figure 6.14 (lower part right) shows the respective optical band gaps [19].

Electrical series connection (two-terminal devices) of tandems, triples etc., requires an accurate adjustment of the generation rate in each of the subcells by tuning absorption coefficients, thicknesses, and collection efficiencies at maximum power output (mpp), since the current in each cell has to match exactly for optimum operation. Here, local, as well as temporal and seasonal variations of the spectral distribution of the solar light become a crucial issue for competition with single-threshold devices.

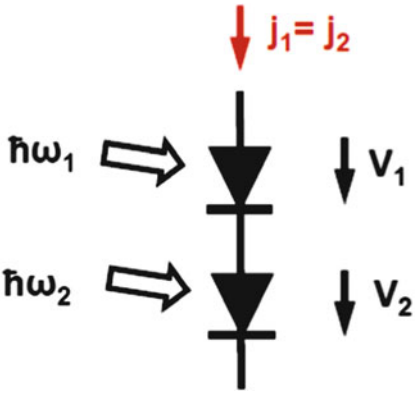

Fig. 6.15 Circuit comprising two illuminated ideal diodes connected in series and requiring current continuity (current matching)

In a simple analytical calculation, we may understand the sensitive dependence of the output power for departures from the ideal current match in tandem cells. We consider two cells in optical and electrical series connection, as sketched in Fig. 6.15 with individual j–V curves:

$$j_i = j_{0,i}\left(\exp\left(\frac{eV_i}{kT_i}\right) - 1\right) - j_{\text{phot},\,i}\ , \tag{6.9}$$

where the index i is either $i = 1$ or $i = 2$. For reasons of simplicity, we assume $T_1 = T_2 = T$. In addition, electrical series connection requires $j_1 = j_2 = j$. The corresponding voltages are

$$eV_i = kT \ln\left[1 + \frac{j_i}{j_{0,i}} - \frac{j_{\text{phot},\,i}}{j_{0,i}}\right]\ , \tag{6.10}$$

which in series connection with boundary condition $j_1 = j_2 = j$ sum to give

$$eV = e(V_1 + V_2) = kT\left(\ln\left[1 + \frac{j}{j_{0,1}} - \frac{j_{\text{phot},1}}{j_{0,1}}\right] + \ln\left[1 + \frac{j}{j_{0,2}} - \frac{j_{\text{phot},2}}{j_{0,2}}\right]\right)\ . \tag{6.11}$$

For decent photoexcitation, we neglect the '1' in the logarithm and arrive at

$$\begin{aligned} eV &= kT\left(\ln\left[\frac{j}{j_{0,1}} - \frac{j_{\text{phot},1}}{j_{0,1}}\right] + \ln\left[\frac{j}{j_{0,2}} - \frac{j_{\text{phot},2}}{j_{0,2}}\right]\right) \\ &= kT\left(\ln\left[\frac{1}{j_{0,1}}\left(j - j_{\text{phot},1}\right)\right] + \ln\left[\frac{1}{j_{0,2}}\left(j - j_{\text{phot},2}\right)\right]\right)\ , \end{aligned} \tag{6.12}$$

or equivalently,

$$eV = kT\left(\ln\left[j - j_{\text{phot},1}\right] + \ln\left[j - j_{\text{phot},2}\right] - \ln\left[j_{0,1}\right] - \ln\left[j_{0,2}\right]\right) \ . \tag{6.13}$$

For identical generation rates in cell 1 and cell 2, i.e., $j_{\text{phot},1} = j_{\text{phot},2} = j_{\text{phot}}$, we can write

$$\begin{aligned} eV &= kT\left(2\ln\left[j - j_{\text{phot}}\right] - \ln\left[j_{0,1}\right] - \ln\left[j_{0,2}\right]\right) \\ &= kT\left(2\ln\left[\tilde{j}\right] - \ln\left[j_{0,1}\right] - \ln\left[j_{0,2}\right]\right) \ , \end{aligned} \tag{6.14}$$

where $\tilde{j} = j - j_{\text{phot}}$. We compare identical generation rates in the two series connected cells with a departure from the symmetric excitation such as $j_{\text{phot},1} = j_{\text{phot}} - \Delta$ and $j_{\text{phot},2} = j_{\text{phot}} + \Delta$, or equivalently, $\left(\tilde{j} + \Delta\right)$ and $\left(\tilde{j} - \Delta\right)$, and finally arrive at the voltage V for identical generation rates versus the voltage $\tilde{V}$ for departure Δ from symmetric behavior:

$$\begin{aligned} eV &= kT\left(2\ln\left[\tilde{j}\right] - \ln\left[j_{0,1}\right] - \ln\left[j_{0,2}\right]\right) \\ &> kT\left(\ln\left[\tilde{j} + \Delta\right] + \ln\left[\tilde{j} - \Delta\right] - \ln\left[j_{0,1}\right] - \ln\left[j_{0,2}\right]\right) = e\tilde{V} \ , \end{aligned} \tag{6.15}$$

or briefly $V > \tilde{V}$, for any values of the current densities j, j_{phot}, $j_{0,1}$, and $j_{0,2}$ (see Fig. 6.16).

In most of these cases, the exchange of luminescence photons between the absorbers and their neighbors, which also couples their individual quasi-Fermi levels, has not been taken into account. Although it is an effect that does not substantially modify the overall tandem- or triple-cell efficiency, but from a principal point of view, it remains an instructive exercise (see Fig. 6.17) [18].

In molecular absorbers, the high-energy photons from the Sun are not absorbed due to the decrease in absorption coefficient for energies sufficiently above the optical threshold. Here the use of the full solar spectrum by the optical series connection of absorber species with different HOMO–LUMO thresholds is as beneficial as it seems to be obviously self-consistent.

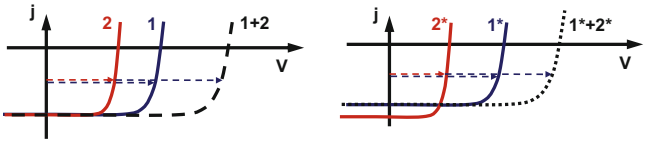

Fig. 6.16 Current-density–voltage curves of two illuminated series-connected ideal diodes with identical individual photocurrents (*left*) and with different photocurrents (*right*) that superimpose to a common set of output voltage and output current density

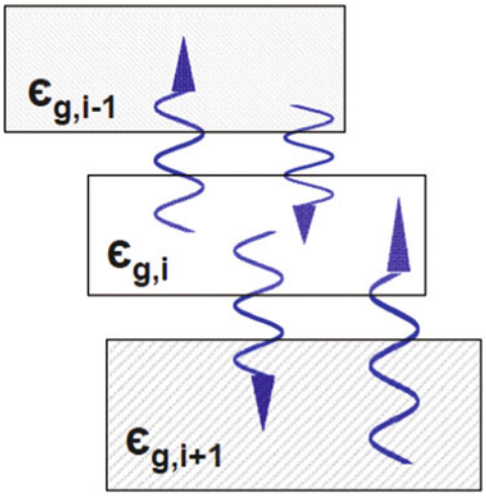

Fig. 6.17 Schematics of luminescence photon exchange and interconnected photoexcitation of optically series-connected triple devices; the mutual photon exchange strongly depending on the geometric constellation of the individual absorbers influence their particular photoexcited state

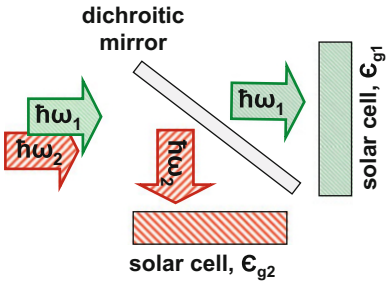

Fig. 6.18 Principle of spectrum splitting by a dichroic mirror guiding the separated spectral parts to absorbers with appropriate optical band gaps

6.2.2 Spectrum Splitting by Optical Components

In addition to the optical series connection of semiconductor absorbers, spectrum splitting can also be achieved by separating the relevant spectral regimes into different directions and angles. Although not particularly suitable for practical application, one conceptually simple arrangement uses dichroic mirrors and exposes different-band-gap cells to the corresponding part of the spectrum (see Fig. 6.18).

Another approach for spectrum splitting, technically much more relevant, is based on spectral dispersion of photons with different wavelengths in a hologram, with simultaneous light concentration of up to a factor of 100. These holograms contain a thin transparent film with a periodic lateral variation of refractive indices,

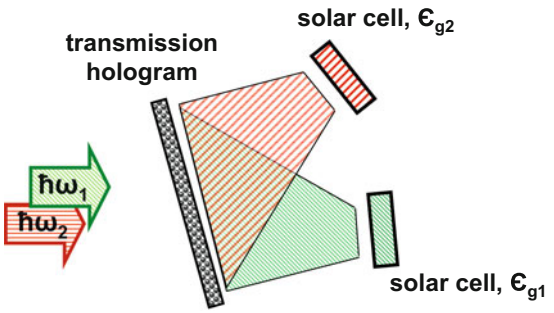

Fig. 6.19 Principle of spectrum splitting and simultaneous light concentration by a hologram guiding the separated spectral parts to solar cells with suitably adjusted optical band gaps

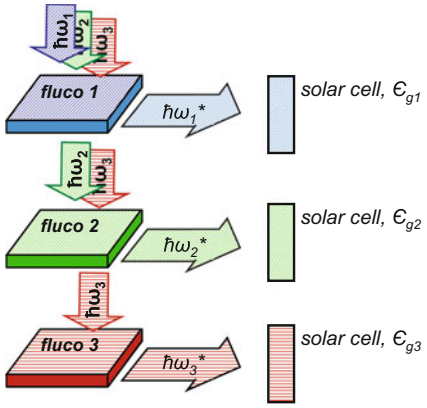

Fig. 6.20 Schematic arrangement of optically series-connected fluorescence collectors for spectral splitting (with Stokes shift of emission by excited dyes) and simultaneous solar light concentration [4]

e.g., spin coated on a glass substrate, and act either in transmission (see Fig. 6.19) or in reflection mode [20].

Since molecular dye absorbers exhibit considerable absorption only in a comparatively small wavelength range, a sequence of these can be arranged in optical series connection, which is of course nothing but a multispectral approach. In Fig. 6.20, this obviously favorable attempt is sketched for a sequence of fluorescence collectors [4].

6.2.3 *Subdivision of a Homogeneous Single Gap Absorber*

An informative gedanken experiment consists of the subdivision of an absorber with total thickness d into several layers, for example, n layers with individual thicknesses $(d_{i+1} - d_i)$ such that the generation of electron–hole pairs in each of the layers is identical, i.e.,

$$g_i = \frac{g_{\text{tot}}}{n} = \frac{1}{n}\left[1 - \exp(-\alpha d)\right] = \int_{d_i}^{d_{i+1}} \alpha \exp(-\alpha x)\mathrm{d}x \ .$$

The ideal short-circuit current density in each of the subcells is

$$j_i \sim g_i = \frac{g_{\mathrm{tot}}}{n} ,$$

whereas the total voltage is the sum of the individual voltages governed by the excess carrier concentrations:

$$V_{\mathrm{oc},i} = kT \ln \left[\frac{n_i}{n_0} \right] .$$

The subcell excess densities n_i originate from identical generation rates g_i and identical lifetimes $\tau_i = \tau$, but with increasing depth, the corresponding thickness across which the excess carriers spread out (e.g., by diffusion) rises due to the exponential decay of the residual photon flux. Figure 6.21 exemplifies depth profiles for the subdivision into two absorber layers, while the ratio $(V_{\mathrm{oc},1} + V_{\mathrm{oc},2})/V_{\mathrm{oc},d}$ of the voltage contribution from the two cells to the open-circuit voltage of one thick absorber is displayed in Fig. 6.22. Evidently, the reduction of the short-circuit current density by a factor of $n = 2$ is overcompensated by enhancement of the total voltage, since the excess carriers in the subdivided absorber do not spread out as much as in the thick absorber. In thermodynamic language, in thin absorbers there is less mixing of intensive variables, and hence higher output.

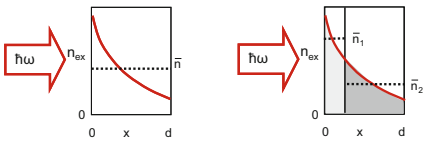

Fig. 6.21 Depth profiles of photogenerated excess carriers and average excess densities in a single absorber (*left*) and for comparison in an absorber subdivided into two local regimes with identical total excess carrier number and two different average excess densities (*right*)

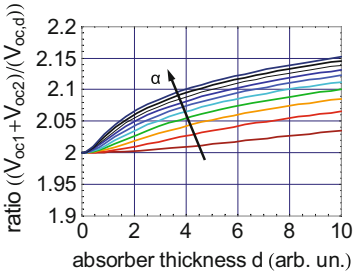

Fig. 6.22 Gain in the open-circuit voltage $(V_{\mathrm{oc},1} + V_{\mathrm{oc},2})/V_{\mathrm{oc},d}$ of an absorber subdivided into $d_1 + d_2 = d$ in such a way that the total generation in the two parts is identical as compared with a non-subdivided absorber of thickness d. Note that the possible short-circuit current density of the subdivided structure amounts to only 0.5 of that of the absorber with thickness d

6.3 Photon Conversion

6.3.1 Photon Up-Conversion

In photon-up conversion, the electronic transition from an initial state with energy $\epsilon_i = \epsilon_0$ to a final state at $\epsilon_f = \epsilon_2^*$ might be initiated by two photons $\hbar\omega_1$ and $\hbar\omega_2$, each of lower energy than the band gap $\hbar\omega_{1,2} < \epsilon_g$. The transitions are performed via intermediate levels, firstly by excitation with $\hbar\omega_1$ from ϵ_0 to ϵ_1 and subsequent relaxation $\epsilon_1 \rightarrow \epsilon_1^*$ [singlet to triplet state transfer to prevent a fast back reaction $(\epsilon_1 \rightarrow \epsilon_0)$] and secondly with $\hbar\omega_2$ from ϵ_1^* to ϵ_2 and again with relaxation to ϵ_2^*. The resulting radiative transition with

$$\hbar\omega_{up} = \left(\hbar\omega_1 - (\epsilon_1 - \epsilon_1^*)\right) + \left(\hbar\omega_2 - (\epsilon_2 - \epsilon_2^*)\right) = (\epsilon_2^* - \epsilon_0)$$

serves for the excitation when coupled in to an absorber with optical threshold $\epsilon_g \leq \hbar\omega_{up}$. This procedure is shown schematically in Fig. 6.23 with a mirror at the rear side of the up-converter to reflect photons towards the absorber [21].

Currently analyzed materials for up-conversion are rare-earth-doped ceramics or glasses, such as Er-doped materials, whose fluorescence with low photon energy excitation fits the band gap of crystalline silicon (see Fig. 6.24).

With the up-converter above, the schematic increase in external quantum efficiency of c-Si solar cells shows a rise in the below-gap regime (Fig. 6.25) [21]. However, since the up-conversion depends non-linearly on the light flux, this rise in external quantum efficiency for non-concentrated sunlight remains of the order of 10^{-4}.

A substantial increase in up-conversion contribution to quantum efficiency may be expected by an artificial local increase of the photon flux via plasmonic effects through small (few nm diameter) metallic nanoparticles between the absorber rear surface and the front of the up-converter (see Sect. 6.6).

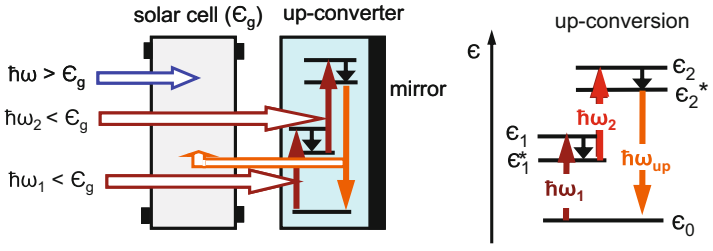

Fig. 6.23 Schematics of up-conversion in a converter at the rear of a solar cell by using low-energy photons with $\hbar\omega_1 < \epsilon_g$, $\hbar\omega_2 < \epsilon_g$ which are not absorbed in the solar cell (schematic energy diagram *right*); the upconverted photon $[\hbar\omega_{up} = \hbar\omega_1 + \hbar\omega_2 - (\epsilon_1 - \epsilon_1^*) - (\epsilon_2 - \epsilon_2^*)]$ is fed to the solar cell (*left*) where it can be absorbed because $\hbar\omega_{up} \geq \epsilon_g$

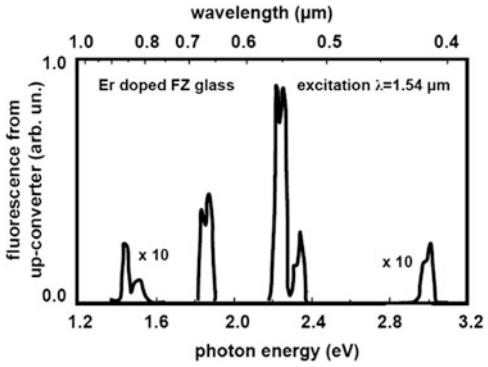

Fig. 6.24 Example of spectral emission by a photon up-converter (Er-doped FZ glass) after excitation with IR photons with $\lambda = 1.54\,\mu\text{m}$ [21]

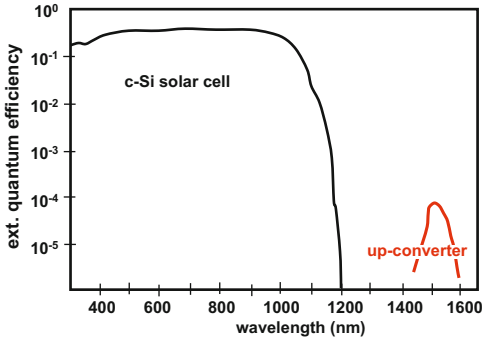

Fig. 6.25 Exemplary external quantum efficiency of a solar cell with and without photon up-conversion versus wavelength λ [21]

6.3.2 Photon Down-Conversion

Photon down-conversion does not strictly belong to the approaches for surpassing the Shockley–Queisser (SQ) limit, since in the SQ approach each of the photons with $\hbar\omega \geq \epsilon_g$ is assumed to be absorbed, contributing with probability unity to the external quantum yield.

Since high-energy photons in semiconductor absorbers are trapped close to the light-entrance surface as a consequence of the comparatively high absorption coefficient and basically suffer from front-surface recombination, an appropriate shift in their energy and corresponding absorption deeper in the bulk is beneficial for the lifetime and extraction of photoexcited carriers. The proposed down-conversion of photons is commonly performed by a suitable dye, optimally matching the band gap of the absorber. As a consequence of the Stokes shift between absorption

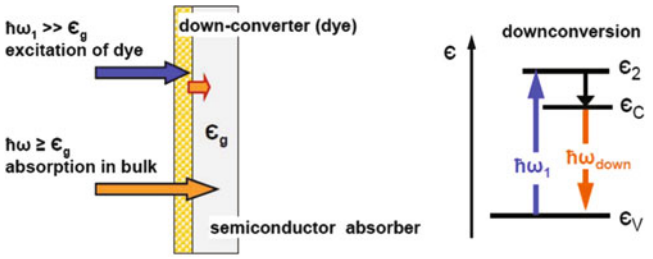

Fig. 6.26 Design principle of a of photon down-converter in conjunction with a solar cell. In order to avoid the generation of electron–hole pairs by high energy photons in the vicinity of the absorber front surface, where rates of surface recombination are rather large, the high-energy photons are converted (Stokes-shifted) to lower energies and consequently absorbed deeper in the bulk of the semiconductor where they suffer less from surface recombination (*left*); schematic energy diagram for down-conversion (*right*)

and fluorescence emission, the red shift is achieved by the 'natural' behavior of molecular structures (see the schematics in Fig. 6.26).

This technological effort has so far been applied successfully to enhance the spectral quantum yield in thin-film CdTe solar cells in the wavelength regime $450\,\text{nm} \leq \lambda \leq 550\,\text{nm}$ by prevention of carrier generation and equivalent recombination in the highly doped, comparatively thick CdS window layer [22].

For the general application of photon down-converters, the balance between loss by front-surface recombination without down-converter versus fluorescence quantum yield multiplied by the solid angle for fluorescence photons towards the absorber seems to have been not yet appropriately met. In addition, efficient down-converters are not available for many of the desired spectral regimes.

6.4 Intermediate-Band-Gap Cells

A concept very close to multispectral converters is employed by the intermediate-band-gap cell [23], which comprises a relatively large-band-gap semiconductor absorber with a comparatively narrow intermediate band (IMB) in the gap (Fig. 6.27). This resembles conceptually the two-terminal-triple cell sketched in Fig. 6.13 (left).

The intermediate band must not be confused with a defect band arising from localized states, since its electronic wave functions in the ideal case are infinitely extended, and the Fermi level is adjusted somewhere in the center of the intermediate band. Illumination of this ideal three-band system provides for generation and recombination rates in each of the three bands which are exclusively radiative. The charge transport for transferring the photoexcited state to the boundaries of the absorber takes place in the conduction and in the valence band, whereas the intermediate band serves only for the storage of photoexcited charges. We recognize

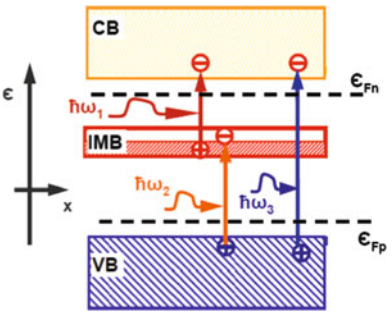

Fig. 6.27 Band diagram of an intermediate band gap absorber with transitions for excitation within photon energy regimes ($\hbar\omega_1$, $\hbar\omega_2$, $\hbar\omega_3 = \hbar\omega_1 + \hbar\omega_2$). Reverse rates accounting for the radiative back-reactions to the respective ground states are not indicated [23]

that the excitation from IMB to CB is definitely not a two-photon process of the kind that occurs in an up-converter, but rather is a consecutive absorption of photons with appropriate energy to lift an electron to CB. In this sense the intermediate-band system is an extension of the two-band system, and its performance has to be treated analogously with the Shockley–Queisser procedure.

In order to harvest the solar light fed to three regimes with photon energies $\hbar\omega_1 < \hbar\omega_2 < \hbar\omega_3$, only two of the energy levels can be freely selected, say $\hbar\omega_1$ and $\hbar\omega_2$ with $\hbar\omega_3 = (\hbar\omega_1 + \hbar\omega_2)$. This approach resembles for the derivation of the theoretical efficiency, even quantitatively, a triple cell with only two independently adjustable band gap energies (see Fig. 6.27); thus its theoretical efficiency is, of course, higher than that of an ideal tandem cell. In steady-state, the net rates of transitions from VB to IMB and from IMB to CB (including the reverse rates via radiative transitions to the respective ground states) have to ideally match:

$$r_{\mathrm{VB}\rightarrow\mathrm{IMB,net}} = r_{\mathrm{IMB}\rightarrow\mathrm{CB,net}} \ ,$$

in order to satisfy current continuity, avoiding depletion or oversaturation of the intermediate band states. The asymmetry of the configuration needed to separate charges of different polarity (electrons from holes) has—by the strategy of the inventors of the IMB-cell—to be achieved with a *pin* structure, in which the intrinsic layer consists of the IMB absorber.

The open-circuit voltage of such a device is governed by the regular band gap, means, the separation of CB–VB states, where the thermal equilibrium carrier densities n_0 in the conduction band and p_0 in the valence band are enhanced by illumination. Equivalently, with a single barrier, the open-circuit voltage is

$$e \cdot V_{\mathrm{oc}} \leq kT \ln\left[\frac{np}{n_0 p_0}\right] \ ,$$

but the excess carrier densities which enter logarithmically into V_{oc} and linearly into j_{sc} are substantially enhanced by absorption via the intermediate gap. This gain raises V_{oc}, j_{sc}, and thus the efficiency as well, above the values for single gap structures.

Figure 6.28 shows the theoretical efficiencies of cells with intermediate band absorbers [24], operated at 300 K and under maximum solar light concentration

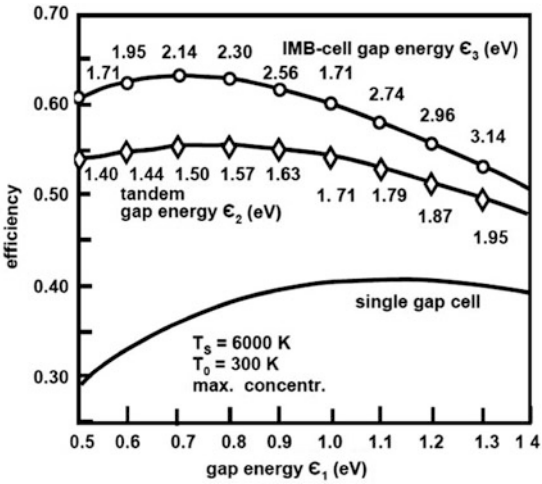

Fig. 6.28 Theoretical efficiencies of ideal solar cells with intermediate-band-gap and tandem-gap absorbers versus energy gap ϵ_1 of single-band gap absorber. In each of the options, ϵ_1 denotes the optical threshold of the low gap absorber. In the IMB cell the energy difference $(\epsilon_3 - \epsilon_1)$ does not equal the upper gap energy ϵ_2 of the tandem cell [24]

versus the low gap ϵ_1 in comparison with a single gap and an optimum gap tailored tandem. Respective values for optimum gaps, viz., ϵ_2 for tandems and ϵ_3 for the CB–VB separation in intermediate-gap cells, are indicated in the figure.

6.5 Use of Photon Excess Energy

A substantial portion of the energy of solar photons not used in conventional single-gap cells is their excess above the band gap $(\hbar\omega - \epsilon_g)$. Even in the early days of photovoltaic research, this waste of energy initiated concepts for possible better use of this part. For example, in the late 1970s, proposals were made to exploit the so-called hot electrons (by Fan et al. [41]). In the course of the last decade, these ideas have been rediscovered and repeatedly proposed under the heading of third-generation photovoltaics.

6.5.1 Hot Carriers

The excess energy of electrons and holes above the band gap immediately after photogeneration, i.e., before thermalization by interaction with phonons, is the largest amount of energy wasted in a conventional electronic band system.[8]

[8]Recall that the entire energy of free electrons and holes after relaxation is composed of the band separation plus average kinetic energy $(3/2)kT$ of both type of carriers

$$\epsilon = \epsilon_g + 3kT \ ,$$

where the temperature is that of the lattice $T = T_{\text{phon}}$.

The extraction of these 'hot-carrier' energies would substantially increase the yield of solar light conversion, but it turns out to be an extremely challenging task, since hot carrier relaxation by interaction with phonons in three-dimensional structures occurs on timescales shorter than a picosecond, that is, 10^{-12}–10^{-13} s. (Relaxation of electrons by interactions with other electrons is even faster.)

To slow down the phonon interaction, dimensionally reduced structures such as particular two-dimensional II–VI type absorbers, or small clusters named quantum dots (QDs), were first proposed in the early 1980s.[9] Firstly, geometrically reduced structures allow the extraction lengths to be small enough to let carriers escape before phonon interaction becomes significant and, secondly, energy and wave-vector relaxation times can be longer compared to the 3D extended states, according to some evidence [25]. Furthermore, the 'cold' carriers in metal leads connecting the absorber must not interact with the hot electrons, although the wave function of the hot electron must overlap with those of the metal electrons to allow for a transition to the contacts.

Currently there are two concepts for exploiting the energy of hot electrons. On the one hand, use of the high kinetic energy $\epsilon = \epsilon(k)$ would contribute to higher open-circuit voltages, provided these electrons can leave the absorber at an appropriate energy level (see Fig. 6.29). These exits would act like a higher-band-gap absorber that allows for a larger splitting of quasi-Fermi levels (see Sects. 4.2.3 and 5.1.4). On the other hand, the energy of hot carriers might serve to generate more than one electron–hole pair per absorbed photon by carrier multiplication, also termed

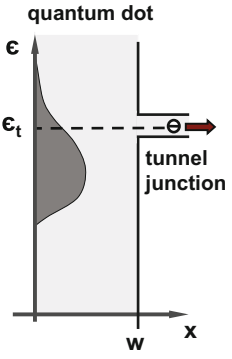

Fig. 6.29 Schematic outlet for hot electrons from an absorber through an energy selective tunnel junction. Here, cooling of electrons/holes by electron–phonon interactions, is assumed to be strongly attenuated or even completely switched off

[9]The reduction of the dimensions in condensed matter systems leads to discrete energy levels for electrons and holes, separated on the average, by a typical 'level spacing' $\Delta\epsilon$. As a rule of thumb $\Delta\epsilon \approx \chi/N$ where N is the number of respective electrons (e.g., in the valence band) and χ the energetic width of the according band. For sufficient energy separation of these levels compared with longitudinal optical phonon energies $\Delta\epsilon > \hbar\omega_{\text{phon, LO}}$ the cooling of 'hot electrons' requires the generation of more than one phonon (multi-phonon emission), which is less likely compared to one-phonon emission. Thus the transfer of electron energies to the lattice is reduced and might increase the relaxation time by more than one order of magnitude. This effect is called the phonon bottleneck.

impact ionization. The increase mainly contributes to a higher photocurrent density, reflected in larger short-circuit currents of the solar cells, but in addition contributes to a slight increase in open-circuit voltage through the logarithmic dependence of V_{oc} on excess carrier density, $eV_{\mathrm{oc}} \approx kT \ln\left[\frac{np}{n_0 p_0}\right] = kT \ln\left[\frac{np}{n_i^2}\right]$. The proposals for appropriate 'exits' for these hot carriers include tunnel junctions and thermoelectric barriers. However, the problem of aligning those exits, in particular in each of the relevant direction in k-space, seems hard to realize[10] [40, 42].

The second option, the generation of more than one excited species (electron–hole pairs, excitons) per absorbed photon (likewise termed impact ionization) was experimentally detected as early as the late 1950s, but also in the mid-1970s in Ge and Si [26, 27], when applying blue light (photon energies $\hbar\omega > 3\,\mathrm{eV}$), before being rediscovered in the 1990s [28, 29]. In indirect semiconductors like Ge and Si, the comparatively large excess photon energy above the (indirect) band gap needed for this impact ionization to occur is strongly governed by the necessity to involve phonons for wave-vector conservation.

A hot electron transfers its excess energy $\Delta(\hbar\omega) \approx (1-3)\epsilon_{\mathrm{g}}$ to a VB electron in a bonding state to excite the latter to the conduction band. It should be noted that the main portion of the photon energy exceeding the band gap goes to the electron. This is because of the stronger band curvature in the conduction band compared to that of the valence band, which determines the hole effective mass m^* by the second derivative

$$\frac{\partial^2 \epsilon(\mathbf{k})}{\partial k^2} \sim \frac{1}{m_{\mathrm{n}}^*} .$$

In a detailed analysis [30], the energy redistribution of solar-light-generated hot electron–hole pairs has been formulated neglecting the electron–phonon interaction. The rates of electron–electron scattering for establishing the energy redistribution are much higher than the rates of radiative transitions (recombination), which are negligible for the steady-state energy distribution within a band. Moreover, the rates of carrier extraction from the system (current density) are much lower still, and thus their contribution to establishing the energy distribution is marginal and can be omitted. The balance of the fluxes light-in ($\Gamma_{\gamma,in}$) and light-out ($\Gamma_{\gamma,out}$) together with the particular chemical potential only serves to determine the output current density.

The results in terms of system efficiency of this concept are shown schematically in Fig. 6.30 versus optical band gap for unconcentrated sunlight (AM0 illumination) and for maximum light concentration (47,000 × AM0). As a nice coincidence with results in previous chapters, for zero-band gap absorber (ideal Planck black body)

[10] In order to collect hot electrons in each of the directions in the **k**-space the respective exits would have to be attached to each CB minimum of the Brillouin zone [in Si exist six CB minima (ellipsoidal pockets with long axes directed along the < 100 > direction) or eight CB minima in Ge (half ellipsoids with long axes along < 111 >)].

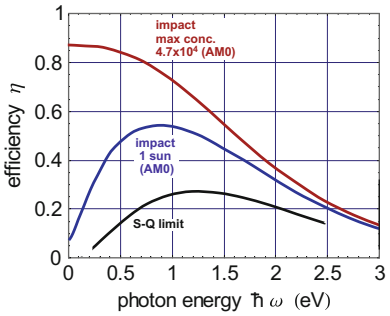

Fig. 6.30 Efficiencies of ideal photovoltaic converters with impact ionization/charge generation by 'hot photons' versus optical band gap under AM0 illumination and under maximum concentrated sunlight (47,000 × AM0) compared with the efficiency of a single gap absorber in the radiative limit (Shockley-Queisser limit) [30]

and maximum sunlight concentration, we get the well known number for maximum sunlight conversion efficiency $\eta \approx 0.86$.

An efficient method for the generation of multiple excited species, in particular of excitons (bi-excitons[11]) by absorption of a single photon has been proposed to occur preferentially in nanocrystals. This multiple exciton generation (MEG) has attracted a considerable amount of interest, particularly in quantum dots.[12] MEG has been proven experimentally to occur effectively in PbSe quantum dots, see for example [31–33].

Figure 6.31 shows the experimental results for multiple carrier generation in terms of quantum efficiency per absorbed photon in PbSe QDs as a function of photon energy. The dotted lines have been estimated on the basis of the balance for absorbed photon energies and the creation of electron–hole pairs (EHPs):

$$\Delta\epsilon = \epsilon_{\text{loss}} = \left(\hbar\omega - \epsilon_{\text{g}}\right) - (m-1)\,\epsilon_{\text{g}} = \hbar\omega - m\epsilon_{\text{g}}\ ,$$

where $\Delta\epsilon$ is the energy loss for absorption of one photon. Due to the requirement of integer numbers m in the ideal case of unit probability for multigeneration this approach leads to a staircase behavior of the quantum efficiency versus photon energy $\hbar\omega$.

From experimental data [32, 33], instead of a staircase behavior of the quantum yield, above a particular threshold a linear increase versus photon energy has been found. This has been fitted by the dashed lines in Fig. 6.31 with probability

[11] An electron-hole-pair coupled by Coulomb interaction has to be regarded as single quasi-particle (exciton); two such pairs (a bi-exciton) with sufficient spatial overlap of their wave functions behave, like a 'molecule' composed of two quasi-particles.

[12] A quantum dot (QD) results from the reduction of the geometrical size of matter in three dimension with the effect of sufficient separation of energy levels (see footnote 5 in Sect. 6.5.1).

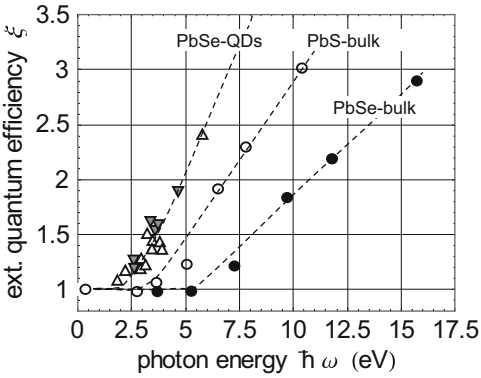

Fig. 6.31 External quantum efficiencies for multiple electron–hole pair generation (EHPM) in PbSe quantum dots in comparison to PbSe and PbS bulk absorbers versus photon energy [33]

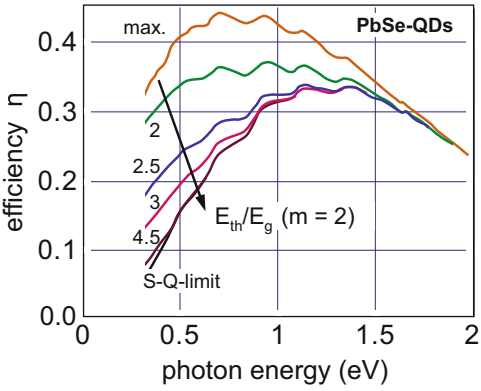

Fig. 6.32 Efficiencies of solar light conversion in PbSe quantum dots, including multiple electron–hole pair generation. EHPM effects with different ratios $m = \epsilon_{\text{thresh}}/\epsilon_{\text{g}} = 2, \ldots, 4.5$ (after [33]). The Shockley–Queisser limit and theoretical maximum EHPM (energetically max. number of EHMP) lines are shown for comparison

$\eta_{\text{EHPM,PbSe,QD}} = 0.6$ for electron–hole pair multiplication (EHPM) in the PbSe QDs, whereas in bulk absorbers the efficiency turned out to be substantially lower ($\eta_{\text{EHPM,PbSe}} = 0.31$, $\eta_{\text{EHPM,PbS}} = 0.45$).

The introduction of these EHPM quantum efficiencies into the radiative limit approach yields the efficiency of solar light conversion versus photon energy of the optical gap (threshold energy of the QDs), shown in Fig. 6.32 for illumination with an AM1.5 solar spectrum.[13]

Theoretically, this approach for 'hot electron-hole' energy use has been supported by investigating the probability for impact-like multiplication processes in nanocrystals of different sizes and material composition via band structure calculations and the behavior of Coulomb-coupled exciton states (bi-exciton states). In essence, out of numerous II–V, II–IV, and group IV element semiconductors, the most promising candidates for direct carrier multiplication (DCM) are PbSe, CdSe, GaAs, InP, and c-Si [34].

[13]Since AM1.5 spectra contain scattering and absorption of photons in the terrestrial atmosphere, e.g., by water vapor, ripples occur in the solar light flux as well as in the spectral performance of converters.

6.6 Plasmonic Effects for Increase in Local Photon Density

The exposure of metals to electromagnetic waves may lead to a collective excitation of the conduction-electron ensemble in a narrow frequency regime (plasmons). This collective excitation is commonly formulated in the independent-particle picture as oscillatory motion of 'free' (non-bound) electrons:

$$m^* \frac{\partial^2 x}{\partial t^2} + m^* \frac{1}{\tau_\mathrm{m}} \frac{\partial x}{\partial t} = E^0_\mathrm{loc} \exp(\mathrm{i}\omega_\mathrm{ext} t) \ ,$$

with effective mass m^*, momentum relaxation time in the band τ_m, and amplitude and frequency of the local electric field E^0_loc and ω_ext, respectively. The transition from the average local displacement $\mathbf{x}(t, \omega_\mathrm{ext})$ due to the dielectric susceptibility $\varepsilon(\omega_\mathrm{ext})$ via the electric dipole moment $e \cdot \mathbf{x}(t, \omega_\mathrm{ext})$ and polarization $\mathbf{P} = n_v e \cdot \mathbf{x}(t, \omega_\mathrm{ext})$, where n_v is the volume density of polarizable sites (dipoles),[14] is given by [40]

$$\begin{aligned} \varepsilon(\omega_\mathrm{ext}) &= 1 + \chi_\mathrm{el,\,bound} + \chi_\mathrm{el,\,free} = \varepsilon_\mathrm{el,\,bound} + \chi_\mathrm{el,\,free} \\ &= \varepsilon_\mathrm{el,\,bound} \left[1 - \frac{n_\mathrm{v,\,free} e^2}{\varepsilon_0 \varepsilon_\mathrm{el,\,bound} m^* \omega_\mathrm{ext} \left(\omega_\mathrm{ext} - \mathrm{i}/\tau_\mathrm{m} \right)} \right] . \end{aligned} \tag{6.16}$$

For metals in the visible wavelength range $\omega_\mathrm{ext} \gg 1/\tau_\mathrm{m}$ with the free electron density $n_\mathrm{v,free}$, this reduces to

$$\varepsilon\left(\omega_\mathrm{ext}\right) \approx \varepsilon_\mathrm{el,\,bound} \left(1 - \frac{n_\mathrm{v,\,free} e^2}{\varepsilon_0 \varepsilon_\mathrm{el,\,bound} m^* \omega_\mathrm{ext}^2} \right) = \varepsilon_\mathrm{el,\,bound} \left[1 - \left(\frac{\omega_\mathrm{plasma}}{\omega_\mathrm{ext}} \right)^2 \right] , \tag{6.17}$$

with the abbreviation

$$\omega_\mathrm{plasma} = \sqrt{\frac{n_\mathrm{v,\,free} e^2}{\varepsilon_0 \varepsilon_\mathrm{el,\,bound} m^*}} \ . \tag{6.18}$$

6.6.1 Plasmons in Small Metal Clusters

For dimensionally reduced metals such as clusters of a length scale of few nanometers (nanoparticles), the plasma resonance frequency of extended bulk metals can be

[14] We remember that polarizable sites may be introduced generally by bound and by free electrons al well as by ions; the polarization effect to be described also in terms of the appropriate susceptibility tensor as $\mathbf{P} = \varepsilon_0 \overline{\chi}$.

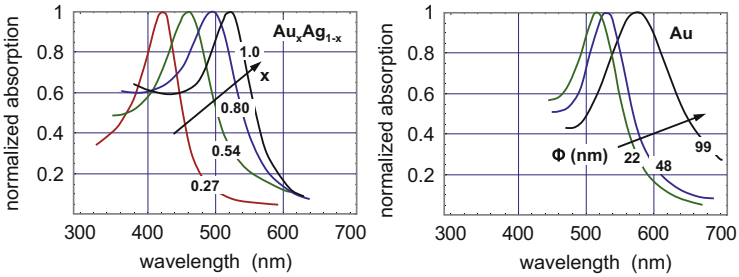

Fig. 6.33 Spectral absorbances (normalized to unity) of 20 nm diameter Au_xAg_{1-x} nanoparticles with different composition x (*left*) and Au nanoparticles with different diameters ø (*right*) [36, 37]

substantially modified and even tailored by the shape of the clusters, e.g., spherical or elongated. In the presence of electromagnetic waves, the nanoparticles act as antennas, for reception and emission of electromagnetic radiation [35]. As an example, absorption by Au nanoparticles of different sizes and with different Ag admixtures, both factors influencing the plasmon resonance energy significantly, is plotted in Fig. 6.33 [36, 37] .

The emission by antennas contains various contributions depending on the distance $|\mathbf{r}|$ at which, in the far field, the portion of electric field $|\mathbf{E}| \sim 1/|\mathbf{r}|$, exceeds each of the $|\mathbf{E}|$- and $|\mathbf{H}|$ components depending on higher power on $|\mathbf{r}|$. However, in the near field, the so-called evanescent (non-propagating) modes with $|\mathbf{E}| \sim 1/|\mathbf{r}|^n$, $n > 1$, emerge strongly. As a consequence, in the near field these modes in the vicinity of the resonance frequency provide for strong enhancement of the electric field strength, and hence also its square, which we know to be equivalent to the 'evanescent' photon density $|\mathbf{E}|^2|$.

6.6.2 Local Increase in Photon Density

The local enhancement in photon density of the incoming flux by plasmonic effects [38], even if it occurs as evanescent modes, can be successfully used to initiate nonlinear effects in matter such as up-conversion of two long-wavelength photons into one of shorter wavelength.

The contact of nanoparticles with a corresponding dielectric or semiconductor absorber (with optical threshold ϵ_{thresh} substantially above the resonance energy), in which the non-linear excitation, e.g., by $2\hbar\omega_{\text{plasma}}$ to ϵ_{thresh}, is desired (see Fig. 6.34), will enhance the high evanescent field. This is a consequence of the conservation of the normal component of the dielectric displacement $\mathbf{D}_{\text{n}} = \varepsilon_0\varepsilon(\omega)\mathbf{E}_{\text{n}}$ at the interface between two different phases.

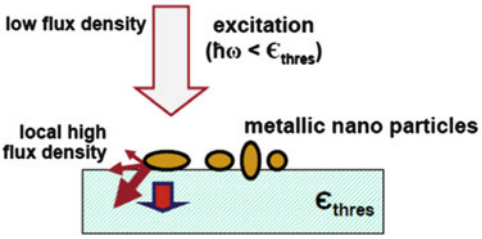

Fig. 6.34 Metallic nanoparticles located at an absorber surface to increase the local electric field strength (evanescent field) in the absorber for the initiation of nonlinear charge-generation effects

The enhancement of the photon flux in terms of local redistribution of the electric field, additionally supported by the geometrical shape of the nanoparticle, such as elongated ones, is not unlimited, of course. As absorption and emission in matter are generally coupled, the same limits exist like those which hold for the concentration of light by optical methods and for the Stokes-shifted photon fluxes in dye absorbers, like in fluorescent collectors.

6.7 Thermophotovoltaic Energy Conversion

Thermophotovoltaics can be conceptually linked to an ideal solar light absorber and an ideal conversion engine, proposed in the 1950s and 1960s at conferences, workshops, and in unpublished lectures (P. Aigrain, C.D. White, and B.D. Wedlock and reviewed later [39]). Concentrated sunlight is fed into an absorber which heats up to a temperature T_{ab} depending on the light entrance flux, the geometrical design of the absorber, the entrance aperture, and so on. The absorber emits thermal equilibrium radiation according to its temperature and emissivity, and this is fed to a solar cell through a (reflective) band filter allowing transmission only of photons with appropriate energy with respect to the band gap of the cell. So only photons convertible in the solar cell with comparatively high yield are extracted from the absorber, while others are reflected back to the radiation source by the filter (see schematics in Fig. 6.35).

Despite the very high theoretical efficiency of this approach in reality, heat losses by radiation, convection, and conduction in the absorber at the required high temperature lower the efficiency of the few existing demonstration systems to $\eta \approx 0.3$. Moreover, problems developing suitable materials and the comparatively high cost of the equipment requiring vacuum technology, have prevented so far every attempt of commercialization. For details, see the review by Coutts [39].

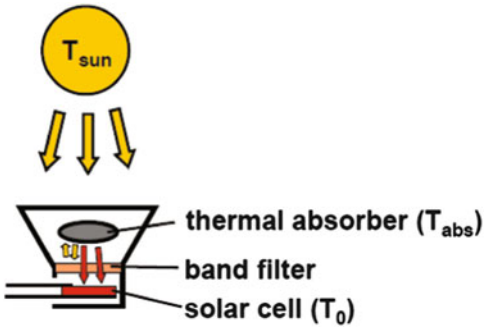

Fig. 6.35 Configuration of a thermophotovoltaic device: concentrated sunlight (from an imaging or non-imaging concentrating element) heats a thermal absorber of which the thermal equilibrium radiation is fed through a narrow (reflective) band gap filter ϵ_{filter} to a solar cell with appropriate band gap $\epsilon_g = \epsilon_{\text{filter}}$. Absorber photons with energies outside the filter transmission are 'given back' to the thermal absorber and only the energy of those photons passing the filter has to be replaced by the solar light. Thus the solar cell only sees spectrally selected photons, in order to minimize the excess photon energies as well as those photons with energies below the band gap

References

1. W. Shockley, H.-J. Queisser, J. Appl. Phys. **32**, 510 (1961)
2. W.T. Welford, R. Winston, *The Optics of Non-imaging Concentrators* (Academic, New York, 1978)
3. W.H. Weber, J. Lambe, Appl. Opt. **15**, 2299 (1976)
4. A. Goetzberger, W. Greubel, Appl. Phys. **14**, 123 (1977)
5. E. Yablonovich, J. Opt. Soc. Am. **70**, 1362 (1980)
6. G. Smestad et al., Sol. Energy Mater. **21**, 99 (1990)
7. T. Markvart, J. Opt. A Pure Appl. Opt. **10**, 015008 (2008)
8. T. Markvart, J. Appl. Phys. **99**, 026101 (2006)
9. U. Rau et al., Appl. Phys. Lett. **87**, 171101 (2005)
10. E. Yablonovitch, J. Opt. Soc. Am. **72**, 899 (1982)
11. C. Ulbrich et al., Phys. Status Solidi (a) **205**, 2831 (2008)
12. A. Bielawny et al., Phys. Status Solidi (a) **205**, 2796 (2008)
13. S. Knabe et al., Phys. Status Solidi (RRL) **4**, 118 (2010)
14. L. Shaffer, Sol. Energy **2**, 21 (1958)
15. C. Liebert, R. Hibbard, Sol. Energy **6**, 84 (1962)
16. A. De Vos, J. Phys. D: Appl. Phys. **13**, 839 (1980)
17. P. Baruch, J. Appl. Phys. **57**, 1347 (1985)
18. G.H. Bauer et al., in *Proceedings of the 2nd World Conference on Photovoltaic Solar Energy Conversion*, European Commission / Directorate General Joint Research Centre Environment Institute Renewable Energies Unit Ispra (I), (ISBN 92-828-5179-6) 1998, p. 132
19. A. Marti, G.L. Araujo, Sol. Energy Mater. Sol. Cells **43**, 203 (1996)
20. W.H. Bloss et al., in *Proceedings of 3rd European Photovoltaic Solar Energy Conference* (Reidel Publishing Company, Dordrecht, 1981), p. 401
21. J. Fischer et al., J. Appl. Phys. **108**, 044912 (2010)
22. E. Klampaftis et al., Sol. Energy Mater. Sol. Cells **93**, 1182 (2009)

23. A. Luque et al., J. Appl. Phys. **96**, 903 (2004)
24. A. Luque, A. Marti, Phys. Rev. Lett. **78**, 5014 (1997)
25. R.T. Ross, A.J. Nozik, J. Appl. Phys. **53**, 3813 (1982); A.J. Nozik, Physica E **14**, 115 (2002)
26. V.S. Vavilov, J. Phys. Chem. Solids **8**, 223 (1959)
27. O. Christensen, J. Appl. Phys. **47**, 689 (1976)
28. F.J. Wilkinson et al., J. Appl. Phys. **54**, 1172 (1983)
29. S. Kolodinsky et al., Appl. Phys. Lett. **63**, 2405 (1993)
30. P. Würfel et al., Progr. Photovolt. Res. Appl. **13**, 277 (2005)
31. R.J. Ellington et al., Nano Lett. **5**, 865 (2005)
32. G. Allan, C. Delerue, Phys. Rev. B **73**, 205423 (2006)
33. M.C. Beard et al., Nano Lett. **10**, 3019 (2010)
34. J.-W. Luo et al., Nano Lett. **8**, 3174 (2008)
35. F. Hallermann et al., Phys. Status Solidi (a) **205**, 2844 (2008)
36. S. Link et al., J. Phys. Chem. B **103**, 3529 (1999)
37. S. Link et al., J. Phys. Chem. B **103**, 4212 (1999)
38. S. Pillai et al., J. Appl. Phys. **101**, 093105 (2007)
39. T.J. Coutts, Sol. Energy Mater. Sol. Cells **66**, 443 (2000)
40. N.W.Ashcroft, N.D. Mermin, *Solid State Physics/International Edition* (W.B. Saunders Company, Philadelphia, 1976)
41. J.C.C. Fan, G.W. Turner, R.GP. Gale, C.O. Bozler, in *Conference Record of 14th IEEE Photovoltaic Specialists Conference* (IEEE, New York, 1980), p. 1102
42. Khz. Seeger, *Semiconductor Physics*. Springer Series in Solid State Sciences, vol. 40 (Springer, Berlin, 1989)

Appendix A
Radiation in Condensed Matter

A.1 Propagation and Attenuation

The spatio-temporal behavior of electromagnetic radiation propagating in matter or across phase boundaries therein is appropriately treated with Maxwell's equations. For example, combining

$$\nabla \times \mathbf{E} = -\mu_0 \mu \frac{\partial \mathbf{H}}{\partial t} \tag{A.1}$$

with[1]

$$\nabla \times \mathbf{H} = \varepsilon_0 \varepsilon \frac{\partial \mathbf{E}}{\partial t} + \mathbf{j} = \varepsilon_0 \varepsilon \frac{\partial \mathbf{E}}{\partial t} + \sigma \left[\mathbf{E} + (\mathbf{v} \times \mu_0 \mu \mathbf{H}) \right] , \tag{A.2}$$

then neglecting the effect of the magnetic field on charge transport, i.e., setting

$$\sigma (\mathbf{v} \times \mu_0 \mu \mathbf{H}) \approx 0 ,$$

and applying the boundary conditions

$$\nabla \cdot (\mu_0 \mu \mathbf{H}) = 0 \qquad \text{(no magnetic monopoles)}$$

and

$$\nabla \cdot \mathbf{E} = \frac{\rho}{\varepsilon_0 \varepsilon} \approx 0 \qquad \text{(space charge in the relevant spatial scale negligible)} ,$$

[1]The constants $\mu_0, \mu, \varepsilon_0, \varepsilon$, designate magnetic permeability and dielectric susceptibility, each in vacuum (subscript "0") and in matter, where σ represents the stationary state electric conductivity.

G.H. Bauer, *Photovoltaic Solar Energy Conversion*, Lecture Notes in Physics 901,
DOI 10.1007/978-3-662-46684-1

the electric field strength can be written

$$\Delta \mathbf{E} = \mu_0 \varepsilon_0 \mu \varepsilon \frac{\partial^2 \mathbf{E}}{\partial t^2} + \mu_0 \mu \sigma \frac{\partial \mathbf{E}}{\partial t} \,. \tag{A.3}$$

For a harmonic wave like $\mathbf{E} = \mathbf{E}^0 \exp(\mathrm{i}\mathbf{k} \cdot \mathbf{x}) \exp(-\mathrm{i}\omega t)$, we find the solution for propagation in the x-direction to combine the (complex) wave vector $\tilde{k}_x$ with material properties ϵ, μ, σ, etc.:

$$k_x^2 = \varepsilon_0 \mu_0 \varepsilon \mu \omega^2 + \mathrm{i} \mu_0 \mu \sigma \omega = \frac{\varepsilon \mu}{c_0^2} + \mathrm{i} \frac{\mu \sigma}{\varepsilon_0 c_0^2} \,, \tag{A.4}$$

$$\tilde{k}_x = \pm \frac{\omega}{c_0} \sqrt{\varepsilon \mu + \mathrm{i} \frac{\sigma \mu}{\varepsilon_0 \omega}} \,, \tag{A.5}$$

where $c_0^2 = 1/\varepsilon_0 \mu_0$ is the square of the vacuum speed of light. Since the ratio of the wave vector to the vacuum wave vector, viz.,

$$\frac{\tilde{k}_x}{k_0} = \tilde{n} = n_1 + \mathrm{i} n_2 \,,$$

represents the refractive index (also a complex magnitude), we arrive at the solution for the harmonic ansatz above by introducing $\tilde{k}_x(\varepsilon, \varepsilon_0, \mu, \sigma, \omega)$. The imaginary part of the refractive index $\mathrm{i}n_2$ can be extracted in the form

$$n_2^2 = \frac{1}{2} \varepsilon \left[\sqrt{1 + \left(\frac{\sigma}{\omega \varepsilon_0 \varepsilon} \right)^2} - 1 \right] \,. \tag{A.6}$$

It determines the attenuation of the amplitude[2] versus propagation length

$$\mathbf{E}(x) = \mathbf{E}^0(x) \exp(\mathrm{i} k_{0,x} n_1 x) \exp(-\mathrm{i}\omega t) \exp(-k_{0,x} n_2 x) \,.$$

The damping of the electric field strength $\mathbf{E}(x)$ versus x is translated into the attenuation of the photon flux $\Gamma_{\mathrm{phot}} \sim \mathbf{E}^2(x)$, we get the optical absorption coefficient

$$\alpha(\omega) = 2\omega \sqrt{\varepsilon_0 \mu_0} n_2 = 2\omega \sqrt{\varepsilon_0 \mu_0} \times \frac{1}{2} \varepsilon \left[\sqrt{1 + \left(\frac{\sigma}{\omega \varepsilon_0 \varepsilon} \right)^2} - 1 \right] \,. \tag{A.7}$$

[2]The amplitude of the electric field strength propagating in x-direction $\mathbf{E}(x)$ consists, of course, of components in y- and z-direction, E_y, E_z.

A.2 Propagation Across Interfaces

The propagation of electromagnetic waves across interfaces between matter with properties indexed 1 and 2 is again formulated with Maxwell's equations and the appropriate boundary conditions expressing conservation of the tangential components of the electric and magnetic fields

$$\mathbf{E}_{\mathrm{t},1} = \mathbf{E}_{\mathrm{t},2} \text{ and } \mathbf{H}_{\mathrm{t},1} = \mathbf{H}_{\mathrm{t},2},$$

and also their normal components

$$\varepsilon_0\varepsilon_1\mathbf{E}_{\mathrm{n},1} = \mathbf{D}_{\mathrm{n},1} = \mathbf{D}_{\mathrm{n},2} = \varepsilon_0\varepsilon_2\mathbf{E}_{\mathrm{n},2} \text{ and } \mu_0\mu_1\mathbf{H}_{\mathrm{n},1} = \mathbf{B}_{\mathrm{n},1} = \mathbf{B}_{\mathrm{n},2} = \mu_0\mu_2\mathbf{H}_{\mathrm{n},2}.$$

Generally, for each of the two media, one has to assume amplitudes of waves $A_{1,2}^{\mathrm{f,r}}$, such as $E_{1,2}^{\mathrm{f,r}}$ and $H_{1,2}^{\mathrm{f,r}}$ traveling in forward as well as reverse directions, denoted by superscripts f and r here. For simplicity, we shall only discuss normal incidence on the interface. In addition, we shall only consider non-magnetic materials ($\mu_1 = \mu_2 = 1$).

We choose a harmonic ansatz $A = A_0 \exp(\mathrm{i}kx) \exp(-\mathrm{i}\omega t)$ for the electric and magnetic field components, bearing in mind that propagation in the x-direction implies y- and z-components of the fields. (Recall that, for linear interaction of radiation with matter, any shape of wave may be generated by superposing harmonic waves with different amplitudes, wave vectors, and frequencies.) We then balance the left- and right-hand sides at the interface (located at $x = 0$) for the electric field with known amplitude E_{10}^{f}, frequency ω, and wave vector

$$k_1 = k_0\tilde{n}_1 = \frac{\omega}{c_0}\tilde{n}_1$$

of the electric field in medium 1:

$$\begin{aligned} E_1 &= E_{10}^{\mathrm{f}} \exp\left(\mathrm{i}\frac{\omega}{c_0}\tilde{n}_1 x\right) \exp(-\mathrm{i}\omega t) + E_{10}^{\mathrm{r}} \exp\left(-\mathrm{i}\frac{\omega}{c_0}\tilde{n}_1 x\right) \exp(\mathrm{i}\omega t) \\ &= E_2 = E_{20}^{\mathrm{f}} \exp\left(\mathrm{i}\frac{\omega}{c_0}\tilde{n}_2 x\right) \exp(-\mathrm{i}\omega t)\ , \end{aligned} \tag{A.8}$$

and get

$$E_{10}^{\mathrm{f}} + E_{10}^{\mathrm{r}} = E_{20}^{\mathrm{f}}\ . \tag{A.9}$$

A second equation for the determination of the two unknown amplitudes E_{10}^{r} and E_{20}^{f} can be formulated via the magnetic field balance:

$$\begin{aligned} H_1 &= H_{10}^{\mathrm{f}} \exp\left(\mathrm{i}\frac{\omega}{c_0}\tilde{n}_1 x\right) \exp(-\mathrm{i}\omega t) + H_{10}^{\mathrm{r}} \exp\left(-\mathrm{i}\frac{\omega}{c_0}\tilde{n}_1 x\right) \exp(\mathrm{i}\omega t) \\ &= H_2 = H_{20}^{\mathrm{f}} \exp\left(\mathrm{i}\frac{\omega}{c_0}\tilde{n}_2 x\right) \exp(-\mathrm{i}\omega t) \ , \end{aligned} \tag{A.10}$$

where the z-component is coupled to the y-component of the electric field and vice versa. From $\nabla \times \mathbf{E} = -\mu_0 \mu \partial \mathbf{H}/\partial t$, the $\mathbf{H}$ relation is converted into the second $\mathbf{E}$ equation which reads, again at the interface position $x = 0$,

$$i\tilde{n}_1 \frac{\omega}{c_0} E_{10}^{\mathrm{f}} - i\tilde{n}_1 \frac{\omega}{c_0} E_{10}^{\mathrm{r}} = i\tilde{n}_2 \frac{\omega}{c_0} E_{20} \ , \tag{A.11}$$

or

$$E_{10}^{\mathrm{f}} - E_{10}^{\mathrm{r}} = \frac{\tilde{n}_2}{\tilde{n}_1} E_{20}^{\mathrm{f}} \ . \tag{A.12}$$

Combining these two equations, we obtain the transmission and reflection factors for the amplitudes (bearing in mind that both quantities are generally complex):

$$\tilde{r}_{1,2} = \frac{E_{10}^{\mathrm{r}}}{E_{10}^{\mathrm{f}}} = \left(\frac{\tilde{n}_1}{\tilde{n}_2} - 1\right)\left(\frac{\tilde{n}_1}{\tilde{n}_2} + 1\right)^{-1} = \frac{\tilde{n}_1 - \tilde{n}_2}{\tilde{n}_1 + \tilde{n}_2} \ , \tag{A.13}$$

and finally,

$$\tilde{t}_{1,2} = \frac{2\tilde{n}_1}{\tilde{n}_1 + \tilde{n}_2} \ . \tag{A.14}$$

Note, that $r_{1,2}$ and $t_{1,2}$ definitely do not sum up to unity; energy flux conservation reads differently:

The square of the amplitude reflection and transmission factors times the corresponding propagation wave vector represents the energy fluxes for forward and reverse directions, and these do sum up to unity:

$$\left(E_{10}^{\mathrm{f}}\right)^2 n_1 = \left(E_{10}^{\mathrm{r}}\right)^2 n_1 + \left(E_{20}^{\mathrm{f}}\right)^2 n_2 \ ,$$

or

$$1 = (r_{1,2})^2 + (t_{1,2})^2 \frac{n_2}{n_1} \ .$$

A.3 Matrix Transfer Formalism

The optical properties of multilayer sequences available in many solar cells for combinations of antireflective coatings with absorbers, for heterojunctions, for tandem structures, etc., are preferably formulated by a matrix transfer formalism that combines the forward and reverse propagation of electromagnetic fields in a particular layer i with those from and to its neighbor layers $(i-1)$ and $(i+1)$ (Fig. A.1).

In layer i we find the amplitudes of forward (f) and reverse components (r)

$$A_i^{\mathrm{f}} = A_{i-1}^{\mathrm{f}} \tilde{t}_{i-1,i} \exp(\mathrm{i}k_0 \tilde{n}_{i-1} d_{i-1}) + A_i^{\mathrm{r}} \tilde{r}_{i,i-1} \exp(\mathrm{i}k_0 \tilde{n}_i d_i) \tag{A.15}$$

and

$$A_i^{\mathrm{r}} = A_i^{\mathrm{f}} \tilde{r}_{i,i+1} \exp(\mathrm{i}k_0 \tilde{n}_i d_i) + A_{i+1}^{\mathrm{r}} \tilde{t}_{i-1,i} \exp(\mathrm{i}k_0 \tilde{n}_{i+1} d_{i+1}) \,. \tag{A.16}$$

This set of equations with neighbor layer inputs into i from both sides $(i-1)$ and $(i+1)$ is not very comfortable to work with. However, we have

$$A_i^{\mathrm{f}} = \alpha A_{i-1}^{\mathrm{f}} + \beta A_i^{\mathrm{r}} \tag{A.17}$$

and

$$A_i^{\mathrm{r}} = \gamma A_i^{\mathrm{f}} + \delta A_{i+1}^{\mathrm{r}} \,, \tag{A.18}$$

and it can thus be translated into a version that is easier to apply with input magnitudes only from one side, i.e., from $i+1$ or from $i-1$:

$$\begin{pmatrix} A_i^{\mathrm{f}} \\ A_i^{\mathrm{r}} \end{pmatrix} = \begin{bmatrix} \alpha - \dfrac{\beta\gamma^*}{\delta^*} & \dfrac{\beta}{\delta^*} \\ -\dfrac{\gamma^*}{\delta^*} & \dfrac{1}{\delta^*} \end{bmatrix} \begin{pmatrix} A_{i-1}^{\mathrm{f}} \\ A_{i-1}^{\mathrm{r}} \end{pmatrix} \tag{A.19}$$

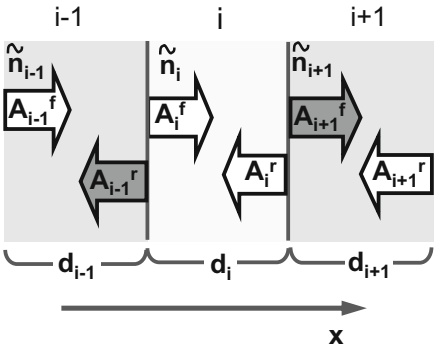

Fig. A.1 Amplitudes, e.g., electric field strength, propagating back and forth in layer i of a multilayer configuration with refractive indices $\ldots, \tilde{n}_{i-1}, \tilde{n}_i, \tilde{n}_{i+1}, \ldots$, each complex with real and imaginary parts, and across interfaces on the left and right sides, for formulation of the matrix transfer ansatz

On the basis of this representation we are able to calculate the magnitudes of interest (amplitudes including attenuation and interference effects) from the entrance interface (layer 0) to the rear end of the layer sequence in which the reverse wave is either explicitly given or does not exist.

The coefficients in the matrix above read, with phase accumulation and attenuation,

$$\alpha = t_{i-1,i} \exp(\mathrm{i}k_0 \bar{n}_{i-1} d_{i-1}) \exp(-\lambda_{i-1} d_{i-1}) \,, \tag{A.20}$$

$$\beta = r_{i,i-1} \exp(\mathrm{i}k_0 \bar{n}_i d_i) \exp(-\lambda_i d_i) \,, \tag{A.21}$$

$$\gamma^* = r_{i-1,i} \exp(\mathrm{i}k_0 \bar{n}_{i-1} d_{i-1}) \exp(-\lambda_{i-1} d_{i-1}) \,, \tag{A.22}$$

$$\delta^* = t_{i,i-1} \exp(\mathrm{i}k_0 \bar{n}_i d_i) \exp(-\lambda_i d_i) \,, \tag{A.23}$$

where $\bar{n}$ denotes the real part of the respective refractive index and λ is the amplitude attenuation coefficient (imaginary part of the refractive index $\lambda = in_2$).

Appendix B
Absorption of Photons in Condensed Matter

The electronic transition from an initial valence band state ψ_i to a final state ψ_f in the conduction band initiated by the interaction of photons with electrons in a semiconductor is basically treated as a perturbation problem in quantum mechanics (for details see [1]). The photon is expressed by a vector potential

$$\mathbf{A}(\mathbf{r},t) = \frac{1}{2}A_0\boldsymbol{\varepsilon}\left\{\exp\left[\mathrm{i}\left(\mathbf{k}_\mathrm{p}\cdot\mathbf{r}-\omega t\right)\right] + \exp\left[-\mathrm{i}\left(\mathbf{k}_\mathrm{p}\cdot\mathbf{r}-\omega t\right)\right]\right\}, \tag{B.1}$$

where $\boldsymbol{\varepsilon}$ is the normalized polarization vector, and the magnetic field $\mathbf{H}$ is given by $\mathbf{H} = \nabla\times\mathbf{A}$. The Hamiltonian $\hat{H}_0$ of electrons in the unperturbed system is modified due to the magnetic field into $\hat{H} = \hat{H}_0 + \hat{H}_1$, where

$$\hat{H}_1 = \frac{e}{mc}\hat{p}\mathbf{A}\,,$$

and the momentum operator reads $\hat{p} = -\mathrm{i}\hbar\nabla$. The Schrödinger equation is thus

$$\left[-\frac{\hbar^2}{2m}\nabla^2 + \frac{\mathrm{i}e\hbar}{2mc}(\nabla\mathbf{A}) + \frac{\mathrm{i}e\hbar}{2mc}(\mathbf{A}\nabla) + \frac{e^2}{2mc^2}(\mathbf{A})^2 + V(\mathbf{r})\right]\psi = -\mathrm{i}\hbar\frac{\partial\psi}{\partial t}\,. \tag{B.2}$$

Introducing the relation $\mathbf{A}\hat{p} = \hat{p}\mathbf{A}$ and the unit polarization vector $\mathbf{e}$, and assuming a small perturbation so that the term in $\mathbf{A}^2$ can be neglected, the probability for 'direct' transitions ω_VC from initial state $|\mathrm{v}\mathbf{k}\rangle$ (valence band) to final state $|\mathrm{c}\mathbf{k}'\rangle$ (conduction band) becomes [1]

$$\omega_\mathrm{VC} = \frac{\pi e^2}{2\hbar m^2}A_0^2\left|\langle\mathrm{c}\mathbf{k}'|\exp(\mathrm{i}\mathbf{k}_\mathrm{p}\cdot\mathbf{r})\mathbf{e}\cdot\hat{p}|\mathrm{v}\mathbf{k}\rangle\right|^2 \times \delta\left[\epsilon_\mathrm{C}\left(\mathbf{k}'\right) - \epsilon_\mathrm{V}(\mathbf{k}) - \hbar\omega\right]. \tag{B.3}$$

G.H. Bauer, *Photovoltaic Solar Energy Conversion*, Lecture Notes in Physics 901,
DOI 10.1007/978-3-662-46684-1

With Bloch functions $|j\mathbf{k}\rangle = u_{j\mathbf{k}}(\mathbf{r})\exp(\mathrm{i}\mathbf{k}\cdot\mathbf{r})$, where j represents either v or c, and $\mathbf{k}_\mathrm{p}$ is the photon wave vector, and with wave vector conservation

$$\mathbf{k}_\mathrm{p} + \mathbf{k} - \mathbf{k}' = \mathbf{G}_\mathrm{m} \ ,$$

where $\mathbf{G}_\mathrm{m}$ denotes any reciprocal lattice vector. Assuming that the photon wave vector is negligible $\mathbf{k}_\mathrm{p} \approx 0$ in comparison with lattice wave vectors in the first Brillouin zone, one arrives finally, after some additional intermediate equations, at the imaginary part of the dielectric constant ε_2, which is composed of contributions from the individual valence–conduction band transitions:

$$\varepsilon_2 = \frac{\pi e^2}{\varepsilon_0 m^2 \omega^2} \sum_{k,k'} |\mathbf{e}\cdot\mathbf{p}_\mathrm{cv}|^2 \delta\big[\epsilon_\mathrm{c}(\mathbf{k}') - \epsilon_\mathrm{v}(\mathbf{k}) - \hbar\omega\big]\delta_{\mathbf{k}\mathbf{k}'} \ , \tag{B.4}$$

or

$$\varepsilon_2 \sim (\hbar\omega)^{-2} |M_\mathrm{i,f}|^2 (\hbar\omega - \epsilon_\mathrm{g})^{1/2} \ . \tag{B.5}$$

This can be converted into the absorption coefficient $\alpha(\hbar\omega)$ for direct transitions, viz.,

$$\alpha(\hbar\omega) = \frac{\omega}{c_0}\varepsilon_2(\hbar\omega) \ , \tag{B.6}$$

where ω is the frequency and c_0 the vacuum speed of light.

For valence band–conduction band transitions which are accompanied by fulfillment of wave vector conservation with the participation of phonons, an analogous treatment leads to the corresponding relation for the imaginary part of the refractive index and the absorption coefficient of indirect semiconductors:

$$\varepsilon_2 = \frac{\pi e^2}{\varepsilon_0 m^2 \omega^2} \sum_{m,\alpha,\pm} |M_\mathrm{cv}^{m,\alpha,\pm}|^2 \times \sum_{\mathbf{k},\mathbf{k}'} \delta\left[\epsilon_\mathrm{c}(\mathbf{k}') - \epsilon_\mathrm{v}(\mathbf{k}) - \hbar\omega \pm \hbar\omega_\mathbf{q}^\alpha\right] \ . \tag{B.7}$$

Here, the first summation is to be carried out for a virtual state $|m\rangle$ and the phonon mode α, either in absorption (+) or in emission (−), with the appropriate probability for phonons $n_\mathbf{q}^{\alpha+1}$, $n_\mathbf{q}^\alpha$ approximated by phonon statistics from the Bose–Einstein distribution function. The second summation is performed in the $\mathbf{k}$-space, in the neighborhood of the top of the valence and the minimum of the conduction band, located at different wave vector positions and associated with corresponding

curvature (second derivatives) representing the effective masses of holes ($m^*_{\mathrm{p}x,y,z}$ in VB) and of electrons ($m^*_{\mathrm{n}x,y,z}$ in CB):

$$\sum_{\mathbf{k},\mathbf{k}'} \delta\left[\epsilon_{\mathrm{c}}(\mathbf{k}') - \epsilon_{\mathrm{v}}(\mathbf{k}) - \hbar\omega \pm \hbar\omega^{\alpha}_{\mathbf{q}}\right]$$
$$= \sum_{k,k'} \delta\Bigg[\epsilon_{\mathrm{c}0} - \epsilon_{\mathrm{v}0} + \frac{\hbar^2}{2}\left(\frac{k_x^2}{m^*_{\mathrm{p}x}} + \frac{k_y^2}{m^*_{\mathrm{p}y}} + \frac{k_z^2}{m^*_{\mathrm{p}z}} + \frac{k_x'^2}{m^*_{\mathrm{n}x}} + \frac{k_y'^2}{m^*_{\mathrm{n}y}} + \frac{k_z'^2}{m^*_{\mathrm{n}z}}\right)$$
$$-\hbar\omega \pm \hbar\omega^{\alpha}_{\mathbf{q}}\Bigg]. \tag{B.8}$$

Finally, the imaginary part of the refractive index is obtained as

$$\varepsilon_2 = \frac{\pi e^2}{\varepsilon_0 m^2 \omega^2}\frac{K}{(4\pi)^3}\sum_{m,\alpha,\pm}\left\{\left|A^{m,\alpha,+}_{\mathrm{cv}}\right|^2 \frac{\left[\hbar\omega - \hbar\omega^{\alpha}_{\mathbf{q}} - (\epsilon_{\mathrm{c}0} - \epsilon_{\mathrm{v}0})\right]^2}{1 - \exp\left(-\hbar\omega^{\alpha}_{\mathbf{q}}/kT\right)}\right\}$$
$$+\frac{\pi e^2}{\varepsilon_0 m^2 \omega^2}\frac{K}{(4\pi)^3}\sum_{m,\alpha,\pm}\left\{\left|A^{m,\alpha,-}_{\mathrm{cv}}\right|^2 \frac{\left[\hbar\omega + \hbar\omega^{\alpha}_{\mathbf{q}} - (\epsilon_{\mathrm{c}0} - \epsilon_{\mathrm{v}0})\right]^2}{-1 + \exp\left(+\hbar\omega^{\alpha}_{\mathbf{q}}/kT\right)}\right\}. \tag{B.9}$$

Here, the first term corresponds to absorption of a photon associated with the emission (generation) of a phonon of mode α and energy $\hbar\omega^{\alpha}_{\mathbf{q}}$, with wave vector $\mathbf{q}$, whereas the second term represents photon absorption with absorption of a phonon ('borrowed' from the lattice) with appropriate energy and wave vector. The abbreviation of the contribution of the effective hole and electron masses reads

$$K = \left(\frac{2}{\hbar^2}\right)^3 \sqrt{\left(m_{\mathrm{p}x} m_{\mathrm{p}y} m_{\mathrm{p}z}\right)\left(m_{\mathrm{n}x} m_{\mathrm{n}y} m_{\mathrm{n}z}\right)}\,.$$

For these phonon-associated transitions, the absorption coefficient $\alpha(\hbar\omega)$ in a simplified version with $\epsilon_{\mathrm{c}0} - \epsilon_{\mathrm{v}0} = \epsilon_{\mathrm{g}}$ is written analogously [1]:

$$\alpha(\hbar\omega) = C^{\text{phon, absorb}}\frac{1}{\omega^2}\left(\hbar\omega + \hbar\omega_{\text{phon}} - \epsilon_{\mathrm{g}}\right)^2 + C^{\text{phon, emiss}}\frac{1}{\omega^2}\left(\hbar\omega - \hbar\omega_{\text{phon}} - \epsilon_{\mathrm{g}}\right)^2. \tag{B.10}$$

Reference

1. C. Hamaguchi, *Basic Semiconductor Physics* (Springer, Berlin, 2001)

Appendix C
Photon Density in Matter

The photon density in matter out of thermal equilibrium results from perturbations from outside, e.g., from an external photon field. In steady state the chemical potential of the photons μ_γ equals the chemical potential of the electron system $\mu_{\rm np}$, provided no charge carriers are extracted from or injected to the material. As $\mu_{\rm np}$ rises—with good approximation—logarithmically with electron and hole densities, for solar light conversion, the goal is to maximize likewise the internal photon density in matter.

In the language of statistical ray optics [1], the stationary energy density in non- or weakly absorbing solid matter, e.g., in dielectrics with refractive index n, be it in thermal equilibrium ($\mu = 0$) or in an excited state, and characterized by Planck's generalized law ($\mu > 0$), can be written

$$u(\omega) = \frac{2k^2}{(2\pi)^3}(\hbar\omega)\frac{1}{\exp\left(\dfrac{\hbar\omega - \mu}{kT}\right) - 1}\,\mathrm{d}\Omega\,\mathrm{d}k\ , \tag{C.1}$$

where the first factor is the density of photon states in k-space, the second is the photon energy, and the third is the Bose factor. As usual, $\mathrm{d}\Omega$ represents the solid angle.

For ergodic optical behavior of solid matter, this relation can be converted into the energy flux using $k = n\omega/c$ and the group velocity $v_{\rm gr} = c = \mathrm{d}\omega/\mathrm{d}k$

$$\Gamma_\varepsilon = v_{\rm gr}u(\omega) = \frac{2n^2\omega^2}{(2\pi)^2c^2}(\hbar\omega)\frac{1}{\exp\left(\dfrac{\hbar\omega - \mu}{kT}\right) - 1}\mathrm{d}\,\Omega\,\mathrm{d}\omega\ . \tag{C.2}$$

Ergodicity means that the variables time t and space x in the description of the flux properties cannot be exchanged or, in other words, after sufficient time and propagation path the photons have 'forgotten' which direction they originally

G.H. Bauer, *Photovoltaic Solar Energy Conversion*, Lecture Notes in Physics 901,
DOI 10.1007/978-3-662-46684-1

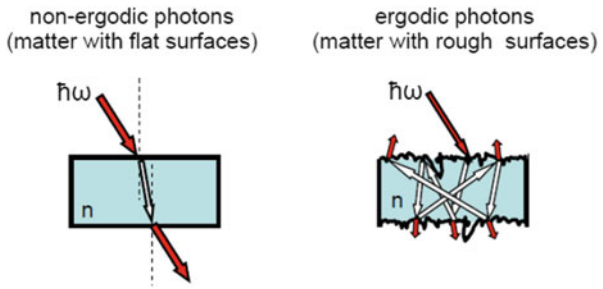

Fig. C.1 Non-ergodic (*left*) and ergodic photon behavior (*right*) due to surface scattering properties of dielectric matter

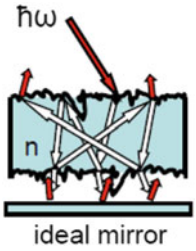

Fig. C.2 Ergodic photon behavior due to surface scattering properties of dielectric matter with ideal back-reflector

came from. Typical ergodic behavior of photons can be generated by an ideally (wavelength independent and isotropic to the solid angle 2π) scattering surface (see Fig. C.1).

The energy flux depends on n^2 what simply results from the 'compression' of the wave modes in the three-dimensional k-space due to the presence of a refractive index n. (The more modes can be fitted into the energy interval dω, the more they are squeezed through the refractive index n.)

A further increase of the internal photon flux Γ_ϵ by a factor of 2 can be achieved using an ideally reflecting rear surface of the dielectric matter which returns the photons (see Fig. C.2). In essence, compared to the energy flux outside $\Gamma_{\epsilon,\,\mathrm{out}} = \Gamma_{u,\,\mathrm{incident}}$, the internal energy flux $\Gamma_{\epsilon,\,\mathrm{int}}$ becomes in the best case $\Gamma_{\epsilon,\,\mathrm{int}} = (2n)^2 \Gamma_{\epsilon,\,\mathrm{incident}}$.

Reference

1. E. Yablonovitch, J. Opt. Soc. Am. **72**, 899 (1982)

Appendix D
Surface Recombination and Carrier Depth Profiles

D.1 Carrier Flux at the Surface

As a consequence of the interrupted periodic potential at the surface of a crystal due to missing neighbors and non-saturated bonding sites (dangling bonds) at the surface electronic states are generated, in addition to those in the bands resulting from the bulk properties.[1] These surface states allow for a surplus in recombination rates for excess carriers. In our picture, the surface states act as an additional sink for photoexcited carriers which, depending on the concentration of these states, may substantially reduce the overall excess carrier density.

In the steady state, the carrier current at the surface (x_s) is conserved[2] and reads for positions $x_s - \delta$ and $x_s + \delta$ (see Fig. D.1):

$$\Gamma\,(x_s - \delta) = \Gamma\,(x_s + \delta)\ .$$

The general electric current density of a particle species (i.e., electrons) with concentration n and mobility μ_n reads

$$\mathbf{j}_n = en\mu_n \left(-\nabla_{\mathbf{x}} \left(\frac{1}{e}\epsilon_{Fn}(\mathbf{x})\right)\right)\ . \tag{D.1}$$

[1] Stationary state electronic wave functions at a potential barrier, like at a surface exhibit an imaginary wave vector causing the amplitude to decay exponentially with distance into the barrier. Such wave functions provide electronic states in the barrier material even without the existence of non-saturated dangling bonds.

[2] In one dimension the treatment in terms of current and current density is identical.

G.H. Bauer, *Photovoltaic Solar Energy Conversion*, Lecture Notes in Physics 901,
DOI 10.1007/978-3-662-46684-1

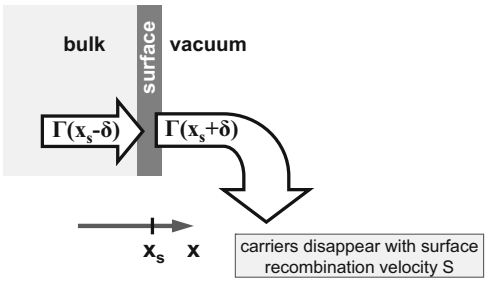

Fig. D.1 Schematic current continuity at the surface at x_s. The carrier current arriving at x_s is removed from the surface with a particular velocity S, called the surface recombination velocity

Writing

$$\epsilon_{\mathrm{Fn}} = kT \ln\left[\frac{n}{n_0}\right] = kT \ln\left[\frac{\Delta n + n_0}{n_0}\right] ,$$

we get the spatial derivative

$$\nabla_{\mathbf{x}} (\epsilon_{\mathrm{Fn}}) = \nabla_{\mathbf{x}} \left(kT \ln\left[\frac{n}{n_0}\right]\right) .$$

Assuming spatially independent temperature $T \neq T(\mathbf{x})$, and spatially independent $n_0 \neq n_0(\mathbf{x})$, which implies $n(\mathbf{x}) = n_0 + \Delta n(\mathbf{x})$, so that diffusion is the sole driving force, we continue with

$$\mathbf{j}_{\mathrm{n}} = e(n_0 + \Delta n) \left(\frac{\mu_{\mathrm{n}} kT}{e}\right) \left(\frac{n_0}{n_0 + \Delta n}\right) \left[-\nabla_{\mathbf{x}} \left(\frac{\Delta n}{n_0}\right) - \nabla_{\mathbf{x}} \left(\frac{n_0}{n_0}\right)\right] .$$

We substitute in $(\mu_{\mathrm{n}} kT/e) = D_{\mathrm{n}}$ and get the well known expression for a diffusion current density:

$$\mathbf{j}_{\mathrm{n}} = eD_{\mathrm{n}} \left(-\nabla_{\mathbf{x}} \big[\Delta n(\mathbf{x})\big]\right) .$$

In one dimension we accordingly find at x_s:

$$-eD_{\mathrm{n}} \partial(\Delta n)/\partial x = eS\Delta n,$$

where S represents the surface recombination velocity, in other words, this velocity with which excess carriers are removed from contributing to charge transport.

D.2 Surface Recombination and Carrier Diffusion

The excess carrier concentration $\Delta n(\mathbf{x})$ in homogeneous absorbers is usually derived using the steady-state continuity equation with a linear recombination term: the input parameters of the carrier depth profile are governed by properties of the bulk, such as diffusion length L and lifetime τ, and by those of the surfaces, which are usually expressed in surface recombination velocities at the front (S_0) and rear side (S_d) of the absorber. It goes without saying that the profile of the excess carrier generation also enters into the resulting depth dependence $n(\mathbf{x})$. Hence,

$$\frac{\partial(\Delta n(\mathbf{x}))}{\partial t} + \nabla\big[\Delta n(\mathbf{x})\big] = g(\mathbf{x}) - r(\mathbf{x}) \; . \tag{D.2}$$

We apply a one-dimensional ansatz in the x-direction, steady-state conditions, and carrier motion exclusively driven by diffusion with a particle flux

$$\frac{1}{e} j_x = -D_\mathrm{n} \frac{\partial(\Delta n(x))}{\partial x} \; .$$

We assume a generation rate $g(x) = g_0 \exp\left(-\alpha(\hbar\omega)x\right)$ with absorption coefficient α and recombination with a rate linear in the carrier density $r = \Delta n(x)/\tau$, and hence get a differential equation of second order in which generation occurs as a perturbation of the homogeneous equation:

$$\tau D_\mathrm{n} \frac{\partial^2(\Delta n(x))}{\partial x^2} + \Delta n(x) = \tau g_0 \exp(-\alpha x) \; . \tag{D.3}$$

We separate the above relation into a homogeneous part containing two exponential terms

$$\Delta n_\mathrm{hom}(x) = A \exp\left(+\frac{x}{L}\right) + B \exp\left(-\frac{x}{L}\right) \; ,$$

with diffusion length of electrons $L = \sqrt{D_\mathrm{n}\tau}$, together with an inhomogeneous part. The result is finally[3]

$$\begin{aligned} \Delta n(x) &= \Delta n_\mathrm{hom}(x) + \Delta n_\mathrm{inhom}(x) \\ &= A \exp\left(+\frac{x}{L}\right) + B \exp\left(-\frac{x}{L}\right) + \frac{\tau g_0}{1 - (\alpha L)^2} \exp(-\alpha x) \; . \end{aligned} \tag{D.4}$$

The coefficients A and B are determined by the boundary conditions at the absorber front ($x = 0$) and rear side ($x = d$), where the concentrations are controlled by the

[3]The solution below only holds for $(\alpha L)^2 \neq 1$. The ansatz for the solution of the so-called resonance case $(\alpha L)^2 = 1$ reads $\Delta n(x) = x \exp(\beta x)$.

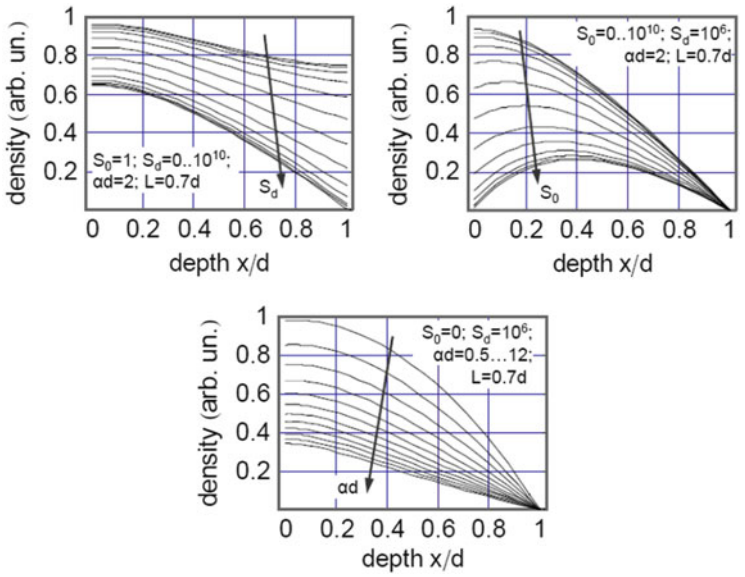

Fig. D.2 Example diffusion profiles of excess carriers $\Delta n(x)$ versus normalized depth x/d for a variation of front and rear surface recombination velocities S_0 and S_d and different absorption factors αd

surface recombination velocities $S_j(x_j)$ through

$$\Delta n(x)S(x) = -D_\mathrm{n}\partial(\Delta n(x))/\partial x$$

with $S(x=0) = S_0$ and $S(x=d) = S_d$. The final solutions for the prefactors A and B are

$$A = \left(\frac{\tau g_0}{1-(\alpha L)^2}\right)\left(\exp\left(-\frac{d}{L}\right)\left(LS_0S_d - D_\mathrm{n}S_0 - \alpha D_\mathrm{n}^2 + D_\mathrm{n}\alpha LS_d\right)\right)\left(\frac{1}{\Xi}\right) + \left(\frac{\tau g_0}{1-(\alpha L)^2}\right)\left(\exp(-\alpha d)\left(\alpha D_\mathrm{n}^2 + \alpha D_\mathrm{n}LS_0 - DS_d - LS_0S_d\right)\right)\left(\frac{1}{\Xi}\right) \tag{D.5}$$

and

$$B = \left(\frac{\tau g_0}{1-(\alpha L)^2}\right)\left(exp\left(-\frac{d}{L}\right)\left(LS_0S_d + D_\mathrm{n}S_0 + \alpha D_\mathrm{n}^2 + D_\mathrm{n}\alpha LS_d\right)\right)\left(\frac{1}{\Xi}\right) + \left(\frac{\tau g_0}{1-(\alpha L)^2}\right)\left(\exp(-\alpha d)\left(\alpha D_\mathrm{n}^2 - \alpha D_\mathrm{n}LS_0 - DS_d + LS_0S_d\right)\right)\left(\frac{1}{\Xi}\right) \tag{D.6}$$

with denominator

$$\Xi = 2\left[\left(\frac{D_{\mathrm{n}}^2}{L} + LS_0S_d\right)\sinh\left[\frac{d}{L}\right] + D\left(S_0 + S_d\right)\cosh\left[\frac{d}{L}\right]\right] \tag{D.7}$$

To visualize depth profiles and the influences of surface and bulk properties, see the examples in Fig. D.2.

Appendix E
Finite Length of a Homogeneous Diode

The current density–voltage relation of a homogeneous *pn*-junction was derived in Sect. 5.1.2 with the assumption that the p- and n-layers had infinite spatial extent. In particular, in the expression for the reverse saturation current density j_0, regarding the boundary conditions of the infinitely extended layers, it was assumed that the perturbation of the minority density away from the junction at infinite distance asymptotes exponentially towards the thermal equilibrium values.

For finite length of the individual layers, however, terminated with a metal as contact material, the excess density vanishes at finite distances $-x_\mathrm{p}$ and x_n in Fig. E.1. The relevant minority carrier densities at $-x_\mathrm{p}$, x_n are introduced by comparatively high ('infinite') surface recombination velocities $S(-x_\mathrm{p}) \to \infty$ and $S(x_\mathrm{n}) \to \infty$. In each of the solutions for the spatially dependent minorities, two exponential terms now appear, one with positive and one with negative argument. The particular spatial densities are thus formulated in terms of hyperbolic functions with arguments containing the magnitudes of the surface recombination velocity S_j, minority diffusion length L_j, diffusion coefficient D_j, thickness of layer x_j, and of course the elementary charge $e = +1.6 \times 10^{-19}$ As. In essence, only the reverse saturation current density j_0 is modified by the spatial limitation of the diode, while the qualitative behavior in the dark and under illumination $j = j(V)$ remains unchanged:

$$j_0 = en_{\mathrm{p}0}\left(\frac{D_\mathrm{n}}{L_\mathrm{n}}\right)\left(\frac{\frac{L_\mathrm{n}S_\mathrm{p}}{D_\mathrm{p}}\cosh\left[\frac{w_\mathrm{p}}{L_\mathrm{n}}\right]+\sinh\left[\frac{w_\mathrm{p}}{L_\mathrm{n}}\right]}{\cosh\left[\frac{w_\mathrm{p}}{L_\mathrm{n}}\right]+\frac{L_\mathrm{n}S_\mathrm{p}}{D_\mathrm{n}}\sinh\left[\frac{w_\mathrm{p}}{L_\mathrm{n}}\right]}\right)$$
$$+ep_{\mathrm{n}0}\left(\frac{D_\mathrm{p}}{L_\mathrm{p}}\right)\left(\frac{\frac{L_\mathrm{p}S_\mathrm{n}}{D_\mathrm{p}}\cosh\left[\frac{w_\mathrm{n}}{L_\mathrm{p}}\right]+\sinh\left[\frac{w_\mathrm{n}}{L_\mathrm{p}}\right]}{\cosh\left[\frac{w_\mathrm{n}}{L_\mathrm{p}}\right]+\frac{L_\mathrm{p}S_\mathrm{n}}{D_\mathrm{p}}\sinh\left[\frac{w_\mathrm{n}}{L_\mathrm{p}}\right]}\right) \qquad \text{(E.1)}$$

G.H. Bauer, *Photovoltaic Solar Energy Conversion*, Lecture Notes in Physics 901,
DOI 10.1007/978-3-662-46684-1

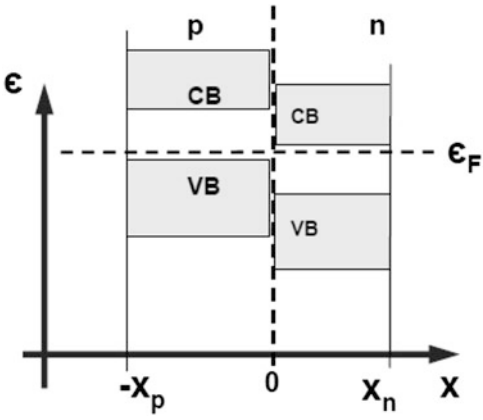

Fig. E.1 Sketch of spatially limited homogeneous *pn*-junction. Space charge regions are neglected

Here, the widths $w_\mathrm{p} \approx x_\mathrm{p}$ and $w_\mathrm{n} \approx x_\mathrm{n}$ are approximations, since these widths correspond to the lengths/thicknesses of the *p*- and the *n*-type doped layers after subtraction of the widths of the space-charge regions.

For detailed analytical formulations of finite *pn*-junctions, the interested reader is referred to [1, 2].

References

1. S.M. Sze, *Physics of Semiconductor Devices* (Wiley, New York, 1981)
2. H.G. Wagemann, H. Eschrich, *Grundlagen der Photovoltaischen Energiewandlung* (Teubner, Stuttgart, 2010)

Appendix F
Boltzmann Transport Equation

In solids the one-electron states bear the quantum rules (**k**,S) with $\mathbf{k} = (k_x, k_y, k_z)$ and spin quantum number S. The latter ($S = \pm 1/2$) accounts for the fact that each **k** state can be occupied by two electrons (here S0 effects are neglected). The quasi-classical description of the transport of an ensemble of species assumes that the effect of external fields like an electric (**E**) and a magnetic field (**B**) lead to the following equations of motion:

$$\dot{\mathbf{r}} = \mathbf{v_n}(\mathbf{k}) = \frac{1}{\hbar}\frac{\partial \epsilon_n(\mathbf{k})}{dk},$$
$$\hbar\,\dot{\mathbf{k}} = -e\,[\mathbf{E}(\mathbf{r},t) + \mathbf{v_n}(\mathbf{k}) \times \mathbf{B}(\mathbf{r},t)]$$

This approach is valid if the carriers can be viewed as wave packets with an uncertainty $\Delta\mathbf{k}$ allowing a spatial confinement **r** to $\Delta\mathbf{r} \approx 1/\Delta\mathbf{k}$. Hence the behavior of a charge carrier can be described by a distribution function $f(\mathbf{k}, \mathbf{r}, t)$ [1, 2]:

$$\frac{\partial f}{\partial t} + \dot{\mathbf{r}}\nabla_{\mathbf{r}}[f] + \dot{\mathbf{k}}\nabla_{\mathbf{k}}[f] = \frac{\partial f}{\partial t}|_{\text{relax}}$$

with the relaxation time approximation[1]

$$\frac{\partial f}{\partial t}|_{\text{relax}} = \frac{f(\mathbf{k}) - f_0(\mathbf{k})}{\tau_m},$$

containing the thermal-equilibrium distribution $f_0(\mathbf{k})$.

[1]The representation of carrier scattering for wave vector and energy relaxation, which is controlled by static and dynamic effects of carriers and the lattice are extremely complex; the easiest ansatz thus consists of a phenomenological relaxation time constant τ_m for particular cases determined by respective experiments.

G.H. Bauer, *Photovoltaic Solar Energy Conversion*, Lecture Notes in Physics 901,
DOI 10.1007/978-3-662-46684-1

Replacing $\dot{\mathbf{r}} = \mathbf{v}$ and $\dot{\mathbf{k}}$ by a general force $\dot{\mathbf{k}} = (1/\hbar)\mathbf{F}$ we arrive for stationarity $(\partial f/\partial t = 0)$ at

$$f(\mathbf{k}) = f_0(\mathbf{k}) + \tau_{\mathrm{m}}(\mathbf{v} \cdot \nabla_{\mathbf{r}}[f] + (1/\hbar)\mathbf{F} \cdot \nabla_{\mathbf{k}}[f])$$

The stationary non-thermal-equilibrium distribution contains a term for spatial variation of $\mathbf{v} \cdot \nabla_{\mathbf{r}}[f]$ in which, e.g., a spatially dependent temperature and concentration profiles generated by illumination can be accommodated, as well as the external forces, $(1/\hbar)\mathbf{F} \cdot \nabla_{\mathbf{k}}[f])$.

For spatial homogeneous structures $(\nabla_{\mathbf{r}} = 0)$ and for small departures from thermal equilibrium we approximate $\nabla_{\mathbf{v}} f(\mathbf{v}) \approx \nabla_{\mathbf{v}} f_0$, and finally get

$$f = f_0 + \tau_{\mathrm{m}}(1/\hbar)\mathbf{F} \cdot \nabla_{\mathbf{k}}[f_0],$$

which is known as Boltzmann's linearization, in which the stationary non-equilibrium distribution function has thus been related to the thermal-equilibrium Fermi-Dirac distribution function $f_0(\mathbf{k})$.

The expression of the external forces is usually replaced by

$$\frac{\mathbf{F}}{\hbar}\nabla_{\mathbf{k}}\big[f_0\big] = \frac{\mathbf{F}}{\hbar}\frac{\partial f_0\big(\epsilon(\mathbf{k})\big)}{\partial \epsilon} \cdot \nabla_{\mathbf{k}}\big[\epsilon(\mathbf{k})\big] = \frac{\mathbf{F}}{\hbar} \cdot \frac{\partial f_0(\epsilon)}{\partial \epsilon}\hbar\nabla_{\mathbf{k}}\omega \ . \tag{F.1}$$

With $\nabla_{\mathbf{k}}\omega = \mathbf{v}_{\mathrm{group}} = \hbar\mathbf{k}/m^*$, we arrive at

$$\frac{\mathbf{F}}{\hbar} \cdot \nabla_{\mathbf{k}}\big[f_0\big] = \frac{\mathbf{F}}{m^*} \cdot \mathbf{k}\frac{\partial f_0(\epsilon)}{\partial \epsilon}\hbar \ , \tag{F.2}$$

where $\mathbf{F}$ might represent an electric and/or magnetic field component, in which case $\mathbf{F} = e\mathbf{E} + e\mathbf{v} \times \mathbf{B}$.

In the quasi-classical approximation discussed here, the effect of the periodic crystal potential on the dynamics of charge carriers is treated quantum mechanically (via Bloch states). The wave packet formed of the states are than treated as classical objects subject to external fields.

For semiconductors with typically only few carriers in the conduction and valence bands, the Fermi-Dirac distribution function can be replaced by the Boltzmann energy-distribution function, as been discussed in detail in Sect. 4.2.

As a consequence of the above linearization, in the particular case of spatial homogeneity $(\nabla_{\mathbf{x}} = 0)$, where the only gradient is in the electrostatic potential, with say an electric field $\mathbf{E}$, a small perturbation of the thermal equilibrium distribution in the wave vector space ($\mathbf{k}$-space) results in a displacement of the symmetric distribution by $\delta\mathbf{k} \sim \mathbf{E}$, as shown schematically in Fig. F.1.

For charge carrier transport in solar cells, the contribution of magnetic fields are usually neglected, and the remaining driving forces are electric fields for drift of charge carriers, concentration gradients for their diffusion, and—mostly neglected as well—temperature gradients, which initiate thermoelectric transport effects.

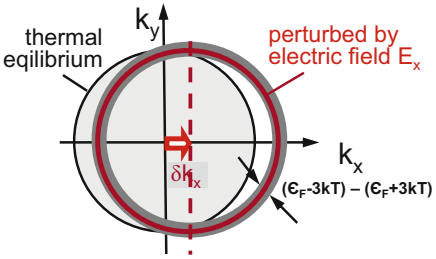

Fig. F.1 Schematic representation of electron distribution in k-space (spherical shape for cases with $\epsilon \sim k^2$) with perturbation of the k_x-distribution by an electric field $\mathbf{E} = \{E_x\,,\ 0\,,\ 0\}$, $(E_x < 0)$. Only electrons in the wave vector regime perturbed by the electric field (*bold circle*) contribute to charge transport (in metals the main contribution to transport results from the regime which spans approximately from $(\epsilon_\mathrm{F} - 3kT)$ to $(\epsilon_\mathrm{F} + 3kT)$ around the bold ϵ_F-contour line; in semiconductors transport electrons and holes may be formulated by replacing the corresponding Fermi-Dirac distribution function by the Boltzmann energy distribution)

References

1. S.R. Elliott, *The Physics and Chemistry of Solids* (Wiley, New York, 2006)
2. S. Hunklinger, *Festkörperphysik* (Oldenbourg Wissenschaftsverlag, München (F.R.G.), 2007)

Index

G.H. Bauer, *Photovoltaic Solar Energy Conversion*, Lecture Notes in Physics 901,
DOI 10.1007/978-3-662-46684-1